

# Structure-assisted design of enzyme inhibitors

Pavλίna Maloy Řezáčová

Institute of Organic Chemistry and Biochemistry, Czech Academy of Sciences  
Institute of Molecular Genetics, Czech Academy of Sciences  
Prague, Czech Republic

## Habilitation thesis

Field: Biophysics

Faculty of Science

University of South Bohemia, České Budějovice, Czech Republic

2019

## Table of Contents

List of papers included in the thesis .....	3
Introduction .....	4
Results .....	6
Design of carborane inhibitors of HIV protease .....	6
Design of carborane inhibitors of human carbonic anhydrases .....	9
Design of inhibitors of human 5'(3')-deoxynucleotidases .....	12
Summary and future perspective .....	16
References .....	18
Papers <b>P1-P9</b> .....	19



## List of papers included in the thesis

### *HIV protease*

---

- P1. Cigler, P., Kozisek, M., **Rezacova, P.**, Brynda, J., Otwinowski, Z., Pokorna, J., Plesek, J., Gruner, B., Doleckova-Maresova, L., Masa, M., Sedlacek, J., Bodem, J., Krausslich, H. G., Kral, V. & Konvalinka, J. (2005) From nonpeptide toward noncarbon protease inhibitors: Metallacarboranes as specific and potent inhibitors of HIV protease, *Proc Natl Acad Sci USA*. **102**, 15394-15399.
- P2. Kožíšek, M., Cigler, P., Lepsik, M., Fanfrlik, J., **Rezacova, P.**, Brynda, J., Pokorna, J., Plesek, J., Gruner, B., Saskova, K. G., Vaclavikova, J., Kral, V. & Konvalinka, J. (2008) Inorganic polyhedral metallacarborane inhibitors of HIV protease: A new approach to overcoming antiviral resistance, *J Med Chem*. **51**, 4839-4843.
- P3. **Rezacova, P.**, Pokorna, J., Brynda, J., Kozisek, M., Cigler, P., Lepsik, M., Fanfrlik, J., Rezac, J., Saskova, K. G., Sieglova, I., Plesek, J., Sicha, V., Gruner, B., Oberwinkler, H., Sedlacek, J., Krausslich, H. G., Hobza, P., Kral, V. & Konvalinka, J. (2009) Design of HIV Protease Inhibitors Based on Inorganic Polyhedral Metallacarboranes, *J Med Chem*. **52**, 7132-7141.

### *Human carbonic anhydrases*

---

- P4. Mader, P., Brynda, J., Gitto, R., Agnello, S., Pachel, P., Supuran, C.T., Chimirri, A., **Rezacova P.** (2011) Structural basis for the interaction between carbonic anhydrase and 1,2,3,4-tetrahydroisoquinolin-2-ylsulfonamides. *J Med Chem*. **54**:2522-2526.
- P5. Brynda, J., Mader, P., Sicha, V., Fabry, M., Poncova, K., Bakardiev, M., Gruner, B., Cigler, P. & **Rezacova, P.** (2013) Carborane-based carbonic anhydrase inhibitors, *Angew Chem Int Edit*. **52**, 13760-13763.
- P6. Mader, P., Pecina, A., Cigler, P., Lepsik, M., Sicha, V., Hobza, P., Gruner, B., Fanfrlik, J., Brynda, J. & **Rezacova, P.** (2014) Carborane-based carbonic anhydrase inhibitors: Insight into CAII/CAIX specificity from a high-resolution crystal structure, modeling, and qQuantum chemical calculations, *Biomed Res Int*. **2014**, 389869.

### *Human 5'(3')-deoxynucleotidases*

---

- P7. Simak, O., Pachel, P., Fabry, M., Budesinsky, M., Jandusik, T., Hnizda, A., Sklenickova, R., Petrova, M., Veverka, V., **Rezacova, P.**, Brynda, J. & Rosenberg, I. (2014) Conformationally constrained nucleoside phosphonic acids - potent inhibitors of human mitochondrial and cytosolic 5'(3')-nucleotidases, *Org Biomol Chem*. **12**, 7971-7982.
- P8. Pachel, P., Simak, O., **Rezacova, P.**, Fabry, M., Budesinsky, M., Rosenberg, I. & Brynda, J. (2015) Structure-based design of a bisphosphonate 5'(3')-deoxyribonucleotidase inhibitor, *Medchemcomm*. **6**, 1635-1638.
- P9. Pachel, P., Simak, O., Buděšínský, M., Brynda, J., Rosenberg, I., & **Rezacova, P.** (2018) Structure-based optimization of bisphosphonate nucleoside inhibitors of human 5'(3')-deoxyribonucleotidases. *Eur J OrgChem* **2018**, 5144–5153

## Introduction

Structure-assisted ligand design, a method used as an alternative to screening random compounds, is the process of identifying new drugs through rational design of molecules based on knowledge of the structure of their biological target (Madsen *et al.*, 2002, Anderson *et al.*, 2015, Macalino *et al.*, 2015). Structural information is obtained through experimental methods such as X-ray crystallography and NMR spectroscopy, or through homology modeling.

Enzymes involved in pathologies are good targets for rational design. Enzymes usually have a well-defined active site to bind substrates, and many have allosteric sites that bind regulators. These sites can be targeted by small molecules that mimic the structure of the substrate or regulator. Knowledge of the 3D structure of the enzyme, especially in complex with its natural ligand, is beneficial to lead the design. During the iterative process of rational design, the structure of the ligand is progressively altered to maximize the shape and charge complementarity to the enzyme binding site (Figure 1). Design also can be guided to ensure that the ligand has little to no affinity towards other off-target enzymes to prevent undesirable side effects.

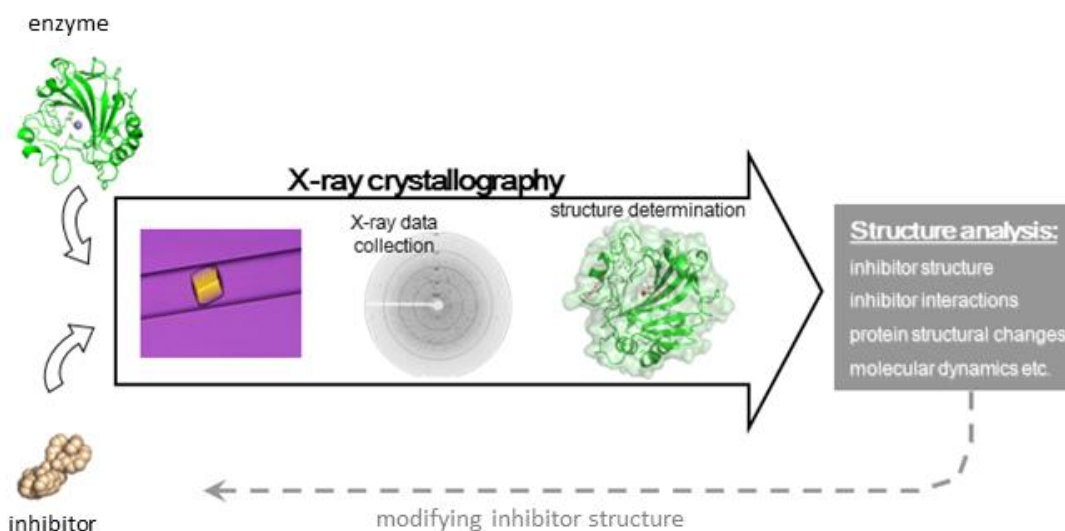


**Figure 1:** Schematic overview of structure-based drug design. The 3D structure of the enzyme-inhibitor complex is determined by X-ray crystallography and structural information is used to modify the inhibitor structure. This process proceeds in multiple cycles until the lead compound is optimized.

This habilitation thesis discusses nine selected publications by Pavlína Maloy Řezáčová to document her contributions to structure-assisted design of enzyme inhibitors that potentially may be further developed for treatment of human diseases. Her specific contributions to the published studies were X-ray crystallography analyses of enzyme-inhibitor complexes and subsequent structural analyses used in structure-guided drug design efforts.

Three papers (**P1-P3**) focus on design of human immunodeficiency virus protease (HIV PR) inhibitors, yielding potential novel drug candidates against drug-resistant HIV infections. Papers **P4-P6** document efforts in design of human carbonic anhydrase (CA) inhibitors, which may serve as potential anti-cancer drugs. Papers **P7-P9** deal with design of inhibitors targeting human deoxynucleotidases in an effort to overcome resistance to clinically used virostatics.

## Results

### Design of carborane inhibitors of HIV protease

The aspartic protease of HIV is responsible for cleavage of viral polyprotein precursors into mature, functional viral structural proteins and enzymes. This process, called viral maturation, leads to the final morphological rearrangements and is indispensable for production of infectious viral particles (Kohl *et al.*, 1988).

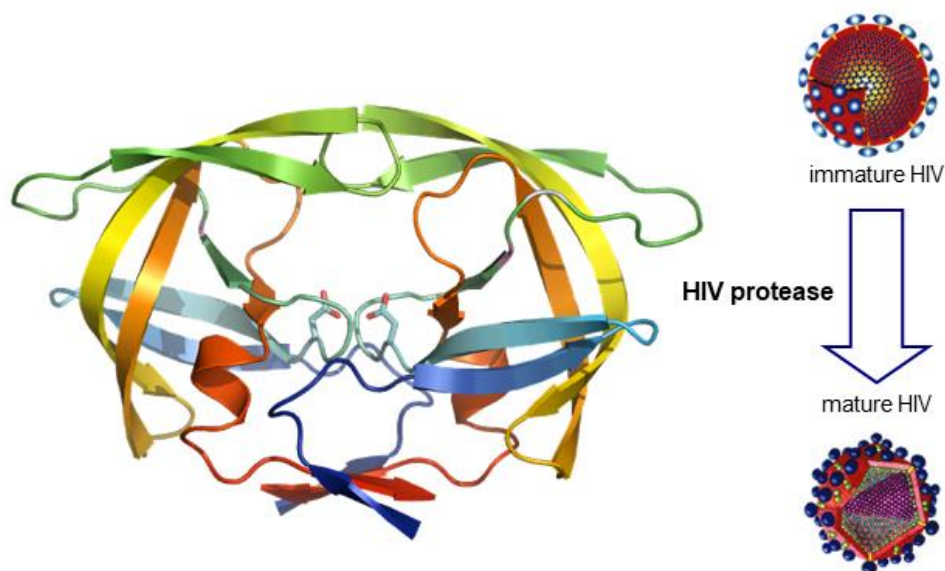


**Figure 2:** Schematic of the role of HIV PR in the viral replication cycle (right) and crystal structure of HIV PR (left, PDB code 4LL3, Kožíšek *et al.*, 2014).

Due to its essential role in the viral replication cycle, HIV PR is one of the primary targets for anti-HIV drug design. Since the first protease inhibitor (PI) was introduced in 1996, structure-based rational drug design has led to the development of hundreds of inhibitory compounds, ten of which are currently approved for clinical treatment of HIV infection. Their effectiveness, however, has been hampered by the emergence of drug-resistant HIV variants (Pokorná *et al.*, 2009). Development of new PIs effective against these resistant viruses will therefore be essential for the successful treatment of many HIV-positive patients.

During a search for unconventional chemical structures with inhibitory activity, we identified icosahedral metallocarboranes as selective inhibitors of HIV PR, as reported in **P1** (Cigler *et al.*, 2005). Screening identified these inorganic compounds, which inhibit HIV PR with  $K_i$  values in the nanomolar range (Table 1), as a novel class of non-peptidic PIs with an unknown inhibition mechanism.

**Table 1:** Inhibition of wild-type HIV PR and a PI-resistant variant.

Compound <sup>a</sup>	K <sub>i</sub> (HIV PR) <sup>b</sup>	K <sub>i</sub> (HIV PR <sup>RES</sup> ) <sup>c</sup>
GB-18	66 nM <sup>b</sup>	210 nM <sup>b</sup>
GB-80	4.9 nM <sup>b</sup>	13 nM <sup>b</sup>

<sup>a</sup> see Figure 3 for chemical structures, <sup>b</sup> reported in Kožíšek et al., 2008,

<sup>c</sup> HIV PR selected under the pressure of clinically available PIs and isolated from an HIV-positive patient receiving highly active antiretroviral therapy. HIV PR<sup>RES</sup> contains substitutions: L10I/L24I/L33F/M46L/I54V/L63P/A71V/V82A/I84V

Carboranes, icosahedral clusters containing boron, carbon, and hydrogen, are bulky pharmacophores used to replace various hydrophobic structures in biologically active molecules (Grimes, 2011, Lesnikowski, 2007). They are an abiotic species that are very stable towards catabolism and degradation by enzymes and thus the use of boron clusters as components of new pharmacological agents has been increasing, recently.

To decipher the mechanism of inhibition, we determined the three-dimensional crystal structure of HIV PR in complex with the lead metallacarborane compound (GB-18, PDB code 1ZTZ). The crystal structure revealed a unique binding mode that differs from that of all other HIV PIs. Two bis(dicarbollide) clusters bind in the HIV PR active site, but do not interact with the catalytic residues. Rather, the clusters interact with hydrophobic pockets in the flap-proximal region of the HIV PR active site (Figure 3A). This crystal structure was indispensable for understanding the mode of action of this class of compounds, and the structural information was used in modeling studies and subsequent structure-based design of other metallacarborane inhibitors.

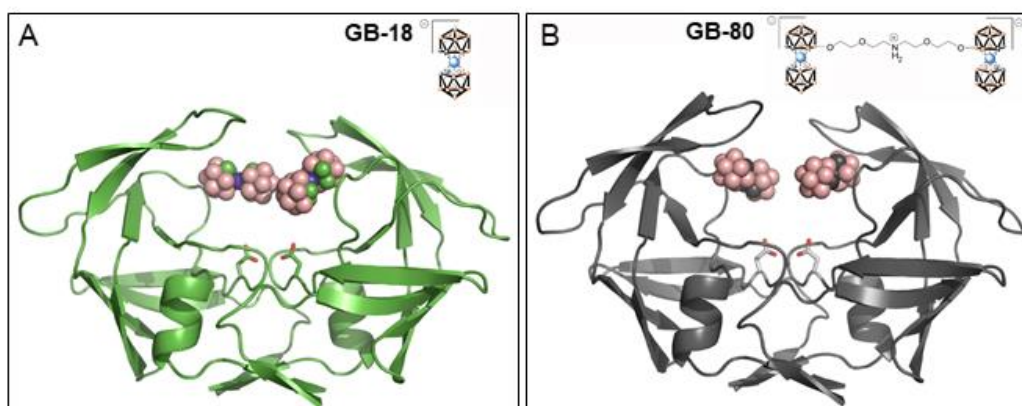


**Figure 3:** Crystal structures of HIV PR in complex with metallacarborane inhibitors.

**A.** The complex with GB-18 (PDB code 1ZTZ) shows binding of two inhibitor molecules to the flap-proximal region of each HIV PR monomer. **B.** The complex with GB-80 (PDB code 3I8W) shows binding of one inhibitor molecule to the flap-proximal region of each HIV PR monomer. The linker connecting the two cages was disordered and could not be modelled into electron density maps.

We next confirmed the activity of metallacarborane compounds against drug-resistant HIV PR variants and used the crystal structure for molecular modeling experiments to explain the inhibition profile of metallacarborane compounds, as reported in **P2** (Kožíšek *et al.*, 2008). We found that metallacarboranes bind HIV PR pockets *via* unconventional proton-hydride hydrogen bonds (dihydrogen bonds) and that they are able to adjust the position of the metallacarborane cluster within the HIV PR substrate-binding cleft. Thanks to these features, metallacarborane compounds are able to inhibit PI-resistant HIV PR variants containing mutations in the inhibitor-binding pockets (Table 1).

Using the structural information from the GB-18 complex, we designed a second series of compounds in which two cobalt bis(dicarbollide) clusters were connected *via* linkers of various lengths and properties. As discussed in **P3** (Rezacova *et al.*, 2009), we explored the inhibitory properties of these compounds, determined the crystal structure of HIV PR with one compound (GB-80), and computationally explored the conformational space of the linker. The crystal structure of GB-80 in complex with HIV PR (PDB code 3I8W) revealed a slightly different positioning of the cluster in the HIV PR binding pocket compared to that of GB-18 (Figure 3B). This finding was consistent with results from modeling studies with resistant HIV PR variants reported in **P2** (Kožíšek *et al.*, 2008), which predicted the flexibility of cluster positioning within the active site.

Overall, our results established linker-substituted, dual-cage cobalt bis(dicarbollides) as lead compounds for the design of more potent inhibitors of HIV PR, including resistant variants.

## Design of carborane inhibitors of human carbonic anhydrases

Human CAs are metalloenzymes with important roles in various physiological and pathological processes (e.g., tumorigenicity, obesity, and epilepsy). There are 14 CA isoforms in humans, several of which are established diagnostic and therapeutic targets (Supuran, 2008). In particular, there is significant interest in the development of selective inhibitors targeting CA isoform IX (CAIX). CAIX is a tumor-associated transmembrane isoenzyme, the overexpression of which is induced by hypoxia. CAIX serves as a tumor marker and as a prognostic factor for several human cancers and thus represents a valuable target for antitumor therapy (Swietach *et al.*, 2009).

Design of a novel generation of selective inhibitors is the current challenge in the development of new therapeutic agents able to inhibit specific CA isoenzymes. Currently used CA inhibitors lack selectivity and cause numerous unwanted side effects. Conventional CA inhibitors contain a sulfonamide, sulfamate or sulfamide group connected to an organic moiety usually composed of an aromatic ring or conjugated ring system. In our structure-assisted design of CA inhibitors, we focused on designing inhibitors containing substituted boron clusters instead of the organic ring system.

The idea to use boron clusters and the first compound design were conceived from the analysis of X-ray structures of CAII in complex with isoquinoline-based inhibitors that we reported in **P4** (PDB codes 3IGP and 3PO6, Mader *et al.*, 2011). Two related isoquinoline-based inhibitors inhibited CAIX with  $K_i$  values in the nanomolar range (Table 2, **1** and **2**). Crystal structures of the enzyme-inhibitor complexes revealed two different binding modes within the active site of CAII and engagement of two opposite sides of the active site cavity (Figure 4A). Following this analysis, we hypothesized that the binding space within the enzyme active site cavity could be effectively filled by an inhibitor bearing a three-dimensional, hydrophobic scaffold.

**Table 2:** Inhibition of selected carbonic anhydrase isozymes.

Compound <sup>a</sup>	$K_i$ (CAII)	$K_i$ (CAIX)
<b>1</b>	94.5 nM <sup>b</sup>	9.5 nM <sup>b</sup>
<b>2</b>	87.3 nM <sup>b</sup>	6.4 nM <sup>b</sup>
<b>3</b>	0.7 $\mu$ M <sup>c</sup>	0.38 $\mu$ M <sup>c</sup>

<sup>a</sup> see Figure 4 for chemical structures, <sup>b</sup> reported in Mader *et al.*, 2011, <sup>c</sup> reported in Brynda *et al.*, 2013.

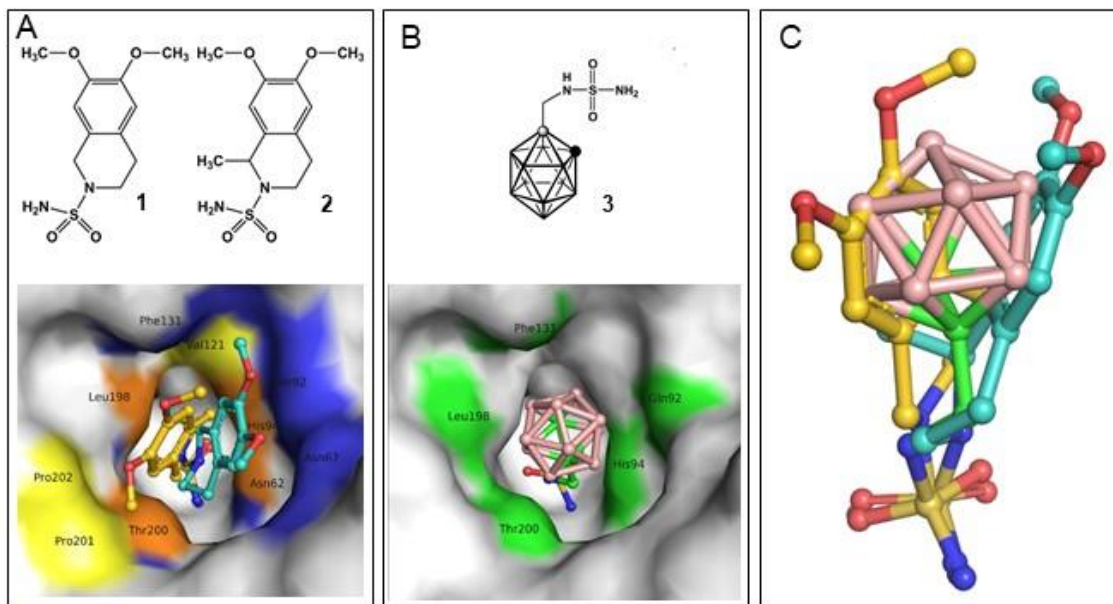


**Figure 4:** Structure-inspired design of carborane inhibitors of human CAII.

**A.** Structural formulas of two isoquinoline-based compounds that inspired design of carborane sulfonamide inhibitors are shown along with a detailed overview of their binding to CAII (PDB codes 3IGP and 3PO6). The active site of CAII is shown in surface representation; residues interacting with **1** and **2** are colored yellow and blue, respectively. Residues interacting with both compounds are highlighted in orange. **B.** Structural formula of the lead carborane sulfonamide compound is shown along with its interactions with the CAII active site (PDB code 3MDG). **C.** Superposition of **1-3** as they bind to the CAII active site.

Using molecular docking, we designed a molecule containing a sulfamide group connected to a carborane cluster, as reported in **P5** (Brynda *et al.*, 2013). This molecule, 1-methylenesulfamide-1,2-dicarba-*closo*-dodecaborane (**3**, Figure 4B), inhibited CA activity with  $K_i$  values in the submicromolar range and showed nearly 2-times higher potency toward the tumor-associated isoform CAIX over the widespread CAII isoform. The crystal structure of CAII in complex with **3** determined at 1.3 Å resolution (PDB code 3MDG) confirmed binding to the enzyme active site in the predicted pose and revealed key interactions responsible for inhibitor binding and enzyme inhibition (Figure 4B). Subsequently, we designed and investigated a series of compounds containing *closo* and *nido* carborane clusters and further established that selectivity towards cancer-specific CAIX can be achieved.

In **P6** (Mader *et al.*, 2014), we presented the structure of CAII in complex with **3** refined to 1 Å atomic resolution (PDB code 4Q78) and described its use in molecular modeling experiments.



A virtual glycine scan revealed the contributions of individual residues to the energy of binding of **3** to CAII and CAIX.

These modeling results were further used to develop a series of more than 70 sulfamides incorporating carborane clusters. The lead compounds from this series inhibited CAIX with  $K_i$  values in the low nanomolar or subnanomolar range, with some inhibitors being more than 1000-fold more selective for tumor-specific CAIX than CAII present in normal tissue. The compounds demonstrated favorable *in vitro* toxicology and pharmacokinetics profiles and reduced tumor size in mice (unpublished results). This series of compounds became the subject of successful patent applications.

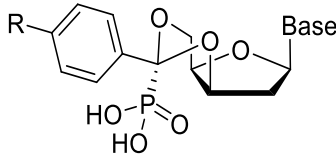
In summary, our contribution to the development of specific CAIX inhibitors was the design of novel and original inhibitors containing a sulfamide group connected to a carborane cluster that optimally fills the CA active site cavity.

## Design of inhibitors of human 5'(3')-deoxynucleotidases

Human 5'(3')-deoxynucleotidases catalyze the dephosphorylation of deoxyribonucleoside monophosphates to the corresponding deoxyribonucleosides and thus help maintain the balance between pools of nucleosides and nucleotides (Hunsucker *et al.*, 2005; Bianchi *et al.*, 1986). In addition to their physiological role, these enzymes also participate in deactivation of nucleoside analogues used as antiviral and anticancer agents, resulting in drug resistance. Human 5'(3')-deoxynucleotidases are thus targets for development of inhibitors that would protect nucleoside-based drugs in their active form as nucleotides (Mazzon *et al.*, 2003). Humans have two 5'(3')-deoxynucleotidases that share 61% sequence identity and differ in cellular localization: cytosolic cdN and mitochondrial mdN. The obvious challenge lies in designing inhibitors that can discriminate between the two highly similar enzymes.

As an initial approach described in P7 (Šimák *et al.*, 2014), we used (S)-1-[2-deoxy-3,5-O-(phosphonobenzylidene)-β-D-threo-pentofuranosyl]thymine (**1**, see Table 3) as a lead compound to design a series of compounds bearing various substituents in the *para* position of the benzylidene. A detailed kinetic study revealed that the presence of certain substituents increases inhibitory potency, and some substitutions induce a shift in selectivity toward cdN (Table 3).

**Table 3:** Inhibition of 5'(3')-deoxynucleotidase isoenzymes.

				
#	base	R	K <sub>i</sub> (cdN) <sup>a</sup>	K <sub>i</sub> (mdN) <sup>a</sup>
1	T	-H	610 μM	11.6 μM
2	T	-I	416 μM	2.71 μM
3	U	-I	115 μM	19.7 μM
4	T	-IO <sub>2</sub>	6.6 μM	5.9 μM
5	U	-IO <sub>2</sub>	12.1 μM	43 μM
6	T	-COOH	11.6 μM	7.9 μM
7	U	-COOH	10.9 μM	16.9 μM

<sup>a</sup> reported in Šimák *et al.*, 2014

X-ray structures of mdN in complex with inhibitors **2** and **6** provided evidence for the existence of two different binding orientations in the enzyme active site (Figure 5). Binding modes for cdN were investigated using NMR spectroscopy. We proposed that inhibitors selective for mdN preferentially bind to both the mitochondrial and cytosolic enzymes in the orientation represented by **2** (Figure 5B), while cdN-selective inhibitors favor an opposite orientation similar to that of **6** (Figure 5A).

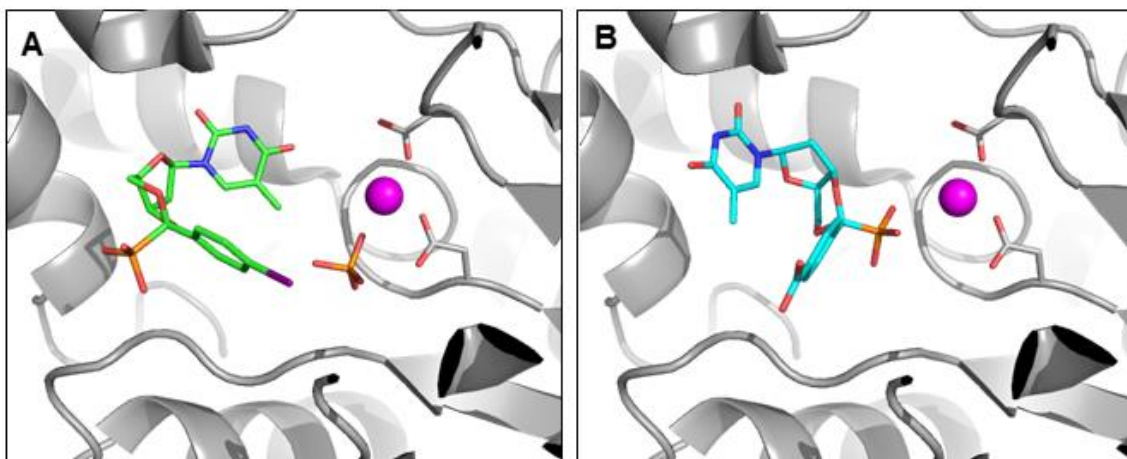


**Figure 5:** Structure-inspired design of 5'(3')-deoxynucleotidase inhibitors.

**A.** Crystal structure of **2** bound to mdN (PDB code 4L6C). Compound **2** is shown as sticks with green carbon atoms, and the active site magnesium ion is shown as a pink sphere along with coordinating catalytic aspartates. A phosphate ion originating from the crystallization solution is also bound in the active site. **B.** Crystal structure of **6** bound to mdN (PDB code 4MWO). Compound **6** is shown as sticks with green carbon atoms; the active site magnesium ion is shown as a pink sphere along with coordinating catalytic aspartates.

As a second approach to design specific mdN and cdN inhibitors, we modified the base moiety of lead compound **1** with a second phosphonate group. The results are described in **P8** and **P9** (Pachl *et al.*, 2015, Pachl *et al.*, 2018). Addition of the phosphonate group was intended to mimic the position of the phosphate ion found in crystal structures of mdN in complex with **1** and **2**. This phosphate ion, originating from the crystallization solution, interacts with the catalytic residues and magnesium ion and mimics the position of the substrate 3'-phosphate in the active site (Figure 6A). The distance between the methyl carbon at the C5 position of the thymine base in **1** and the oxygen atom of the phosphate is 3.0 Å (Figure 6A). Thus, we proposed attaching the phosphonate group to C5 of the thymine base *via* various linkers, giving rise to a series of bisphosphonate compounds (Figure 6B).

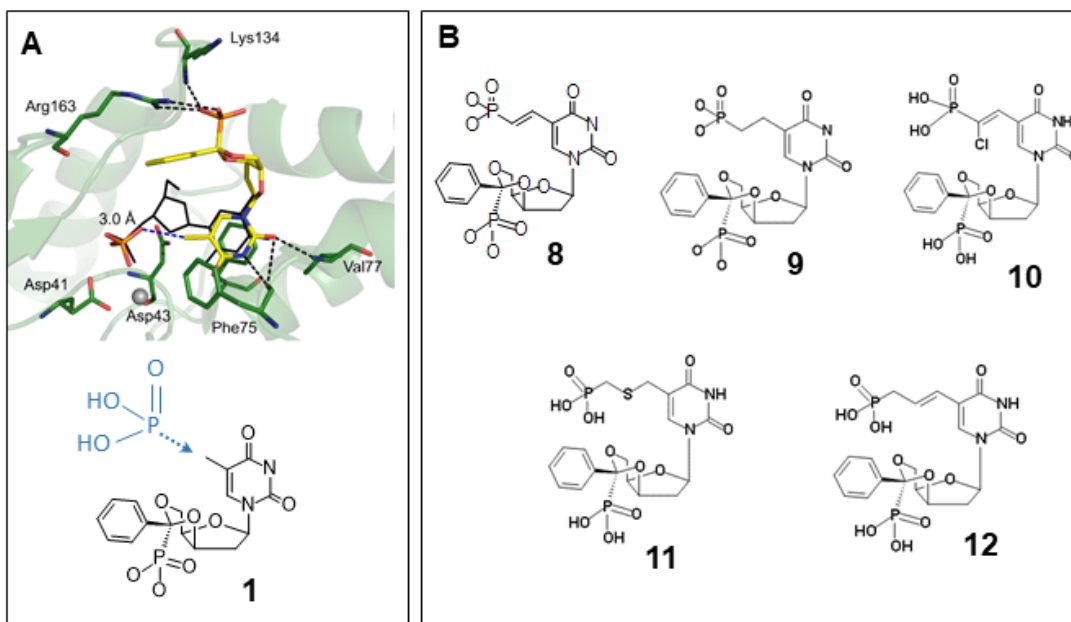


**Figure 6:** Structure-inspired design of bisphosphonate human 5'(3')-deoxynucleotidase inhibitors. **A.** Structure of mdN (green) in complex with **1** (yellow sticks, PDB code 1Q91) superimposed with the position of dTMP from its complex with an inactive mdN mutant (solid black lines, PDB code 1Z4L). The dashed blue line indicates the distance (3 Å) between the base methyl and the phosphate oxygen, which was used to design attachment of a second phosphonate group to the base. **B.** Bisphosphonate compounds designed to explore the optimal linker connecting the phosphonate to the base.

**Table 4:** Inhibition of 5'(3')-deoxynucleotidase isoenzymes.

# <sup>a</sup>	base	substituent	K <sub>i</sub> (cdN)	K <sub>i</sub> (mdN)
<b>1</b>	T		610 μM	11.6 μM
<b>8</b>	U	-(CH) <sub>2</sub> PO <sub>3</sub>	21.7 μM	128 nM
<b>9</b>	U	-(CH <sub>2</sub> ) <sub>2</sub> PO <sub>3</sub>	2.3 μM	27.7 nM
<b>10</b>	U	-CH=CClPO <sub>3</sub>	34.6 μM	310 nM
<b>11</b>	U	-CH <sub>2</sub> -S-CH <sub>2</sub> PO <sub>3</sub>	2.1 μM	68 nM
<b>12</b>	U	-(CH) <sub>2</sub> -CH <sub>2</sub> PO <sub>3</sub>	72 nM	15.1 nM

<sup>a</sup> see Figure 6 for compound structures

The addition of a second phosphonate group substantially improved the inhibitory properties and also increased selectivity towards cdN (Table 4). The strongest compound inhibited both enzymes at concentrations in the nanomolar range, making it the most potent inhibitor of these enzymes reported to date. In addition, some compounds showed selectivity for the cdN variant. Crystal structures solved for several inhibitors in complex with mdN or cdN (PDB codes 6G22, 6G2L, 6G2M, and 6G2N; Pahl et al., 2018) provided a structural basis for understanding the inhibition profile of bisphosphonate compounds.

In conclusion, we succeeded in rational design of conformationally constrained nucleoside phosphonic acid inhibitors of mitochondrial and cytosolic 5'(3')-nucleotidases. We obtained high-resolution structural information about the interactions of inhibitors with cdN and mdN and uncovered two possible binding modes. Structural information about interactions with the mdN and cdN active sites can be applied to future inhibitor design efforts.

## Summary and future perspective

This thesis describes the application of structure-based design principles to develop specific inhibitors of several enzymes involved in human pathologies, namely HIV PR, human CA and human deoxynucleotidases. X-ray structures, determined at high or even atomic resolution, were indispensable for this process. In all three projects included in this thesis, structural information led chemical design efforts to yield inhibitors with high affinity and high selectivity for certain enzyme isoforms.

Unconventional HIV PR inhibitors containing metallacarborane clusters were discovered to inhibit the wild-type enzyme as well as enzymes from patients with HIV resistant to clinically used drugs. This inhibitor class was first identified through random screening, and there was no information available about its inhibition mode. Our first crystal structure (PDB code 1ZTZ), reported in **P1** (Cigler *et al.*, 2005), revealed the binding of two hydrophobic clusters into a hydrophobic pocket in the enzyme active site. This structure was used in the molecular modeling experiments described in **P2** (Kožíšek *et al.*, 2008). Modeling showed that that mechanism of inhibition of resistant enzymes relies on adjustment of the cluster position in response to mutations in the PR binding pocket. Structural information was further used to design a second generation of compounds with two metallacarborane cages connected *via* a flexible linker, as discussed in **P3** (Rezacova *et al.*, 2009). A crystal structure (PDB code 3I8W) confirmed the predicted binding mode and provided structural information that could be used for subsequent design. Clinical development of metallacarborane HIV PR inhibitors, however, is hindered by their unfavorable pharmacokinetic properties. Although metallacarboranes can inhibit viral infectivity in tissue culture, these compounds are prone to aggregation and precipitation.

Carborane-containing molecules were also used in the design of inhibitors of human CAs, especially the cancer-specific isoform CAIX. Unlike the HIV PR inhibitors, in which the lead compound was identified through screening, our first CA inhibitor was the result of rational structure-assisted design. The design process was guided by the structural information reported in **P4** (Mader *et al.*, 2011). We observed that two related isoquinoline-based inhibitors bound within the active site of CAII in two different modes and engaged opposite sides of the active site cavity. This information was used to design compounds with a three-dimensional, space-filling cluster replacing the organic ring structure of the isoquinoline-based inhibitors. A compound containing a carborane cluster connected to a sulfonamide inhibited CAIX with  $K_i$  values in the submicromolar range and served as a lead molecule for design of the first carborane series described in **P5** (Brynda

*et al.*, 2013). Crystal structures of several carborane compounds bound to CAII were determined and used in molecular modeling studies (**P6**, Mader *et al.*, 2014) to uncover interactions important for binding to CAII and CAIX. Next, we designed a second-generation series of approximately 70 compounds. Preclinical tests showed favorable *in vitro* pharmacokinetics and pharmacodynamics and reduced tumor size in a mouse model. These compounds and their activity toward the cancer-specific CAIX isoform have been patented, and extensive preclinical trials are now in progress in collaboration with the Institute of Molecular and Translational Medicine in Olomouc.

The third project included in this habilitation thesis focused on design of inhibitors targeting human deoxynucleotidases to overcome resistance to clinically used virostatics. The compounds are derivatives of nucleoside phosphonic acids. Two approaches were applied to design specific inhibitors of the mitochondrial and cytosolic variants of the enzyme. The first inhibitor series, described in **P7** (Simak *et al.*, 2014), comprises compounds with various substituents on the benzaldehyde ring that have inhibition constants in the low micromolar range. Crystal structures led design in a new direction: attachment of a secondary phosphonic group that mimics the position of a phosphate ion repeatedly found in crystal structures to bind the active site along with inhibitory compounds. This second series of compounds (described in **P8** and **P9**, Pachel *et al.*, 2015, Pachel *et al.*, 2018) had  $K_i$  values in the low nanomolar range and showed selectivity for cdN or mdN. Crystal structures revealed that the specificity is determined by two alternative binding modes. However, compounds with phosphonic acid moieties generally have unfavorable pharmacokinetic properties. Prodrug compounds must be prepared to penetrate the cell membrane. We are currently working in this direction, with the aim of testing the effect of deoxynucleotidase inhibitors in cell culture experiments.

## References

- Anderson, A. C. *Drug Design Chemistry & Biology* (2003) **10**: 787–797.
- Bianchi, V., Pontis, E., Reichard, P. *Proc. Natl. Acad. Sci. U. S. A.* (1986) **83**, 986–990.
- Brynda, J., Mader, P., Sicha, V., Fabry, M., Poncova, K., Bakardiev, M., Gruner, B., Cigler, P., Rezacova, P. *Angew Chem Int Edit.* (2013) **52**, 13760-13763.
- Cigler, P., Kozisek, M., Rezacova, P., Brynda, J., Otwinowski, Z., Pokorna, J., Plesek, J., Gruner, B., Doleckova-Maresova, L., Masa, M., Sedlacek, J., Bodem, J., Krausslich, H. G., Kral, V., Konvalinka, J., *Proc Natl Acad Sci USA.* (2005) **102**, 15394-15399.
- Grimes, R. N., *Carboranes*, 2<sup>nd</sup> Ed., Academic Press Publications (Elsevier, Inc.), London-Amsterdam- Burlington- San Diego- Oxford, 2011 and references therein.
- Hunsucker, S. A., Mitchell, B. S.; Sychala, J. *Pharmacol. Ther.* (2005) **107**, 1–30.
- Lesnikowski, Z. J. *Collect. Czech. Chem. Commun.* (2007) **72**, 1646-1658.
- Macalino SJ, Gosu V, Hong S, Choi S I. *Arch Pharm Res.* (2015) **38**, 1686-701.
- Madsen U, Krogsgaard-Larsen P, Liljefors T (2002). Textbook of Drug Design and Discovery. Washington, DC: Taylor & Francis. ISBN 0-415-28288-8.
- Mader P., Brynda J., Gitto R., Agnello S., Pachel, P., Supuran C.T., Chimirri A., Rezacova P. *J Med Chem.* (2011) **54**:2522-2526.
- Mader, P., Pecina, A., Cigler, P., Lepsik, M., Sicha, V., Hobza, P., Gruner, B., Fanfrlik, J., Brynda, J. & Rezacova, P. *Biomed Res Int.* (2014) **2014**, 389869.
- Mazzon, C., Rampazzo, C., Scaini, M. C., Gallinaro, L., Karlsson, A., Meier, C., Balzarini, J., Reichard, P., Bianchi, V. *Biochem. Pharmacol.* (2003) **66**, 471–479.
- Kohl, N.E., Emini, E.A., Schleif, W.A., Davis, L.J., Heimbach, J.C., Dixon, R.A., Scolnick, E.M., Sigal, I.S. *Proc. Natl. Acad. Sci. U S A* (1988) **85**, 4686-4690.
- Kozisek, M., Cigler, P., Lepsik, M., Fanfrlik, J., Rezacova, P., Brynda, J., Pokorna, J., Plesek, J., Gruner, B., Saskova, K. G., Vaclavikova, J., Kral, V., Konvalinka, J. *J Med Chem.* (2008) **51**, 4839-4843.
- Kozisek, M., Lepsik, M., Saskova, K. G., Brynda, J., Konvalinka, J. & Rezacova, P. Thermodynamic and structural analysis of HIV protease resistance to darunavir - analysis of heavily mutated patient-derived HIV-1 proteases, *FEBS J.* (2014) **281**, 1834-1847.
- Pachel, P., Simak, O., Rezacova, P., Fabry, M., Budesinsky, M., Rosenberg, I., Brynda, J. *Medchemcomm.* (2015) **6**, 1635-1638.
- Pachel P., Šimák O., Buděšínský M., Brynda J., Rosenberg I., Rezacova, P. *Eur. J. Org. Chem.* (2018) **2018**, 5144–5153.
- Pokorná J., Machala L., Rezacova, P., Konvalinka J.: Current and Novel Inhibitors of HIV Protease. *Viruses* (2009), **1**: 1209-1239.
- Rezacova, P., Pokorna, J., Brynda, J., Kozisek, M., Cigler, P., Lepsik, M., Fanfrlik, J., Rezac, J., Saskova, K. G., Sieglova, I., Plesek, J., Sicha, V., Gruner, B., Oberwinkler, H., Sedlacek, J., Krausslich, H. G., Hobza, P., Kral, V., Konvalinka, J. *J Med Chem.* (2009) **52**, 7132-7141.
- Simak, O., Pachel, P., Fabry, M., Budesinsky, M., Jandusik, T., Hnizda, A., Sklenickova, R., Petrova, M., Veverka, V., Rezacova, P., Brynda, J., Rosenberg, I. *Org Biomol Chem.* (2014) **12**, 7971-7982.
- Supuran, C. T. *Nat. Rev. Drug. Discov.* (2008) **7**, 168-181.
- Swietach, P., Patiar, S., Supuran, C. T., Harris, A. L., Vaughan-Jones, R. D. *J. Biol. Chem.* (2009) **284**, 20299-20310.



## Papers P1-P9

- P1. Cigler, P., Kozisek, M., **Rezacova, P.**, Brynda, J., Otwinowski, Z., Pokorna, J., Plesek, J., Gruner, B., Doleckova-Maresova, L., Masa, M., Sedlacek, J., Bodem, J., Krausslich, H. G., Kral, V. & Konvalinka, J. (2005) From nonpeptide toward noncarbon protease inhibitors: Metallacarboranes as specific and potent inhibitors of HIV protease, *Proc Natl Acad Sci USA*. **102**, 15394-15399.
- P2. Kožíšek, M., Cigler, P., Lepsik, M., Fanfrlik, J., **Rezacova, P.**, Brynda, J., Pokorna, J., Plesek, J., Gruner, B., Saskova, K. G., Vaclavikova, J., Kral, V. & Konvalinka, J. (2008) Inorganic polyhedral metallacarborane inhibitors of HIV protease: A new approach to overcoming antiviral resistance, *J Med Chem*. **51**, 4839-4843.
- P3. **Rezacova, P.**, Pokorna, J., Brynda, J., Kozisek, M., Cigler, P., Lepsik, M., Fanfrlik, J., Rezac, J., Saskova, K. G., Sieglöva, I., Plesek, J., Sicha, V., Gruner, B., Oberwinkler, H., Sedlacek, J., Krausslich, H. G., Hobza, P., Kral, V. & Konvalinka, J. (2009) Design of HIV Protease Inhibitors Based on Inorganic Polyhedral Metallacarboranes, *J Med Chem*. **52**, 7132-7141.
- P4. Mader, P., Brynda, J., Gitto, R., Agnello, S., Pachel, P., Supuran, C.T., Chimirri, A., **Rezacova P.** (2011) Structural basis for the interaction between carbonic anhydrase and 1,2,3,4-tetrahydroisoquinolin-2-ylsulfonamides. *J Med Chem*. **54**:2522-2526.
- P5. Brynda, J., Mader, P., Sicha, V., Fabry, M., Poncova, K., Bakardiev, M., Gruner, B., Cigler, P. & **Rezacova, P.** (2013) Carborane-based carbonic anhydrase inhibitors, *Angew Chem Int Edit*. **52**, 13760-13763.
- P6. Mader, P., Pecina, A., Cigler, P., Lepsik, M., Sicha, V., Hobza, P., Gruner, B., Fanfrlik, J., Brynda, J. & **Rezacova, P.** (2014) Carborane-based carbonic anhydrase inhibitors: Insight into CAII/CAIX specificity from a high-resolution crystal structure, modeling, and qQuantum chemical calculations, *Biomed Res Int*. **2014**, 389869.
- P7. Simak, O., Pachel, P., Fabry, M., Budesinsky, M., Jandusik, T., Hnizda, A., Sklenickova, R., Petrova, M., Veverka, V., **Rezacova, P.**, Brynda, J. & Rosenberg, I. (2014) Conformationally constrained nucleoside phosphonic acids - potent inhibitors of human mitochondrial and cytosolic 5'(3')-nucleotidases, *Org Biomol Chem*. **12**, 7971-7982.
- P8. Pachel, P., Simak, O., **Rezacova, P.**, Fabry, M., Budesinsky, M., Rosenberg, I. & Brynda, J. (2015) Structure-based design of a bisphosphonate 5'(3')-deoxyribonucleotidase inhibitor, *Medchemcomm*. **6**, 1635-1638.
- P9. Pachel P., Simak, O., Buděšínský M., Brynda J., Rosenberg I., & **Rezacova, P.** (2018) Structure-based optimization of bisphosphonate nucleoside inhibitors of human 5'(3')-deoxyribonucleotidases. *Eur J OrgChem* **2018**, 5144–5153

# From nonpeptide toward noncarbon protease inhibitors: Metallacarboranes as specific and potent inhibitors of HIV protease

Petr Cígler<sup>\*,†,‡</sup>, Milan Kožiček<sup>\*,§</sup>, Pavlína Řezáčová<sup>\*,§¶</sup>, Jiří Brynda<sup>§</sup>, Zbyszek Otwinowski<sup>¶</sup>, Jana Pokorná<sup>\*</sup>, Jaromír Plešek<sup>¶</sup>, Bohumír Grüner<sup>¶</sup>, Lucie Dolečková-Marešová<sup>\*</sup>, Martin Máša<sup>\*</sup>, Juraj Sedláček<sup>§</sup>, Jochen Bodem<sup>\*\*</sup>, Hans-Georg Kräusslich<sup>\*\*</sup>, Vladimír Král<sup>†,¶</sup>, and Jan Konvalinka<sup>\*,†,§¶</sup>

Institutes of <sup>\*</sup>Organic Chemistry and Biochemistry and <sup>§</sup>Molecular Genetics, Academy of Sciences of the Czech Republic, Flemingovo náměstí 2, 166 10 Prague 6, Czech Republic; <sup>†</sup>Department of Analytical Chemistry, Institute of Chemical Technology, Technická 5, 166 28 Prague 6, Czech Republic; <sup>¶</sup>Department of Biochemistry, University of Texas Southwestern Medical Center, 5323 Harry Hines Boulevard, Dallas, TX 75390-8816; <sup>||</sup>Institute of Inorganic Chemistry, Academy of Sciences of the Czech Republic, Area of Research Institutes 1001, 250 68 Husinec-Rez near Prague, Czech Republic; <sup>\*\*</sup>Department of Virology, University of Heidelberg, Im Neuenheimer Feld 324, D-69120 Heidelberg, Germany; and <sup>‡‡</sup>Department of Biochemistry, Faculty of Natural Science, Charles University, Hlavova 2030, Prague 2, 128 43 Czech Republic

Communicated by Josef Michl, University of Colorado, Boulder, CO, August 31, 2005 (received for review June 2, 2005)

HIV protease (PR) represents a prime target for rational drug design, and protease inhibitors (PI) are powerful antiviral drugs. Most of the current PIs are pseudopeptide compounds with limited bioavailability and stability, and their use is compromised by high costs, side effects, and development of resistant strains. In our search for novel PI structures, we have identified a group of inorganic compounds, icosahedral metallacarboranes, as candidates for a novel class of nonpeptidic PIs. Here, we report the potent, specific, and selective competitive inhibition of HIV PR by substituted metallacarboranes. The most active compound, sodium hydrogen butylimino bis-8,8-[5-(3-oxa-pentoxo)-3-cobalt bis(1,2-dicarbollide)]di-ate, exhibited a  $K_i$  value of 2.2 nM and a submicromolar  $EC_{50}$  in antiviral tests, showed no toxicity in tissue culture, weakly inhibited human cathepsin D and pepsin, and was inactive against trypsin, papain, and amylase. The structure of the parent cobalt bis(1,2-dicarbollide) in complex with HIV PR was determined at 2.15 Å resolution by protein crystallography and represents the first carborane–protein complex structure determined. It shows the following mode of PR inhibition: two molecules of the parent compound bind to the hydrophobic pockets in the flap-proximal region of the S3 and S3' subsites of PR. We suggest, therefore, that these compounds block flap closure in addition to filling the corresponding binding pockets as conventional PIs. This type of binding and inhibition, chemical and biological stability, low toxicity, and the possibility to introduce various modifications make boron clusters attractive pharmacophores for potent and specific enzyme inhibition.

rational drug design | aspartic proteases | carboranes | x-ray structure analysis | virostatics

HIV protease (PR) is responsible for cleaving viral polyprotein precursors into mature, functional viral enzymes and structural proteins. This process, called viral maturation, is required for the progeny virion to become replication competent and infectious. Chemical inhibition or inactivation by mutation of PR blocks the infectivity of the virus (1). PR has thus become a prime target for therapeutic intervention in AIDS. Academic and industrial research has led to the rapid development of eight effective inhibitors that are currently in clinical use, with several others still in the pipeline (for review, see refs. 2 and 3).

Despite the considerable success of rational drug design, the need for effective PR inhibitors (PIs) is still urgent. Most of the current PIs are pseudopeptide compounds with limited bioavailability and stability. Moreover, their clinical use is compromised by high production cost, various side effects, and rapid development of resistant viral strains (4). Therefore, there is a continuing need for

the design of new PIs with an emphasis on broad specificity against PI-resistant HIV mutants (5, 6).

Molecular modeling and/or random testing of compound libraries revealed several PR inhibitors with unexpected structures. Most of the first-generation PIs were pseudopeptides. Some recent compounds involve nonpeptidic structures, such as cyclic ureas, sulfonamides, etc. (2). However, even inorganic compounds, Nb-containing polyoxometalates, specifically inhibit HIV PR with submicromolar  $EC_{50}$  values in tissue cultures (7). In this case, the inhibitors were shown to be noncompetitive, and a model suggested binding to the cationic pocket on the outer surface of the flaps. There is also an evidence for compounds with unexpected chemistry capable to target the active site of the enzyme. The HIV PR-binding cleft was shown to accommodate  $C_{60}$  fullerenes, hydrophobic and electrophilic spheric compounds, and some fullerene derivatives are indeed weak inhibitors of HIV PR (8–11).

We searched for other types of unconventional chemical structures that would fit into the PR-binding cleft, would be biologically stable, and would enable facile chemical modification. When screening a number of structural motifs, we identified a group of inorganic compounds, icosahedral boranes, carboranes, and namely 12-vertex metal bis(dicarbollides), as promising frameworks for a novel class of nonpeptide PIs. These boron/carbon clusters are polyhedra based on a three-dimensional skeleton with triangular facets.

Boron-containing polyhedral compounds have been intensively studied because of their use in boron neutron capture therapy (12) and in radioimaging (13, 14). From the structural point of view, the variety of known structural types of boranes, heteroboranes, and metallaboranes represents an interesting counterpart to organic compounds, especially to aromates. With the icosahedral cage being only slightly larger than the phenyl ring rotation envelope, carboranes were used as stable hydrophobic pharmacophores (e.g., refs. 15–17). There is little information on the use of carboranes as

Freely available online through the PNAS open access option.

Abbreviations: MIA, mouse intracisternal A particles; PR, protease; PI, HIV PR inhibitor; PDB, Protein Data Bank.

Data deposition: The atomic coordinates and structure factors have been deposited in the Protein Data Bank, [www.rcsb.org/pdb](http://www.rcsb.org/pdb) (PDB ID code 1ZTZ).

<sup>†</sup>P.C., M.K., and P.Ř. contributed equally to this work.

<sup>††</sup>To whom correspondence may be addressed at: Department of Analytical Chemistry, Institute of Chemical Technology, Technická 5, 166 28 Prague 6, Czech Republic. E-mail: [vladimir.kral@vscht.cz](mailto:vladimir.kral@vscht.cz).

<sup>§§</sup>To whom correspondence may be addressed at: Institute of Organic Chemistry and Biochemistry, Academy of Sciences of the Czech Republic, Flemingovo nám. 2, 166 10 Prague 6, Czech Republic. E-mail: [konval@uochb.cas.cz](mailto:konval@uochb.cas.cz).

© 2005 by The National Academy of Sciences of the USA

**Table 1. Structures and activities of metallacarborane inhibitors**

Compound no.	Structure	Molecular weight of anion	$K_i$ , nM	$EC_{50}$ , $\mu$ M
1		323.74	$66 \pm 30$	6
2		339.74	$6,800 \pm 500$	20
3		427.85	$2,500 \pm 400$	6
4		624.09	$20 \pm 5$	13
5		837.71	$4.9 \pm 2.1$	3
6		893.82	$2.2 \pm 1.2$	0.25

All compounds were prepared as their sodium salts. Color coding: orange, BH groups; black, CH groups; blue, Co atom. For details see *Materials and Methods*.

enzyme inhibitors. Few examples reported in the literature involve benzolactams bearing dicarba-*closo*-dodecaborane (16, 18) or carborane substitution of the phenyl ring in the phenyl-phthalimidoimid, yielding a tumor necrosis factor- $\alpha$  modulator with the activity comparable with the parental compound (19). Porphyrins substituted with dicarba-*closo*-dodecaboranes were found as inhibitors of HIV PR, with  $IC_{50}$  in the submicromolar range (20).

Our main attention has been focused on ionic metal bis(dicarborollides) that consist of two dicarborollide subclusters sandwiching the central metal atom. In metal bis(dicarborollides), the equal 11-vertex dicarborollide subclusters are connected by a *commo* metal vertex, forming two 12-vertex metal dicarborollide subclusters. These *closo* 26-electron compounds with “peanut-like 12-vertex geometry” were described as early as 1965 by Hawthorne *et al.* (21) and thus form basic stones in metallacarborane chemistry.

Among other transition metal metallacarboranes (22), cobalt bis(1,2-dicarborollide) ion (23) shows certain unique features: synthetic availability, wide possibilities of *exo*-skeletal modifications, high stability, charge delocalization, low nucleophilicity, strong acidity of conjugated acids, and high hydrophobicity. These properties are reflected in unique solution properties and ion-pairing behavior of this ion, which in turn led to its known applications in extraction chemistry (24, 25) and in the development of lowest coordinating anions (26) and compounds for radioimaging (14). However, the metal bis(dicarborollides) have never been considered as biologically active compounds or pharmacophores.

In this article, we report the potent, specific, and selective inhibition of HIV PR by parental and substituted metallacarbo-

ranes, namely cobalt bis(1,2-dicarborollides). We provide evidence for the mechanism of action of these compounds, show their antiviral activity in tissue cultures, analyze their binding toward the enzyme by x-ray crystallography, and show the potential of this class of compounds to become a novel pharmacophore for enzyme inhibition.

## Materials and Methods

**Chemical Syntheses.** Compound 1 (Table 1) was converted to

**Table 2. Data collection and refinement statistics for crystallographic structure determination**

Space group	C2
Unit cell	$a = 85.3 \text{ \AA}$ , $b = 67.2 \text{ \AA}$ , $c = 42.5 \text{ \AA}$ , $\beta = 95.0^\circ$
Data collection resolution, $\text{\AA}$	52.7–2.14
Completeness, %	99.2 (99.2)*
Average $I/\sigma(I)$	9.3 (3.0)*
$R_{\text{merge}}$ , <sup>†</sup> %	5.6 (22.8)*
Refinement resolution, $\text{\AA}$	30–2.15
$R$ factor <sup>‡</sup> / $R_{\text{free}}$ factor, <sup>§</sup> %	17.59/23.25
No. of atoms (protein/water/others)	1,535/202/46
rms deviation bond length/angles, $\text{\AA}/^\circ$	0.009/1.92

\*Values in parentheses refer to the highest resolution shell 2.19–2.14.

<sup>†</sup> $R_{\text{merge}} = \sum_{hkl} |I - \langle I \rangle| / \sum_{hkl} I$ .

<sup>‡</sup> $R = \sum |F_{\text{calc}} - F_{\text{obs}}| / \sum |F_{\text{obs}}|$ .

<sup>§</sup>The  $R_{\text{free}}$  as defined in ref. 45 was calculated for 5% of reflections.

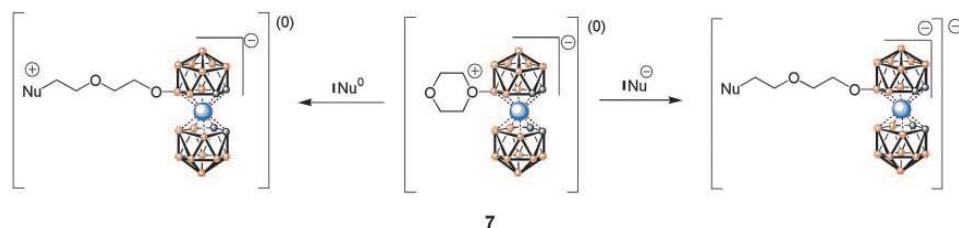


**Fig. 1.** Ring opening reaction of 8-dioxane-3-cobalt bis(1,2-dicarbollide) **7** by different nucleophiles  $\text{Nu}^0$  (e.g.,  $\text{NH}_3$ ) and  $\text{Nu}^-$  (e.g.,  $\text{RO}^-$ ) yielding zwitterionic and anionic compounds, respectively.

sodium salt from the commercially available cesium salt (Katchem, Rez u Prahy, Czech Republic) by using the extraction procedure described in ref. 27. Compound **2** was obtained by direct hydroxylation of **1** by using warm diluted sulfuric acid according to procedures in ref. 28. The starting dioxanate intermediate was prepared as described in ref. 29. The synthesis of compounds **3–6** is described in *Supporting Materials and Methods*, which is published as supporting information on the PNAS web site.

**Enzymes.** The expression, refolding, and purification of HIV-1 PR, HIV-2 PR, and the HIV-1 PR variant (Q7K, L33I, L63I) bearing three mutations that minimize the autoproteolytic cleavage (30) were performed as described (31). PRs from mouse intracisternal A particles (MIA14 PR) (32), human cathepsin D, and pepsin were prepared as described (33, 34). Porcine  $\alpha$ -amylase, bovine trypsin, and papain were purchased from Sigma.

**Inhibition Assays. Inhibition of HIV PRs.** The  $\text{IC}_{50}$  and  $K_i$  values were determined by spectrophotometric assay with the chromogenic substrate KARVNleNphEANle-NH<sub>2</sub> as described (31). The inhibition constants were estimated by using a competitive inhibition equation according to ref. 35. The mechanisms of inhibition were derived from initial reaction rates versus concentrations of substrate in the presence of various concentrations of inhibitor by using a Lineweaver–Burk plot.

**Inhibition of MIA14 protease.** A spectrophotometric assay was used to determine inhibition characteristics by using chromogenic substrate DSAYNphVVS as described (32).

**Inhibition of human cathepsin, pepsin, trypsin, papain, and  $\alpha$ -amylase.** For experimental details, see *Supporting Materials and Methods*.

**Testing of Antiviral Activities in Tissue Cultures.** Antiviral activity was analyzed by using PM-1 cells infected with HIV-1 strain NL4-3 modified from a published procedure (36). PM-1 cells were infected

by coculture and washed 4 h after infection, and compounds **1–6** or the solvent DMSO, respectively, was added after the wash. Newly produced virus was harvested at 48 h postinfection and cleared by brief centrifugation, and infectious titer was determined on TZM cells, which express  $\beta$ -galactosidase from a Tat-responsive promoter. Viral titers and standard deviations are derived from three independent experiments.

**Crystallization, Data Collection, and Structure Solution.** The complex for crystallization was prepared by mixing HIV-1 PR (Q7K, L33I, L63I) with 3.7-fold molar excess of compound **1** dissolved in DMSO and concentrated by ultrafiltration to final concentration of 7.5 mg/ml. The crystals were grown by hanging drop vapor diffusion technique at 19°C by using 0.1 M Tris-HCl (pH 8.5) and 2.0 M ammonium dihydrogen phosphate as the precipitating solution. Diffraction data were collected at 100 K by using synchrotron radiation of wavelength 0.8 Å [X13 beamline, Deutsches Elektronen-Synchrotron (DESY) Hamburg, Germany] and were processed by using the HKL 2000 software package (37). The HIV PR structure was solved by molecular replacement by using protein coordinates from Protein Data Bank (PDB) structure 1NH0 (38). The structure solution and refinement were performed by using the CCP4 program suite.

Crystal parameters and data collection statistics are summarized in Table 2. Atomic coordinates and structure factors have been deposited to PDB: code 1ZTZ. The details of structure determination are found in Table 4, which is published as supporting information on the PNAS web site.

## Results and Discussion

**Inhibitor Design and Synthesis.** Most of the HIV PIs currently used in clinics are pseudopeptide or peptide mimetics based on a limited number of structural building blocks. Our intention was to identify novel core structures and thus expand chemical space available for

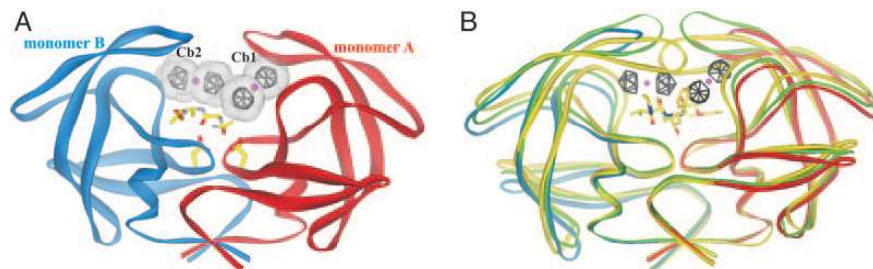


**Fig. 2.** X-ray structure analysis of the binding of compound **1** to HIV-PR. (A) Overall structure of the HIV-PR–compound **1** complex. The PR dimer is in ribbon representation with the two catalytic aspartates shown in sticks. Two compound **1** molecules are represented by their van der Waals surfaces and gray stick model, with cobalt ions shown as magenta spheres. Autoproteolytic peptide product is represented as stick model. (B) Superposition of PR–compound **1** complex with the free PR structure. Protease complex with lopinavir (PDB ID code 1MUI) is represented in yellow ribbons, lopinavir is shown as a stick model, free PR structure (PDB ID code 1HHP) is shown in green ribbons, and color coding for PR–compound **1** complex is the same as in A.



the development of PIs with novel qualities. We have identified 12-vertex metallocarborane clusters as suitable hydrophobic, stable, nontoxic structural analogues of aromatic compounds. In our initial tests, substituted metallocarboranes showed the most promising results.

Our synthetic approach started from easily accessible parent cobalt bis(dicarbollide) ion **1** to yield either 8-hydroxyderivative **2** (**28**) or the 8-dioxane-3-cobalt bis(1,2-dicarbollide) (**29**) reagent **7** (see Fig. 1). This reagent was then reacted under mild conditions, giving rise to a series of *exo*-skeletonally modified metallocarborane cluster anions **3–6** for testing. For synthesis of compounds **3–6**, ring cleavage reaction of **7** with *O*- and *N*-nucleophiles was used (see Fig. 1), thus producing ionic species if the ring opener is an anion, and betain-type zwitterions if the base is not charged.

The ring opening procedure of **7** zwitterion has already become a widely applicable method for attachment of the cobalt bis(dicarbollide) moiety to various organic substances (39–41). However, compounds **5** and **6** represent examples of zwitterionic-anionic structures containing two cobalt bis(1,2-dicarbollide) subunits bonded via flexible organic spacer chain.

**Inhibition Constants and Antiviral Activities.** Compounds **1–6** were tested as potential inhibitors of HIV PR *in vitro* and in tissue cultures. The corresponding inhibition constants ( $K_i$  values) and antiviral activities ( $EC_{50}$  values) are summarized in Table 1. All compounds exhibit classical competitive binding (data shown in *Supporting Materials and Methods* and Fig. 4, which is published as supporting information on the PNAS web site). This kinetic analysis suggests that tested cobalt bis(dicarbollide) competes with the peptide substrate and, therefore, binds to the active cleft of the enzyme. This suggestion has been confirmed by x-ray analysis of the complex of HIV PR with compound **1** (see below). Parent compound **1** shows tight inhibition *in vitro* and micromolar antiviral potency. Derivatization of compound **1** by hydroxyl and 2-(2-hydroxyethoxy) ethoxy groups yielded compounds **2** and **3**, exhibiting much weaker activity *in vitro* and comparable antiviral activities in tissue cultures. Simple visual inspection of the size of compounds **1–3** (Table 1) in comparison with the volume of the closed form of the HIV PR active cleft led to the notion that these compounds would not have sufficient contacts with the corresponding substrate-binding clefts. The solvent accessible area of compound **1** is more than two times lower when compared with a representative conventional pseudopeptide PI, lopinavir (LPV). However, the x-ray structure analysis solved this apparent contradiction, showing that two inhibitor units are needed for the efficient binding to the PR active cleft (see Figs. 2 and 3). Because the relative molecular weight of compound **1** is one of the lowest ever reported to inhibit HIV PR, it provides enough room for further improvement by means of structure-activity analyses, and therefore it was selected as the lead compound of our series of metallocarborane inhibitors of HIV PR.

Approximately a 100-fold improvement of the  $K_i$  value was achieved by enlarging the side chain of compound **3** in position 8 of the cage by the addition of a 1,2-diphenyl-2-hydroxy-ethoxy group, yielding compound **4** with 20 nM  $K_i$ . The binding of the compound was further improved four times by designing a symmetric compound **5** and, even further, by alkylating the secondary amino group with a butyl moiety (compound **6**), which represents the most active inhibitor of the compound series, with a  $K_i$  value of 2.2 nM and submicromolar antiviral activity in tissue culture. The mode of binding of this compound and its interaction with the enzyme-binding pockets could be inferred from the structure of the parent compound **1**.

It is striking that compound **6** showed an  $EC_{50}$  for inhibition of HIV-1 in tissue culture of 250 nM, which was  $\approx 10$ -fold better than that observed for the structurally very similar compound **5**. In contrast, the  $K_i$  value for PR inhibition *in vitro* exhibited only a 2-fold difference. This result indicates that subtle differences in

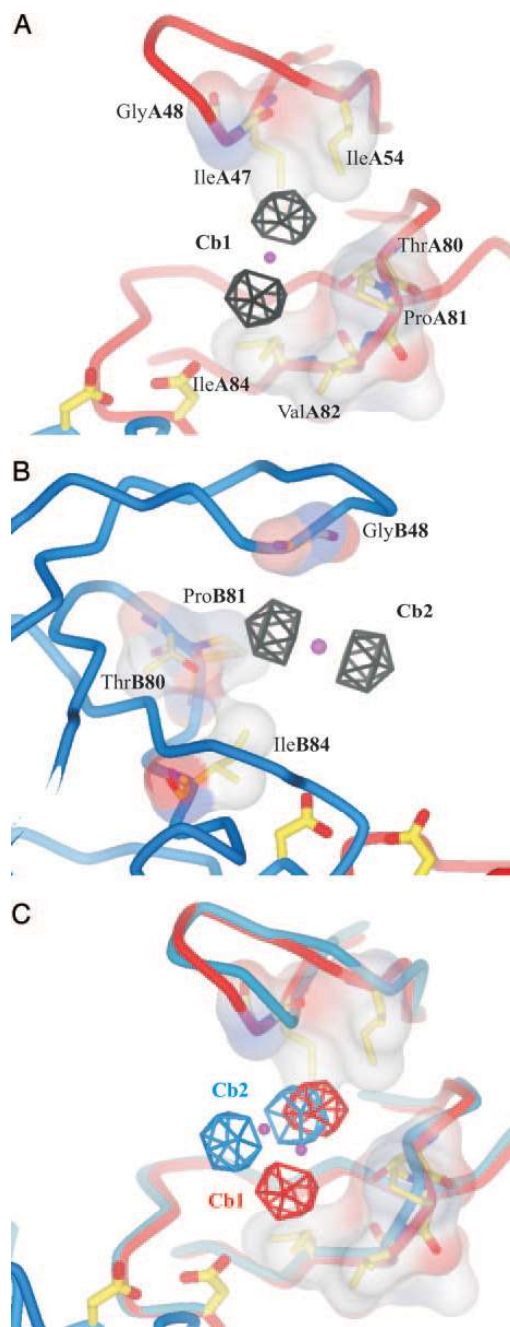


**Fig. 3.** Interactions of compound **1** with the amino acid residues in the corresponding PR-binding pocket. (A) Binding of compound **1** molecule Cb1 by PR monomer A (red tube). (B) Binding of compound **1** molecule Cb2 by PR monomer B (blue tube). Compound **1** is represented by a stick model in gray, with cobalt shown as a magenta sphere. PR residues in contact with compound **1** are represented by stick models, and their solvent-accessible surfaces are colored by atom charge (blue, positive; red, negative). (C) Superposition of the two compound **1**-binding modes. The color scheme and representation for PR is the same as in A and B, and atoms in compound **1** are colored with the color of the interacting PR chain.

**Table 3. The IC<sub>50</sub> values that demonstrate specificity and selectivity of individual compounds as analyzed with other retroviral PRs, representatives of aspartic, serine and cysteine PRs, and amylase**

Enzyme	Compound			
	1	4	5	6
WT HIV-1 PR	1.4 $\mu$ M (66 $\pm$ 30 nM)	0.13 $\mu$ M (20 $\pm$ 5 nM)	0.14 $\mu$ M (4.9 $\pm$ 2.1 nM)	0.10 $\mu$ M (2.2 $\pm$ 1.2 nM)
WT HIV-2 PR	1.5 $\mu$ M (220 $\pm$ 34 nM)	0.76 $\mu$ M (140 $\pm$ 8 nM)	0.35 $\mu$ M (110 $\pm$ 17 nM)	0.31 $\mu$ M (39 $\pm$ 1 nM)
MIA14 PR	1.0 $\mu$ M (85 $\pm$ 17 nM)	0.21 $\mu$ M (22 $\pm$ 7 nM)	0.63 $\mu$ M (60 $\pm$ 22 nM)	0.59 $\mu$ M (85 $\pm$ 4 nM)
Human cathepsin D	2.1 $\mu$ M (1,100 $\pm$ 100 nM)	1.3 $\mu$ M (670 $\pm$ 30 nM)	1.9 $\mu$ M (960 $\pm$ 30 nM)	0.50 $\mu$ M (250 $\pm$ 30 nM)
Pepsin	1.5 $\mu$ M (760 $\pm$ 90 nM)	0.86 $\mu$ M (430 $\pm$ 40 nM)	1.3 $\mu$ M (630 $\pm$ 160 nM)	0.73 $\mu$ M (360 $\pm$ 50 nM)
Trypsin	$\geq$ 50 $\mu$ M	$\geq$ 50 $\mu$ M	10 $\mu$ M (ND)	$\geq$ 50 $\mu$ M
Papain	$\geq$ 50 $\mu$ M	$\geq$ 50 $\mu$ M	46 $\mu$ M (ND)	$\geq$ 50 $\mu$ M
Amylase	$\geq$ 50 $\mu$ M	$\geq$ 50 $\mu$ M	3 $\mu$ M (ND)	17 $\mu$ M (ND)

The experimental error in the IC<sub>50</sub> determination is <10% of the given value. The inhibition constants  $K_i$  are shown in parentheses when applicable.

structure may lead to significant alterations in potency and suggests that further derivatization of this new group of PIs may significantly enhance their potential as antiretroviral drugs.

Analysis of the polyprotein processing by Western blotting shows a processing defect in the virus grown in the presence of active compounds (data not shown). No significant toxicity of tested compounds in tissue cultures was observed in the concentration range up to 50  $\mu$ M.

**Specificity and Selectivity Testing.** The selectivities of the lead compound **1** and the more potent compounds **4–6** were tested on a panel of seven enzymes, including PR from the highly homologous HIV-2 virus, PR from more distantly related retrovirus MIA 14, prototype human aspartic PRs cathepsin D and pepsin, serine PR trypsin, cysteine PR papain, and amylase as a representative of nonproteolytic enzymes with an anionic active-site cleft. The results are summarized in Table 3 in terms of IC<sub>50</sub> values; the corresponding  $K_i$  values are shown in parentheses when appropriate.

All tested compounds inhibit homologous HIV-2 PR and MIA PR, although less tightly, suggesting that they might be active against mutated resistant PR species selected under the pressure of clinically used PIs in HIV-positive patients. The activity of tested compounds toward cathepsin D and pepsin is two orders of a magnitude lower in terms of  $K_i$  when compared with HIV-1 PR. The tested compounds do not significantly inhibit any other enzyme analyzed.

**Crystal Structure of PR–Compound 1 Complex.** Structure of HIV PR–compound **1** complex was determined at 2.15 Å resolution with  $R$  factor of 17.6% and  $R_{\text{free}}$  of 23.6%. The final model comprises a PR dimer (chains A and B) with two molecules of compound **1** bound in the active site (labeled Cb1 and Cb2 in Fig. 2A). Because compound **1** is highly symmetrical in shape, it is not, however, possible to distinguish unambiguously the positions of carbons and borons in electron density maps at 2.15 Å resolution.

With the two molecules of compound **1** bound, the overall conformation of the PR is similar to the open conformation typical for free PR. Most of the structures of substrate-based active site inhibitor complexes exhibit flaps closed over the active site. However, the PR complexed with **1** can be superimposed with the unliganded PR structure [PDB ID code 1HHP (42)] with an rms deviation in  $\alpha$ -carbon positions of 0.99 Å (Fig. 2B). Flaps are obviously held in the open conformation by binding of the inhibitor molecules to the flap-proximal, “upper” part of the active site cleft

(Fig. 2). The structure thus provides evidence that the hitherto unexplored class of inhibitors shows an unexpected mode of inhibition. So far, the open conformation of flap was reported only for unliganded PR, whereas all inhibitor-bound structures of wild-type HIV PR show closed flap conformation. Here, we describe the structure of a complex of PR with a relatively potent inhibitor bound uniquely in the enzyme open form. Because the conformation of flap in PR is functionally very important, this finding might suggest that inhibition mechanism of these compounds is blocking the flap closure rather than filling the specific bonding pockets in the active site cleft.

Compound **1** is bound in the hydrophobic pockets formed by side-chains of PR residues Pro-81, Ile-84, and Val-82 and covered by flap residues Ile-47, Gly-48, and Ile-54 (Fig. 3). These pockets correspond approximately to S3 and S3' substrate-binding subsites. Although the inhibitor-binding site is identical in both monomers, the positions of the two compound **1** molecules are different (Fig. 3C). Inhibitor molecule Cb1 makes 21 van der Waals contacts with seven residues in monomer A (Fig. 3A) whereas inhibitor molecule Cb2 makes 12 van der Waals contacts with four monomer B residues (Fig. 3B). On average, 84% contacts are made with PR nonpolar atoms. The two Cb1 and Cb2 molecules contact each other with 3 van der Waals contacts. Compound **1** loses 89% of its total solvent-accessible surface upon complex formation, and good shape complementarity between both S3 and S3' PR subsites and compound **1** molecules is illustrated by an average gap volume index of 0.45. This result is slightly lower than an average value for enzyme–inhibitor complexes (43).

The PR compound **1** complex crystallized in C2 crystal form, unique among all 169 HIV PR structures deposited in PDB. In the crystal, symmetrically related PR complexes are oriented head-to-head by their active sites. As a result of this crystal packing, symmetrical flaps are in contact with each other and molecules of compound **1** are in contact with their symmetry mates, as well as with flaps belonging to neighboring symmetry molecule. Thus, in addition to the above described contacts, interactions of compound **1** with PR based on crystal contacts can be observed with residues Gly-48, Gly-49, Ile-50, and Phe-53. However, formation of these interactions in solution seems unlikely because assembly of a complex consisting of two PR dimers and four inhibitor molecules is highly improbable.

Five of the PR residues that are in contact with compound **1** are often mutated in drug-resistant PR variants (Ile-47, Ile-48, Ile-54, Val-82, and Ile-84). The question whether the presence of these

mutations affects compound **1** binding needs to be answered by further biochemical and structural studies. Nevertheless, compound **1** binds by two different modes to two identical binding pockets formed by monomers A and B (Fig. 3C). Thus, we can expect that compound **1** is able to adapt its position so that it could bind into an appropriate pocket altered by mutations.

In addition to the two inhibitor molecules, a continuous electron density map at the bottom of the PR active site allowed modeling of the tetrapeptide Ala-Gly-Ala-Ala, which represents a product of PR autoproteolytic cleavage, often observed during cocrystallization of PR with weak active-site inhibitors. The product of PR degradation is then found in the active site instead of inhibitor (ref. 46; PDB ID code 1SP5). In the present structure, however, the peptide and compound **1** occupy different sites of the active cleft, and, therefore, they can bind simultaneously. Nevertheless, high temperature factors of the peptide main chain atoms point to high mobility and/or its probable lower occupancy. The lack of electron density for side chains further suggests that several peptides originating from three possible cleavage sites (44) are present in the structure. Therefore, we presume that the presence of peptide in the active site is not required for compound **1**-specific binding.

In conclusion, we have shown that boron clusters represent convenient building blocks that can create important interactions with hydrophobic patches of the HIV PR-binding site. X-ray structure analysis of the metallaborane-PR complex brings up

compelling evidence about the inhibitor-binding site and type of interaction. *Exo*-skeletal substitution of the parent metallaborane cluster tecton introduces additional noncovalent interactions leading to the dramatic improvement in inhibition efficacy and selectivity. The combination of the hydrophobic interactions of the scaffold with substitutions allowing for specific H-bonding and coulombic interactions might further increase the potency of this class of nonpeptide PR inhibitors based on an inorganic framework. Chemical and biological stability, low toxicity, and the possibility to introduce heteroatoms into the cage or polar group modifications to the side chains make boron clusters very attractive pharmacophores.

We thank the X13 Consortium for Protein Crystallography for access to their facility at the Deutsches Elektronen-Synchrotron (DESY), Hamburg; Tomáš Baše from the Institute of Inorganic Chemistry, Rez u Prahy, for measurements of a part of the NMR spectra; and Hillary Hoffmann for critical proofreading of the manuscript. This work was supported by Grant QLK2-CT-2001-02360 from the 5th Framework of the European Commission and by a grant from the Ministry of Education (MSMT) of the Czech Republic within Program 1M6138896301, "Research Centre for new Antivirals and Antineoplastics." The project was further supported by Research Plans AVZ40550506 and AVOZ40320502 (from the Academy of Science of the Czech Republic). The synthesis of new compounds was partly supported by Research Centre LC523, "Perspective Inorganic Materials" (from MSMT).

- Kohl, N. E., Emini, E. A., Schleif, W. A., Davis, L. J., Heimbach, J. C., Dixon, R. A. F., Scolnick, E. M. & Sigal, I. S. (1988) *Proc. Natl. Acad. Sci. USA* **85**, 4686–4690.
- Prejdova, J., Soucek, M. & Konvalinka, J. (2004) *Curr. Drug Targets: Infect. Disord.* **4**, 137–152.
- Clavel, F. & Hance, A. J. (2004) *N. Engl. J. Med.* **350**, 1023–1035.
- Coffin, J. M. (1995) *Science* **267**, 483–489.
- Surleraux, D. L. N. G., De Kock, H. A., Verschuere, W. G., Pille, G. M. E., Maes, L. J. R., Peeters, A., Vendeville, S., De Meyer, S., Azijn, H., Pauwels, R., et al. (2005) *J. Med. Chem.* **48**, 1965–1973.
- Surleraux, D. L. N. G., Tahri, A., Verschuere, W. G., Pille, G. M. E., De Kock, H. A., Jonckers, T. H. M., Peeters, A., De Meyer, S., Azijn, H., Pauwels, R., et al. (2005) *J. Med. Chem.* **48**, 1813–1822.
- Judd, D. A., Nettles, J. H., Nevins, N., Snyder, J. P., Liotta, D. C., Tang, J., Ermolieff, J., Schinazi, R. F. & Hill, C. L. (2001) *J. Am. Chem. Soc.* **123**, 886–897.
- Bosi, S., Da Ros, T., Spalluto, G. & Prato, M. (2003) *Eur. J. Med. Chem.* **38**, 913–923.
- Friedman, S. H., DeCamp, D. L., Sijbesma, R. P., Srdanov, G., Wudl, F. & Kenyon, G. L. (1993) *J. Am. Chem. Soc.* **115**, 6506–6509.
- Sijbesma, R., Srdanov, G., Wudl, F., Castoro, J. A., Wilkins, C., Friedman, S. H., DeCamp, D. L. & Kenyon, G. L. (1993) *J. Am. Chem. Soc.* **115**, 6510–6512.
- Zheng, Z., Juodawlkis, A. S., Wirtz, S. S., Schinazi, R. F., Zeng, H., Bellavia, C., Wudl, F. & Hill, C. L. (1998) in *Fullerenes: Recent Advances in the Chemistry and Physics of Fullerenes and Related Materials*, eds. Kadish, K. M. & Ruoff, R. S. (Electrochem. Soc., San Diego, CA), Vol. 6, No. PV98-8.
- Hawthorne, M. F. (1993) *Angew. Chem.* **105**, 997–1033.
- Soloway, A. H., Tjarks, W., Barnum, B. A., Rong, F. G., Barth, R. F., Codogni, I. M. & Wilson, J. G. (1998) *Chem. Rev. (Washington, DC)* **98**, 1515–1562.
- Hawthorne, M. F. & Maderna, A. (1999) *Chem. Rev. (Washington, DC)* **99**, 3421–3434.
- Endo, Y., Ohta, K., Yoshimi, T. & Yamaguchi, K. (2004) *Phosphorus Sulfur Silicon Relat. Elem.* **179**, 799–802.
- Valliant, J. F., Guenther, K. J., King, A. S., Morel, P., Schaffer, P., Sogbein, O. O. & Stephenson, K. A. (2002) *Coord. Chem. Rev.* **232**, 173–230.
- Fujii, S., Hashimoto, Y., Suzuki, T., Ohta, S. & Endo, Y. (2005) *Bioorg. Med. Chem. Lett.* **15**, 227–230.
- Endo, Y., Yoshimi, T., Kimura, K. & Itai, A. (1999) *Bioorg. Med. Chem. Lett.* **9**, 2561–2564.
- Tsuji, M., Koiso, Y., Takahashi, H., Hashimoto, Y. & Endo, Y. (2000) *Biol. Pharm. Bull.* **23**, 513–516.
- DeCamp, D. L., Babe, L. M., Salto, R., Lucich, J. L., Koo, M. S., Kahl, S. B. & Craik, C. S. (1992) *J. Med. Chem.* **35**, 3426–3428.
- Hawthorne, M. F., Young, D. C. & Wegner, P. A. (1965) *J. Am. Chem. Soc.* **87**, 1818–1819.
- Saxena, A. K. & Hosmane, N. S. (1993) *Chem. Rev. (Washington, DC)* **93**, 1081–1124.
- Sivaev, I. B. & Bregadze, V. I. (1999) *Collect. Czech. Chem. Commun.* **64**, 783–805.
- Plešček, J. (1992) *Chem. Rev. (Washington, DC)* **92**, 269–278.
- Rais, J. & Gruner, B. (2005) in *Solvent Extraction*, eds. Marcus, I. & SenGupta, A. K. (Dekker, New York), pp. 243–334.
- Reed, C. A. (1998) *Acc. Chem. Res.* **31**, 133–139.
- Plešček, J., Base, K., Mares, F., Hanousek, F., Stibr, B. & Hermanek, S. (1984) *Collect. Czech. Chem. Commun.* **49**, 2776–2789.
- Plešček, J., Gruner, B., Baca, J., Fusek, J. & Cisarova, I. (2002) *J. Organomet. Chem.* **649**, 181–190.
- Plešček, J., Hermanek, S., Franken, A., Cisarova, I. & Nachtigal, C. (1997) *Collect. Czech. Chem. Commun.* **62**, 47–56.
- Mildner, A. M., Rothrock, D. J., Leone, J. W., Bannow, C. A., Lull, J. M., Reardon, I. M., Sarcich, J. L., Howe, W. J. & Tomich, C. S. (1994) *Biochemistry* **33**, 9405–9413.
- Weber, J., Mesters, J. R., Lepšik, M., Prejdova, J., Svec, M., Sponarova, J., Mlcochova, P., Skalicka, K., Strisovsky, K., Uhlikova, T., et al. (2002) *J. Mol. Biol.* **324**, 739–754.
- Strisovsky, K., Smrz, D., Fehrmann, F., Kracusslich, H. G. & Konvalinka, J. (2002) *Arch. Biochem. Biophys.* **398**, 261–268.
- Mares, M., Meloun, B., Pavlik, M., Kostka, V. & Baudys, M. (1989) *FEBS Lett.* **251**, 94–98.
- Kucerova, Z., Pohl, J. & Korbova, L. *J. Chromatogr.* **376**, 409–412.
- Williams, J. W. & Morrison, J. F. *Methods Enzymol.* **63**, 437–467.
- Benyoucef, S., Hober, D., Shen, L., Ajana, F., De Groote, D., Bocket-Mouton, L., Gerard, Y., Lion, G., Vilain, V. & Wattré, P. (1997) *Microbiol. Immunol.* **41**, 939–946.
- Otwinowski, Z. & Minor, W. (1997) *Methods Enzymol.* **276**, 307–326.
- Brynda, J., Řezáčová, P., Fabry, M., Horejsi, M., Stouracova, R., Soucek, M., Hradilek, M., Konvalinka, J. & Sedláček, J. (2004) *Acta Crystallogr. D Biol. Crystallogr.* **60**, 1943–1948.
- Gruner, B., Plešček, J., Baca, J., Cisarova, I., Dozol, J. F., Rouquette, H., Vinas, C., Selucky, P. & Rais, J. (2002) *New J. Chem.* **26**, 1519–1527.
- Sivaev, I. B., Starikova, Z. A., Sjoberg, S. & Bregadze, V. I. (2002) *J. Organomet. Chem.* **649**, 1–8.
- Olejniczak, A. B., Plešček, J., Kriz, O. & Lesnikowski, Z. J. (2003) *Angew. Chem. Int. Ed.* **42**, 5740–5743.
- Spinelli, S., Liu, Q. Z., Alzari, P. M., Hirel, P. H. & Poljak, R. J. (1991) *Biochimie* **73**, 1391–1396.
- Jones, S. & Thornton, J. M. (1996) *Proc. Natl. Acad. Sci. USA* **93**, 13–20.
- Rose, R. B., Craik, C. S. & Stroud, R. M. (1998) *Biochemistry* **37**, 2607–2621.
- Bruenger, A. T. (1992) *Nature* **355**, 472–475.
- Buchtelova, E., Hasek, J., Dohnalek, J., Petvokova, H., Duskova, J., Skalova, T., Brynda, J., Sedláček, J., Hradilek, J., Konvalinka, J., et al. (2001) *Mater. Struct.* **8**, 31–32.



## Inorganic Polyhedral Metallacarborane Inhibitors of HIV Protease: A New Approach to Overcoming Antiviral Resistance

Milan Kožíšek,<sup>†,‡</sup> Petr Cígler,<sup>†,§</sup> Martin Lepšík,<sup>†</sup> Jindřich Fanfrlík,<sup>†</sup> Pavlína Řezáčová,<sup>†,||</sup> Jiří Brynda,<sup>†,||</sup> Jana Pokorná,<sup>†</sup> Jaromír Plešek,<sup>⊥</sup> Bohumír Grüner,<sup>⊥</sup> Klára Grantz Šašková,<sup>†,‡</sup> Jana Václavíková,<sup>†</sup> Vladimír Král,<sup>§</sup> and Jan Konvalinka<sup>\*,†,‡,||</sup>

Gilead Sciences and IOCB Research Center Prague, Institute of Organic Chemistry and Biochemistry, Academy of Sciences of the Czech Republic, Flemingovo nám. 2, 166 10 Praha 6, Czech Republic, Department of Biochemistry, Faculty of Science, Charles University, Hlavova 8, Praha 2, Czech Republic, Department of Analytical Chemistry, Institute of Chemical Technology, Technická 5, 166 28 Praha 6, Czech Republic, Institute of Molecular Genetics, Academy of Sciences of the Czech Republic, Flemingovo nám. 2, 166 37 Praha 6, Czech Republic, Institute of Inorganic Chemistry, Academy of Sciences of the Czech Republic, Area of Research Institutes 1001, 250 68 Husinec-Rež u Prahy, Czech Republic

Received March 5, 2008

HIV protease (PR) is a prime target for rational anti-HIV drug design. We have previously identified icosahedral metallacarboranes as a novel class of nonpeptidic protease inhibitors. Now we show that substituted metallacarboranes are potent and specific competitive inhibitors of drug-resistant HIV PRs prepared either by site-directed mutagenesis or cloned from HIV-positive patients. Molecular modeling explains the inhibition profile of metallacarboranes by their unconventional binding mode.

### Introduction

HIV protease (PR)<sup>1</sup> cleaves the Gag and Gag-Pol polyproteins of the virus into structural proteins and replication enzymes to yield infectious viral particles. Prevention of this processing by mutation or chemical inhibition of PR leads to the production of immature progeny virus particles;<sup>1</sup> inhibitors of HIV PR are therefore effective virostatics. There are nine FDA-approved PR inhibitors currently on the market, and several others are making their way through the pharmaceutical pipeline.<sup>2</sup> All of the clinically active compounds identified to date are competitive inhibitors that target the PR active site. Most of them contain nonhydrolyzable peptide isosteres that mimic the transition state of substrate hydrolysis.

The evolution of drug resistant PR variants due to the rapid selection of resistant viral strains is a major complication of anti-HIV therapy.<sup>3,4</sup> The development of new, effective PR inhibitors with a novel mechanism of action capable of inhibiting multidrug resistant species and/or showing a high genetic barrier to resistance development<sup>4,5</sup> is still very relevant.

In our search for new structural types of versatile compounds that inhibit HIV PR, we identified a group of inorganic carbon/boron cluster complexes as promising frameworks for a novel class of nonpeptide PR inhibitors (PIs).<sup>6</sup> Our main attention has been focused on cobaltacar-

boranes, specifically the [3-cobalt bis(1,2-dicarbollide)]<sup>−</sup> ion **GB-18** (see Figure 1). There are several reports describing boron cluster-containing compounds as potential pharmaceuticals (antineoplastic and cytotoxic agents, estrogen agonists and antagonists, protein kinase C modulators), building blocks for BNCT (boron neutron capture therapy) pharmaceuticals, and agents for radioimaging.<sup>7</sup> On the other hand, not much is known about the toxicity of metallacarboranes in animals. Some early studies suggest low toxicity of metallacarboranes of the structural type of [3-cobalt bis(1,2-dicarbollide)]-ion in rats.<sup>8</sup>

In this paper, we show that cobaltacarboranes are able to inhibit a panel of recombinant HIV-1 PR species bearing signature resistance-conferring mutations for various FDA-approved PR inhibitors as well as highly resistant PR species amplified from HIV-positive patients failing antiretroviral therapy using HIV PR inhibitors. We provide a molecular model based on the recently published X-ray structure of a PR–metallacarborane complex that illuminates the structural reason for the activity of this novel family of HIV PR inhibitors.

### Chemistry

The synthesis and characterization of all metallacarboranes, discussed in this paper, has been described previously.<sup>6</sup> Briefly, the cesium salt of **GB-18** was converted to a sodium salt by simple extraction metathesis.<sup>9</sup> The ring opening of 8-dioxane-3-cobalt bis(1,2-dicarbollide)<sup>10</sup> under mild conditions provided a series of *exo*-skeletonally modified metallacarborane cluster anions **GB-21**, **GB-48**, and **GB-80**.<sup>6</sup> Compounds **GB-48** and **GB-80** involve the same symmetric structural pattern, in which two cobalt bis(1,2-dicarbollide) subunits are connected via a flexible hydrophilic spacer. The presence of an amino group in the center of the chain originates their unique zwitterionic-anionic character.

### Results and Discussion

Selected metallacarboranes (Figure 1) were tested in vitro as potential inhibitors of the recombinant PR variants listed in Table 1. PRs 1–4 are variants prepared by in vitro

\* To whom correspondence should be addressed. Phone: 420-220183218. Fax: 420-220183578. E-mail: konval@uochb.cas.cz. Address: Institute of Organic Chemistry and Biochemistry, Academy of Sciences of the Czech Republic, Flemingovo nám. 2, 166 10 Praha 6, Czech Republic.

<sup>†</sup> Gilead Sciences and IOCB Research Center Prague, Institute of Organic Chemistry and Biochemistry, Academy of Sciences of the Czech Republic.

<sup>‡</sup> Department of Biochemistry, Faculty of Science, Charles University.

<sup>§</sup> Department of Analytical Chemistry, Institute of Chemical Technology.

<sup>||</sup> Institute of Molecular Genetics, Academy of Sciences of the Czech Republic.

<sup>⊥</sup> Institute of Inorganic Chemistry, Academy of Sciences of the Czech Republic.

<sup>‡</sup> Abbreviations: BNCT, boron neutron capture therapy; FDA, Food and Drug Administration; HAART, highly active antiretroviral therapy; HIV-1, human immunodeficiency virus type 1;  $k_{\text{cat}}$ , catalytic rate constant;  $K_i$ , inhibition constant;  $K_m$ , Michaelis constant; Nle, norleucine; Nph, *p*-nitrophenylalanine; PR, protease; QM, quantum mechanics; wt, wild-type.



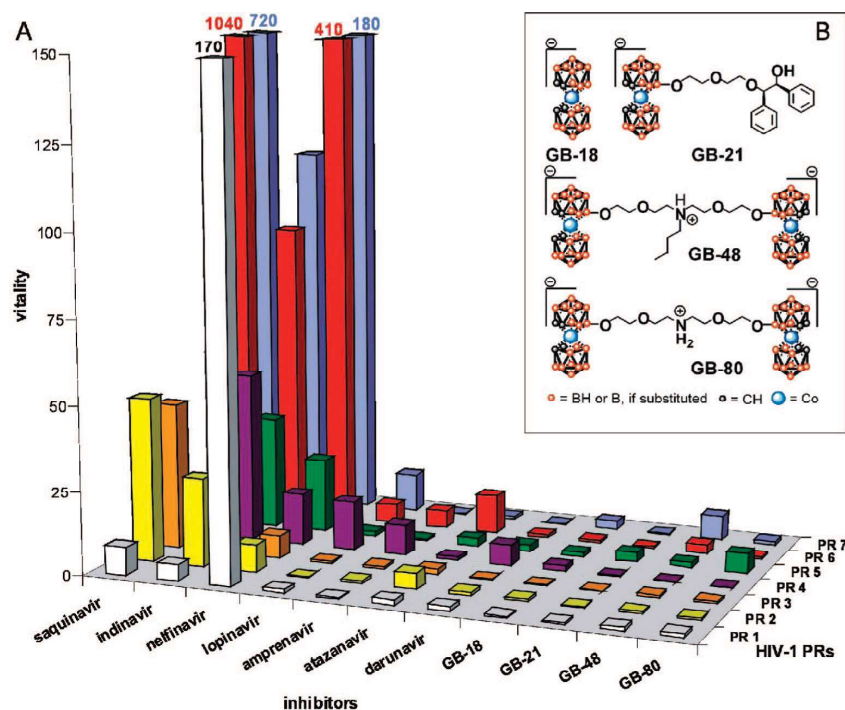


**Figure 1.** (A) Vitalities of seven clinical inhibitors and metallacarborane compounds with the panel of PR mutants. (B) Structural formulas of metallacarborane inhibitors used in this work. All compounds were prepared as  $\text{Na}^+$  salts.

mutagenesis that bear signature primary mutations responsible for decreased susceptibility to nelfinavir, ritonavir, indinavir, and lopinavir, whereas PRs 5–7 are enzymes amplified from HIV-1 positive patients heavily pretreated with various PR inhibitors. Note that the latter group of PRs have up to 17 amino acid exchanges compared to the wild-type enzyme (PR7). All of the proteases were expressed in *Escherichia coli*, refolded from inclusion bodies, purified to homogeneity, and fully enzymologically characterized as previously reported.<sup>11,12</sup> Their enzyme kinetic parameters ( $K_m$  and  $k_{cat}$ ) are summarized in Table S1 (see Supporting Information).

**In Vitro Resistance Profile.** Four metallacarborane compounds were selected and tested for their ability to inhibit a panel of selected proteases. These compounds exhibit classical competitive binding (data not shown), and no significant toxicity in tissue cultures was observed in the concentration range up to  $50 \mu\text{M}$ . For comparison, seven clinically available inhibitors (saquinavir, indinavir, nelfinavir, lopinavir, amprenavir, atazanavir, and darunavir) were included in our inhibition assay. Table 1 summarizes the inhibition constants ( $K_i$  values) and relative increases in  $K_i$  values compared to the wild-type PR. Metallacarborane compounds proved to be potent inhibitors of wild-type PR and preserved their inhibitory capacity toward all tested PRs. The relative inhibition values ( $K_i$  mutant PR/ $K_i$  wt PR) for compounds **GB-18**, **GB-21**, **GB-48**, and **GB-80** range from 0.6 to 20, whereas relative inhibition values for the clinically available inhibitors range from 0.8 to 4500.

To correlate the relative  $K_i$  values with the changes in catalytic efficiency caused by the mutations in PR, the catalytic efficiency of the mutated PRs must be taken into account. The term “vitality” was introduced<sup>13</sup> as a measure

of the relative capability of a mutated enzyme to cleave its substrate in the presence of an inhibitor. It is defined as  $v = (K_i k_{cat}/K_m)_{\text{MUT}} / (K_i k_{cat}/K_m)_{\text{WT}}$  and predicts the therapeutic effect of a given PI. Figure 1 depicts the relative vitalities of the panel of resistant PR species PR1–PR7 with compounds **GB-18**, **GB-21**, **GB-48**, and **GB-80** and comparison with clinically available inhibitors. Metallacarboranes show a low relative loss of activity, as demonstrated by the values of vitalities for all PR variants tested (Figure 1). While the specific mutations in the PR lead to dramatic (50-fold to 1000-fold) increases in vitality for saquinavir, indinavir, and nelfinavir, the increase in vitality is less dramatic for lopinavir, amprenavir, and darunavir (PR4, which harbors mutations V321 and I47A, shows the highest vitality). Metallacarborane compounds **GB-18**, **GB-21**, **GB-48**, and **GB-80** show a rather low relative loss of inhibition potency, as seen from the relative values of vitalities for all the PR variants in Figure 1.

**Inhibitor Binding to HIV PR.** The crystal structure of the wild-type enzyme in complex with **GB-18** (PDB accession 1ZTZ) revealed a unique binding mode of metallacarboranes in the HIV PR active site.<sup>6</sup> Two molecules of **GB-18** bind to the flap-proximal part of the enzyme active site cleft and hold the flaps in a semi-open conformation, occupying two hydrophobic pockets that are formed by the side chains of residues Pro81, Ile84, and Val82 and covered by the flap residues Ile47, Gly48, and Ile54. Interestingly, the two molecules (designated Cb1 and Cb2) of **GB-18** bind asymmetrically into the symmetrical active site (Figure 2A).

Mutations in the residues that form the inhibitor binding site are present in several of the protease variants tested. The primary mutations I47A, I54V, V82A, and I84V cause spatial

Table 1.  $K_i$  Values [nM] for the Inhibition of PR Mutants by Seven Clinically Available Inhibitors and by Metallacarboranes GB-18, GB-21, GB-48, and GB-80<sup>a</sup>

inhibitor	wild-type	PR 1	PR 2	PR 3	PR 4	PR 5	PR 6	PR 7
saquinavir	0.04 ± 0.01 (1)	0.51 ± 0.07 (13)	13 ± 2 (25)	12 ± 1 (290)	0.22 ± 0.01 (5.5)	2.9 ± 0.3 (73)	180 ± 15 (4500)	71 ± 6 (1800)
indinavir	0.12 ± 0.02 (1)	0.88 ± 0.07 (7)	21 ± 4 (180)	13 ± 1.2 (110)	56 ± 6 (470)	5.5 ± 0.3 (46)	47 ± 3 (390)	33 ± 1 (280)
nelfinavir	0.07 ± 0.01 (1)	18 ± 1 (260)	3.8 ± 1.1 (54)	3.2 ± 0.2 (46)	10 ± 1 (140)	2.1 ± 0.3 (30)	130 ± 9 (1800)	32 ± 2 (450)
lopinavir	0.018 ± 0.009 (1)	0.026 ± 0.006 (1.5)	0.029 ± 0.007 (1.6)	0.060 ± 0.004 (3.3)	2.4 ± 0.5 (130)	0.029 ± 0.006 (1.6)	0.44 ± 0.09 (24)	0.50 ± 0.03 (28)
amprenavir	0.18 ± 0.02 (1)	0.13 ± 0.04 (0.7)	0.90 ± 0.10 (5)	0.82 ± 0.13 (4.5)	15 ± 3 (82)	0.15 ± 0.05 (0.8)	4.1 ± 0.3 (22)	0.13 ± 0.05 (0.7)
atazanavir	0.024 ± 0.005 (1)	0.055 ± 0.006 (2.3)	0.76 ± 0.04 (32)	0.23 ± 0.01 (9.4)	0.17 ± 0.02 (7.1)	0.076 ± 0.004 (3.2)	1.2 ± 0.4 (50)	0.054 ± 0.003 (2.3)
darunavir	0.0053 ± 0.0036 (1)	0.011 ± 0.001 (2)	0.032 ± 0.011 (6)	0.0043 ± 0.0007 (0.8)	0.31 ± 0.04 (88)	0.015 ± 0.004 (2.8)	0.02 ± 0.06 (3.7)	<0.001 (<0.2)
GB-18	66 ± 30 (1)	39 ± 14 (0.6)	330 ± 5 (5)	150 ± 35 (2.2)	870 ± 44 (1.3)	120 ± 20 (1.8)	210 ± 20 (3.1)	410 ± 30 (6.2)
GB-21	20 ± 5 (1)	13 ± 0.5 (0.7)	34 ± 9 (1.7)	39 ± 4 (2)	41 ± 1 (2.1)	82 ± 6 (4.1)	41 ± 5 (2.1)	9.1 ± 3.7 (0.5)
GB-48	2.2 ± 1.2 (1)	3.7 ± 2.2 (1.7)	9.0 ± 3.4 (4.1)	11 ± 4 (5)	2.7 ± 1.3 (1.2)	4.6 ± 2.7 (2.1)	24 ± 5 (11)	39 ± 6 (18)
GB-80	4.9 ± 2.1 (1)	8.1 ± 1.5 (1.7)	22 ± 5 (4.5)	21 ± 8 (4.3)	5.0 ± 1.1 (1)	40 ± 17 (8.1)	13 ± 3 (2.6)	14 ± 1 (2.9)

<sup>a</sup> These inhibition constants were determined by spectrophotometric assay at the pH optimum of the protease (pH 4.7). Numbers in parentheses show relative increases in  $K_i$  values for the corresponding recombinant mutant proteases as compared with wild-type. The recombinant proteases bear the following mutations in comparison to the consensus wild-type HIV PR strain BH10: PR 1-D30N/N88D; PR 2-M46I/A71/V82T/I84V; PR 3-A71/V82T/I84V; PR 4-V32I/I47A; PR 5-L10I/I15V/E35D/N37S/R41K/I62V/LG3P/A71V/G73S/L90M; PR 6-L10I/L24I/L33F/M46L/I54V/L63P/A71V/V82A/I84V; PR 7-L10F/L19I/K20R/L33F/E35D/M36I/R41K/F53L/I54V/L63P/H69K/A71V/I74P/I84V/L89M/L90M/I93L.

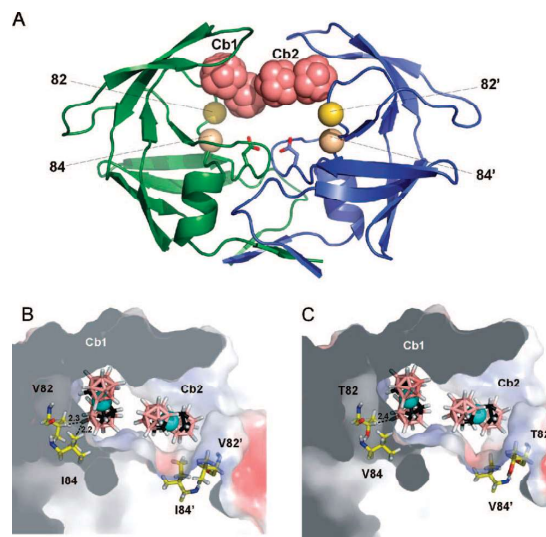


**Figure 2.** (A) Overall view of wild-type PR–GB-18 complex crystal structure (PDB code 1ZTZ<sup>6</sup>). The PR dimer is shown in ribbon representation with two molecules of GB-18 (represented as spheres) bound to the flap-proximal part of the enzyme active site. The two mutations at positions 82 and 84, which were studied by molecular modeling, are indicated (B). (C) Detail of two molecules of GB-18 (Cb1 and Cb2) bound to the active site of PR wild-type (panel B) and to the V82T/I84V variant (panel C). Metallacarboranes (pink, boron; black, carbon; white, hydrogen; cyan, cobalt) as well as residues 82/82' and 84/84' of PR (yellow, carbon; white, hydrogen; red, oxygen; blue, nitrogen) are shown as sticks. Also, the PR solvent accessible surface is shown colored by charge from positive (blue) to negative (red). Dihydrogen bonds are shown as dashed lines with  $d_{HH}$  distances in Å. The figure was prepared with PyMol 0.99 (DeLano Scientific LLC, 2002).

enlargement of the S3 and S3' substrate binding pockets. We employed molecular modeling to study the impact of mutations at residues 82/82' and 84/84' on interaction with GB-18. Metallacarboranes interact with biomolecules via unconventional B–H···H–X dihydrogen bonds, where X stands for N, O, or C atoms. The characteristic distance between interacting hydrogens  $d_{HH}$  is 1.8–2.3 Å.<sup>14</sup> In our optimized active-site structural models, we searched for differences in dihydrogen bonding between GB-18 and either wild-type PR or a V82T/I84V PR mutant. In the mutant, the dihydrogen bond between the first molecule of GB-18 (Cb1) and Thr82 is weaker than the interaction with Val82 ( $d_{HH}$  is longer by 0.1 Å), while the interaction with residue 84 is lost due to the I84V mutation (Figure 2B,C). Residues 82' and 84' are unable to interact with the second molecule of GB-18 (Cb2) in the V82T/I84V PR variant due to distance constraints.

The strength of C–H···H–B dihydrogen bonds in carborane–amino acid complexes has been calculated as 2.1–5.8 kcal/mol.<sup>14</sup> Our experimental data show that the presence of primary mutations in the S3/S3' subsites does not have a dramatic effect on metallacarborane inhibition compared to other inhibitors that occupy these subsites (e.g. saquinavir and indinavir). We observed 2- and 6-fold decreases in the binding affinity of GB-18 toward PRs 2 and 3 (which contain V82T and I84V substitutions), respectively, as compared to the wild-type PR (Table 1). The changes in Gibbs free energy are thus 0.4 and 1 kcal/mol, respectively. These values are smaller than our estimate of 2.1–5.8 kcal/

mol, corresponding to the loss of the dihydrogen bond found in our models. We propose that repositioning of **GB-18** in the mutated PR binding site might explain the preserved inhibitory capacity of metallacarboranes. Indeed, two different modes of binding into identical binding sites were observed in the crystal structure,<sup>6</sup> implying that the metallacarborane cage has a certain degree of freedom in its binding position and that this position can be adjusted in response to binding pocket alterations.

## Conclusions

Substituted metallacarboranes are potent, specific, and selective competitive inhibitors of wild-type and mutated HIV PRs. We explain their potential to inhibit a variety of PI-resistant PR species due to their novel binding mode in the PR binding pockets via unconventional proton–hydride hydrogen bonds (dihydrogen bonds) and their ability to adjust the position of the metallacarborane cage within the HIV PR substrate binding cleft. We conclude that boron clusters are promising pharmacophores for potent and specific inhibition of drug-resistant HIV protease mutants.

## Experimental Methods

Resistant PRs were prepared by site-directed mutagenesis (HIV-1 PR 1–4) as previously described<sup>11,12</sup> or selected under the pressure of clinically available PIs (HIV-1 PR 5–7).<sup>15</sup> HIV-positive patients receiving highly active antiretroviral therapy (HAART) at the Faculty Clinic Bulovka in Prague within a long-term epidemiological study have been followed for the presence of resistant HIV species. Selection of the patients for this study was based on genotyping and clinical markers suggesting development of resistance to protease inhibitors.<sup>15,16</sup>

**Inhibition Assay.** The inhibition constants ( $K_i$ ) were determined by spectrophotometric assay using the chromogenic peptide substrate LysAlaArgValNle\*<sup>6</sup>NphGluAla<sup>6</sup>Nle-NH<sub>2</sub> as previously described.<sup>11</sup> Typically, 8–10 pmol of PR was added to 1 mL of 0.1 M sodium acetate buffer, pH 4.7, 0.3 M NaCl, and 4 mM EDTA, containing substrate at a concentration near the  $K_m$  of the enzyme and various concentrations of inhibitor dissolved in DMSO. The final concentrations of DMSO were kept below 2.5% (v/v). Substrate hydrolysis was followed as a decrease in absorbance at 305 nm using a UNICAM UV500 UV–vis spectrophotometer (Thermo, Cambridge, MA). The HIV PR remained stable over the whole reaction time. Inhibition data were analyzed using the equation for competitive inhibition according to Williams and Morrison.<sup>17</sup>

**Inhibitor Synthesis.** The synthesis and characterization of all metallacarboranes, discussed in this paper, has been described previously.<sup>6</sup>

**Molecular Modeling.** The effects of the Val82Thr and Ile84Val mutations in HIV-1 PRs 2 and 3 on the binding of compound **GB-18** were studied using molecular modeling. We added hydrogen atoms to the X-ray structure of the complex of wild-type HIV-1 PR with **GB-18** (PDB code: 1ZTZ)<sup>6</sup> using the program InsightII 2000 (Accelrys Software Inc., 2000). For quantum calculations, we selected the two molecules of **GB-18**, designated Cb1 and Cb2, and parts of active-site PR residues (Val32, Ile47, Gly48, Gly49, Ile54, Thr80, Pro81, Val82, Ile84, Ile47', Gly48', Thr80', Pro81', Ile84') together with the peptide found in the PR active site and three structural water molecules. The model for the resistant variant was created by replacing the C $\gamma$ 2 atoms of Val82/Val82' by O $\gamma$ 1, followed by deleting C $\delta$  methyl groups from residues Ile84/Ile84' and subsequent protonation.

Quantum chemical optimizations of the models were performed: (i) for hydrogen atoms only of the wild-type PR–compound **GB-18** complex and (ii) for the whole model except the anchoring atoms of the resistant PR variant–**GB-18** complex. The QM calculations

were performed with the Turbomole 5.7<sup>18</sup> program package augmented with London dispersion energy.<sup>19</sup>

**Acknowledgment.** This work was supported by a grant from the sixth Framework of the European Commission (LSHP-CT-2007-037693), by grants from the Ministry of Education (MSMT) of the Czech Republic within programs 1M0508, LC523, and LC 512, and by a grant from the Ministry of Health Care of the Czech Republic NR-8571-3. The project was further supported by Research Plans AV0Z40550506, AV0Z50520514, and AV0Z40320502 from the Academy of Sciences of the Czech Republic.

**Supporting Information Available:** List of PR variants analyzed in this study, including the specific mutations and enzyme characteristics ( $K_m$ ,  $k_{cat}$ , and catalytic efficiencies [ $k_{cat}/K_m$ ]). This material is available free of charge via the Internet at <http://pubs.acs.org>.

## References

- (1) Kohl, N. E.; Emini, E. A.; Schleif, W. A.; Davis, L. J.; Heimbach, J. C.; Dixon, R. A.; Scolnick, E. M.; Sigal, I. S. Active human immunodeficiency virus protease is required for viral infectivity. *Proc. Natl. Acad. Sci. U.S.A.* **1988**, *85*, 4686–4690.
- (2) Mastrolorenzo, A.; Rusconi, S.; Scozzafava, A.; Supuran, C. T. Inhibitors of HIV-1 protease: 10 years after. *Expert. Opin. Ther. Pat.* **2006**, *16*, 1067–1091.
- (3) Prejdova, J.; Soucek, M.; Konvalinka, J. Determining and overcoming resistance to HIV protease inhibitors. *Curr. Drug Targets Infect. Disord.* **2004**, *4*, 137–152.
- (4) Yin, P. D.; Das, D.; Mitsuya, H. Overcoming HIV drug resistance through rational drug design based on molecular, biochemical, and structural profiles of HIV resistance. *Cell. Mol. Life Sci.* **2006**, *63*, 1706–1724.
- (5) Rusconi, S.; Vigano, O. New HIV protease inhibitors for drug-resistant viruses. *Therapy* **2006**, *3*, 79–88.
- (6) Cigler, P.; Kozisek, M.; Rezacova, P.; Brynda, J.; Otwinowski, Z.; Pokorna, J.; Plesek, J.; Gruner, B.; Doleckova, L.; Masa, M.; Sedlacek, J.; Bodem, J.; Krausslich, H.-G.; Kral, V.; Konvalinka, J. From nonpeptide toward noncarbon protease inhibitors: metallacarboranes as specific and potent inhibitors of HIV protease. *Proc. Natl. Acad. Sci. U.S.A.* **2005**, *102*, 15394–15399.
- (7) Lesnikowski, Z. J. Boron units as pharmacophores: new applications and opportunities of boron cluster chemistry. *Collect. Czech. Chem. Commun.*; 2007 16461658, and the references therein.
- (8) Spryskova, R. A.; Karaseva, L. I.; Bratsev, V. A.; Serebryakov, N. G. Toxicity of functional derivatives of polyhedral carboranes. *Med. Radiol.* **1981**, *26*, 62–64.
- (9) Plesek, J.; Base, K.; Mares, F.; Hanousek, F.; Stibr, B.; Hermanek, S. Potential uses of metallocarborane sandwich anions for analysis, characterization and isolation of various cations and organic bases. *Collect. Czech. Chem. Commun.* **1984**, *49*, 2776–2789.
- (10) Plesek, J.; Hermanek, S.; Franken, A.; Cisarova, I.; Nachtigal, C. Dimethyl sulfate induced nucleophilic substitution of the [bis(1,2-dicarbollido)-3-cobaltate(1–)] ion. Syntheses, properties and structures of its 8,8'-*m*-sulfato, 8-phenyl, and 8-dioxane derivatives. *Collect. Czech. Chem. Commun.* **1997**, *62*, 47–56.
- (11) Weber, J.; Mesters, J. R.; Lepsik, M.; Prejdova, J.; Svec, M.; Sponarova, J.; Mlcochova, P.; Skalicka, K.; Strisovsky, K.; Uhlíkova, T.; Soucek, M.; Machala, L.; Stankova, M.; Vondrasek, J.; Klimkait, T.; Krausslich, H. G.; Hilgenfeld, R.; Konvalinka, J. Unusual binding mode of an HIV-1 protease inhibitor explains its potency against multi-drug-resistant virus strains. *J. Mol. Biol.* **2002**, *324*, 739–754.
- (12) Kozisek, M.; Bray, J.; Rezacova, P.; Saskova, K.; Brynda, J.; Pokorna, J.; Mammano, F.; Rulisek, L.; Konvalinka, J. Molecular analysis of the HIV-1 resistance development: enzymatic activities, crystal structures, and thermodynamics of nefinavir-resistant HIV protease mutants. *J. Mol. Biol.* **2007**, *374*, 1005–1016.
- (13) Gulnik, S. V.; Suyorov, L. I.; Lju, B.; Yu, B.; Anderson, B.; Mitsuya, H.; Erickson, J. W. Kinetic characterization and cross-resistance patterns of HIV-1 protease mutants selected under drug pressure. *Biochemistry* **1995**, *34*, 9282–9287.
- (14) Fanfrlik, J.; Lepsik, M.; Horinek, D.; Havlas, Z.; Hobza, P. Interaction of carboranes with biomolecules: formation of dihydrogen bonds. *ChemPhysChem* **2006**, *7*, 1100–1105.
- (15) Kozisek, M.; Prejdova, J.; Soucek, M.; Machala, L.; Stankova, M.; Linka, M.; Bruckova, M.; Konvalinka, J. Characterisation of mutated proteinases derived from HIV-positive patients: enzyme activity,

- vitality and inhibition. *Collect. Czech. Chem. Commun.* **2004**, *69*, 703–714.
- (16) Vaclavikova, J.; Weber, J.; Machala, L.; Reinis, M.; Linka, M.; Bruckova, M.; Vandasova, J.; Stankova, M.; Konvalinka, J. Long-term analysis of the resistance development in HIV-1 positive patients treated with protease and reverse transcriptase inhibitors: correlation of the genotype and disease progression. *Acta Virol.* **2005**, *49*, 29–36.
- (17) Williams, J. W.; Morrison, J. F. The kinetics of reversible tight-binding inhibition. *Methods Enzymol.* **1979**, *63*, 437–467.
- (18) Ahlrichs, R.; Bar, M.; Haser, M.; Horn, H.; Kolmel, C. Electronic structure calculations on workstation computers: The program system Turbomole. *Chem. Phys. Lett.* **1989**, *162*, 165–169.
- (19) Jurecka, P.; Cerny, J.; Hobza, P.; Salahub, D. R. Density functional theory augmented with an empirical dispersion term. Interaction energies and geometries of 80 noncovalent complexes compared with ab initio quantum mechanics calculations. *J. Comput. Chem.* **2007**, *28*, 555–569.

JM8002334



## Design of HIV Protease Inhibitors Based on Inorganic Polyhedral Metallacarboranes<sup>†</sup>

Pavlna Řezáčová,<sup>\*,‡,§</sup> Jana Pokorná,<sup>‡,||</sup> Jiří Brynda,<sup>‡,§</sup> Milan Kožíšek,<sup>‡,||</sup> Petr Cigler,<sup>‡,⊥</sup> Martin Lepšík,<sup>‡</sup> Jindřich Fanfrlík,<sup>‡</sup> Jan Řezáč,<sup>‡</sup> Klára Grantz Šašková,<sup>‡,||</sup> Irena Siegllová,<sup>‡,§</sup> Jaromír Plešek,<sup>#</sup> Václav Šícha,<sup>#</sup> Bohumír Grüner,<sup>#</sup> Heike Oberwinkler,<sup>∇</sup> Juraj Sedláček,<sup>§</sup> Hans-Georg Kräusslich,<sup>∇</sup> Pavel Hobza,<sup>‡</sup> Vladimír Král,<sup>⊥</sup> and Jan Konvalinka<sup>‡,§,||</sup>

<sup>‡</sup>Institute of Organic Chemistry and Biochemistry, Academy of Sciences of the Czech Republic, v.v.i., Gilead Sciences and IOCB Research Center, Flemingovo nám. 2, 16610 Praha 6, Czech Republic, <sup>§</sup>Institute of Molecular Genetics, Academy of Sciences of the Czech Republic v.v.i., Flemingovo nám. 2, 166 10 Praha 6, Czech Republic, <sup>||</sup>Department of Biochemistry, Faculty of Science, Charles University, Hlavova 8, 128 43 Praha 2, Czech Republic, <sup>⊥</sup>Department of Analytical Chemistry, Institute of Chemical Technology, Technická 5, 166 28 Praha 6, Czech Republic, <sup>#</sup>Institute of Inorganic Chemistry, Academy of Sciences of the Czech Republic, v.v.i., Area of Research Institutes 1001, 250 68 Husinec-Rež u Prahy, Czech Republic, and <sup>∇</sup>Department of Virology, University of Heidelberg, Im Neuenheimer Feld 324, D-69120 Heidelberg, Germany

Received July 31, 2009

HIV protease (HIV PR) is a primary target for anti-HIV drug design. We have previously identified and characterized substituted metallacarboranes as a new class of HIV protease inhibitors. In a structure-guided drug design effort, we connected the two cobalt bis(dicarbollide) clusters with a linker to substituted ammonium group and obtained a set of compounds based on a lead formula  $[\text{H}_2\text{N}-(8-(\text{C}_2\text{H}_4\text{O})_2-1,2-\text{C}_2\text{B}_9\text{H}_{10})(1',2'-\text{C}_2\text{B}_9\text{H}_{11})-3,3'-\text{Co}]_2\text{Na}$ . We explored inhibition properties of these compounds with various substitutions, determined the HIV PR:inhibitor crystal structure, and computationally explored the conformational space of the linker. Our results prove the capacity of linker-substituted dual-cage cobalt bis(dicarbollides) as lead compounds for design of more potent inhibitors of HIV PR.

### Introduction

The human immunodeficiency virus protease (HIV PR<sup>a</sup>), an enzyme belonging to the aspartic protease family, is responsible for cleavage of the Gag and Gag-Pol polyprotein precursors necessary for production of infectious viral particles.<sup>1</sup> Since the demonstration that HIV PR plays an essential role in the HIV replication cycle, this enzyme has become one of the primary targets for antiviral drug design leading to the development of hundreds of inhibitory compounds. Nine of these are currently FDA-approved for clinical use and several others are in the pipeline of pharmaceutical companies (reviewed in ref 2). All FDA-approved drugs represent competitive inhibitors that occupy the enzyme active site and share a similar structural scaffold mimicking the peptide substrate. The major problem that limits the therapeutic efficiency of protease inhibitors (PIs) is drug resistance caused by extensive mutations in PR.<sup>3</sup> Development of new inhibitors acting by an alternative mode of inhibition and capable of inhibiting multidrug resistant species is thus essential for the sustained successful treatment of HIV-positive patients.

In our search for novel structural types of unconventional chemical compounds, we have recently identified a group of

inorganic carbon/boron (carborane) cluster complexes, namely cobalt bis(dicarbollides), as promising frameworks for nonpeptide PIs.<sup>4</sup> These clusters form icosahedral sandwich complexes of two icosahedral  $\text{C}_2\text{B}_9\text{H}_{11}^{2-}$  dicarbollide cages and a central  $\text{Co}^{3+}$  ion.<sup>5</sup> (Metalla)carborane compounds show remarkable stability originating from delocalized bonding within their triangular boron facets and over the whole cage, a phenomenon referred to as three-dimensional aromaticity.<sup>6,7</sup> The use of boron clusters as hydrophobic pharmacophores have lately been gaining in importance (reviewed in refs 8,9). Specifically, various carboranes were introduced for use in boron neutron capture therapy,<sup>9–11</sup> radioimmunodetection, and radioimmunotherapy.<sup>12,13</sup> Other biologically active carborane derivatives include carborane-based insect neuropeptides, antineoplastic and cytotoxic agents, estrogen agonists and antagonists, retinoids, protein kinase C modulators, and others.<sup>9</sup>

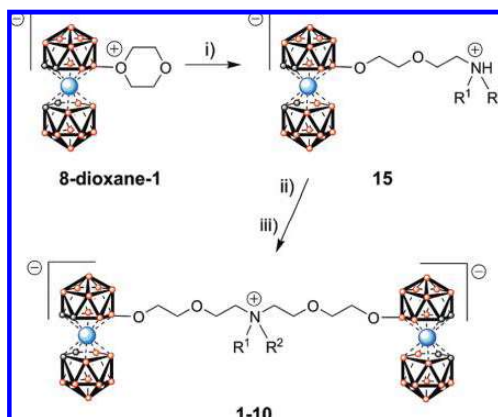
We have shown in our previous works that substituted cobalt bis(dicarbollides) are specific inhibitors of HIV PR<sup>4</sup> and also effective inhibitors of HIV-1 PR variants resistant to clinical inhibitors.<sup>14</sup> The tested compounds showed little toxicity in tissue culture and exhibited substantial chemical and biological stability. The crystal structure of the parent cluster, cobalt bis(1,2-dicarbollide) ion in complex with wild-type HIV-1 PR, revealed a unique binding mode. Two inhibitor molecules occupied in a nonsymmetrical manner symmetric hydrophobic pockets in the flap-proximal region of the S3 and S3' subsites of the enzyme active site.<sup>4</sup> In a structure-guided drug design effort, we connected the two parent clusters with a linker to yield compounds with significantly increased inhibitory potency toward HIV-1 PR.

In this work, we have designed and synthesized a set of compounds set of double (triple) cluster compounds

<sup>†</sup>PDB ID: Atomic coordinates and experimental structure factors have been deposited with the Protein Data Bank with the code 3I8W.

\*To whom correspondence should be addressed. Phone: + 420220183135. Fax: + 420220183280. E-mail: rezacova@uochb.cas.cz.

<sup>a</sup>Abbreviations: ADP, atomic displacement parameter; FDA; Food and Drug Administration; HIV PR; human immunodeficiency virus protease;  $K_i$ , inhibition constant;  $K_m$ , Michaelis constant; PI, protease inhibitor; rmsd, root-mean square deviation; QM, quantum mechanics; WT, wild-type.

**Scheme 1.** Synthetic Method Used for Construction of the Anionic Molecules **1–10**<sup>a</sup>

<sup>a</sup> (i) Toluene:ethyleneglycol dimethyl ether (DME) 4:1, 60 °C, 4 h; (ii) NaH, toluene: DME 4: 1, (iii) 8-dioxane-1, room temperature.

(Table 1 and Scheme 1) of general formulation  $[R^1R^2RN-(8-(C_2H_4O)_2-1,2-C_2B_9H_{10})(1',2'-C_2B_9H_{11})-3,3'-Co)_2]^{n-}$  (where  $R^1 = H, -C_2H_5, -n-C_4H_9, -C_2H_4OH, -t-C_4H_9, -C(CH_2OH)_3, -C_3H_6COO^-, -C_2H_4SO_3^-, -CH_2C_6H_5, -SO_2C_6H_5-3-CH_3, -7-CB_{10}H_{11}^-, -1-CB_{11}H_{11}, -[\mu-8,8'-(1,2-C_2B_{10}H_{10})-3,3'Co]$ ,  $R^2 = \text{none, H, } -C_2H_5, n = 1 \text{ and } 2$ ) (**1–13**) or  $[n-C_4H_9H_2N-(10-(C_2H_4O)_2-nido-7,8-C_2B_9H_{10})_2]^-$  (**14**) and investigated their HIV PR inhibition properties. We have determined the crystal structure of the parental compound  $[H_2N-(8-(C_2H_4O)_2-1,2-C_2B_9H_{10})(1',2'-C_2B_9H_{11})-3,3'-Co)_2]Na$  (designated here **1**) in complex with wild-type HIV-1 PR. As the lack of a continuous electron-density map in the crystal structure suggested numerous possible linker conformations, we explored the conformational space of the linker computationally. This study demonstrates the capacity of linker-substituted dual-cage cobalt bis(dicarbollides) as lead compounds for design of more potent HIV PIs.

## Results

**Inhibitor Design and Synthesis.** The structural formulas of the compounds studied in this work are shown in Table 1. The series involves symmetric molecules designed based on the most effective structures from our previous study.<sup>4</sup> These zwitterionic–anionic molecules contain two or three carborane clusters bonded via an N-substituted bis(ethyleneglycol)amine linker. We focused on the substitution of the central part. In addition to hydrocarbon/functional group substituents, we also used various boron hydride clusters differing distinctively in hydrophobicity and acidity. It should be noted here that the total negative charge of several tested members of the series is increased to  $-2$  due to the presence of the third anionic cluster or due to the substitution pattern.

The selection of synthetic routes was limited to double (triple) ring-opening of the 8-dioxane cobalt-bis(dicarbollide) zwitterion by a variety of organic amines or carborane and metallacarborane building blocks substituted with amine/ammonium functions as shown in Scheme 1 and Table 1.

Compounds containing three boron cages **11–13** are also available through this approach if a boron cluster substituted with ammonium function (deprotonated using NaH) is used instead of the organic amine in the first ring-opening step.

These synthetic routes are efficient, reliable, and almost quantitative for the majority of compounds presented in this article.

The synthesis of compound **14** was also based on this methodology but using 10-dioxane-*nido*-7,8- $C_2B_9H_{11}$  (**15**) reactive building block instead of **1**. The 11 vertex carborane derivative 155-P has been known for a long time from reactions of the parent *nido*- $[7,8-C_2B_9H_{12}]^-$  anion with dioxane promoted by formaldehyde/HCl<sup>15</sup> or  $HgCl_2$ .<sup>16</sup> We report here that the compound 155-P can be obtained more effectively if the neutral *nido*-7,8- $C_2B_9H_{13}$  carborane is heated in toluene in the presence of an excess of dioxane. For details on the synthetic procedures, see the Supporting Information.

**Enzyme and Antiviral Inhibition Studies.** The inhibitory properties of all compounds were tested in an in vitro spectrophotometric enzyme assay using a chromogenic substrate and recombinant wild-type HIV-1 PR. The results are shown in Table 1. First, the  $IC_{50}$  values were measured to screen for inhibition potency. The  $IC_{50}$  values in submicromolar range proved the inhibition potency for all dual-cage cobalt bis(dicarbollide) compounds. Significantly higher  $IC_{50}$  values for compound **14** provided evidence for the requirement of a bulkier cobalt bis(dicarbollide) moiety for effective inhibition of HIV PR.

Inhibition mechanism was determined using double reciprocal Lineweaver–Burk plot<sup>17</sup> (Figure S1 in Supporting Information). The tested compounds exhibited various inhibition types: competitive, noncompetitive, and for four compounds **2, 9, 10, and 12**, the inhibition mechanism was dependent on the compound concentration (Table 1). At low concentrations, the inhibition mechanism was noncompetitive or mixed, and with the increasing concentration the mechanism shifted toward the competitive mode (Figure S1C in Supporting Information).

For six compounds with competitive mode of inhibition, inhibition constants ( $K_i$  values) were determined (Table 1). These values can be directly compared in order to draw conclusions on the relation between compound structure and inhibition efficiency. Connection of the two parental cobalt bis(dicarbollide) clusters with a hydrophilic linker in **1** resulted in an approximately 14-fold improvement of the  $K_i$  value compared to value for parent cobalt bis(1,2-dicarbollide) ion.<sup>4</sup> Further improvement of the in vitro inhibitory potency (about two times lower  $K_i$  values) was attained by subsequent substitutions of the central secondary amino group of the linker by small hydrophobic groups, e.g., the butyl moiety in **3** or *tert*-butyl (1,1-dimethylethyl) moiety in **5**. The addition of small substituents with a polar group (e.g., hydroxyethyl in **4** or carboxypropyl in **7**) had no significant effect on the  $K_i$  value. Interestingly, the addition of a bridged cobalt(III) bis (dicarbollide) substituent in **13** significantly improved the inhibitory efficiency ( $K_i$  values lowered 20 times compared to **1**).

The inhibition potency against resistant HIV PR variants was tested for selected competitive inhibitors from this series and seven HIV PR variants representing enzyme mutations for various FDA-approved protease inhibitors. Four of the HIV PR variants (PR1–4, Figure 1) used in the inhibition assay were prepared by site-directed mutagenesis, whereas three highly resistant HIV PR species (PR5–7, Figure 1) were amplified from HIV-positive patients failing antiretroviral therapy with HIV PR inhibitors. In Figure 1, the resistance profile for four compounds is expressed as a

**Table 1.** Structures and Inhibitory Constants of Metallocarborane Inhibitors of HIV-1 PR

General formula <sup>a</sup>			14 <sup>a</sup>		
Compound description			in vitro enzyme assay		
No.	R <sup>1</sup>	R <sup>2</sup>	IC <sub>50</sub>	Mechanism	K <sub>i</sub> (nM)
1	H	H	140 nM	competitive	4.9 ± 2.1
2			160 μM	concentration dependent <sup>b</sup>	N.D.
3		H	100 nM	competitive	2.2 ± 1.2
4		H	140 nM	competitive	4.7 ± 1.2
5		H	130 nM	competitive	2.7 ± 1.1
6		H	190 nM	noncompetitive	N.D.
7		H	110 nM	competitive	4.2 ± 1.5
8		H	110 nM	noncompetitive	N.D.
9		H	140 nM	concentration dependent <sup>b</sup>	N.D.
10		none	70 nM	concentration dependent <sup>b</sup>	N.D.
11 <sup>c</sup>		H	50 nM	noncompetitive	N.D.
12 <sup>c</sup>		H	58 nM	concentration dependent <sup>b</sup>	N.D.
13 <sup>c</sup>			250 nM	competitive	0.27 ± 0.33
14	see Fig. above		8.5 μM	N.D.	N.D.

<sup>a</sup> Color coding: orange, BH groups or B (if substituted); black, CH groups or C (if substituted); blue, Co atom. <sup>b</sup> With the increasing concentration, the inhibition mechanism changes from noncompetitive through mixed toward competitive. <sup>c</sup> The carborane or metallocarborane cluster substituents are covalently bound to the central nitrogen atom of the linker in the case of compound 13 by a bridging manner.

vitality value representing a measure of the relative capacity of the mutated enzyme to cleave its substrate in the presence of an inhibitor.<sup>18</sup> For comparison, seven clinically used inhibitors (saquinavir, indinavir, nelfinavir, lopinavir, amprenavir, atazanavir, and darunavir) were included in our inhibition assay. Tested cobaltacarborane compounds show low relative loss of activity as indicated by low values of vitalities for all tested HIV-1 PR variants and proved thus to be specific inhibitors of the mutated HIV-1 PRs. Similar inhibition profiles were obtained previously for 3, 1, and other cobaltacarborane compounds and the molecular mechanism of inhibition potency toward PI-resistant HIV PR species was studied by molecular

modeling.<sup>14</sup> Strikingly, the compound 13, which shows the highest in vitro inhibitory efficiency, loses its potency against four of the tested HIV PR variants. The vitality values could not be determined for compound 13 and proteases PR6 and PR7 because the inhibitor concentration needed to inhibit these enzyme variants was above the compound solubility limit. This, however, indicates high resistance of PR6 and PR7 species against 13. Interestingly, the comparison of values for PR2 and PR3 variants (differing only by the presence or absence of mutation M46I, respectively) shows 4.5-fold increase in vitality value for PR2. This suggests a role of residue 46 in compound 3 binding.

**Crystal Structure.** To gain structural information on binding of metallocarborane compounds containing two linked cobalt bis(1,2-dicarbollide) clusters to the HIV PR, we have determined the crystal structure of wild-type HIV-1 PR in complex with the parent compound of this series, the inhibitor **1**. Crystals of the complex exhibited the symmetry of orthorhombic space group  $C222$  and contained one protease monomer in the asymmetric unit with a solvent content of 50%. The crystal structure was determined by molecular replacement and was refined using data to 1.7 Å resolution. The final model contains complete HIV-1 PR monomer (99 residues) and 23 non-hydrogen atoms of one cobalt bis(1,2-dicarbollide) cluster of the compound **1**. The biologically relevant unit, the HIV PR dimer, can be generated through crystal symmetry operations (rotation along 2-fold axis, Figure 2A). In addition to dimer, a crystallographic tetramer with two dimers arranged head-to-head

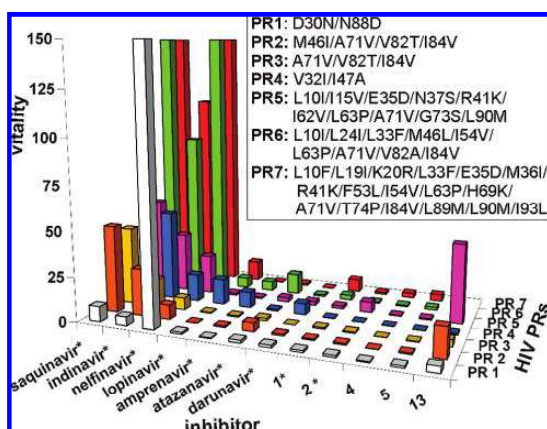


**Figure 1.** Vitality values of seven clinical inhibitors and five cobalt-tacarborane compounds analyzed with the panel of HIV-1 PR resistant species. Mutations in HIV-1 PR variants are shown in the figure inset. The vitality<sup>18</sup> is defined as  $(K_i k_{cat}/K_m)_{MUT}/(K_i k_{cat}/K_m)_{WT}$ , where MUT and WT are mutated and wild-type enzyme variant, respectively. The vitality values could not be determined for compound **13** and proteases PR6 and PR7 because the inhibitor concentration needed to inhibit these enzyme variants was above the compound solubility limit. Enzyme characteristics and  $K_i$  values are summarized in Tables S1 and S2 in Supporting Information. The asterisks mark data published in our previous work.<sup>14</sup>

by their active sites is also observed for this structure. This crystal packing was also present in previously determined crystal structure of HIV PR in complex with the parent cobalt bis(1,2-dicarbollide) ion (PDB code 1ZTZ<sup>4</sup>). The biological relevance of this crystallographic oligomer in solution, however, remains to be addressed by further studies.

Overall, the enzyme structure resembles the structure of an apoenzyme with open flap conformation rather than closed conformation typical for complexes with active-site inhibitors; however, the conformation of the flaps' tips (residues 47–55) is unique. The cobalt bis(1,2-dicarbollide) cluster of **1** could be modeled into well-defined electron density, however, no continuous map for the linker connecting the two cobalt bis(1,2-dicarbollide) clusters of **1** was observed (Figure 2B). This part is thus missing in the final crystallographic structure. The fact that the linker is disordered in the crystal structure of the PR:**1** complex suggests that it is inherently flexible and is able to adopt alternative conformations. To determine which of these **1** conformers would be energetically feasible in the enzyme cavity, we employed computational procedures.

Comparison of the HIV PR:**1** complex with the previously determined crystal structure of HIV PR in complex with the parent cobalt bis(1,2-dicarbollide) ion (PDB code 1ZTZ<sup>4</sup>) revealed an overall similar inhibitor binding mode but uncovered numerous differences in protein–inhibitor interactions. The overall deviation (rmsd) of the main-chain atoms of HIV PR dimers in **1** and cobalt bis(1,2-dicarbollide) ion complexes is 0.87 Å, suggesting that the inhibitor binding slightly alters the protein structure. Significant structural differences (with the rmsd values for main-chain atoms  $>0.7$  Å<sup>19</sup>) are localized in the tip of flap residues 46–55 (Figure 3) and solvent exposed inherently flexible surface loop (residues 66–71).

In both crystal structures, the cobalt bis(1,2-dicarbollide) cluster occupies a hydrophobic pocket whose bottom is formed by enzyme residues Pro81, Val82, and Ile84 and is covered by the flap residues Ile47, Gly48, and Ile54. This site corresponds approximately to S3 and S3' substrate-binding subsites. Two cobalt bis(1,2-dicarbollide) clusters bind to HIV PR dimer, and their binding blocks the closing of the two flexible flaps over the enzyme active site (Figure 3A).

While the HIV PR complex structure with parent cobalt bis(dicarbollide) ion shows an asymmetric binding of the two

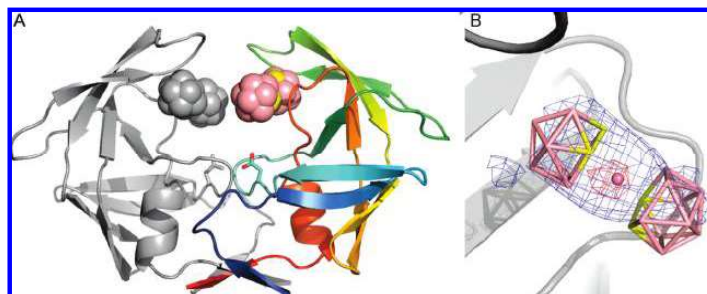


**Figure 2.** (A) Overall view of the crystal structure of the HIV PR:**1** complex. The HIV PR main-chain is represented as a cartoon with catalytic aspartates shown in sticks. Atoms of cobalt bis(1,2-dicarbollide) cluster of **1** are shown as spheres with boron and carbon atoms colored pink and yellow, respectively. One HIV PR monomer with cobalt bis(1,2-dicarbollide) cluster of **1** present in the crystal asymmetric unit is represented in rainbow coloring (N-terminus blue, C-terminus red), while gray colors represent the symmetrically related molecule. (B) Close view on the **1** cobalt bis(1,2-dicarbollide) cluster bound to HIV PR monomer with  $F_o - F_c$  omit map contoured at  $2.0\sigma$  (blue) and  $8.0\sigma$  (red).



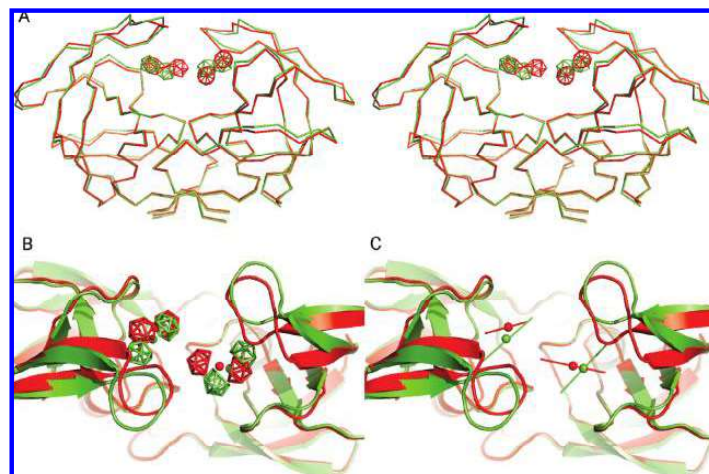


**Figure 3.** Comparison of cobalt bis(1,2-dicarbollide) ion and **1**:HIV-1 PR complex structures. (A) Stereo view of a superposition of the overall structures of HIV-1 PR with cobalt bis(dicarbollide) ion (PDB code 1ZTZ<sup>4</sup>) and **1** compounds, respectively, bound to the enzyme dimer. The enzyme is represented by its C $\alpha$  trace, and cobaltacarboranes are shown as sticks. HIV PR:cobalt bis(1,2-dicarbollide) ion and HIV:**1** complexes are colored red and green, respectively. The linker connecting two cobaltacarborane clusters in **1** is disordered and thus missing in the crystallographic model. (B) Close-up top view into the enzyme active site showing differences in HIV PR:cobalt bis(1,2-dicarbollide) ion (red) and HIV PR:**1** (green) structures. Carbon and boron atoms in cobaltacarboranes are shown as sticks with central cobalt atom represented by a sphere. (C) Same view and color coding as in (B). Cobalt bis(1,2-dicarbollide) clusters are represented by their longitudinal axes with the central cobalt atom shown as a sphere.

cobalt bis(1,2-dicarbollide) clusters into two symmetrical binding sites present in the enzyme dimer, in the HIV PR:**1** complex, the two cobalt bis(1,2-dicarbollide) clusters of **1** occupy their binding sites symmetrically. The symmetry in binding of the two clusters of **1** into the symmetric protease dimer is also reflected in higher symmetry of the HIV PR:**1** crystals. The HIV PR:cobalt bis(dicarbollide) crystals belonged to the monoclinic space group *C2* with one protease dimer related by noncrystallographic 2-fold axis in one asymmetric unit.<sup>4</sup> On the other hand, the HIV PR:**1** crystallized in the orthorhombic space group *C222* with a crystallographic 2-fold axis relating the two protease monomers with bound metallacarborane cluster of **1**.

Although the inhibitor binding site is conserved in both complexes, the orientation of the parent metallacarborane cluster and **1** differ (Figure 3B). The clusters' central cobalt atoms in **1** are shifted by 1.5 and 1.3 Å compared to the corresponding atoms in parent bis(1,2-dicarbollide) cluster. Also, the **1** clusters are rotated by 37 and 44° with respect to the two clusters of bis(1,2-dicarbollide) ion. As a result of these cluster position rearrangements, the extent of interactions with individual protein residues differs. Compound **1** forms more interactions with flap residues (Ile 47, Gly 48, and Ile 54) than with the bottom of the binding site.

**Binding Mode of the Linker in 1.** Molecular modeling and calculations were employed to explore the conformational space of the inherently flexible linker of **1**. By use of molecular-dynamics based quenching technique (MD/Q) (for details, see Supporting Information), accessible conformations of the **1** linker within the HIV PR active site were computationally sampled. Quantum mechanics/molecular mechanics (QM/MM) optimizations for 20 snapshots from the MD/Q protocol resulted in a set of conformers differing substantially in energy (differences up to 40 kcal/mol). On the basis of a criterion of copopulation/interchangeability in the enzyme–inhibitor complex, we selected five lowest-energy

structures differing in the linker conformation with an energy span of at most 3 kcal/mol (for a discussion of the energy cutoff, see ref 20). These five **1** conformers shared the common position of the central nitrogen atom of the linker secondary amino group. Interestingly, in the crystal structure, a spherical electron density is noticeable in the vicinity of this predicted nitrogen atom position (distance of 1.5–3.4 Å). This electron density was modeled in the crystal structure as a water molecule (W110). However, this electron density peak can also be explained by a common position of the central nitrogen atom shared by various conformations of the disordered linker. Further refinement of the models was therefore carried out using QM/MM calculations, where the central nitrogen atom was constrained to the position of the spherical electron density map yielding the final predicted linker conformations. Four resulting lowest-energy conformers fall within the range of 3 kcal/mol and are thus predicted to be copopulated in the complex structure (Figure 4A).

## Discussion

In this study, we focused on substituted cobalt bis(dicarbollides) as specific inhibitors of HIV PR.<sup>4</sup> We explored the inhibition properties of compounds based on the parent formula [H<sub>2</sub>N-(8-(C<sub>2</sub>H<sub>4</sub>O)<sub>2</sub>-1,2-C<sub>2</sub>B<sub>9</sub>H<sub>10</sub>)(1',2'-C<sub>2</sub>B<sub>9</sub>H<sub>11</sub>-3,3'-Co)<sub>2</sub>]Na (compound **1**, Table 1). In an attempt to map steric requirements of substituents at the central nitrogen atom as well as the influence of the hydrogen bonding potential on the activity of compounds, we focused on the substitution of the central part by a variety of groups differing in functionality/bulkiness/charge of the substituent. We used reactions on a cobalt bis(dicarbollide)(1–) cage (Scheme 1), based on Plešek's original synthetic concept,<sup>21,22</sup> which have recently become a versatile approach for incorporating metallaborane clusters into various functional molecules and materials (see Semioshkin et al., 2008, for a recent review<sup>23</sup>).

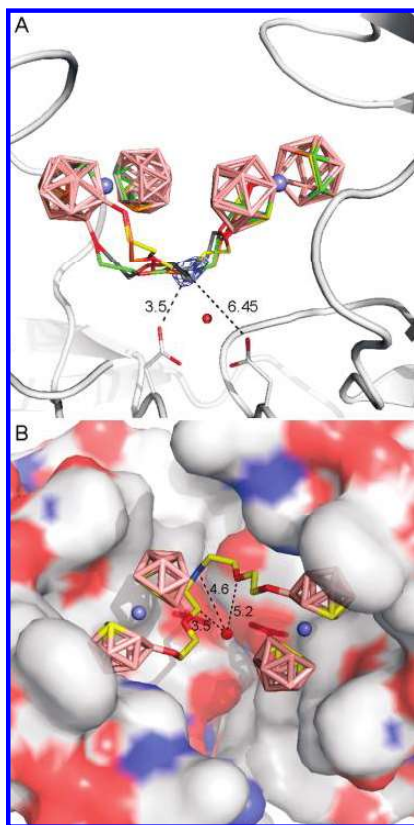


**Figure 4.** Molecular modeling of the **1** linker. (A) The four lowest-energy **1** conformers obtained from molecular modeling and calculations are represented by stick model with differentially colored carbon atoms and oxygen atoms in red. Boron and cobalt atoms are colored pink and blue, respectively. The  $2F_o - F_c$  map modeled as a water molecule in the crystallographic model is shown at  $1.0 \sigma$ . The position of this water molecule (shown as gray sphere) was used to fix the position of the nitrogen atom of the linker's central secondary amino group. The dashed lines and numbers represent the distances to catalytic aspartates (in Å), catalytic water is shown as a red sphere. (B) Top view into the HIV PR active site with the lowest energy model of the compound **1** linker. Protease is represented by its solvent accessible surface colored by the atom type (carbon gray, oxygen red, and nitrogen blue). The closest distances between linker atoms and the catalytic water (red sphere) are shown as dashed lines and numbers (in Å).

The *in vitro* inhibition assays proved their inhibition efficiency toward wild-type HIV PR as well as toward resistant variants. Strikingly, it also revealed various modes of inhibition for various compounds in our series: competitive, mixed, and noncompetitive.

The competitive mode of inhibition implies that the inhibitor competes with the substrate for binding to the enzyme active site. This mode of action is supported by previously published crystal structure of the parent bis(1,2-dicarbollide) ion<sup>4</sup> bound to the active site of HIV PR as well as by the crystal structure of compound **1**:enzyme complex presented in this work.

Mixed and noncompetitive types of inhibition might suggest specific binding of compounds outside the enzyme active site. The binding site most likely involves a functionally

important part of the enzyme other than the active site, i.e., the dimerization interface or the flap region. A noncompetitive mode of inhibition might also be explained by the activity of inhibitor aggregates that bind outside of the enzyme active site cavity. The aggregation behavior of cobalt bis(dicarbollides) in solution was previously described and studied in detail.<sup>24</sup> Light scattering and atomic force microscopy techniques revealed that the behavior of aggregates of cobalt(III) bis(1,2-dicarbollide) compounds in aqueous solutions is fairly complex and depends on numerous factors, including compound concentration.<sup>24,25</sup> Interestingly, the formation of larger aggregates upon dilution of cobalt bis(dicarbollide) ion solutions was observed.<sup>25</sup> Indeed, for some compounds in this study, we observed concentration-dependent inhibition mode. For high compound concentration, the inhibition mechanism was distinctly competitive, while for low compound concentration, the transition to mixed and noncompetitive inhibition mechanism was obvious (Figure S1C3 in Supporting Information). Potential binding of the aggregates to the enzyme, however, must be tested experimentally and will be a subject of our further studies.

The X-ray structure of **1** bound to the wild-type HIV-1 PR is the second structure of this enzyme with bound metalla-carborane in the active site. Although the linker part of **1** molecule is disordered in our crystal structures, the position of cobalt bis(1,2-dicarbollide) cluster and especially the position of the sandwiched cobalt atom was supported by well-defined electron density maps (Figure 2B). This map was used to model and refine one bis(1,2-dicarbollide) cluster to one enzyme monomer in the asymmetric unit. The average atomic displacement parameter (ADP) for the cluster atoms is higher by about 35% compared to the average ADP for the protein atoms (52 vs 38.2 Å<sup>2</sup>), suggesting partial static or dynamic disorder of this part within the crystal. Comparison with our previous structure of HIV-1 PR in complex with parent cobalt bis(dicarbollide) ion<sup>4</sup> revealed that the metalla-carborane cluster can acquire various positions within the common inhibitor binding site. Freedom in positions was indeed already proposed from modeling of parent cobalt bis(dicarbollide)(1<sup>-</sup>) binding into resistant protease species with mutations in S3 and S3' substrate-binding subsites.<sup>14</sup>

Computational procedures helped us to model the position of the linker connecting two cobalt bis(1,2-dicarbollide) clusters of **1**. Because of the inherent flexibility of the linker of **1** within the HIV PR active site cavity, there is no continuous experimental electron density for the linker. The set of alternative models with similar energy shared a common position of the nitrogen atom of the linker's central secondary amino group, which is corroborated by the presence of electron density map peak in our crystal structure. The linker is placed asymmetrically within the symmetric cavity of the enzyme active site (with symmetrically bound metalla-carborane clusters). The central nitrogen is within hydrogen bonding distance of 3.5 Å with one of the two catalytic aspartates (Figure 4A) and in a distance of 4.6 Å from the catalytic water (Figure 4B). Another possible hydrogen bonding partner is the main-chain carbonyl oxygen of Gly27 (distance 3.6 Å). The position of the linker in our model allows an opportunity for small substituents on the central amino group to be placed into the hydrophobic groove formed by Val82, Ile84, Leu10, and Leu23 (pointing "upwards" in Figure 4B) or even deeper into the dimeric interface and perhaps result in mixed inhibition by disrupting the active protease dimer. Another option for the substituent binding is to replace catalytic water and

occupy the polar pocket formed by the catalytic aspartate dyad (Figure 4B).

Our model can be used to propose potential binding mode of the compounds with the competitive mode of inhibition (Table 1). The nonpolar substituents of **2** and **5** could be accommodated in the hydrophobic pocket, and this interaction could account for the slight increase in their inhibition potency compared to compound **1**. To accommodate the *tert*-butyl moiety of **5** into the rather narrow hydrophobic groove structural rearrangements in PR would have to occur to achieve a productive binding conformation. The polar chains of **4** and **7** could fit well into the polar groove with a possibility of hydrogen bonding interactions to the catalytic aspartates. Our model is unable to explain binding of the compound **13**, as modeling of the bulky metallacarborane substituent produces sterical clashes with PR. Larger structural rearrangements in PR as well as in the compound **13** are needed for inhibitor binding. The binding mode of compound **13** probably differs substantially from the other substituent in our series. This is, indeed, indicated by the differential resistance profile of **13** (Figure 1) compared to other metallacarborane competitive inhibitors. To evaluate our hypotheses, the enzyme–inhibitor cocrystal structures are needed. However, our current models can be used in future compound optimization and design. Specifically, in our future design we will address the issue of optimal size and flexibility of the linker and also focus our optimization effort on improving physicochemical properties of the compounds to increase solubility and prevent aggregation.

In conclusion, our structure-based design led to the development of HIV PR inhibitors utilizing a novel boron-cage scaffold. Our X-ray structure analysis and modeling of a protein–inhibitor complex uncovered potentially important molecular interactions useful in the design of more potent inhibitors based on substituted cobalt bis(dicarbollides).

## Experimental Procedures

**Chemical Syntheses. Instrumental Methods Used for Compounds Characterization and Purity Check.** A combination of instrumental methods was used for identification, characterization, and purity check of all compounds. The  $^1\text{H}$  and  $^{11}\text{B}$  and  $^{13}\text{C}$  NMR spectra were recorded on Varian Mercury 400 Plus instrument. The spectral pattern and peak intensities corresponded to a particular structure and substitution pattern on each cluster molecule. Mass spectrometry measurements were carried out on a Thermo-Finnigan LCQ-Fleet ion trap instrument using electrospray ionization (ESI) in a negative mode. In most cases, negative ions corresponding to the molecular ion were observed with 100% abundance for the highest peak in the isotopic distribution plot. Molecular ions  $[\text{M}]^-$  were detected for all univalent anions (compounds **1–6**, **9**, and **14**).  $[\text{M}]^{2-}$  and  $[\text{M} + \text{H}]^-$  or  $[\text{M} + \text{Na}]^-$  ions were observed for the divalent anions (compounds **7**, **8**, and **10–13**). The isotopic distribution in the boron plot of  $[\text{M}]^{2-}$  peaks was in agreement with the charge, showing distances of 1/2 mass units for dianionic compounds. Full agreement of the experimental and calculated isotopic distribution pattern was observed for all the compounds.

As previously verified, the data of elemental analyses of sodium salts of cobalt bis(dicarbollides) are often misleading due to variable content of water or other solvent molecules associated with the cation and cannot be considered as appropriate criterion of purity.<sup>26</sup> The identity of the reported compounds has been unambiguously proven by their spectral data and the purity assessed by analytical HPLC. A Merck-Hitachi HPLC system LaChrom 7000 series was used through the study employing an Ion-Pair RP chromatographic method with an

isocratic elution based on the methods previously reported<sup>27</sup> for the separation of hydrophobic borate anions. The purity of all compounds, as determined by HPLC, was better than 98.0%.

**Chemical Syntheses of Inhibitors (General Procedure).** The synthesis of **1** and **3** was already reported in the previous paper along with the corresponding data for the compound's characterization.<sup>4</sup> The general methods for the synthesis of double-cluster cobalt bis(1,2-dicarbollide) compounds consisted from ring cleavage of the  $[(8\text{-O}(\text{C}_2\text{H}_4)_2\text{O}-1,2\text{-C}_2\text{B}_9\text{H}_{10})\text{-}(1',2'\text{-C}_2\text{B}_9\text{H}_{11})\text{-}3,3'\text{-Co}]^0$  (8-dioxane-**1**) by amines.

The starting cobalt bis(dicarbollide) building block (8-dioxane-**1**, 165 mg, 0.40 mmol) was dissolved in toluene/DME (3:1, 10 mL) solvent mixture and stirred with the respective amine (0.41 mmol) in the same solvent (10 mL) at room temperature. The reaction course was monitored on TLC until the spot of the starting 8-dioxane-**1** disappeared. The intermediate products, i.e., the respective hydrogen 8-(XNH<sub>2</sub>-3-oxa-pentoxo)-3-cobalt bis(1,2-dicarbollide)ate zwitterions were not isolated, but their solutions were directly stirred with NaH 22 mg (dry, 96%, 0.84 mmol) for 2 h. Then one additional equivalent of 8-dioxane-**1** (165 mg, 0.41 mmol) in toluene/DME solution (3:1 v/v, 10 mL) was added dropwise from a syringe and the reaction mixture was stirred 12–16 h at ambient temperature when the spot of 8-dioxane-**1** on TLC diminished. The reaction was quenched by careful addition of methanol (1 mL). Water was added (2 mL) and the resulting solution was neutralized with few drops of acetic acid (1.0 M), and solvents were removed in vacuum. The crude products were dissolved in Et<sub>2</sub>O (25 mL) and shaken with water (2 × 20 mL). The organic layer was filtered, and the solvent was removed under reduced pressure. The purification of the crude product was accomplished by successive column chromatography over silica gel using CH<sub>2</sub>Cl<sub>2</sub>–CH<sub>3</sub>CN mixture (1:4 to 1:3 v/v) as the mobile phase, eventually by crystallization from CH<sub>2</sub>Cl<sub>2</sub> (with few drops of CH<sub>3</sub>OH until dissolution) upon layering with hexane.

Representative examples of compound preparations and their spectral data are summarized below. For yields, NMR, MS, and other data were used for characterization of remaining compounds (see the Supporting Information).

**Sodium Diethylimino Bis-8,8-[5-(3-oxa-pentoxo)-3-cobalt Bis-(1,2-dicarbollide)]diate (1<sup>-</sup>),  $[(\text{C}_2\text{H}_5)_2\text{N}-(8-(\text{C}_2\text{H}_4\text{O})_2-1,2\text{-C}_2\text{B}_9\text{H}_{10})(1',2'\text{-C}_2\text{B}_9\text{H}_{11})\text{-}3,3'\text{-Co}]_2\text{Na}$ , **2**.** Diethylamine was used for the ring cleavage. Yield 305 mg (83%); mp 268 °C (decomp.); TLC (acetonitrile/chloroform 1:2 v/v);  $R_F = 0.27$  (CHCl<sub>3</sub>:CH<sub>3</sub>CN, 2:1); HPLC  $k' = 6.04$ ; MS-ESI ( $m/z$ ): 894.82 (100%) calcd 894.75, 899.78 (2%)  $[\text{M}]^-$  calcd 999.73.  $^1\text{H}$  ( $^{11}\text{B}$ ) NMR (400 MHz, acetone-*d*<sub>6</sub>), [ $^1\text{H}$  ( $^{11}\text{B}_{\text{selective}}$ ) in square brackets]:  $\delta$  4.167 (s, 4H, CH<sub>carb</sub>), 4.092 (s, 4H, CH<sub>carb</sub>), 4.035 (br t,  $J = 4.0$ , 4H, OCH<sub>2</sub>–CH<sub>2</sub>O), 3.746 (t,  $J = 4.4$ , 4H, O–CH<sub>2</sub>–CH<sub>2</sub>O), 3.698 (q,  $J = 7.1$ , 4H, CH<sub>3</sub>–CH<sub>2</sub>–N), 3.627 (t,  $J = 4.6$ , 4H, OCH<sub>2</sub>–CH<sub>2</sub>O), 3.597 (m,  $J = 4.8$ , 4H, O–CH<sub>2</sub>–CH<sub>2</sub>–N), 1.418 (t,  $J = 7.2$ , 6H, CH<sub>3</sub>–N); [2.92] (H10'), [2.79] (H8'), [2.71] (H4', 7'), [2.68] (H10), [2.95 s, 2.05 s, 1.84 s] (H 4, 7, 9, 12, 9', 12'), [1.68] (H6'), [1.62] (H5', 11'), [1.55] (H5, 11), [1.45] (H6).  $^{13}\text{C}$  ( $^1\text{H}$ ) NMR (100 MHz, acetone-*d*<sub>6</sub>):  $\delta$  73.07 (CH<sub>2</sub>–O), 69.75 (CH<sub>2</sub>–O), 65.19 (CH<sub>2</sub>–O), 56.2, 55.5 (CH<sub>2</sub>–N), 54.23 (CH<sub>carb</sub>), 47.45 (CH<sub>carb</sub>), 19.91 (–CH<sub>3</sub>).  $^{11}\text{B}$  NMR (128 MHz, acetone-*d*<sub>6</sub>):  $\delta$  23.89 (s, 2B, B8), 5.48 (d,  $J = 137$ , 2B, B8'), 0.42 (d,  $J = 150$ , 2B, B10'), –2.63 (d,  $J = 150$ , 2B, B10), –4.55 (d,  $J = 149$ , B4', 7'), –7.05 d, –7.67 (2d, overlap B9, 12, 9', 12'), –17.30 (d,  $J = 159$ , 4B, B5', 11'), –20.15 (d,  $J = 161$ , 4B, B5, 11), –22.25 (d,  $J = 158$ , 2B, B6'), –28.73 (d,  $J$  (B,H) = 140, 2B, B6).

**Sodium Hydrogen 2-Hydroxyethylimino Bis-8,8-[5-(3-oxa-pentoxo)-3-cobalt Bis(1,2-dicarbollide)]diate (1<sup>-</sup>),  $[(\text{HOCH}_2\text{CH}_2)\text{-NH}-(8-(\text{C}_2\text{H}_4\text{O})_2-1,2\text{-C}_2\text{B}_9\text{H}_{10})(1',2'\text{-C}_2\text{B}_9\text{H}_{11})\text{-}3,3'\text{-Co}]_2\text{Na}$ , **4**.** Ethanolamine was used as the respective reagent. Yield of the sodium salt: 323 mg (89%). TLC (CHCl<sub>3</sub>/CH<sub>3</sub>CN 2:1 v/v)  $R_F = 0.22$ ; HPLC  $k' = 3.37$ ; MS 883.80 (100) (calc 883.71),  $m/z = 887.68$  (2)  $[\text{M}]^-$  (calc 887.68).  $^1\text{H}$  ( $^{11}\text{B}$ ) NMR [ $^1\text{H}$  ( $^{11}\text{B}_{\text{selective}}$ ) in square brackets], (400 MHz, acetone-*d*<sub>6</sub>):  $\delta$  7.82 br s (2H, NH),



**Table 2.** X-ray Crystallography Statistics<sup>a</sup>

Data Collection Statistics	
space group	C222
cell parameters (Å)	58.16, 92.34, 48.95
wavelength (Å)	0.975
resolution (Å)	50–1.7 (1.76–1.7)
unique reflections	14821
redundancy	8.2 (5.9)
completeness (%)	95.4 (70.1)
$R_{\text{merge}}^b$	4.9 (30.8)
average $I/\sigma(I)$	55.87 (4.3)
Wilson $B$ (Å <sup>2</sup> )	21.0
Refinement Statistics	
resolution range (Å)	23.8–1.7 (1.76–1.7)
no. of reflections in working set	13436 (694)
no. of reflections in test set	703 (30)
$R$ value (%) <sup>c</sup>	17.6 (24.3)
$R_{\text{free}}$ value (%) <sup>d</sup>	21.2 (29.5)
rmsd bond length (Å)	0.013
rmsd angle (deg)	3.76
no. of atoms in a.u.	945
protein atoms	806
ligand atoms	23
water molecules	111
mean $B$ value (Å <sup>2</sup> )	39.2
protein atoms ADP (Å <sup>2</sup> )	38.2
inhibitor atoms ADP (Å <sup>2</sup> )	52.1
solvent atoms ADP (Å <sup>2</sup> )	45.7
Ramachandran plot	
residues in favored regions (%)	96.2
residues in allowed regions (%)	3.8

<sup>a</sup> The data in parentheses refer to the highest-resolution shell. ADP, atomic displacement parameter. <sup>b</sup>  $R_{\text{merge}} = \sum_{hkl} \sum_i |I_i(hkl) - \langle I(hkl) \rangle| / \sum_{hkl} \sum_i I_i(hkl)$ , where the  $I_i(hkl)$  is an individual intensity of the  $i$ th observation of reflection  $hkl$  and  $\langle I(hkl) \rangle$  is the average intensity of reflection  $hkl$  with summation over all data. <sup>c</sup>  $R$  value =  $|F_o| - |F_c| / |F_o|$ , where  $F_o$  and  $F_c$  are the observed and calculated structure factor amplitudes, respectively. <sup>d</sup>  $R_{\text{free}}$  is equivalent to  $R$  value but is calculated for 5% of the reflections chosen at random and omitted from the refinement process.<sup>42</sup>

4.158 s (4H,  $\text{CH}_{\text{carb}}$ ), 4.095 s (4H,  $\text{CH}_{\text{carb}}$ ), 3.94 t (8H,  $^1J(\text{H,H}) = 5.6$  Hz, O- $\text{CH}_2$ - $\text{CH}_2$ -O), 3.749 m (4H, O- $\text{CH}_2$ - $\text{CH}_2$ -O), 3.749 m (6H, O- $\text{CH}_2$ - $\text{CH}_2$ -O; O- $\text{CH}_2$ - $\text{CH}_2$ -N), 3.53 t (5 Hz, 2H, O- $\text{CH}_2$ - $\text{CH}_2$ -N), [2.98] (H10'), [2.85] (H8') [2.69] (H4', 7'), [2.68] (H10), [2.95 s, 2.04 s, 1.84 s] (H 4, 7, 9, 12, 9', 12'), [1.68] (H6'), [1.61] (H5', 11'), [1.54] (H5, 11), [1.45] (H6). <sup>13</sup>C{<sup>1</sup>H} NMR (100 MHz, acetone- $d_6$ ):  $\delta$  72.99 (CH<sub>2</sub>-O), 69.73 (CH<sub>2</sub>-O), 65.11 (CH<sub>2</sub>-O), 56.31 (O- $\text{CH}_2$ - $\text{CH}_2$ -N), 54.65 (HO- $\text{CH}_2$ - $\text{CH}_2$ -N), 53.76 (CH<sub>carb</sub>), 53.25 (HO- $\text{CH}_2$ - $\text{CH}_2$ -N), 47.44 (CH<sub>carb</sub>). <sup>11</sup>B NMR (128 MHz, acetone- $d_6$ ):  $\delta$  24.01 (s, 2B, B8), 5.65 (d, 137 Hz, 2B, B8'), 0.42 (d, 142 Hz, 2B, B10'), -2.58 (d, 143 Hz, 2B, B10), -4.74 (d, 143 Hz, 4B, B4', 7') -7.00 (3d overlap, 12B, B4, 7, 9, 12, 9', 12'), -17.28 (d,  $^1J(\text{B,H}) = 156$  Hz, 4B, B5', 11'), -20.27 (d, 158 Hz, 4B, B5, 11), -22.22 (d, 173, Hz, 2B, B6'), -28.6 (d, 142 Hz, 2B, B6).

**Sodium Hydrogen 3-Cobalt-bis(1,2-dicarbollid)- $\mu$ -8,8'-yl-imino-bis-8,8-[5-(3-oxa-pentoxo)-3-cobalt Bis(1,2-dicarbollide)]diate (2-), [(1'',2''-C<sub>2</sub>B<sub>9</sub>H<sub>10</sub>)<sub>2</sub>-3'-Co)-8''- $\mu$ -N-(8-(C<sub>2</sub>H<sub>4</sub>O)<sub>2</sub>-1,2-C<sub>2</sub>B<sub>9</sub>H<sub>10</sub>)(1',2'-C<sub>2</sub>B<sub>9</sub>H<sub>10</sub>)-3,3'-Co)]Na<sub>2</sub>, 13.** The [8,8'- $\mu$ -NH<sub>2</sub>-(1,2-C<sub>2</sub>B<sub>9</sub>H<sub>10</sub>)<sub>2</sub>-3,3'-Co] bridge derivative<sup>4</sup> (135 mg, 0.40 mmol) was dissolved in toluene/DME (3:1, 15 mL) and treated with sodium hydride (22 mg, 0.84 mmol) under stirring for 2 h. Then solution of 8-dioxane-1 (165 mg, 0.41 mmol) in toluene/DME (3:1, 15 mL) was injected. After stirring for 16 h, an additional portion of sodium hydride (11 mg, 0.42 mmol) was added, followed by dropwise addition of the second equivalent of 8-dioxane-1 (165 mg, 0.41 mmol). The product was purified by chromatography and crystallization as described in general

synthetic method above. Yield 215 mg (45%); mp 243 °C; TLC (acetonitrile/ chloroform 1:2 v/v)  $R_F = 0.20$ ; HPLC  $k' = 2.20$ ; MS 579.25 (100),  $m/z = 581.90$  (8) [M]<sup>2-</sup> (calc 581.92), (4); 1180.88 (55), 1190.89 (1) [M + Na]<sup>-</sup> (calc 1190.88). <sup>1</sup>H {<sup>11</sup>B} NMR (400 MHz, CD<sub>3</sub>CN) [<sup>1</sup>H{<sup>11</sup>B<sub>selective</sub>} in square brackets]:  $\delta$  4.186 (s, 4H, CH<sub>carb</sub>), 4.123 (s, 4H, CH<sub>carb</sub>), 3.727 (t,  $J = 6.0$ , 4H, O- $\text{CH}_2$ - $\text{CH}_2$ -O), 3.608 (s, 4H, CH<sub>carb</sub>), 3.481 (t,  $J = 4.2$ , 4H, OCH<sub>2</sub>- $\text{CH}_2$ -O), 3.399 (t,  $J = 4.3$ , 4H, O- $\text{CH}_2$ - $\text{CH}_2$ -O), 3.204 br. (s, 4H, O- $\text{CH}_2$ - $\text{CH}_2$ -N); [3.72, 3.49] (H4'', 7'', 9'', 12''), [3.4] (H10''), [2.79] (H10'), [2.606] (H10), [2.57] (H4', 7'), [2.42] (H8'), [2.78, 1.88 s, 1.62 s] (H 4, 7, 9, 12, 9', 12'), [1.66] (H5'', 11''), [1.62] (H6'), [1.57] (H5', 11'), [1.54] (H6''), [1.47] (H5, 11), [1.45] (H6). <sup>13</sup>C{<sup>1</sup>H} NMR, (100 MHz, CD<sub>3</sub>CN):  $\delta$  72.90 (CH<sub>2</sub>-O), 69.10 (CH<sub>2</sub>-O), 65.30 (CH<sub>2</sub>-O), 56.08 (CH<sub>2</sub>-N), 54.93 (4C, CH<sub>carb</sub>), 47.57 (8C, CH<sub>carb</sub>). <sup>11</sup>B NMR (128 MHz, CD<sub>3</sub>CN):  $\delta$  22.97 (s, 2B, B8), 9.64 (s, 2B, B8'), 3.74 (d,  $J = 138$ , 2B, B8'), -0.58 (d,  $J = 142$ , 2B, B10'), -0.85 (d, overlap, 2B, B10'), -2.65 (d,  $J = 153$ , 2B, B10), -4.81 (d,  $J = 144$ , 2B, B4', 7'), -8.174 (d, overlap, 16B, B9, 12, 9', 12', 4', 7', 9', 12''), 15.8 d (d, 2B, B5', 11'), -17.44 (d,  $J = 153$ , 4B, B5', 11'), -20.53 (d,  $J = 153$ , 4B, B5, 11), -21.8 (d,  $J = 164$ , 2B, B6'), -24.5 (br d, 2B, B6''), -28.43 (d,  $J = 162$ , 2B, B6).

**Enzymes.** For enzymatic assays, wild-type HIV-1 PR and its resistant variants were used. Resistant PRs were prepared by site-directed mutagenesis (HIV-1 PR 1–3) as described earlier<sup>28</sup> or selected under pressure of clinically used PIs (HIV-1 PR 4–6).<sup>29</sup> For crystallographic studies, HIV-1 PR variant bearing three mutations (Q7K, L33I, L63I) that minimize the autoproteolytic cleavage without changing other enzyme properties<sup>30</sup> was used. The expression, refolding, and purification of HIV-1 PR were performed as described previously.<sup>28</sup>

**Enzymatic Assays.** The inhibition analyses were performed by spectrophotometric assay using the chromogenic peptide substrate KARVNle\*NpHEANle-NH<sub>2</sub> as previously described.<sup>28</sup>

Substrate was added to final concentration near the  $K_m$  of the enzyme to 1 mL of 0.1 M sodium acetate buffer, pH 4.7, 0.3 M NaCl containing 6–8 pmol of PR and various concentrations of inhibitor dissolved in DMSO. The final concentrations of DMSO were kept below 2.5% (v/v). Substrate hydrolysis was followed as a decrease in absorbance at 305 nm using a UNICAM UV500 UV-vis spectrophotometer (Thermo, Cambridge, MA). The data were analyzed using the equation for competitive inhibition according to Williams and Morrison.<sup>31</sup> IC<sub>50</sub> values were calculated for a given inhibitors by determining concentration needed to lower the initial HIV PR activity velocity to half using GraFit 5 software. The mechanism of inhibition was determined by Lineweaver–Burk plot.<sup>17</sup> Double reciprocal fits of initial rates versus concentration of substrate carried out at three fixed inhibitor concentrations were overlaid and yielded a pattern of lines characteristic of a particular mode of inhibition (Supporting Information).

**Crystallographic Analysis.** The complex for crystallization was prepared by mixing HIV-1 PR with 5-fold molar excess of compound 1 dissolved in DMSO. The complex was concentrated by ultrafiltration using Microcon-10 (Millipore) to concentration 7–9 mg/mL, and initial crystallization conditions were obtained by the vapor diffusion method in hanging drop mode using Wizard I and II crystallization screens (Emerald Biostructures). Optimal crystals were prepared by mixing 1  $\mu$ L of protein at 7 mg/mL (in buffer containing 50 mM sodium phosphate pH 6.5, 75 mM sodium chloride, 1 mM EDTA, 0.05% (v/v)  $\beta$ -mercaptoethanol, and 20% (v/v) glycerol) with 1  $\mu$ L of reservoir solution (0.1 M *N*-cyclohexyl-3-aminopropanesulfonic acid (CAPS) pH 10.5, 1.2 M sodium dihydrogen phosphate, 0.2 M potassium hydrogen phosphate, and 0.2 M lithium sulfate, final pH 6.0) and equilibration at 20 °C over 1 mL of reservoir solution.

Plate-like crystals grew to final size of 0.25  $\times$  0.2  $\times$  0.08 mm<sup>3</sup> within 3 days. For cryoprotection, the crystals were transferred into reservoir solution supplemented with 20% (v/v) ethylene

glycol, flash-cooled by plunging into liquid nitrogen and stored in liquid nitrogen until used for X-ray diffraction experiments.

Diffraction data were collected at 100 K at beamline 19-ID of the Structural Biology Center at the Advanced Photon Source, Argonne National Laboratory, Argonne, IL. Diffraction data were processed using the HKL-3000 suite of programs.<sup>32</sup> Crystal parameters and data collection statistics are given in Table 2.

The structure solution and refinement were performed using CCP4 program suite<sup>33</sup> graphical interface. HIV PR structure was solved by molecular replacement with the program MolRep<sup>34</sup> using protease monomer from Protein Data Bank structure 1ZTZ<sup>4</sup>. Initial  $F_o - F_c$  difference Fourier map clearly showed presence of high positive maxima in the enzyme active cavity, indicating position of cobalt atom present in compound **1**. At this stage, the metallacarborane cluster of **1** was included into the model and the model was subjected to consecutive cycles of refinement using program Refmac<sup>35</sup> and model building using program Coot.<sup>36</sup> The final steps included TLS refinement.<sup>37</sup> Atomic coordinates and experimental structure factors have been deposited with the Protein Data Bank with the code 3I8W. Refinement statistics is given in Table 2. The quality of the final model was validated with Molprobity.<sup>38</sup> All figures showing structural representations were prepared with the programs PyMOL.<sup>39</sup> The following services were used to analyze the structures: PISA server<sup>40</sup> and protein-protein interaction server.<sup>41</sup>

**Molecular Modeling and Calculations.** The structural model for the calculations was based on the PR:1 crystal structure (this work). The linker was modeled connecting the two metal bis(dicarbollide) cages. A computational screening of accessible conformations of the compound **1** linker was performed using a molecular dynamics based quenching technique (MD/Q) followed by quantum mechanics/molecular mechanics (QM/MM) optimizations. Details of this procedure are summarized in the Supporting Information.

**Acknowledgment.** We thank members of the Structural Biology Center at Argonne National Laboratory, the Advanced Photon Source, and Zbyszek Otwinowski (UT Southwestern Medical Center at Dallas) for their help with conducting X-ray data collection and Devon Maloy for critical proofreading of the manuscript. This work was supported by the European Commission sixth Framework no. LSHP-CT-2007-037693 and in part by the research projects nos. AV0Z50520514, AV0Z40320502, and AV0Z0550506 awarded by the Academy of Sciences of the Czech Republic, Grant IAAX00320901 from the Grant Agency of the Academy of Sciences of the Czech Republic, and LC512 and LC523 from the Ministry of Education of the Czech Republic. We are indebted to Praemium Academiae awarded to Pavel Hobza in 2007.

**Supporting Information Available:** List of mutations and enzyme characteristics [ $K_m$ ,  $k_{cat}$ , and catalytic efficiencies ( $k_{cat}/K_m$ )] of PR variants analyzed in this study.  $K_i$  values [nM] for the inhibition of PR mutants by seven clinically available inhibitors and by metallacarboranes **1**, **3**, **4**, and **5**. The inhibition constants were determined by spectrophotometric assay at the pH optimum of the protease (pH 4.7). Examples of plots used for determination of inhibition mechanisms using double reciprocal Lineweaver-Burk plot. Competitive inhibition of **7**, noncompetitive inhibition **8**, inhibitor concentration dependent inhibition **12**. Experimental procedure on chemical syntheses and molecular modeling. This material is available free of charge via the Internet at <http://pubs.acs.org>.

## References

- (1) Kohl, N. E.; Emini, E. A.; Schleif, W. A.; Davis, L. J.; Heimbach, J. C.; Dixon, R. A.; Scolnick, E. M.; Sigal, I. S. Active human immunodeficiency virus protease is required for viral infectivity. *Proc. Natl. Acad. Sci. U.S.A.* **1988**, *85*, 4686-4690.
- (2) Mastrolorenzo, A.; Rusconi, S.; Scozzafava, A.; Barbaro, G.; Supuran, C. T. Inhibitors of HIV-1 protease: current state of the art 10 years after their introduction. From antiretroviral drugs to antifungal, antibacterial and antitumor agents based on aspartic protease inhibitors. *Curr. Med. Chem.* **2007**, *14*, 2734-2748.
- (3) Condra, J. H.; Schleif, W. A.; Blahy, O. M.; Gabryelski, L. J.; Graham, D. J.; Quintero, J. C.; Rhodes, A.; Robbins, H. L.; Roth, E.; Shivaprakash, M.; et al. In vivo emergence of HIV-1 variants resistant to multiple protease inhibitors. *Nature* **1995**, *374*, 569-571.
- (4) Cigler, P.; Kozisek, M.; Rezacova, P.; Brynda, J.; Otwinowski, Z.; Pokorna, J.; Plesek, J.; Gruner, B.; Doleckova-Maresova, L.; Masa, M.; Sedlacek, J.; Bodem, J.; Krausslich, H. G.; Kral, V.; Konvalinka, J. From nonpeptide toward noncarbon protease inhibitors: metallacarboranes as specific and potent inhibitors of HIV protease. *Proc. Natl. Acad. Sci. U.S.A.* **2005**, *102*, 15394-15399.
- (5) Grimes, R. N. Metallacarboranes in the new millennium. *Coord. Chem. Rev.* **2000**, *200*, 773-811.
- (6) King, R. B. Three-dimensional aromaticity in polyhedral boranes and related molecules. *Chem. Rev.* **2001**, *101*, 1119-1152.
- (7) Chen, Z. F.; King, R. B. Spherical aromaticity: Recent work on fullerenes, polyhedral boranes, and related structures. *Chem. Rev.* **2005**, *105*, 3613-3642.
- (8) Lesnikowski, Z. J.; Paradowska, E.; Olejniczak, A. B.; Studzinska, M.; Seekamp, P.; Schussler, U.; Gabel, D.; Schinazi, R. F.; Plesek, J. Towards new boron carriers for boron neutron capture therapy: metallacarboranes and their nucleoside conjugates. *Bioorg. Med. Chem.* **2005**, *13*, 4168-4175.
- (9) Sivaev, I. B.; Bregadze, V. V. Polyhedral Boranes for Medical Applications: Current Status and Perspectives. *Eur. J. Inorg. Chem.* **2009**, 1433-1450.
- (10) Plesek, J. Potential Applications of the Boron Cluster Compounds. *Chem. Rev.* **1992**, *92*, 269-278.
- (11) Olejniczak, A. B.; Plesek, J.; Kriz, O.; Lesnikowski, Z. J. A nucleoside conjugate containing a metallacarborane group and its incorporation into a DNA oligonucleotide. *Angew. Chem., Int. Ed.* **2003**, *42*, 5740-5743.
- (12) Beatty, B. G.; Paxton, R. J.; Hawthorne, M. F.; Williams, L. E.; Rickard-Dickson, K. J.; Do, T.; Shively, J. E.; Beatty, J. D. Pharmacokinetics of an anti-carcinoembryonic antigen monoclonal antibody conjugated to a bifunctional transition metal carbonyl complex (venus flytrap cluster) in tumor-bearing mice. *J. Nucl. Med.* **1993**, *34*, 1294-1302.
- (13) Paxton, R. J.; Beatty, B. G.; Hawthorne, M. F.; Varadarajan, A.; Williams, L. E.; Curtis, F. L.; Knobler, C. B.; Beatty, J. D.; Shively, J. E. A transition metal complex (Venus flytrap cluster) for radioimmunodetection and radioimmunotherapy. *Proc. Natl. Acad. Sci. U.S.A.* **1991**, *88*, 3387-3391.
- (14) Kozisek, M.; Cigler, P.; Lepsik, M.; Fanfrlik, J.; Rezacova, P.; Brynda, J.; Pokorna, J.; Plesek, J.; Gruner, B.; Grantz Saskova, K.; Vaclavikova, J.; Kral, V.; Konvalinka, J. Inorganic polyhedral metallacarborane inhibitors of HIV protease: a new approach to overcoming antiviral resistance. *J. Med. Chem.* **2008**, *51*, 4839-4843.
- (15) Plesek, J.; Jelinek, T.; Mares, F.; Hermanek, S. Unique Dialkylsulfonio-Methylation of the 7,8-C<sub>2</sub>B<sub>9</sub>H<sub>12</sub>(-) Ion to the 9-R<sub>2</sub>S-Ch<sub>2</sub>-7,8-C<sub>2</sub>B<sub>9</sub>H<sub>11</sub> Zwitterions by Formaldehyde and Dialkyl Sulfides—General Synthesis of the Compounds 10-R<sub>2</sub>e-7,8-C<sub>2</sub>B<sub>9</sub>H<sub>11</sub> (E=O,S). *Collect. Czech. Chem. Commun.* **1993**, *58*, 1534-1547.
- (16) Stogniy, M. Y.; Abramova, E. N.; Lobanova, I. A.; Sivaev, I. B.; Bragin, V. I.; Petrovskii, P. V.; Tsupreva, V. N.; Sorokina, O. V.; Bregadze, V. I. Synthesis of functional derivatives of 7,8-dicarbido-undecaborate anion by ring-opening of its cyclic oxonium derivatives. *Collect. Czech. Chem. Commun.* **2007**, *72*, 1676-1688.
- (17) Lineweaver, H.; D., B. The determination of enzyme dissociation constants. *J. Am. Chem. Soc.* **1934**, *56*, 656-666.
- (18) Gulnik, S. V.; Suvorov, L. I.; Liu, B.; Yu, B.; Anderson, B.; Mitsuya, H.; Erickson, J. W. Kinetic characterization and cross-resistance patterns of HIV-1 protease mutants selected under drug pressure. *Biochemistry* **1995**, *34*, 9282-9287.
- (19) Betts, M. J.; Sternberg, M. J. E. An analysis of conformational changes on protein-protein association: implications for predictive docking. *Protein Eng.* **1999**, *12*, 271-283.
- (20) Fanfrlik, J.; Brynda, J.; Rezac, J.; Hobza, P.; Lepsik, M. Interpretation of protein/ligand crystal structure using QM/MM calculations: case of HIV-1 protease/metallacarborane complex. *J. Phys. Chem. B* **2008**, *112*, 15094-15102.
- (21) Selucky, P.; Plesek, J.; Rais, J.; Kyrs, M.; Kadlecova, L. Extraction of Fission-Products into Nitrobenzene with Dicobalt Tris-Dicarbollide

- and Ethyleneoxy-Substituted Cobalt Bis-Dicarbollide. *J. Radioanal. Nucl. Chem.* **1991**, *149*, 131–140.
- (22) Plešek, J.; Hermanek, S.; Franken, A.; Cisarova, I.; Nachtigal, C. Dimethyl sulfate induced nucleophilic substitution of the [bis(1,2-dicarbollido)-3-cobalt(1-)]ate ion. Syntheses, properties and structures of its 8,8'-mu-sulfato, 8-phenyl and 8-dioxane derivatives. *Collect. Czech. Chem. Commun.* **1997**, *62*, 47–56.
- (23) Semioshkin, A. A.; Sivaev, I. B.; Bregadze, V. I. Cyclic oxonium derivatives of polyhedral boron hydrides and their synthetic applications. *Dalton Trans.* **2008**, 977–992.
- (24) Kubat, P.; Lang, K.; Cigler, P.; Kozisek, M.; Matejcek, P.; Janda, P.; Zelinger, Z.; Prochazka, K.; Kral, V. Tetraphenylporphyrin-cobalt(III) bis(1,2-dicarbollide) conjugates: from the solution characteristics to inhibition of HIV protease. *J. Phys. Chem. B* **2007**, *111*, 4539–4546.
- (25) Matejcek, P.; Cigler, P.; Prochazka, K.; Kral, V. Molecular assembly of metallacarboranes in water: light scattering and microscopy study. *Langmuir* **2006**, *22*, 575–581.
- (26) Gruner, B.; Mikulasek, L.; Baca, J.; Cisarova, I.; Bohmer, V.; Danila, C.; Reinoso-Garcia, M. M.; Verboom, W.; Reinhoudt, D. N.; Casnati, A.; Ungaro, R. Cobalt bis(dicarbollides)(1-) covalently attached to the calix[4]arene platform: The first combination of organic bowl-shaped matrices and inorganic metallaborane cluster anions. *Eur. J. Org. Chem.* **2005**, 2022–2039.
- (27) Gruner, B.; Plzák, Z. *J. Chromatogr., A* **1997**, *789*, 497–517.
- (28) Weber, J.; Mesters, J. R.; Lepsik, M.; Prejdova, J.; Svec, M.; Sponarova, J.; Mlcochova, P.; Skalicka, K.; Strisovsky, K.; Uhlíkova, T.; Soucek, M.; Machala, L.; Stankova, M.; Vondrasek, J.; Klímkait, T.; Kraeusslich, H. G.; Hilgenfeld, R.; Konvalinka, J. Unusual binding mode of an HIV-1 protease inhibitor explains its potency against multi-drug-resistant virus strains. *J. Mol. Biol.* **2002**, *324*, 739–754.
- (29) Vaclavikova, J.; Weber, J.; Machala, L.; Reinis, M.; Linka, M.; Bruckova, M.; Vandasova, J.; Stankova, M.; Konvalinka, J. Long-term analysis of the resistance development in HIV-1 positive patients treated with protease and reverse transcriptase inhibitors: correlation of the genotype and disease progression. *Acta Virol.* **2005**, *49*, 29–36.
- (30) Mildner, A. M.; Rothrock, D. J.; Leone, J. W.; Bannow, C. A.; Lull, J. M.; Reardon, I. M.; Sarcich, J. L.; Howe, W. J.; Tomich, C. S.; Smith, C. W.; et al. The HIV-1 protease as enzyme and substrate: mutagenesis of autolysis sites and generation of a stable mutant with retained kinetic properties. *Biochemistry* **1994**, *33*, 9405–9413.
- (31) Williams, J. W.; Morrison, J. F. The kinetics of reversible tight-binding inhibition. *Methods Enzymol.* **1979**, *63*, 437–467.
- (32) Minor, W.; Cymborowski, M.; Otwinowski, Z.; Chruszcz, M. HKL-3000: the integration of data reduction and structure solution—from diffraction images to an initial model in minutes. *Acta Crystallogr., Sect. D: Biol. Crystallogr.* **2006**, *62*, 859–866.
- (33) CCP4. The CCP4 suite: programs for protein crystallography. *Acta Crystallogr., Sect. D: Biol. Crystallogr.* **1994**, *50*, 760–763.
- (34) Vagin, A.; Teplyakov, A. An approach to multi-copy search in molecular replacement. *Acta Crystallogr., Sect. D: Biol. Crystallogr.* **2000**, *56*, 1622–1624.
- (35) Murshudov, G. N.; Vagin, A. A.; Dodson, E. J. Refinement of macromolecular structures by the maximum-likelihood method. *Acta Crystallogr., Sect. D: Biol. Crystallogr.* **1997**, *53*, 240–255.
- (36) Emsley, P.; Cowtan, K. Coot: model-building tools for molecular graphics. *Acta Crystallogr., Sect. D: Biol. Crystallogr.* **2004**, *60*, 2126–2132.
- (37) Winn, M. D.; Isupov, M. N.; Murshudov, G. N. Use of TLS parameters to model anisotropic displacements in macromolecular refinement. *Acta Crystallogr., Sect. D: Biol. Crystallogr.* **2001**, *57*, 122–133.
- (38) Lovell, S. C.; Davis, I. W.; Arendall, W. B., III; de Bakker, P. I.; Word, J. M.; Prisant, M. G.; Richardson, J. S.; Richardson, D. C. Structure validation by Calpha geometry: phi, psi and Cbeta deviation. *Proteins* **2003**, *50*, 437–450.
- (39) De Lano, W. L. *The PyMOL Molecular Graphics System*; DeLano Scientific LLC: San Carlos, CA; <http://www.pymol.org>.
- (40) Krissinel, E.; Henrick, K. Detection of Protein Assemblies in Crystals. In *CompLife 2005, LNBI 3695*; Springer-Verlag: Berlin Heidelberg, 2005; pp 163–174.
- (41) Jones, D. T.; Taylor, W. R.; Thornton, J. M. A Model Recognition Approach to the Prediction of All-Helical Membrane-Protein Structure and Topology. *Biochemistry* **1994**, *33*, 3038–3049.
- (42) Brunger, A. T. Free R-Value—A Novel Statistical Quantity for Assessing the Accuracy of Crystal Structures. *Nature* **1992**, *355*, 472–475.

## Structural Basis for the Interaction Between Carbonic Anhydrase and 1,2,3,4-tetrahydroisoquinolin-2-ylsulfonamides<sup>†</sup>

Pavel Mader,<sup>‡</sup> Jiří Brynda,<sup>‡,§</sup> Rosaria Gitto,<sup>||</sup> Stefano Agnello,<sup>||</sup> Petr Páchl,<sup>‡</sup> Claudiu T. Supuran,<sup>⊥</sup> Alba Chimirri,<sup>||</sup> and Pavlína Řezáčová<sup>\*,‡,§</sup>

<sup>‡</sup>Department of Structural Biology, Institute of Molecular Genetics, Academy of Sciences of the Czech Republic, Prague, Czech Republic

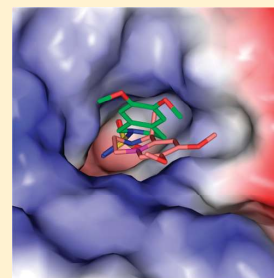
<sup>§</sup>Structural Biology Team, Institute of Organic Chemistry and Biochemistry, Academy of Sciences of the Czech Republic, Prague, Czech Republic

<sup>||</sup>Dipartimento Farmaco-Chimico, Università di Messina, Messina, Italy

<sup>⊥</sup>Laboratorio di Chimica Bioorganica, Università degli Studi di Firenze, Firenze, Italy

**S** Supporting Information

**ABSTRACT:** Isoquinolinesulfonamides inhibit human carbonic anhydrases (hCAs) and display selectivity toward therapeutically relevant isozymes. The crystal structure of hCA II in complex with 6,7-dimethoxy-1-methyl-1,2,3,4-tetrahydroisoquinolin-2-ylsulfonamide revealed unusual inhibitor binding. Structural analyses allowed for discerning the fine details of the inhibitor binding mode to the active site, thus providing clues for the future design of even more selective inhibitors for druggable isoforms such as the cancer associated hCA IX and neuronal hCA VII.



### ■ INTRODUCTION

Human carbonic anhydrases (hCAs, EC 4.2.1.1) form a family of zinc metalloenzymes that play an important role in several physiological and pathological processes. To date, 15 human isozymes have been identified displaying differences in activity, subcellular localization, and tissue expression profiles. They play key roles in intracellular and extracellular pH homeostasis, in the transport of CO<sub>2</sub> and bicarbonate in respiration, and in several biochemical pathways where either CO<sub>2</sub> or bicarbonate is required,<sup>1</sup> with bone resorption, the production of gastric acid, renal acidification, and lipogenesis representing just a few examples. Immense experimental evidence also suggested the role of hCAs in various pathological processes (e.g., tumorigenicity, obesity, and epilepsy). Thus, many isozymes are established diagnostic and therapeutic targets.

About 30 carbonic anhydrase inhibitors are clinically used as antiglaucoma drugs (targeting hCA II, hCA IV, and hCA XII), anticonvulsants (targeting hCA II, hCA VII, and hCA XIV), and antiobesity agents (targeting hCA VA and hCA VB).<sup>2,3</sup> The classical carbonic anhydrase inhibitors (CAIs), which have been known for more than 50 years and which are used in therapy, contain a sulfonamide (e.g., acetazolamide) or a sulfamate (e.g., topiramate) moiety coordinating the Zn(II) ion located in the enzyme catalytic site (reviewed in refs 4 and 5). Nevertheless, most of currently used CA inhibitors lack selectivity, presenting numerous unwanted side effects. The design of a novel generation

of isozyme-selective CA inhibitors is the current challenge in the development of new therapeutic agents able to inhibit specific isozymes.

Recently, several isozymes became popular targets for inhibitor development. Isozyme CA XIV is a transmembrane isoform highly abundant in neurons and axons in the human brain,<sup>6</sup> where it seems to play an important role in modulating excitatory synaptic transmission, and is an emerging target for neuroprotective agents.<sup>7</sup> Neuronal hCA VII is an important target for the development of anticonvulsant agents and neuropathic pain killers.<sup>8</sup> Two transmembrane hCA isozymes (hCA IX and hCA XII) are associated with cancer, and their role in tumor progression was recently established.<sup>9</sup> Targeting these tumor-specific hCA isozymes with specific inhibitors thus became a promising strategy for cancer therapy.<sup>10–12</sup>

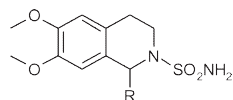
In our previous work, we explored isoquinoline sulfonamides that showed inhibitory effects against some hCA isozymes at nanomolar concentrations.<sup>13,14</sup> One of the most interesting results was the identification of new CAIs displaying a high potency and selectivity toward some therapeutically relevant isozymes (hCA VII, hCA IX, and hCA XIV)<sup>13,14</sup> over the widespread hCA II isozyme. The crystal structure of 6,7-dimethoxy-1,2,3,4-tetrahydroisoquinolin-2-ylsulfonamide as a prototype of this series in

**Received:** January 10, 2011

**Published:** March 11, 2011



**Table 1.** Inhibition of hCA II, hCA VII, hCA IX, and hCA XIV Isoforms by Tetrahydroisoquinoline Derivatives (**1** and **2**), Acetazolamide, and Topiramate



compd	R	$K_i$ (nM) <sup>a</sup>			
		hCA II <sup>b</sup>	hCA VII <sup>c</sup>	hCA IX <sup>b</sup>	hCA XIV <sup>b</sup>
<b>1</b>	H	94.5	5.4	9.5	9.8
<b>2</b>	methyl	87.3	6.4	9.4	9.6
acetazolamide		12	2.5	25	41
topiramate		10	0.9	58	1460

<sup>a</sup> Experimental errors are  $\pm 10\%$  of the reported value, from three different assays. Recombinant full length hCAs II, VII, and XIV and the catalytic domain of hCA IX were used. <sup>b</sup> Values from ref 13. <sup>c</sup> Values from ref 14.

complex with hCA II provided valuable structural information on the protein–inhibitor interaction. Subsequent docking studies suggested that the nature of the C-1 substituent on the isoquinoline scaffold affects the hCA isoform specificity.<sup>13</sup>

To understand the structural basis of interaction of isoquinoline sulfonamide derivatives with hCAs, we report the crystal structure of hCA II in complex with 6,7-dimethoxy-1-methyl-1,2,3,4-tetrahydroisoquinolin-2-ylsulfonamide. Comparison of the inhibitor position within the enzyme active site cavity with the previously determined crystal structure of the prototype compound lacking the methyl substitution on the C-1 position (PDB code 3IGP<sup>13</sup>) revealed striking differences in the inhibitor binding mode. These results obtained by protein crystallography could help in the elucidation of the isoform selectivity of other alkyl-substituted compounds at the C-1 position observed previously and also should be beneficial in future rational drug design.

## RESULTS AND DISCUSSION

Compounds **1** and **2** were synthesized following the previously reported procedure.<sup>13</sup> Both **1** and **2** show inhibitory efficacy toward various CA isoforms *in vitro*, but their selectivity differs substantially from well-known CAs such as acetazolamide and topiramate (Table 1). Compounds **1** and **2** were able to inhibit the widely distributed hCA II with  $K_i$  of 94.5 and 87.3 nM, respectively, but interestingly they were able to inhibit druggable isoforms hCA VII, hCA IX, and hCA XIV with even higher potency ( $K_i$  in the nanomolar range).

Structural information on **1** binding to hCA II was published by us previously.<sup>13</sup> In the present work, the crystal structure of hCA II in complex with 6,7-dimethoxy-1-methyl-1,2,3,4-tetrahydroisoquinolin-2-ylsulfonamide (**2**) was determined and refined using diffraction data to 1.47 Å resolution (Figure 1). Well-defined, non-protein electron densities indicated the binding of an inhibitor molecule into the primary binding site in the enzyme active site and the secondary inhibitor binding site on the surface of the protein molecule near the N-terminus. The secondary binding site, also reported for other hCA II–inhibitor crystal

structures (e.g., PDB codes 3HS4<sup>15</sup> and 2QOA<sup>16</sup>), most likely has no biological relevance and represents a crystallization artifact caused by high concentrations of the inhibitor used in the cocrystallization experiments.

As shown in Figure 1C, **2** binds into the cavity of the hCA II active site with the deeply buried sulfonamide group. The ionized nitrogen atom of the sulfonamide moiety is coordinated to the zinc ion at  $\sim 2.0$  Å. The sulfonamide nitrogen also accepts a hydrogen bond from the hydroxyl group of Thr199 side chain, and one oxygen atom from the sulfonamide moiety forms a hydrogen bond with backbone amine group of Thr199. Positions of the N $\epsilon$  atoms of His 94 and His 96 and N $\delta$  atom of His 119 form a ligand field, which dictates the position of a coordinated Zn<sup>2+</sup> cation and consequently determines the position of acidic group of the sulfonamide to complete the tetrahedral coordination of the central zinc ion. The position of the sulfonamide group and the key hydrogen bond network in the active site are highly conserved in all known structures of hCA II–sulfonamide complexes deposited in PDB.<sup>17–20</sup>

In addition to the polar interactions mediated by the sulfonamide group, the oxygen of the 6-methoxy group of **2** (labeled OAK in Figure 1B) is stabilizing the inhibitor in proximity of  $\beta$ -sheet 8 by forming an additional polar interaction (2.73 Å) with side chain N $\delta$  atom of Asn 67. N $\epsilon$  atom of Gln 92 is positioned 2.89 Å from the oxygen atom (labeled OAL in Figure 1B) of the other methoxy group at the 7-position; however, the overall geometry does not allow additional polar interaction to be formed between these two atoms. Several hydrophobic interactions of the substituted isoquinoline moiety with residues of the central  $\beta$ -sheet (mainly with Gln 92 and Val 121) stabilize the inhibitor within the active site cavity.

Compound **2** was synthesized as a racemic mixture of the two enantiomers and has been used in crystallization trials. Interestingly, the high resolution crystal structure revealed that the absolute configuration of **2** bound in the active site was *R* while the inhibitor bound on the surface was the *S* enantiomer. This suggests that only one enantiomer represents an active compound. This subject will be addressed in future research aimed at the enantiomeric resolution of the active isoquinoline sulfonamide based compounds.<sup>13</sup>

We compared the hCA II–**2** complex with the structure containing the parent, the unsubstituted isoquinoline based inhibitor **1** (6,7-dimethoxy-1,2,3,4-tetrahydroisoquinolin-2-ylsulfonamide; PDB code 3IGP<sup>13</sup>). Although the two compounds differ only by the presence of the methyl group substitution at C-1 in **2** (see Table 1), their binding modes in the enzyme active site are quite dissimilar (Figure 2).

The position of the sulfonamide group is well conserved in the two crystal structures; the major difference is in the arrangement of the isoquinoline moiety within the active site cavity. The rearrangement of **2** compared to **1** is achieved by the rotation around the covalent bond between sulfur and nitrogen atoms (atoms SAS and NAR in Figure 1B) accompanied by the change of the isoquinoline ring puckering. The three dihedral angles defined by atoms of nonaromatic ring CAQ–NAR–CAJ–CAI, CAP–CAQ–NAR–CAJ, and NAR–CAJ–CAI–CAM (Figure 1B) are 0.2°, 30.4°, and  $-30.8^\circ$  for **1** and  $-75.2^\circ$ ,  $52.0^\circ$ ,  $52.8^\circ$  for **2**. The substantial change in position of **2** with respect to **1** within the hCA II active site can also be documented by a distance of more than 4 Å between the two corresponding methoxy oxygen atoms in **1** and **2**, respectively (atoms OAL and OAK in Figure 1B).

The isoquinoline moiety of **1** forms numerous van der Waals interactions with residues Gln 92, Val 121 located on the bottom



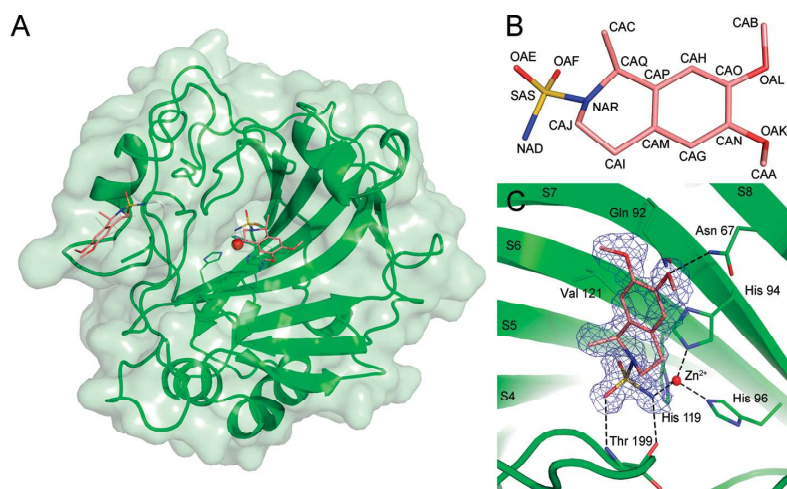


**Figure 1.** (A) Overall view of structure of hCA II in complex with **2**. The main chain of the protein is represented by a ribbon and a transparent solvent accessible surface. The zinc ion is shown as a red sphere with three coordinating histidine residues in sticks. Two molecules of inhibitor **2** bound to hCA II are shown in the stick model with carbon atoms colored salmon and oxygen and nitrogen atoms colored red and blue, respectively. (B) Structure of **2** with atom labels used in the crystal structure coordinate file. (C) Detail of the hCA II active site with **2**. Protein is represented in green with residues forming van der Waals interactions and polar contacts (black dashed lines). Also three histidine residues coordinating the zinc ion are shown. Strands of the central  $\beta$ -sheet are labeled S4–S8. Compound **2** is shown in sticks with the  $2F_o - F_c$  electron density map contoured at  $0.8\sigma$ .

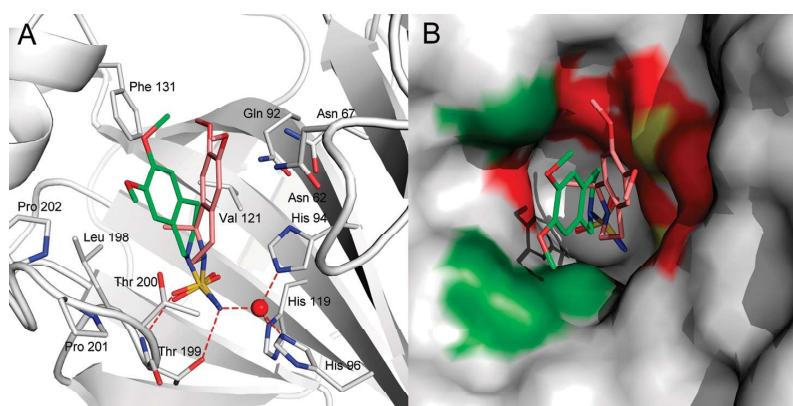


**Figure 2.** Comparison of **1** and **2** binding mode into the hCA II active site. Superposition of the complex structures is based on the best fit for C $\alpha$  atoms of hCA II residues 6–261. Compound **1** is represented with green carbon atoms, while **2** carbon atoms are salmon colored. In (A), the protein is represented by a ribbon and residues involved in the binding of the inhibitor compounds are shown as sticks. Polar interactions between the histidine residues coordinating the Zn ion (red sphere) and also the polar interactions between sulfonamide group and Thr 199 are indicated with dashed lines. (B) shows a top view into the active site where the protein is represented by its van der Waals radii. Atoms making contacts with the isoquinoline moiety of **1** and **2** are highlighted. Atoms within 4.0 Å from **1** and **2** are highlighted in green and red, respectively. Atoms colored yellow make contacts with both compounds. Atoms involved in contacts with the sulfonamide groups are not highlighted.

of the catalytic site and also with residues Ser197–Pro202 located in the loop connecting  $\beta$ -strands S3 and S4. Also, the side chain of Phe131 from helix 4 contributes to interaction with the substituting methoxy groups (Figure 2A, Table S1 in Supporting Information). In contrast, the substituted isoquinoline moiety of **2** is stabilized by the amino acid residues coming from the central part of the strands S6–S8 of the 10-stranded  $\beta$ -sheet<sup>1</sup> located on the opposite side of the active site cavity (residues Asn 62, Asn 67, Gln 92, Val 121; Figure 2A, Table S1 in Supporting Information). The methyl substituent on the isoquinoline scaffold

interacts with Leu 198 from the loop connecting  $\beta$ -strands S3 and S4.

Comparison of the residues interacting with **1** and **2**, respectively, revealed that the isoquinoline moiety can achieve two different binding modes within the hCA II active site and engage different amino acid residues in the interaction (Figure 2B). This finding is quite striking considering that **1** and **2** are very similar in their structure and also in their inhibitory properties (see Table 1).

We have compared the binding modes of **1** and **2** to other hCA II inhibitors that are structurally similar to our isoquinoline

**Table 2.** Crystal Parameters, Data Collection, and Refinement Statistics

parameter	complex of hCA II with 2
space group	$P2_1$
unit cell params	
<i>a</i> (Å)	42.18
<i>b</i> (Å)	41.21
<i>c</i> (Å)	72.00
α (deg)	90
β (deg)	104.31
γ (deg)	90
no. molecules in AU	1
wavelength (Å)	0.954
resolution range (Å)	26.62–1.47 (1.51–1.47)
no. unique reflns	40 809
redundancy	3.6 (3.4)
completeness (%)	99.8 (99.8)
$R_{\text{merge}}^a$	0.053 (0.238)
average $I/\sigma(I)$	7.8 (3.0)
Wilson $B$ (Å <sup>2</sup> )	13.7
refinement statistics	
resolution range (Å)	25.27–1.47 (1.51–1.47)
no. reflns in working set	38 750 (2850)
no. reflns in test set	2045 (132)
$R^b$ (%)	14.3 (18.6)
$R_{\text{free}}^c$ (%)	17.5 (22.4)
rmsd bond length (Å)	0.014
rmsd angle (deg)	1.69
no. atoms in AU	2511
no. protein–inhibitor atoms in AU	2171
no. solvent molecules in AU	340
mean $B$ (Å <sup>2</sup> )	13.8
PDB code	3PO6

<sup>a</sup>  $R_{\text{merge}} = \frac{\sum_{\text{hkl}} \sum_i |I_i(\text{hkl}) - \langle I(\text{hkl}) \rangle|}{\sum_{\text{hkl}} \sum_i I_i(\text{hkl})}$ , where the  $I_i(\text{hkl})$  is an individual intensity of the  $i$ th observation of reflection  $\text{hkl}$  and  $\langle I(\text{hkl}) \rangle$  is the average intensity of reflection  $\text{hkl}$  with summation over all data. <sup>b</sup>  $R = \frac{||F_o| - |F_c||}{|F_o|}$ , where  $F_o$  and  $F_c$  are the observed and calculated structure factors, respectively. <sup>c</sup>  $R_{\text{free}}$  is equivalent to  $R$  value but is calculated for 5% of the reflections chosen at random and omitted from the refinement process.

sulfonamide series. For our analysis, we chose 59 crystal structures of hCA II in complex with inhibitors containing a cyclic or heterocyclic moiety attached directly to the sulfonamide group (Tables S2 and S3 in Supporting Information). Of these, 51 compounds displayed a binding mode highly similar to that of **1**. Eight compounds displayed a slightly altered binding mode in which the inhibitor position was shifted toward the  $\beta$ -strands S7 and S8. Nevertheless, none of the analyzed structures showed a binding mode overlapping with **2**. This analysis also revealed that a change in inhibitor binding in response to such a small structural change in the inhibitor is unique for our isoquinoline-sulfonamide compounds.

## CONCLUSIONS

Comparison of the crystal structures of hCA II in complex with **1** and **2**, respectively, provided structural information about interactions of 1,2,3,4-tetrahydroisoquinolin-2-ylsulfonamides

with the hCA II active site. Although both compounds exhibit similar inhibitory potency toward hCA II, a unique binding mode of the **2** has been observed in response to the presence of a substituent on C-1 on the isoquinoline scaffold. The same inhibitory potency can apparently be achieved by two different binding modes of the inhibitor into the enzyme active site cavity. From a structural point of view, **1** and **2** served as excellent molecular tools for the detailed mapping of active site cavity. These results will be exploited for the rational design of molecules which could be highly selective inhibitors for various hCA isozymes.

## EXPERIMENTAL SECTION

Detailed experimental procedures are given in the Supporting Information. Briefly, the crystals of human hCA II in complex with **2** (6,7-dimethoxy-1-methyl-1,2,3,4-tetrahydroisoquinolin-2-ylsulfonamide) were obtained by adding a 5-fold molar excess of the inhibitor (in dimethylsulfoxide) to a 10 mg/mL protein solution of hCA II (Sigma). The crystallization was performed in hanging drops at 18 °C in 0.1 M Tris-Cl, pH 8.2, 2.5 M (NH<sub>4</sub>)<sub>2</sub>SO<sub>4</sub>, and 0.3 M NaCl. Diffraction data for hCA II in complex with **2** were collected at the Hamburg DESY, beamline X12. The structure of hCA II–**2** complex was solved using the difference Fourier method, using hCA II structure (Protein Data Bank entry 1H9N<sup>21</sup>) as the initial model. Atomic coordinates and experimental structure factors have been deposited with the Protein Data Bank with the code 3PO6. All figures showing structural representations were prepared with the programs PyMOL (DeLano Scientific; <http://www.pymol.org>). Crystal parameters and data collection statistics are summarized in Table 2. Compounds **1** and **2** were synthesized following previously reported procedures, and the spectral data were in accordance with the literature.<sup>13</sup>

## ASSOCIATED CONTENT

**S** Supporting Information. Crystallization conditions, data collection, structure determination, refinement procedures, table of contacts between hCA II and **1** and **2**, respectively, and analysis results of the inhibitor binding mode in 59 hCA II structures. This material is available free of charge via the Internet at <http://pubs.acs.org>.

## Accession Codes

<sup>1</sup>PDB codes for the hCA II structures are 3IGP and 3PO6.

## AUTHOR INFORMATION

### Corresponding Author

\*Phone: +420220183210. Fax: +420220183144. E-mail: rezacova@img.cas.cz.

## ACKNOWLEDGMENT

We thank the X12 beamline staff at the DESY synchrotron radiation facility for expert assistance during data collection. Financial support for this research was awarded by the Academy of Sciences of the Czech Republic (Projects AV0Z50520S14 and AV0Z40550S06), by Grant Agency of the Czech Republic (Grant GA203/09/0820), and by MiUR (Prin2008, Grant 20085HRSJK\_002). This work was also financed in part by the FP7 EU project (Metoxia) to C.T.S. The authors thank Devon Maloy for critical proofreading of the manuscript.

## REFERENCES

- (1) Krishnamurthy, V. M.; Kaufman, G. K.; Urbach, A. R.; Gitlin, I.; Gudiksen, K. L.; Weibel, D. B.; Whitesides, G. M. Carbonic anhydrase as a model for biophysical and physical-organic studies of proteins and protein–ligand binding. *Chem. Rev.* **2008**, *108*, 946–1051.
- (2) Mincione, F.; Scozzafava, A.; Supuran, C. T. The development of topically acting carbonic anhydrase inhibitors as anti-glaucoma agents. *Curr. Top. Med. Chem.* **2007**, *7*, 849–854.
- (3) Supuran, C. T. Carbonic anhydrases as drug targets—an overview. *Curr. Top. Med. Chem.* **2007**, *7*, 825–833.
- (4) Supuran, C. T. Carbonic anhydrases: novel therapeutic applications for inhibitors and activators. *Nat. Rev. Drug Discovery* **2008**, *7*, 168–181.
- (5) Supuran, C. T. Carbonic anhydrase inhibitors. *Bioorg. Med. Chem. Lett.* **2010**, *20*, 3467–3474.
- (6) Parkkila, S.; Parkkila, A. K.; Rajaniemi, H.; Shah, G. N.; Grubb, J. H.; Waheed, A.; Sly, W. S. Expression of membrane-associated carbonic anhydrase XIV on neurons and axons in mouse and human brain. *Proc. Natl. Acad. Sci. U.S.A.* **2001**, *98*, 1918–1923.
- (7) Thiry, A.; Dogne, J. M.; Supuran, C. T.; Masereel, B. Carbonic anhydrase inhibitors as anticonvulsant agents. *Curr. Top. Med. Chem.* **2007**, *7*, 855–864.
- (8) Asiedu, M.; Ossipov, M. H.; Kaila, K.; Price, T. J. Acetazolamide and midazolam act synergistically to inhibit neuropathic pain. *Pain* **2010**, *148*, 302–308.
- (9) Swietach, P.; Patiar, S.; Supuran, C. T.; Harris, A. L.; Vaughan-Jones, R. D. The role of carbonic anhydrase 9 in regulating extracellular and intracellular pH in three-dimensional tumor cell growths. *J. Biol. Chem.* **2009**, *284*, 20299–20310.
- (10) Winum, J. Y.; Rami, M.; Scozzafava, A.; Montero, J. L.; Supuran, C. Carbonic anhydrase IX: a new druggable target for the design of antitumor agents. *Med. Res. Rev.* **2008**, *28*, 445–463.
- (11) Thiry, A.; Supuran, C. T.; Masereel, B.; Dogne, J. M. Recent developments of carbonic anhydrase inhibitors as potential anticancer drugs. *J. Med. Chem.* **2008**, *51*, 3051–3056.
- (12) Tunuguntla, H. S.; Jorda, M. Diagnostic and prognostic molecular markers in renal cell carcinoma. *J. Urol.* **2008**, *179*, 2096–2102.
- (13) Gitto, R.; Agnello, S.; Ferro, S.; De Luca, L.; Vullo, D.; Brynda, J.; Mader, P.; Supuran, C. T.; Chimirri, A. Identification of 3,4-dihydroisoquinoline-2(1H)-sulfonamides as potent carbonic anhydrase inhibitors: synthesis, biological evaluation, and enzyme–ligand X-ray studies. *J. Med. Chem.* **2010**, *53*, 2401–2408.
- (14) Gitto, R.; Agnello, S.; Ferro, S.; Vullo, D.; Supuran, C. T.; Chimirri, A. Identification of potent and selective human carbonic anhydrase VII (hCA VII) inhibitors. *ChemMedChem* **2010**, *5*, 823–826.
- (15) Sippel, K. H.; Robbins, A. H.; Domsic, J.; Genis, C.; Agbandje-McKenna, M.; McKenna, R. High-resolution structure of human carbonic anhydrase II complexed with acetazolamide reveals insights into inhibitor drug design. *Acta Crystallogr., Sect. F: Struct. Biol. Cryst. Commun.* **2009**, *65*, 992–995.
- (16) D'Ambrosio, K.; Masereel, B.; Thiry, A.; Scozzafava, A.; Supuran, C. T.; De Simone, G. Carbonic anhydrase inhibitors: binding of indanesulfonamides to the human isoform II. *ChemMedChem* **2008**, *3*, 473–477.
- (17) Eriksson, A. E.; Jones, T. A.; Liljas, A. Refined structure of human carbonic anhydrase II at 2.0 Å resolution. *Proteins* **1988**, *4*, 274–282.
- (18) Supuran, C. T.; Scozzafava, A.; Casini, A. Carbonic anhydrase inhibitors. *Med. Res. Rev.* **2003**, *23*, 146–189.
- (19) Winum, J. Y.; Scozzafava, A.; Montero, J. L.; Supuran, C. T. Sulfamates and their therapeutic potential. *Med. Res. Rev.* **2005**, *25*, 186–228.
- (20) Srivastava, D. K.; Jude, K. M.; Banerjee, A. L.; Haldar, M.; Manokaran, S.; Kooren, J.; Mallik, S.; Christianson, D. W. Structural analysis of charge discrimination in the binding of inhibitors to human carbonic anhydrases I and II. *J. Am. Chem. Soc.* **2007**, *129*, 5528–5537.
- (21) Lesburg, C. A.; Huang, C.; Christianson, D. W.; Fierke, C. A. Histidine → carboxamide ligand substitutions in the zinc binding site of carbonic anhydrase II alter metal coordination geometry but retain catalytic activity. *Biochemistry* **1997**, *36*, 15780–15791.

## Carborane-Based Carbonic Anhydrase Inhibitors\*\*

Jiří Brynda, Pavel Mader, Václav Šícha, Milan Fábry, Kristýna Poncová, Mario Bakardiev, Bohumír Grüner, Petr Cígler, and Pavlína Řezáčová\*

Human carbonic anhydrases (CAs) are zinc metalloenzymes that play an important role in many physiological processes. To date, 15 human CA isozymes with different subcellular localization and tissue expression profiles have been identified. Vast experimental evidence also suggests the involvement of CAs in various pathological processes (e.g., tumorigenicity, obesity, and epilepsy). Many CA isozymes are thus recognized as diagnostic and therapeutic targets.<sup>[1]</sup>

About 30 CA inhibitors are used clinically, for example, as anti-glaucoma drugs (targeting CAII, CAIV, and CAXII), anti-convulsants (targeting CAII, CAVII, and CAXIV) and anti-obesity agents (targeting CAVA and CAVB).<sup>[2]</sup> Recently, other isozymes, namely the neuronal CAVII and CAXIV, and the cancer-associated forms CAIX and CAXII, have been validated as targets for inhibitor development.<sup>[3]</sup>

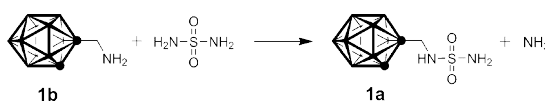
The traditional CA inhibitors contain a sulfonamide or sulfamide moiety that coordinates the zinc cation located in the CA catalytic site.<sup>[4]</sup> Most of the currently used CA inhibitors lack selectivity, and their use causes numerous unwanted side effects. A current challenge is the design of compounds that can inhibit specific isozymes. Although the conical active-site clefts of different human CA isozymes are conserved, variations exist in the amino acid residues at the entrance to the active site. As a result of their differing in shape and hydrophobicity, these surface pockets can be exploited to design specific inhibitors.<sup>[5,6]</sup>

Structural analysis of CAII in complex with numerous inhibitors revealed two general binding modes, each involving a distinct site within the enzyme active site cavity.<sup>[7]</sup> This led us to hypothesize that CA inhibitors could be designed more

effectively based on three-dimensional scaffolds rather than flat structures.

Carboranes, icosahedral clusters containing boron, carbon, and hydrogen are bulky pharmacophores used to replace various hydrophobic structures in biologically active molecules.<sup>[8,9]</sup> The 12-vertex carboranes increase the in vivo stability and bioavailability of biologically active molecules and enhance the hydrophobic interactions between them and their receptors.<sup>[10]</sup> They are an abiotic species that are very stable towards catabolism and degradation by enzymes and thus the use of boron clusters as components of new pharmacological agents has been increasing.<sup>[11–15]</sup>

With the help of manual molecular docking into the active site of CAII, we designed **1a**, which contains a sulfamide group connected to a carborane cluster intended to optimally fill the enzyme active site. The length of the linker between the sulfamide group and carborane cluster was chosen based on comparison with the structures of isoquinoline sulfonamide inhibitors.<sup>[7]</sup> Attachment of the sulfamide moiety was accomplished by using a transamination reaction between aminomethylcarborane **1b** and sulfamide (Scheme 1).



**Scheme 1.** Preparation of **1a** by heating **1b** with sulfamide in dioxane. Vertices represent BH, black spheres CH or C if substituted.

Compound **1a** showed inhibitory activity toward CAII ( $K_i$  value of 0.7  $\mu\text{M}$ ) and showed almost 2-fold higher activity toward the tumor-associated isoform CAIX ( $K_i$  of 0.38  $\mu\text{M}$ ).

The crystal structure of **1a** in complex with CAII determined at 1.35 Å resolution (PDB code 4MDG) confirmed that the inhibitor binds in the enzyme active site as predicted (Figure 1) and revealed key interactions responsible for inhibitor binding and enzyme inhibition.

The sulfamide moiety of **1a** proved to be the anchoring group that completes the coordination sphere of  $\text{Zn}^{2+}$  in the active site and makes the polar interactions with Thr199 that are typical of other CA inhibitors.<sup>[4]</sup> An additional polar interaction is a hydrogen bond between a linker NH group and the side chain  $\text{O}_\gamma$  of Thr200 (Figure 1a). Further interactions of the inhibitor with the active site cavity are mediated through van der Waals interactions between the carborane cluster and amino acid residues Gln92, His94, Phe131, Leu198, and Thr200. For a complete list of interactions, see Table S1 in the Supporting Information. Compound **1a** fills the proximal active site cavity of CAII, but

[\*] Dr. J. Brynda, Dr. P. Mader, Dr. M. Fábry, Dr. P. Řezáčová  
Institute of Molecular Genetics  
Academy of Sciences of the Czech Republic, v.i.  
Václavská 1083, 142 20 Prague 4 (Czech Republic)  
E-mail: rezacova@uochb.cas.cz

Dr. J. Brynda, K. Poncová, Dr. P. Cígler, Dr. P. Řezáčová  
Institute of Organic Chemistry and Biochemistry  
Academy of Sciences of the Czech Republic, v.i.  
Flemingovo nám. 2, 16610 Prague 6 (Czech Republic)  
E-mail: cigler@uochb.cas.cz

Dr. V. Šícha, Dr. M. Bakardiev, Dr. B. Grüner  
Institute of Inorganic Chemistry  
Academy of Sciences of the Czech Republic, v.i.  
250 68 Řež u Prahy (Czech Republic)  
E-mail: gruner@iic.cas.cz

[\*\*] This work was supported by Grant Agency of the Academy of Sciences of the Czech Republic (project IAAX00320901), Technology Agency of the Czech Republic (project TE01020028) and in part by research projects RVO 68378050, 61388963, and 61388980 awarded by the Academy of Sciences of the Czech Republic.

Supporting information for this article is available on the WWW under <http://dx.doi.org/10.1002/anie.201307583>.



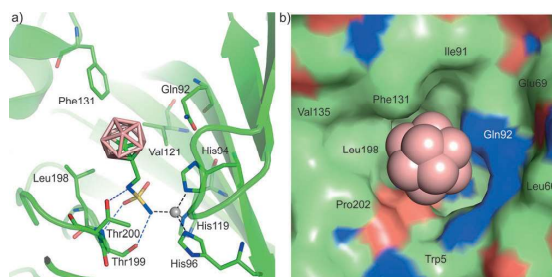


**Figure 1.** Crystal structure of CAII in complex with **1a**. a) The protein is shown as a ribbon diagram; residues involved in interactions with the  $\text{Zn}^{2+}$  ion (gray sphere) and **1a** are shown as stick representations. C green, B pink, S yellow, O red, and N blue atoms are shown. Polar interactions are represented by blue dashed lines;  $\text{Zn}^{2+}$  ion coordination is shown as black dashed lines. b) Top view into the active site, shown as a surface representation. **1a** is shown as a space filling model.

some side pockets at the entrance of the active site could potentially be targeted by cluster substituents (Figure 1b).

Next, we considered several modifications and prepared a series of novel boron cage compounds combining various carborane clusters with a polar sulfamide moiety (Figure 2). Compounds **2a–10a** were prepared in high yields using the transamination reaction depicted in Scheme 1.

Our pilot series of ten CA inhibitors includes the parent compounds **1a** and **4a**, which contain one alkyl sulfamide group and icosahedral *ortho*- and *meta*-carborane units, respectively. A structurally similar, charged derivative based on the  $[\text{CB}_{11}\text{H}_{12}]^-$  cage was also prepared (**6a**). *Closo*-carboranes containing either hydrophobic (**2a** and **3a**) or hydrophilic (second sulfamide moiety; **5a**) substituents and their charged 11-vertex *nido* counterparts (**7a–10a**) complete this structurally diverse series.

The compounds were tested for inhibition of the human CA isozymes CAII and CAIX using a colorimetric enzymatic assay. Most of the compounds tested displayed good CA inhibition profiles, with  $K_i$  values in the low micromolar or submicromolar range (Table 1). Almost all of the compounds showed selectivity for the cancer-specific CAIX isozyme over the more abundant variant CAII.

Analysis of crystal structures of CAII in complex with **4a** and **7a** (PDB codes 4MDL and 4MDM) confirmed that these compounds are positioned similarly in the enzyme active site to **1a**. In fact, **4a** binds to CAII identically to **1a** in terms of conformation and interactions (Figure 3a).

Compound **7a** binds CAII differently and, unlike **1a** and **4a**, does not form a hydrogen bond between its linker NH group and the side chain  $\text{O}_\gamma$  of Thr200 (Figure 3b). The distance between the position of the linker NH group in **1a** and **7a** is 0.18 Å. The *nido*-carborane cluster interacts with His64, Gln92, His94, Leu198, Thr200, and Pro201 (for a complete list of interactions see Table S1 in Supporting Information).

In our pilot series of carborane-based CA inhibitors, we exploited four different carborane cluster types. The effect of cluster type on inhibition can be deduced from comparison of

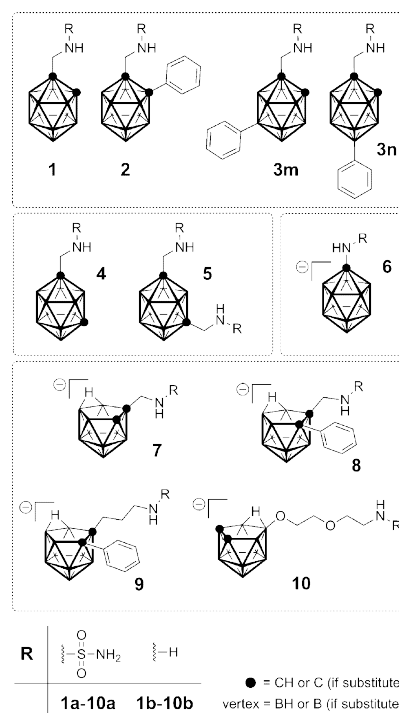


**Figure 2.** Structures of compounds used in this study. Amino groups attached to the anionic clusters (**6b–10b**) are protonated, forming zwitterions. **3** was prepared as an inseparable mixture of two isomers (termed **3m** and **3n**). The substituent in **10b** is located at boron B(10) sitting in the open face and not at a carbon as in **7**.

**Table 1:** In vitro inhibition of selected carbonic anhydrase isozymes.

Compound	$K_i$ (CAII) [ $\mu\text{M}$ ]	$K_i$ (CAIX) [ $\mu\text{M}$ ]	Selectivity Index <sup>[a]</sup>
<b>1a</b>	$0.70 \pm 0.14$	$0.38 \pm 0.11$	1.8
<b>2a</b>	$348 \pm 113$	$161 \pm 37$	2.2
<b>3ma</b> + <b>3na</b>	$0.51 \pm 0.08$	$0.43 \pm 0.17$	1.2
<b>4a</b>	$1.16 \pm 0.24$	$1.12 \pm 0.20$	1.0
<b>5a</b>	$0.38 \pm 0.14$	$0.23 \pm 0.04$	1.7
<b>6a</b>	$8.57 \pm 2.24$	$2.20 \pm 0.48$	3.9
<b>7a</b>	$6.79 \pm 2.01$	$5.09 \pm 2.38$	1.3
<b>8a</b>	$9.00 \pm 2.23$	$2.32 \pm 1.02$	3.9
<b>9a</b>	$2.71 \pm 0.47$	$0.15 \pm 0.06$	18.1
<b>10a</b>	$132 \pm 19$	$26.04 \pm 2.93$	5.1

[a] Selectivity index is the ratio between  $K_i$  (CAII) and  $K_i$  (CAIX).

the  $K_i$  values obtained for **1a**, **4a**, and **7a**. The *o*-carborane derivative **1a** has slightly better inhibitory potency toward CA isozymes than the *m*-carborane derivative **4a**. This could result from the presence of a slightly acidic CH group in the position vicinal to the substituted carbon in **1a**. Compound **7a** (containing *7,8-nido*-carborane) is a less efficient inhibitor of CA isozymes than the *closo*-carborane derivatives; however, it shows a slightly different binding mode. As revealed by the

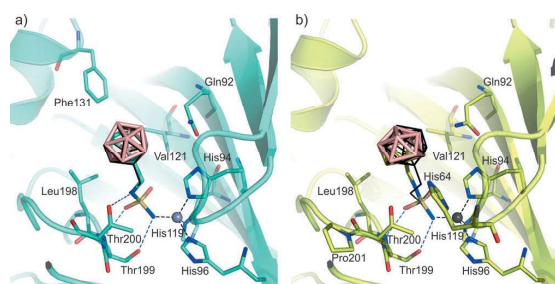


**Figure 3.** Crystal structure of CAII in complex with **4a** (a) or **7a** (b). The protein is shown as ribbon diagram; residues involved in interactions are shown as stick representations. Polar interactions are represented by dashed blue lines;  $\text{Zn}^{2+}$  ion coordination is represented by dashed black lines. The binding mode of **1a** (black line) is superimposed on the crystal structures.

co-crystal structure, the *nido* cluster **7a** has the possibility to adjust its position within the active site, which confers a potential advantage in that it can accommodate additional substituents that might affect selectivity toward a particular CA isozyme.

To explore a greater diversity of carborane clusters, we also prepared **6a**, which contains a 1-carbadodecaborate ion  $[\text{CB}_{11}\text{H}_{12}]^-$ . The removal of one methylene group from the linker and the presence of a negatively charged cluster led to a decrease in efficiency but a substantial increase in selectivity index compared to **1a**, **4a**, and **7a**. This demonstrates that a relatively subtle change in structure can strongly influence inhibitor interactions with a particular CA isozyme.

In our initial molecular design, we hypothesized that tuning compound selectivity to a certain CA isozyme could be achieved by cluster substitutions. In our series, we exploited a phenyl ring as a substituent in synthetically accessible positions on the cluster. Analysis of the crystal structure of **1a** in complex with CAII suggested that a phenyl ring in the *ortho* position on the *closo*-carborane cluster would have steric clashes with amino acids lining the entrance to the enzyme active site. Indeed, this detrimental effect on inhibitory efficiency was illustrated by the 400-fold greater  $K_i$  value obtained for inhibition of CAII with **2a**. On the other hand, the phenyl substituent placed in the *meta*-position, as in **3ma** and **3na**, seems not to experience any steric clash with the bottom of the active site, and the inhibitory potencies toward CAII and CAIX remain virtually unchanged, with  $K_i$  values close to those of parent compound **1a**.

The *nido*-carborane cluster was substituted with a phenyl ring in the *ortho* position, leading to **8a**. We did not observe a loss of inhibitory potency as a result of the addition of a phenyl ring in this position. Derivative **8a** shows only a slightly increased  $K_i$  value for CAIX, while the  $K_i$  value for CAII is lower than that of parent compound **7a**. The smaller *nido* cluster is apparently able to adjust its position in the active site cavity; the phenyl ring can thus be accommodated in a side pocket. Inspection of the crystal structure of CAII in complex with **7a** suggests that a pocket formed by Ile91 and Phe131 (Figure 1b) would be accessible for substituent

binding. In CAIX, this pocket contains Leu91 and Val131 and is more spacious.

In **5a**, an additional sulfamide group was attached by a methylene linker to the *meta* position of the *meta*-carborane cluster. This increased the inhibitory potency compared to that of the parent *m-closo*-carborane by a factor of approximately 2. This increase can be attributed to the presence of two sulfamide groups that can anchor the compound into the catalytic site of the enzyme.

The effect of the linker connecting the cluster to the sulfamide group can be deduced from comparison of the inhibitory properties of **8a** and **9a**, and **7a** and **10a**; two pairs of compounds with the same carborane cage but with linkers differing in length and nature.

Compound **8a** contains the methylene linker designed in the initial docking. Increasing the length of the aliphatic linker to a propylene moiety improved the inhibitory potency of **9a** and made it almost 5-fold more selective toward CAIX. Increasing the length of the cluster-sulfamide linker by two methylene groups probably allows accommodation of the *nido* cluster with its phenyl substituent in side pockets at the entrance of the enzyme active site (Figure S3 in the Supporting Information). With a CAIX/CAII selectivity index of 18.1, Compound **9a** showed the highest selectivity observed within the entire series.

For the parental *nido* cluster, we therefore tested an even longer, 7-atom linker (**10a**). This elongation, however, substantially decreased the inhibitory efficiency of the compound compared to that of the cluster bearing a short methylene linker (**7a**). A possible explanation for this decrease, based on this compound's similarity to ionic metallacarboranes bearing a similar linker, is that complexation with sodium cations may lead to a rigid, crown-ether-like arrangement.<sup>[16]</sup> This would decrease the compound's solubility and its ability to interact with the catalytic cleft. Our observations suggest that both the length and the nature of the cluster-to-sulfamide linker are crucial for inhibitory efficacy and should be carefully tuned in future design.

In conclusion, our results suggest that carborane-based compounds are promising lead structures for the development of inhibitors of CA isozymes. Our experiments demonstrated that various types of hydrophobic, space-filling carborane clusters can be accommodated in the CA active site and that substitution with an appropriately attached sulfamide group and other substituents leads to compounds with high selectivity for the cancer-specific CAIX isozyme over the widespread CAII isozyme. Crystal structures confirmed our hypothesis that three-dimensional scaffolds could be efficiently used in CA inhibitors and provided structural information that can be applied to the structure-based design of specific CAIX inhibitors.

### Experimental Section

Experimental procedures including detailed synthetic procedures for the sulfamide derivatives and their precursors are described in the Supporting Information. Briefly, the sulfamide compounds were prepared from their respective amine or ammonium carborane derivatives (**1b**<sup>[17]</sup> and **6b**<sup>[18]</sup>) were prepared

according to known procedures. **4b** and **5b** were prepared by lithiation of 1,7-carborane, reaction with bromomethyl phthalimide, and removal of the phthalimido group by hydrazine hydrate.<sup>[19–22]</sup> Derivatives **2b** and **3b** were synthesized similarly, but the final steps involved reduction with NaBH<sub>4</sub> and subsequent hydrolysis. Although this pathway has been described as failing for 1-aminomethyl-*o*-carboranes,<sup>[20]</sup> we have demonstrated the feasibility of this approach for compounds **2b** and **3b** bearing methylene connectors. During synthesis of **9b**, an equilibrium mixture of two isomers formed after lithiation of 9-C<sub>6</sub>H<sub>5</sub>-1,2-C<sub>2</sub>B<sub>10</sub>H<sub>11</sub> and subsequent reaction with bromomethyl phthalimide as a result of the presence of two available CH sites with similar reactivity. The isolated mixture of the 9- and 12-phenyl isomers (in a nearly 1:1 ratio) could not be separated by liquid chromatography either as phthalimido-protected amines or after deprotection. This isomeric mixture was therefore used for the synthesis of sulfamide derivatives **3ma** and **3na**. Derivatives **8b** and **9b** were obtained using hydrazine hydrate to convert 1-alkylphthalimido-2-phenyl-*closo*-1,2-carboranes into their respective 11-vertex *nido*-[C<sub>2</sub>B<sub>9</sub>H<sub>12</sub>]<sup>−</sup> ion species, as described in a previous report.<sup>[17]</sup> For the preparation of **7b**, we used a new straightforward one-step deboronation<sup>[8]</sup>/amination of 1-BrCH<sub>2</sub>-1,2-C<sub>2</sub>B<sub>10</sub>H<sub>11</sub>. The reaction proceeds even with 24 % aqueous NH<sub>4</sub>OH, producing a mixture of the target *nido*-derivative **7b** along with two other boron-substituted isomeric species (7-CH<sub>3</sub>-9-NH<sub>2</sub>-1,7-C<sub>2</sub>B<sub>9</sub>H<sub>10</sub>, 7-CH<sub>3</sub>-11-NH<sub>2</sub>-1,7-C<sub>2</sub>B<sub>9</sub>H<sub>10</sub>) in lower yield (ca. 35 %). Compound **7b** could be isolated in good yield (62 %) by column chromatography. Compound **10b** was prepared by cleavage of the dioxane derivative 10-O(CH<sub>2</sub>CH<sub>2</sub>)<sub>2</sub>O-C<sub>2</sub>B<sub>9</sub>H<sub>10</sub> with ammonia, as described in a previous report.<sup>[23]</sup>

Addition of the sulfamide end group was accomplished with high yields by heating the respective amines with sulfamide in dioxane (see Scheme 1). Potassium carbonate was used for the deprotonation of the ammonium groups or to release the respective amines from their hydrochlorides in situ. Nevertheless, the attempted synthesis of 1-H<sub>2</sub>NSO<sub>2</sub>NH-(CH<sub>2</sub>)<sub>2</sub>-2-C<sub>6</sub>H<sub>5</sub>-*closo*-1,2-C<sub>2</sub>B<sub>10</sub>H<sub>10</sub> and [7-H<sub>2</sub>NSO<sub>2</sub>NH-(CH<sub>2</sub>)<sub>2</sub>-8-C<sub>6</sub>H<sub>5</sub>-*nido*-7,8-C<sub>2</sub>B<sub>9</sub>H<sub>10</sub>]<sup>−</sup> (potential members of the series with intermediate chain lengths; the amines prepared analogously to a published procedure<sup>[22]</sup>) failed owing to quantitative elimination of the substituent in the reaction with sulfamide, thus resulting in only the starting phenyl carborane.

Received: August 28, 2013

Published online: November 4, 2013

**Keywords:** carbonic anhydrases · carboranes · drug discovery · inhibitors · structure elucidation

[1] C. T. Supuran, *Nat. Rev. Drug Discovery* **2008**, *7*, 168–181.

[2] C. T. Supuran, A. Scozzafava, A. Casini, *Med. Res. Rev.* **2003**, *23*, 146–189.

- [3] P. Swietach, S. Patiar, C. T. Supuran, A. L. Harris, R. D. Vaughan-Jones, *J. Biol. Chem.* **2009**, *284*, 20299–20310.
- [4] V. M. Krishnamurthy, G. K. Kaufman, A. R. Urbach, I. Gitlin, K. L. Gudiksen, D. B. Weibel, G. M. Whitesides, *Chem. Rev.* **2008**, *108*, 946–1051.
- [5] M. Aggarwal, R. McKenna, *Expert Opin. Ther. Pat.* **2012**, *22*, 903–915.
- [6] C. T. Supuran, *J. Enzyme Inhib. Med. Chem.* **2012**, *27*, 759–772.
- [7] P. Mader, J. Brynda, R. Gitto, S. Agnello, P. Pachel, C. T. Supuran, A. Chimirri, P. Rezacova, *J. Med. Chem.* **2011**, *54*, 2522–2526.
- [8] R. N. Grimes, *Carboranes*, 2nd ed., Academic Press (Elsevier, Inc.), London, **2011**, and references therein.
- [9] Z. J. Lesnikowski, *Collect. Czech. Chem. Commun.* **2007**, *72*, 1646–1658.
- [10] F. Issa, M. Kassiou, L. Rendina, *Chem. Rev.* **2011**, *111*, 5701–5722.
- [11] P. Cigler, M. Kozisek, P. Rezacova, J. Brynda, Z. Otwinowski, J. Pokorna, J. Plešek, B. Gruner, L. Doleckova-Maresova, M. Masa, J. Sedlacek, J. Bodem, H. G. Krausslich, V. Kral, J. Konvalinka, *Proc. Natl. Acad. Sci. USA* **2005**, *102*, 15394–15399.
- [12] Y. Endo, T. Iijima, Y. Yamakoshi, H. Fukasawa, C. Miyaura, M. Inada, A. Kubo, A. Itai, *Chem. Biol.* **2001**, *8*, 341–355.
- [13] S. Fujii, H. Masuno, Y. Taoda, A. Kano, A. Wongmayura, M. Nakabayashi, N. Ito, M. Shimizu, E. Kawachi, T. Hirano, Y. Endo, A. Tanatani, H. Kagechika, *J. Am. Chem. Soc.* **2011**, *133*, 20933–20941.
- [14] M. Scholz, M. Steinhausen, J. T. Heiker, A. G. Beck-Sickinger, E. Hey-Hawkins, *ChemMedChem* **2011**, *6*, 89–93.
- [15] R. C. Reynolds, S. R. Campbell, R. G. Fairchild, R. L. Kisluk, P. L. Micca, S. F. Queener, J. M. Riordan, W. D. Sedwick, W. R. Waud, A. K. W. Leung, R. W. Dixon, W. J. Suling, D. W. Borhani, *J. Med. Chem.* **2007**, *50*, 3283–3289.
- [16] J. Rak, B. Dejlova, H. Lampova, R. Kaplanek, P. Matejcek, P. Cigler, V. Kral, *Mol. Pharm.* **2013**, *10*, 1751–1759.
- [17] J. G. Wilson, A. K. M. Anisuzzaman, F. Alam, A. H. Soloway, *Inorg. Chem.* **1992**, *31*, 1955–1958.
- [18] J. Plešek, T. Jelínek, E. Drdáková, S. Heřmánek, B. Štíbr, *Collect. Czech. Chem. Commun.* **1984**, *49*, 1559–1562.
- [19] S. L. Woodhouse, L. M. Rendina, *J. Chem. Soc. Dalton Trans.* **2004**, 3669–3677.
- [20] Y. Wu, P. J. Carroll, S. O. Kang, W. Quintana, *Inorg. Chem.* **1997**, *36*, 4753–4761.
- [21] A. S. Batsanov, A. E. Goeta, J. A. K. Howard, A. K. Hughes, J. M. Malget, *J. Chem. Soc. Dalton Trans.* **2001**, 1820–1826.
- [22] J. D. Lee, Y. J. Lee, H. J. Jeong, J. S. Lee, C. H. Lee, J. Ko, S. O. Kang, *Organometallics* **2003**, *22*, 445–449.
- [23] P. Rezacova, J. Pokorná, J. Brynda, M. Kožíšek, P. Cigler, M. Lepšík, J. Fanfrlík, J. Řezáč, K. Grantz Šašková, I. Siegllová, J. Plešek, V. Šícha, B. Gruner, H. Oberwinkler, J. Sedláček, H. G. Krausslich, P. Hobza, V. Král, J. Konvalinka, *J. Med. Chem.* **2009**, *52*, 7132–7141.

## Research Article

# Carborane-Based Carbonic Anhydrase Inhibitors: Insight into CAII/CAIX Specificity from a High-Resolution Crystal Structure, Modeling, and Quantum Chemical Calculations

Pavel Mader,<sup>1,2</sup> Adam Pecina,<sup>3</sup> Petr Cígler,<sup>3</sup> Martin Lepšík,<sup>3</sup> Václav Šícha,<sup>4</sup> Pavel Hobza,<sup>3,5</sup> Bohumír Grüner,<sup>4</sup> Jindřich Fanfrlík,<sup>3</sup> Jiří Brynda,<sup>1,3</sup> and Pavlína Řezáčová<sup>1,3</sup>

<sup>1</sup> Institute of Molecular Genetics, Academy of Sciences of the Czech Republic, Vídeňská 1083, 140 00 Prague 4, Czech Republic

<sup>2</sup> Structural Genomics Consortium, University of Toronto, Toronto, ON, Canada M5G 1L7

<sup>3</sup> Institute of Organic Chemistry and Biochemistry, Academy of Sciences of the Czech Republic, Gilead Sciences and IOCB Research Center, Flemingovo nám. 2, 166 10 Prague 6, Czech Republic

<sup>4</sup> Institute of Inorganic Chemistry, Academy of Sciences of the Czech Republic, v.v.i., Hlavní 1001, 250 68 Řež near Prague, Czech Republic

<sup>5</sup> Regional Center of Advanced Technologies and Materials, Department of Physical Chemistry, Palacký University, 77146 Olomouc, Czech Republic

Correspondence should be addressed to Jindřich Fanfrlík; fanfrlik@uochb.cas.cz, Jiří Brynda; brynda@img.cas.cz, and Pavlína Řezáčová; rezacova@uochb.cas.cz

Received 24 April 2014; Accepted 8 June 2014; Published 18 September 2014

Academic Editor: Mariya Al-Rashida

Copyright © 2014 Pavel Mader et al. This is an open access article distributed under the Creative Commons Attribution License, which permits unrestricted use, distribution, and reproduction in any medium, provided the original work is properly cited.

Carborane-based compounds are promising lead structures for development of inhibitors of carbonic anhydrases (CAs). Here, we report structural and computational analysis applicable to structure-based design of carborane compounds with selectivity toward the cancer-specific CAIX isoenzyme. We determined the crystal structure of CAII in complex with 1-methylenesulfamide-1,2-dicarba-*closo*-dodecaborane at 1.0 Å resolution and used this structure to model the 1-methylenesulfamide-1,2-dicarba-*closo*-dodecaborane interactions with CAIX. A virtual glycine scan revealed the contributions of individual residues to the energy of binding of 1-methylenesulfamide-1,2-dicarba-*closo*-dodecaborane to CAII and CAIX, respectively.

## 1. Introduction

Carbonic anhydrases (CAs) play important roles in many physiological and pathophysiological processes. For example, extracellular CAs participate in tumor growth and progression [1]. CAIX, which is selectively expressed in a range of hypoxic tumors, is a validated diagnostic and therapeutic target (recently reviewed in [2–4]). There are 15 human CA isoenzymes, and due to the ubiquity of these enzymes in human tissues, selective inhibition is a very important aspect of drug design.

Three main classes of CA inhibitors have been described to date (reviewed in [5]): (i) metal ion binders (sulfonamides, sulfamides, sulfamates, dithiocarbamates, thiols, and hydroxamates); (ii) compounds that anchor the zinc-coordinated

water molecule/hydroxide ion (phenols, carboxylates, polyamines, esters, and sulfocoumarins); and (iii) coumarins and related compounds that bind further away from the metal ion.

CA inhibitors from the first class (metal ion binders) contain specific functional groups that interact with the catalytic Zn<sup>2+</sup> ion in the CA active site. These metal-binding functionalities are typically joined to a “ring” structure. This moiety is not necessarily aromatic; however, it is usually consisting of a 5- or 6-membered hydrocarbon ring or conjugated ring system containing nitrogen, oxygen, and/or sulfur. Numerous functional groups have been added to the ring structure scaffold to modify inhibitor properties such as specificity toward a particular CA isoenzyme, pK<sub>a</sub>, or solubility (reviewed in [6]). Recently, we reported design of CA inhibitors containing



space-filling carborane clusters in place of the typical ring structure [7]. We showed that various carborane clusters act as CA inhibitors and that modifying these clusters with an appropriately attached sulfamide group and other substituents leads to compounds with selectivity toward the cancer-specific CAIX isoenzyme.

Boron is one of few chemical elements that can form binary hydrides composed of more than two atoms, which leads to formation of boron cluster compounds (boron hydrides or boranes). Their basic structural feature is formation of a polyhedron with triangular facets held together by 3-center 2-electron bonds with an extensive electron delocalization [8]. A typical structural archetype is represented by the divalent *closo*-B<sub>12</sub>H<sub>12</sub><sup>2-</sup> anion, an extremely stable compound with a symmetrical 12-vertex icosahedron structure [9]. Replacement of one or more {BH<sup>-</sup>} in borane cage with {CH} leads to series of carboranes and removal of BH vertices leads to various open-cage (*nido*-) species. Carboranes thus offer a large variety of structural archetypes that provide interesting counterparts to organic compounds [10].

Many features of icosahedral 12-vertex carboranes are useful in the design of biologically active compounds. Carboranes have high thermal and chemical stability; therefore, they generally do not undergo catabolism and are nontoxic to the host organism [11, 12]. The basic *closo*-C<sub>2</sub>B<sub>10</sub>H<sub>12</sub> carborane cluster is highly hydrophobic [13]; however, its controlled deboronation can generate water soluble 11-vertex *nido*-C<sub>2</sub>B<sub>9</sub>H<sub>12</sub><sup>-</sup>. These anions represent important intermediates in the synthesis of a family of mainly anionic metal bis(dicarbollides) accessible via metal insertion. Incorporation of carborane cages into the structures of certain substances of medicinal interest can enhance hydrophobic interactions between the boron cluster-coupled pharmaceuticals and their protein targets, increase *in vivo* stability, and facilitate uptake through cellular membranes [14, 15]. The successful use of boron clusters as hydrophobic pharmacophores has recently been increasing [16, 17]. Examples of carborane pharmacophores include boron-containing antifolates [18], HIV protease inhibitors [19, 20], and estrogen receptor agonists and antagonists [21], among others [16, 22, 23].

Drug design efforts benefit greatly from knowledge of the 3D structures of protein-ligand complexes. X-ray crystallography has contributed considerably to the development of CA inhibitors; more than 500 structures of human CA isoenzymes (wild-type and mutant forms) in complex with various inhibitors have offered unprecedented insight into inhibitor binding modes (reviewed in [24]). Structural information coupled with experimental inhibition data can be used to validate various computational approaches to assess inhibitor binding strength. Once a particular theoretical approach reproduces the known data well, it can be used for prospective design. For studies involving metal ions and unusual compounds such as boranes, the use of quantum chemistry (QM) is warranted [25, 26]. Indeed, we recently used a quantum mechanics/molecular mechanics (QM/MM) methodology to quantitatively describe the binding of two carborane-based sulfamides to CAII [7] and to explain fundamental differences in the binding modes of *closo*- and *nido*-cages [27].

Here, we report the X-ray structure of CAII with bound 1-methylenesulfamide-1,2-dicarba-*closo*-dodecaborane (compound **1**, Figure 1(a)) determined at 1.0 Å resolution. This atomic-level resolution allowed us to assess in detail the positions of carbon and boron atoms in the carborane cage of **1**. Additionally, we modeled the complex of **1** with CAIX. We employed a virtual glycine scan to analyze the differences between the interactions of **1** with CAII and CAIX.

## 2. Materials and Methods

**2.1. Protein Crystallization and Diffraction Data Collection.** For crystallization of human CAII (Sigma, catalogue number C6165) in complex with 1-methylenesulfamide-1,2-dicarba-*closo*-dodecaborane (compound **1**), we adapted a previously described procedure [28]. CAII (at a concentration of 4 mg·mL<sup>-1</sup>, dissolved in water) was incubated in aqueous solution containing a 2-fold molar excess of *p*-hydroxymercuribenzoate (Sigma, catalogue number 55540). The protein was concentrated to 10 mg·mL<sup>-1</sup> and unbound *p*-hydroxymercuribenzoate was removed with Amicon Ultra-4 concentrators (Merck-Millipore MWCO 10 kDa).

The complex of CAII with **1** was prepared by adding a 1.1-fold molar excess of **1** (in DMSO) to the 10 mg·mL<sup>-1</sup> solution of CAII in water without pH adjustment (the final DMSO concentration did not exceed 5% v/v).

The best diffracting crystals were obtained using the hanging-drop vapor diffusion method under the following conditions: 2 μL protein-inhibitor complex solution was mixed with 2 μL precipitant solution [2.5 M (NH<sub>4</sub>)<sub>2</sub>SO<sub>4</sub>, 0.3 M NaCl, and 100 mM Tris-HCl, pH 8.2] and equilibrated over a reservoir containing 1 mL of precipitant solution at 18°C. Crystals with dimensions of 0.3 mm × 0.1 mm × 0.1 mm grew within 7 days.

For cryoprotection, the crystals were incubated in mother liquor supplemented with 25% glycerol for approximately 30 s, flash-frozen, and stored in liquid nitrogen. Diffraction data for the CAII complex were collected at 100 K at the X14.2 BESSY beamline in Berlin, Germany [29]. Data were collected in two passes: the high-resolution range (1.75–1.00 Å) and the low-resolution range (21.08–1.20 Å). The two datasets were integrated with iMOSFLM [30] and merged and scaled with SCALA [31]. Data collection and refinement statistics are summarized in Table 1.

**2.2. Structure Determination, Refinement, and Analysis.** Crystal structures were solved by difference Fourier method using the CAII structure (PDB code 3IGP [34]) as a starting model. The model was refined using REFMAC5 [35], part of the CCP4 program suite [36]. The model was initially refined with isotropic atomic displacement parameters (ADPs); hydrogen atoms in riding positions were added later. For the final rounds of refinement, we used a mixed isotropic-anisotropic model of ADPs: anisotropic ADPs were used for all atoms, and only atoms in alternative conformations were refined isotropically. Atomic coordinates for the structure of **1** were generated by quantum mechanics computation with DFT-D methodology [37] using the B-LYP functional and SVP basis set [38] in the Turbomole program [39].

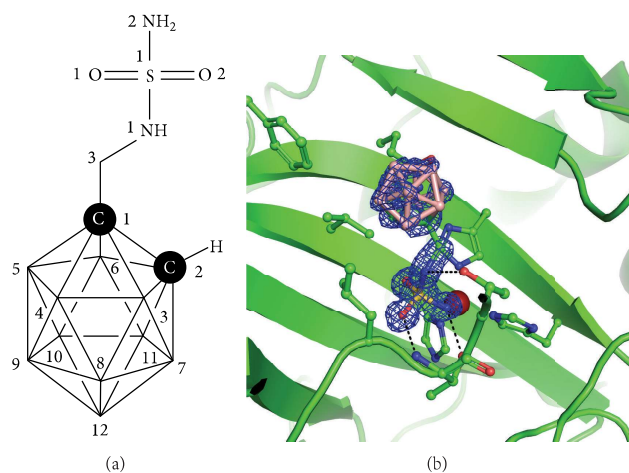


FIGURE 1: (a) Structural formula of **1** with atom numbers used in the crystal structure coordinate file. The vertices in carborane cluster represent BH groups. (b) Crystal structure of CAII in complex with **1**. The CAII active site is shown in cartoon representation; residues involved in interactions with the Zn<sup>2+</sup> ion (purple sphere) and **1** are shown in stick representation with carbon atoms colored green. Boron atoms are colored pink, and other heteroatoms are colored according to standard color coding: oxygen, red; nitrogen, blue; sulfur, yellow. The 2*Fo*-*Fc* electron density map for **1** is contoured at 1  $\sigma$ .

A geometric library for **1** was generated using the Libcheck program from the CCP4 suite. Coot [40] was used for rebuilding. The quality of the refined model was assessed using MolProbity [33]. The coordinates and structure factors were deposited in the PDB under accession code 4Q78. Final refinement statistics are summarized in Table 1. All structural figures were prepared using PyMOL 1.4.1 [41].

**2.3. Model of CAIX-1 Complex.** The complex of CAIX and **1** was modeled by aligning the existing crystal structures of the CAIX catalytic domain (PDB code 3IAI [42]) with the CAII-**1** complex (PDB code 4MDG [7]) using PyMOL version 1.2 [43]. Preparation of structure coordinate files for further calculations was performed as described before for CAII [27].

The complex was fully optimized using a QM/MM procedure. We used ONIOM-like subtractive scheme [44] with link atoms and mechanical embedding to be consistent with our previous studies [27, 45–48]. The QM part is described at the DFT-D TPSS/TZVP//BLYP/SVP level of theory [39] and comprises 218 atoms including the atoms present in **1** and 8 amino acids (Trp5, Asn62, His64, Gln67, Gln92, Val131, Leu135, and Pro202). The MM part constituted the remainder of the protein, and the surrounding solvent was approximated by a generalized Born (GB) implicit model. Detailed description of the procedure was published in [27]. One crystal water molecule (Wat272) bridging the inhibitors and CAII residues Thr199, Glu106, and Tyr7 was retained to maintain the integrity of the active site. Other water molecules present in the crystal structures were omitted.

The positions of the added hydrogen atoms, **1**, and 15 amino acids surrounding the ligand (Trp5, Asn62, Gly63, His64, Gln67, Leu91, Gln92, Leu123, Val131, Leu135, Leu141, Thr200, Pro201, Pro202, and Ala204) were relaxed in a GB implicit solvent model using the FIRE algorithm followed

by 10 ps annealing from 100 K or 150 K to 0 K using the Berendsen thermostat [49] in the SANDER module of the AMBER 10 package [50].

**2.4. Virtual Glycine Scan.** The contribution of the active site amino acids to inhibitor binding was examined by virtual glycine scanning. Individual amino acids in contact with **1** in the CAIX-1 model and CAII-1 crystal structure were substituted with glycine. The energy contributions ( $\Delta\Delta G'_{\text{int}}$ ) were calculated as the difference between the original  $\Delta G'_{\text{int}}$  at the QM/MM level with the wild-type amino acid and the new  $\Delta G'_{\text{int}}$  with the mutated glycine residue [27].

### 3. Results and Discussion

**3.1. Crystal Structure of CAII in Complex with **1** at Atomic Resolution.** The overall structure of CAII in complex with **1** was refined to 1.0 Å resolution. This high resolution allowed us to observe details that could not be fully resolved in the complex structure determined previously at lower resolution. Atomic resolution was achieved by derivatization of CAII using the 4-(hydroxymercury)benzoic acid (abbreviated MBO in the cif library of small molecules) method described by [28]. The mercury atom of MBO covalently binds to S $\gamma$  of Cys206. This modification allows formation of a hydrogen bond between the OZ1 oxygen of the MBO carboxyl group and the main-chain amino group of Tyr40 in the neighboring protein molecule, reinforcing the crystal lattice and increasing the diffraction quality of the crystal. In our structure, MBO is modeled in two alternative conformations with occupancies of 0.6 and 0.2.

When our atomic resolution structure is compared with the structure of the CAII-1 complex determined at 1.35 Å resolution (PDB code 4MDG [7]), the RMSD value for

TABLE 1: Data collection and refinement statistics.

Data collection statistics	
Space group	$P2_1$
Cell parameters (Å; °)	42.20, 41.73, 72.16; 90.0, 104.4, 90.0
Wavelength (Å)	0.9184
Resolution (Å)	21.08–1.00 (1.05–1.00)
Number of unique reflections	108,781 (15,490)
Multiplicity	3.5 (2.5)
Completeness (%)	83.1 (81.4)
$R_{\text{merge}}^a$	0.056 (0.375)
Average $I/\sigma(I)$	10.8 (2.3)
Wilson B (Å <sup>2</sup> )	6.5
Refinement statistics	
Resolution range (Å)	69.90–1.00 (1.03–1.00)
No. of reflections in working set	97,856 (7,831)
No. of reflections in test set	5,426 (412)
R value (%) <sup>b</sup>	17.5 (24.4)
$R_{\text{free}}$ value (%) <sup>c</sup>	20.0 (26.2)
RMSD bond length (Å)	0.011
RMSD angle (°)	1.53
Number of atoms in AU	2297
Number of protein atoms in AU	2081
Number of water molecules in AU	176
Mean ADP value protein/inhibitor (Å <sup>2</sup> )	12.0/17.6
Ramachandran plot statistics <sup>d</sup>	
Residues in favored regions (%)	96.56
Residues in allowed regions (%)	3.44

The data in parentheses refer to the highest-resolution shell.

<sup>a</sup> $R_{\text{merge}} = \sum_{hkl} \sum_i I_i(hkl) - \langle I(hkl) \rangle / \sum_{hkl} \sum_i I_i(hkl)$ , where  $I_i(hkl)$  is the individual intensity of the  $i$ th observation of reflection  $hkl$  and  $\langle I(hkl) \rangle$  is the average intensity of reflection  $hkl$  with summation over all data.

<sup>b</sup> $R$  value =  $\|F_o - |F_c|\| / \|F_o\|$ , where  $F_o$  and  $F_c$  are the observed and calculated structure factors, respectively.

<sup>c</sup> $R_{\text{free}}$  is equivalent to  $R$  value but is calculated for 5% of reflections chosen at random and omitted from the refinement process [32].

<sup>d</sup>as determined by Molprobit [33].

superposition of the  $C\alpha$  atoms of residues 4–261 is 0.142 Å, a value typical for superposition of identical structures [51]. The N-terminal residue His3 is traced differently in the two structures; double conformations of numerous side chains (e.g., Glu14, His64, and Gln74) are resolved in the atomic resolution structure. We found an additional difference in the loop formed by amino acid residues 124–139, with a maximum difference of 0.738 Å for the position of Gln136  $C\alpha$ . Gln136 forms van der Waals contacts with the MBO covalently attached to Cys206. The positions of Phe131 and Val135, which form a hydrophobic rim at the active site, are also influenced by MBO binding. This results in a subtle positional shift of the inhibitor, with an RMSD of 0.145 Å for superposition of 12 atoms in the carborane cage of **1** bound to CAII and CAII derivatized by MBO. This value is below the value observed for superposition of identical structures [51].

Atomic-level resolution allowed us to resolve the carbon and boron atom positions in the symmetrical carborane

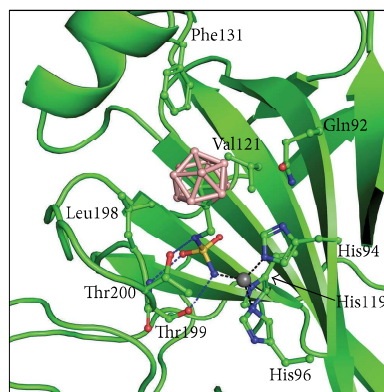


FIGURE 2: Interactions of **1** with CAII. The protein is shown in cartoon representation; residues involved in interactions with the  $Zn^{2+}$  ion (gray sphere) and **1** are shown in stick representation. Polar interactions are represented by blue dashed lines;  $Zn^{2+}$  ion coordination is shown as black dashed lines.

cage of **1**. When analyzing the values of the electron density map at positions of atoms bonded to the C1 atom, we can assume that positions with higher density levels are more likely to be carbon than boron atoms. Similar analysis was done by others for boron-containing inhibitor of human dihydrofolate reductase [18]. The C2 atom of the carborane cage (Figure 1(a)) was modeled into the position with an electron density value of  $1.16 \text{ e}/\text{\AA}^3$ , which was approximately  $0.15 \text{ e}/\text{\AA}^3$  higher than those for the B3, B4, B5, and B6 atoms. To exclude the possibility that higher density is caused by model bias, we altered the composition of the cage by replacing the C2 atom with a boron atom. Electron density values did not change significantly after several rounds of refinement cycles.

Thus, we can conclude that the most probable position of the second carbon atom in the carborane cage of **1** is the position assigned to the C2 atom in our crystal structure. This is in good agreement with the recently published QM/MM modeling study [27].

### 3.2. Detailed Analysis of Inhibitor Interactions with CAII.

The crystal structure of human CAII in complex with **1** determined at 1.0 Å resolution confirmed the key interactions that our group observed previously [7]. The compound fits very well into the CAII active site cavity and makes numerous polar and nonpolar interactions with the residues in the enzyme active site. The sulfamide moiety, which forms key polar interactions with the active site  $Zn^{2+}$  ion, also makes polar interactions with Thr199 typical of other sulfamide inhibitors of CAII (Figure 2). The linker NH group forms an additional polar interaction with Oy of Thr200. The compound makes several van der Waals interactions with residues Gln92, His94, His96, His119, Val121, Phe131, Leu198, and Thr200 (Figure 2). All interactions between the inhibitor and protein are summarized in Table 2.

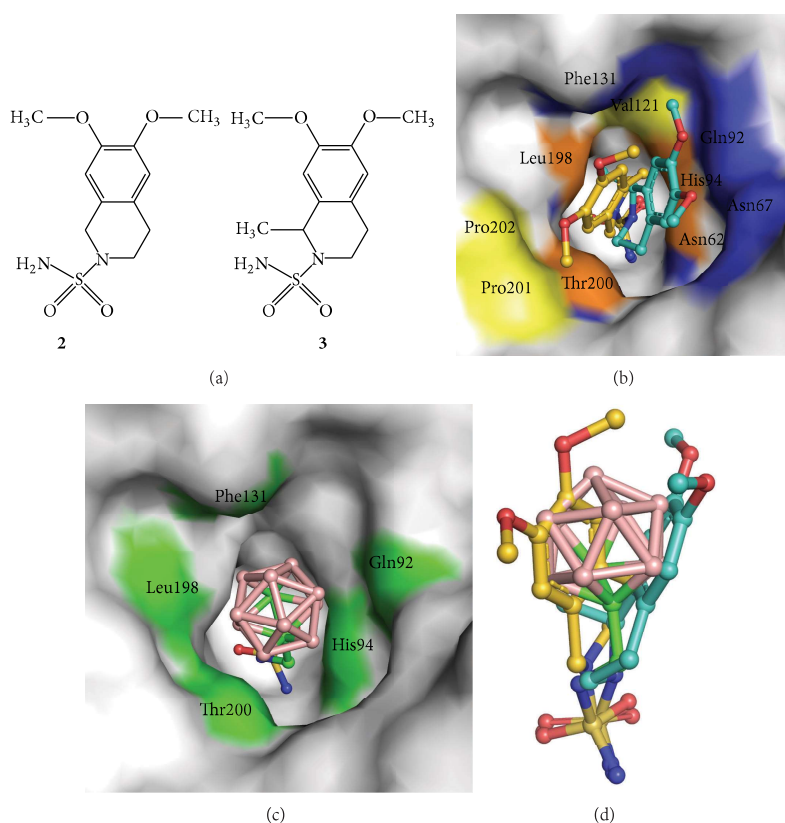


FIGURE 3: (a) Structural formulas of **2** and **3**. (b) Interactions of **2** and **3** with the CAII active site. Compound **2** is represented with golden carbon atoms, while the carbon atoms of **3** are colored turquoise. Surface of residues making contacts with the isoquinoline moiety of **2** and **3** are highlighted in yellow and blue, respectively. Surface of residues colored orange make contacts with both compounds. Atoms involved in contacts with the sulfonamide groups are not highlighted. (c) Interactions of **1** with the CAII active site. Surface of residues making contacts with the carborane and linker moiety of **1** are highlighted in green. Atoms involved in contacts with the sulfonamide groups are not highlighted. (d) Superposition of binding poses of **1**, **2**, and **3** in the CAII active site. Superposition of the complex structures was based on the best fit for C $\alpha$  atoms of CAII residues 6–261.

The idea of designing CA inhibitors containing a carborane cluster moiety originated from our previous structural studies of isoquinoline-containing sulfonamide inhibitors (Figure 3(a)). Structural analysis of CAII in complex with 6,7-dimethoxy-1,2,3,4-tetrahydroisoquinolin-2-ylsulfonamide (**2**, PDB code 3IGP, [34]) and 6,7-dimethoxy-1-methyl-1,2,3,4-tetrahydroisoquinolin-2-ylsulfonamide (**3**, PDB code 3PO6, [52]) revealed two distinct binding modes that engage two opposite sides of the enzyme active site cavity (Figure 3(b)). Following this analysis, we hypothesized that the binding space within the enzyme active site cavity could be effectively filled with a bulky hydrophobic molecule with a spherical structure. This led to design of **1** which exhibited inhibitory property to CAII and CAIX with  $K_i$  values in submicromolar range. Structural analysis of CAII-**1** indicates that our structure-based design was sound. We found that the carborane cluster interacts with both sides of the enzyme active site as predicted (Figure 3(c), Table 3) and that the position of **1**

in the CAII active site superposes well with the two binding modes observed for **2** and **3** (Figure 3(d)).

**3.3. Model of the CAIX-1 Complex.** The CAII-**1** crystal structure was used to model binding of compound **1** into the CAIX active site using QM/MM methods (Figure 4).

The substrate binding sites of CAII and CAIX differ by only six amino acids: Asn67 of CAII is replaced by Gln in CAIX, Ile91 by Leu, Trp123 by Leu, Phe131 by Val, Val135 by Leu, and Leu204 by Ala. These variations result in a differently shaped active site cavity, which accommodated **1** in a slightly different pose (Figure 4). While the position of the sulfamide anchor remained unchanged, the carborane cluster shifted by 2.1 Å (expressed as a difference in the position of B12) away from the central  $\beta$ -sheet. In CAIX-**1**, the carborane interacts more with the opposite site of the active site, specifically with amino acid residues His94, His96, Glu106, Leu198, Thr199, Thr200, and Pro201 (Figure 4, Table 3). All polar and van der



TABLE 2: List of contacts between CAII and **1**.

	CAII		<b>1</b>		Distance [Å] <sup>b</sup>
	Residue	Atom	Atom <sup>a</sup>		
	<b>Zn</b>	<b>ZN</b>	<b>N2</b>		<b>1.87<sup>c</sup></b>
	Zn	ZN	S		3.04
	Zn	ZN	O2		3.05
92	Gln	OE1	B6		3.47
92	Gln	OE1	B11		3.52
92	Gln	CD	B6		3.84
94	His	CE1	O2		2.97
94	His	NE2	N2		3.23
94	His	NE2	O2		3.31
94	His	CE1	C3		3.67
94	His	NE2	S		3.81
94	His	CE1	N2		3.82
94	His	CE1	S		3.84
94	His	NE2	C3		3.94
96	His	NE2	N2		3.14
96	His	CE1	N2		3.56
119	His	ND1	N2		3.39
119	His	ND1	O2		3.88
119	His	CE1	N2		3.96
121	Val	CG2	O2		3.82
131	Phe	CZ	B8		3.83
131	Phe	CZ	B7		3.97
198	Leu	CA	O1		3.09
198	Leu	C	O1		3.36
198	Leu	CB	O1		3.60
198	Leu	CD2	O1		3.63
198	Leu	CD1	B3		3.86
<b>199</b>	<b>Thr</b>	<b>N</b>	<b>O1</b>		<b>2.70</b>
<b>199</b>	<b>Thr</b>	<b>OG1</b>	<b>N2</b>		<b>2.74</b>
199	Thr	OG1	O1		3.58
199	Thr	OG1	S		3.78
199	Thr	N	S		3.83
199	Thr	CA	O1		3.83
199	Thr	CB	N2		3.98
<b>200</b>	<b>Thr</b>	<b>OG1</b>	<b>N1</b>		<b>3.02</b>
200	Thr	OG1	C3		3.14
200	Thr	OG1	B4		3.36
200	Thr	OG1	B3		3.56
200	Thr	OG1	C1		3.66

<sup>a</sup>Atom labels correspond to those shown in Figure 1(a).

<sup>b</sup>All contacts with a distance between ligand and protein (or Zn) atoms less than or equal to 4 Å are listed.

<sup>c</sup>Polar interactions are highlighted in bold.

Waals interactions between CAIX and **1** are summarized in Table 4.

We used a virtual glycine scan to study the roles of individual amino acid side chains in the active sites of CAII and CAIX in binding of **1**. The changes in free energy of

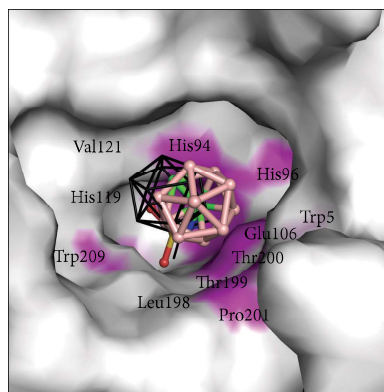


FIGURE 4: Interactions of **1** with the CAIX active site. Atoms making contacts with the carborane and linker moiety of **1** are highlighted in magenta. Atoms involved in contacts with the sulfonamide groups are not highlighted. Superposition of the binding pose of **1** in CAII is shown as black lines. Superposition is based on the best fit for Ca atoms of all residues of CAII onto CAIX.

TABLE 3: CAII or CAIX residues interacting with **1**, **2**, and **3**.

<b>1</b> <sup>a</sup>	CAII <b>2</b> <sup>b</sup>	<b>3</b> <sup>c</sup>	CAIX <b>1</b> <sup>d</sup>
			Trp5
		Asn62	
		<b>Asn67<sup>c</sup></b>	
Gln92	Gln92	Gln92	
His94	His94	His94	His94
His96	His96	His96	His96
			Glu106
His119	His119	His119	His119
Val121		Vall21	Vall21
Phe131	Phe131	Phe131	
	Vall43	Vall43	
Leu198	Leu198	Leu198	Leu198
<b>Thr199</b>	<b>Thr199</b>	<b>Thr199</b>	<b>Thr199</b>
<b>Thr200</b>	Thr200	Thr200	<b>Thr200</b>
	Pro201		Pro201
	Pro202		
	Trp209		Trp209

Interacting residues were identified from <sup>a</sup>crystal structure 4Q78 (this work);

<sup>b</sup>crystal structure 3IGP [34]; <sup>c</sup>crystal structure 3PO6 [52]; <sup>d</sup>computational model (this work); <sup>e</sup>residues making polar interactions are highlighted in bold.

interaction ( $\Delta\Delta G'_{int}$ ) upon mutation of a given amino acid residue to glycine are shown in Figure 5.

The largest energy change (2.6 kcal/mol) occurred for Trp5, which is positioned closer to **1** in CAIX-1 than in CAII-1. The side chain of Trp5 forms several dihydrogen bonds with the carborane cage of **1**. The shortest one has a H...H distance of 2.3 Å. The other major contributor to strong

TABLE 4: Interactions between CAIX and 1.

CAIX Residue	Atom	1 Atom <sup>a</sup>	Distance [Å] <sup>b</sup>	
	<b>Zn</b>	<b>ZN</b>	<b>N2</b>	<b>2.1<sup>c</sup></b>
	Zn	ZN	S	3.3
	Zn	ZN	O2	3.5
5	Trp	CZ2	B5	3.74
5	Trp	CZ2	B10	3.81
94	His	CE1	O2	3.15
94	His	CE1	C3	3.74
94	His	NE2	N2	3.36
94	His	NE2	S	3.88
94	His	NE2	O2	3.45
94	His	NE2	C3	3.76
96	His	CE1	N2	3.99
96	His	NE2	N2	3.49
106	Glu	OE2	N2	3.71
119	His	ND1	N2	3.37
119	His	CE1	N2	3.83
121	Val	CG2	O2	3.58
198	Leu	CA	O1	3.04
198	Leu	CB	O1	3.4
198	Leu	CD2	O1	3.43
198	Leu	C	O1	3.38
199	Thr	N	S	3.88
<b>199</b>	<b>Thr</b>	<b>N</b>	<b>O1</b>	<b>2.79</b>
199	Thr	CA	O1	3.96
199	Thr	CB	N2	3.85
<b>199</b>	<b>Thr</b>	<b>OG1</b>	<b>N2</b>	<b>2.63</b>
199	Thr	OG1	S	3.69
199	Thr	OG1	O1	3.65
200	Thr	OG1	C1	3.77
200	Thr	OG1	B5	3.56
<b>200</b>	<b>Thr</b>	<b>OG1</b>	<b>N1</b>	<b>3.13</b>
200	Thr	OG1	C3	3.31
200	Thr	OG1	B4	3.64
201	Pro	O	B4	3.6
201	Pro	O	B10	3.49
201	Pro	O	B8	3.96
209	Trp	CZ2	O1	3.74

<sup>a</sup>Atom labels correspond to those shown in Figure 1(a).

<sup>b</sup>All contacts with a distance less than or equal to 4 Å between ligand and protein (and Zn) atoms are listed.

<sup>c</sup>Polar interactions are highlighted in bold.

CAIX-1 binding was Asn62; the energy of binding exceeded that in CAII-1 by nearly 1 kcal/mol. These contributions were cancelled out by differences in binding energy contributions of amino acid residues 131 (Phe/Val) and 135 (Val/Leu), which were lower in CAIX by 0.7 and 0.9 kcal/mol, respectively. The energy changes of other residues were small.

When we compared binding of 1 to CAII and CAIX, we noted that the favorable energy changes in CAIX-1 due to the binding of residues Trp5, Asn62, and His64 were slightly

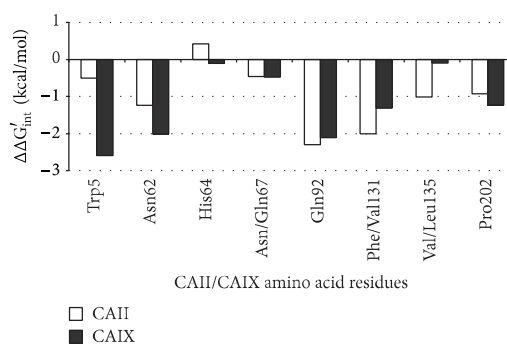


FIGURE 5: Results of virtual glycine scan showing contributions of individual residues to the energy of binding of 1 to CAII and CAIX, respectively.

larger than the unfavorable changes in binding caused by the different amino acids at residues 131 and 135. This is in qualitative agreement with the experimental  $K_i$  values, which are  $700 \pm 141$  nM for inhibition of CAII and  $380 \pm 111$  nM for inhibition of CAIX [7].

#### 4. Conclusions

We determined to atomic resolution the crystal structure of CAII in complex with 1-methylenesulfamide-1,2-dicarba-closo-dodecaborane (1), a parent compound of a recently reported series of CA inhibitors containing carborane cages [7]. Comparing this crystal structure with those of CAII complexes with conventional organic inhibitors showed that the three-dimensional cluster fills the enzyme active site cavity. Atomic-level resolution allowed us to distinguish the positions of carbon and boron atoms in the carborane cage. The crystal structure also served as a model for construction of the CAIX-1 computational model. Virtual glycine scan enabled us to quantify the contributions of individual residues to the energy of binding of 1 to CAII and CAIX and uncover differences of the enzyme active site cavities. Structural and computational analysis will be used in future structure-based design of carborane compounds with selectivity toward the cancer-specific CAIX isoenzyme.

#### Conflict of Interests

The authors declare that there is no conflict of interests regarding the publication of this paper.

#### Authors' Contribution

Pavel Mader and Adam Pecina contributed equally to this work.

#### Acknowledgments

This work was supported by the Technology Agency of the Czech Republic (Project TE01020028) and in part by Research Projects RVO 68378050 and 61388963 awarded by

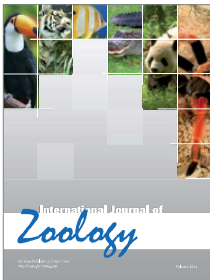
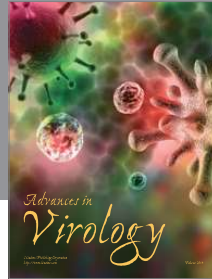
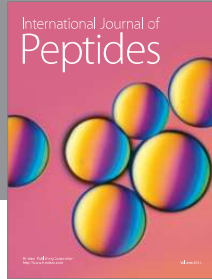
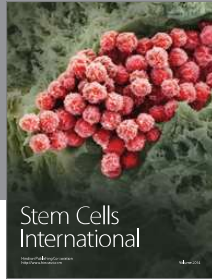
the Academy of Sciences of the Czech Republic. The authors acknowledge the financial support of the Czech Science Foundation (P208/12/G016) and the operational program Research and Development for Innovations of the European Social Fund (CZ.1.05/2.1.00/03/0058). They also thank Gilead Sciences and IOCB Research Centre for financial support. The use of MX14.2 operated by the Helmholtz-Zentrum Berlin at the BESSY II electron storage ring (Berlin-Adlershof, Germany) to collect diffraction data is acknowledged.

## References

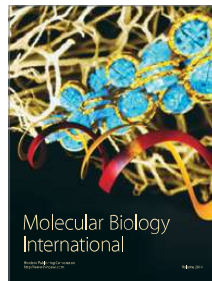
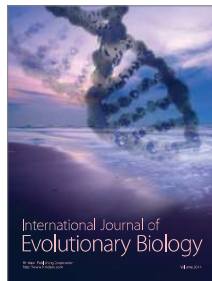
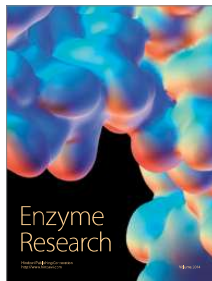
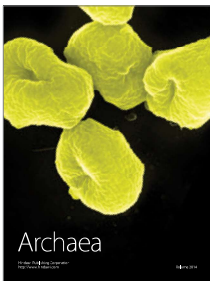
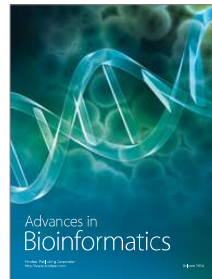
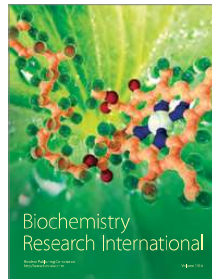
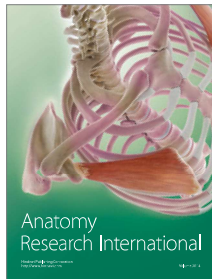
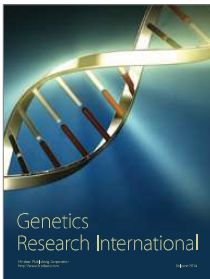
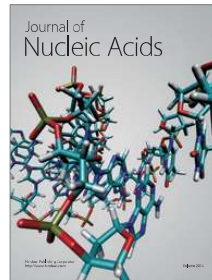
- [1] P. Swietach, S. Patiar, C. T. Supuran, A. L. Harris, and R. D. Vaughan-Jones, "The role of carbonic anhydrase 9 in regulating extracellular and intracellular pH in three-dimensional tumor cell growths," *The Journal of Biological Chemistry*, vol. 284, no. 30, pp. 20299–20310, 2009.
- [2] P. C. McDonald, J. Winum, C. T. Supuran, and S. Dedhar, "Recent developments in targeting carbonic anhydrase IX for cancer therapeutics," *Oncotarget*, vol. 3, no. 1, pp. 84–97, 2012.
- [3] F. E. Lock, P. C. McDonald, Y. Lou et al., "Targeting carbonic anhydrase IX depletes breast cancer stem cells within the hypoxic niche," *Oncogene*, vol. 32, no. 44, pp. 5210–5219, 2013.
- [4] N. K. Tafreshi, M. C. Lloyd, M. M. Bui, R. J. Gillies, and D. L. Morse, "Carbonic anhydrase IX as an imaging and therapeutic target for tumors and metastases," in *Carbonic Anhydrase: Mechanism, Regulation, Links to Disease, and Industrial Applications*, vol. 75 of *Subcellular Biochemistry*, pp. 221–254, 2014.
- [5] S. M. Monti, C. T. Supuran, and G. de Simone, "Anticancer carbonic anhydrase inhibitors: a patent review (2008–2013)," *Expert Opinion on Therapeutic Patents*, vol. 23, no. 6, pp. 737–749, 2013.
- [6] R. McKenna and C. T. Supuran, "Carbonic anhydrase inhibitors drug design," *Subcellular Biochemistry*, vol. 75, pp. 291–323, 2014.
- [7] J. Brynda, P. Mader, V. Sicha et al., "Carborane-based carbonic anhydrase inhibitors," *Angewandte Chemie International Edition in English*, vol. 52, pp. 13760–13763, 2013.
- [8] W. N. Lipscomb, *Boron Hydrides*, W.A. Benjamin, New York, NY, USA, 1963.
- [9] P. R. Schleyer and K. Najafian, "Stability and three-dimensional aromaticity of closo-monocarbaborane anions,  $Cb_{n-1}H_n^-$ , and closo-dicarbaboranes,  $C_2B_{n-2}H_n$ ," *Inorganic Chemistry*, vol. 37, pp. 3454–3470, 1998.
- [10] R. E. Williams, in *The Borane, Carborane and Carbocation Continuum*, J. Casanova, Ed., pp. 3–57, John Wiley & Sons, New York, NY, USA, 1997.
- [11] J. F. Valliant, K. J. Guenther, A. S. King et al., "The medicinal chemistry of carboranes," *Coordination Chemistry Reviews*, vol. 232, no. 1–2, pp. 173–230, 2002.
- [12] Z. J. Lesnikowski, "Boron units as pharmacophores—new applications and opportunities of boron cluster chemistry," *Collection of Czechoslovak Chemical Communications*, vol. 72, no. 12, pp. 1646–1658, 2007.
- [13] J. Plešek, "Potential applications of the boron cluster compounds," *Chemical Reviews*, vol. 92, no. 2, pp. 269–278, 1992.
- [14] J. Seidler, S. L. McGovern, T. N. Doman, and B. K. Shoichet, "Identification and prediction of promiscuous aggregating inhibitors among known drugs," *Journal of Medicinal Chemistry*, vol. 46, no. 21, pp. 4477–4486, 2003.
- [15] M. Sibrian-Vazquez, E. Hao, T. J. Jensen, and M. G. H. Vicente, "Enhanced cellular uptake with a cobaltacarborane-porphyrin-HIV-1 Tat 48–60 conjugate," *Bioconjugate Chemistry*, vol. 17, no. 4, pp. 928–934, 2006.
- [16] M. Scholz, M. Steinhagen, J. T. Heiker, A. G. Beck-Sickinger, and E. Hey-Hawkins, "Asborin Inhibits Aldo/Keto Reductase 1A1," *ChemMedChem*, vol. 6, no. 1, pp. 89–93, 2011.
- [17] F. Issa, M. Kassiou, and L. M. Rendina, "Boron in drug discovery: carboranes as unique pharmacophores in biologically active compounds," *Chemical Reviews*, vol. 111, no. 9, pp. 5701–5722, 2011.
- [18] R. C. Reynolds, S. R. Campbell, R. G. Fairchild et al., "Novel boron-containing, nonclassical antifolates: synthesis and preliminary biological and structural evaluation," *Journal of Medicinal Chemistry*, vol. 50, no. 14, pp. 3283–3289, 2007.
- [19] P. Cigler, M. Kozisek, P. Rezacova et al., "From nonpeptide toward noncarbon protease inhibitors: metallacarboranes as specific and potent inhibitors of HIV protease," *Proceedings of the National Academy of Sciences of the United States of America*, vol. 102, pp. 15394–15399, 2005.
- [20] P. Řezáčová, J. Pokorná, J. Brynda et al., "Design of HIV protease inhibitors based on inorganic polyhedral metallacarboranes," *Journal of Medicinal Chemistry*, vol. 52, no. 22, pp. 7132–7141, 2009.
- [21] Y. Endo, T. Iijima, Y. Yamakoshi et al., "Potent estrogen agonists based on carborane as a hydrophobic skeletal structure: a new medicinal application of boron clusters," *Chemistry & Biology*, vol. 8, no. 4, pp. 341–355, 2001.
- [22] R. L. Julius, O. K. Farha, J. Chiang, L. J. Perry, and M. F. Hawthorne, "Synthesis and evaluation of transthyretin amyloidosis inhibitors containing carborane pharmacophores," *Proceedings of the National Academy of Sciences of the United States of America*, vol. 104, no. 12, pp. 4808–4813, 2007.
- [23] S. Fujii, H. Masuno, Y. Taoda et al., "Boron cluster-based development of potent nonsteroidal vitamin D receptor ligands: direct observation of hydrophobic interaction between protein surface and carborane," *Journal of the American Chemical Society*, vol. 133, no. 51, pp. 20933–20941, 2011.
- [24] V. M. Krishnamurthy, G. K. Kaufman, A. R. Urbach et al., "Carbonic anhydrase as a model for biophysical and physical-organic studies of proteins and protein-ligand binding," *Chemical Reviews*, vol. 108, no. 3, pp. 946–1051, 2008.
- [25] K. Raha, M. B. Peters, B. Wang et al., "The role of quantum mechanics in structure-based drug design," *Drug Discovery Today*, vol. 12, no. 17–18, pp. 725–731, 2007.
- [26] M. Lepšík, J. Řezáč, M. Kolář, A. Pecina, P. Hobza, and J. Fanfrlík, "The semiempirical quantum mechanical scoring function for in silico drug design," *ChemPlusChem*, vol. 78, pp. 921–931, 2013.
- [27] A. Pecina, M. Lepšík, J. Rezac et al., "QM/MM calculations reveal the different nature of the interaction of two carborane-based sulfamide inhibitors of human carbonic anhydrase II," *The Journal of Physical Chemistry B*, vol. 117, pp. 16096–16104, 2013.
- [28] C. A. Behnke, I. Le Trong, J. W. Godden et al., "Atomic resolution studies of carbonic anhydrase II," *Acta Crystallographica D: Biological Crystallography*, vol. 66, no. 5, pp. 616–627, 2010.
- [29] U. Mueller, N. Darowski, M. R. Fuchs et al., "Facilities for macromolecular crystallography at the Helmholtz-Zentrum Berlin," *Journal of Synchrotron Radiation*, vol. 19, no. 3, pp. 442–449, 2012.



- [30] T. G. G. Battye, L. Kontogiannis, O. Johnson, H. R. Powell, and A. G. Leslie, "iMOSFLM: a new graphical interface for diffraction-image processing with MOSFLM," *Acta Crystallographica D*, vol. 67, no. 4, pp. 271–281, 2011.
- [31] P. Evans, "Scaling and assessment of data quality," *Acta Crystallographica Section D: Biological Crystallography*, vol. 62, no. 1, pp. 72–82, 2006.
- [32] A. T. Brunger, "Free R value: a novel statistical quantity for assessing the accuracy of crystal structures," *Nature*, vol. 355, no. 6359, pp. 472–475, 1992.
- [33] S. C. Lovell, I. W. Davis, W. B. Arendall III et al., "Structure validation by C $\alpha$  geometry:  $\phi$ ,  $\psi$  and C $\beta$  deviation," *Proteins*, vol. 50, no. 3, pp. 437–450, 2003.
- [34] R. Gitto, S. Agnello, S. Ferro et al., "Identification of 3,4-dihydroisoquinoline-2(1H)-sulfonamides as potent carbonic anhydrase inhibitors: synthesis, biological evaluation, and enzyme-ligand X-ray studies," *Journal of Medicinal Chemistry*, vol. 53, no. 6, pp. 2401–2408, 2010.
- [35] G. N. Murshudov, A. A. Vagin, and E. J. Dodson, "Refinement of macromolecular structures by the maximum-likelihood method," *Acta Crystallographica D*, vol. 53, no. 3, pp. 240–255, 1997.
- [36] "The CCP4 suite: programs for protein crystallography," *Acta Crystallographica D*, vol. 50, pp. 760–763, 1994.
- [37] P. Jurečka, J. Černý, P. Hobza, and D. R. Salahub, "Density functional theory augmented with an empirical dispersion term. Interaction energies and geometries of 80 noncovalent complexes compared with ab initio quantum mechanics calculations," *Journal of Computational Chemistry*, vol. 28, no. 2, pp. 555–569, 2007.
- [38] F. Weigend and R. Ahlrichs, "Balanced basis sets of split valence, triple zeta valence and quadruple zeta valence quality for H to Rn: design and assessment of accuracy," *Physical Chemistry Chemical Physics*, vol. 7, no. 18, pp. 3297–3305, 2005.
- [39] R. Ahlrichs, M. Bär, M. Häser, H. Horn, and C. Kölmel, "Electronic structure calculations on workstation computers: the program system turbomole," *Chemical Physics Letters*, vol. 162, no. 3, pp. 165–169, 1989.
- [40] P. Emsley and K. Cowtan, "Coot: model-building tools for molecular graphics," *Acta Crystallographica D: Biological Crystallography*, vol. 60, no. 12, pp. 2126–2132, 2004.
- [41] W. L. DeLano, *The PyMOL Molecular Graphics System*, DeLano Scientific LLC, San Carlos, Calif, USA, 2002, <http://www.pymol.org>.
- [42] V. Alterio, M. Hilvo, A. Di Fiore et al., "Crystal structure of the catalytic domain of the tumor-associated human carbonic anhydrase IX," *Proceedings of the National Academy of Sciences of the United States of America*, vol. 106, no. 38, pp. 16233–16238, 2009.
- [43] W. L. DeLano, *The Pymol Molecular Graphics System*, DeLano Scientific, Palo Alto, Calif, USA, 2002.
- [44] M. Svensson, S. Humbel, R. D. J. Froese, T. Matsubara, S. Sieber, and K. Morokuma, "ONIOM: a multilayered integrated MO + MM method for geometry optimizations and single point energy predictions. A test for Diels-Alder reactions and Pt(P(*t*-Bu)<sub>3</sub>)<sub>2</sub> + H<sub>2</sub> oxidative addition," *The Journal of Physical Chemistry*, vol. 100, no. 50, pp. 19357–19363, 1996.
- [45] A. Pecina, O. Přenosil, J. Fanfrlík et al., "On the reliability of the corrected semiempirical quantum chemical method (PM6-DH2) for assigning the protonation states in HIV-1 protease/inhibitor complexes," *Collection of Czechoslovak Chemical Communications*, vol. 76, no. 5, pp. 457–479, 2011.
- [46] P. S. Brahmkshatriya, P. Dobeš, J. Fanfrlík et al., "Quantum mechanical scoring: structural and energetic insights into cyclin-dependent kinase 2 inhibition by pyrazolo[1,5-a]pyrimidines," *Current Computer—Aided Drug Design*, vol. 9, no. 1, pp. 118–129, 2013.
- [47] J. Fanfrlík, M. Kolář, M. Kamlar et al., "Modulation of aldose reductase inhibition by halogen bond tuning," *ACS Chemical Biology*, vol. 8, pp. 2484–2492, 2013.
- [48] J. Fanfrlík, P. S. Brahmkshatriya, J. Řezáč et al., "Quantum mechanics-based scoring rationalizes the irreversible inactivation of parasitic *Schistosoma mansoni* cysteine peptidase by vinyl sulfone inhibitors," *Journal of Physical Chemistry B*, vol. 117, pp. 14973–14982, 2013.
- [49] H. J. C. Berendsen, J. P. M. Postma, W. F. Van Gunsteren, A. Dinola, and J. R. Haak, "Molecular dynamics with coupling to an external bath," *The Journal of Chemical Physics*, vol. 81, no. 8, pp. 3684–3690, 1984.
- [50] D. A. Case, T. E. Cheatham III, T. Darden et al., "The Amber biomolecular simulation programs," *Journal of Computational Chemistry*, vol. 26, no. 16, pp. 1668–1688, 2005.
- [51] M. J. Betts and M. J. E. Sternberg, "An analysis of conformational changes on protein-protein association: implications for predictive docking," *Protein Engineering*, vol. 12, no. 4, pp. 271–283, 1999.
- [52] P. Mader, J. Brynda, R. Gitto et al., "Structural Basis for the Interaction between Carbonic Anhydrase and 1,2,3,4-tetrahydroisoquinolin-2-ylsulfonamides," *Journal of Medicinal Chemistry*, vol. 54, no. 7, pp. 2522–2526, 2011.



**Hindawi**  
Submit your manuscripts at  
<http://www.hindawi.com>





Cite this: *Org. Biomol. Chem.*, 2014, 12, 7971

## Conformationally constrained nucleoside phosphonic acids – potent inhibitors of human mitochondrial and cytosolic 5'(3')-nucleotidases†

Ondřej Šimák,‡<sup>a</sup> Petr Páchl,‡<sup>a,b</sup> Milan Fábry,<sup>b</sup> Miloš Buděšínský,<sup>a</sup> Tomáš Jandušík,<sup>a,c</sup> Aleš Hnízda,<sup>a</sup> Radka Skleničková,<sup>a</sup> Magdalena Petrová,<sup>a</sup> Václav Veverka,<sup>a</sup> Pavlína Řezáčová,<sup>a,b</sup> Jiří Brynda<sup>\*a,b</sup> and Ivan Rosenberg<sup>\*a</sup>

This work describes novel *in vitro* inhibitors of human mitochondrial (mdN) and cytosolic (cdN) 5'(3')-deoxynucleotidases. We designed a series of derivatives of the lead compound (S)-1-[2-deoxy-3,5-O-(phosphonobenzylidene)-β-D-*threo*-pentofuranosyl]thymine bearing various substituents in the *para* position of the benzylidene moiety. Detailed kinetic study revealed that certain *para* substituents increase the inhibitory potency (iodo derivative;  $K_i^{\text{mdN}} = 2.71 \mu\text{M}$ ) and some induce a shift in selectivity toward cdN (carboxy derivative,  $K_i^{\text{cdN}} = 11.60 \mu\text{M}$ ; iodoxy derivative,  $K_i^{\text{cdN}} = 6.60 \mu\text{M}$ ). Crystal structures of mdN in complex with three of these compounds revealed that various *para* substituents lead to two alternative inhibitor binding modes within the enzyme active site. Two binding modes were also identified for cdN complexes by heteronuclear NMR spectroscopy.

Received 27th June 2014,  
Accepted 13th August 2014

DOI: 10.1039/c4ob01332h

www.rsc.org/obc

### Introduction

5'-Nucleotidases are catabolic enzymes that catalyze the dephosphorylation of nucleoside 5'-monophosphates. Together with nucleoside kinases and nucleoside phosphorylases, they regulate cellular nucleotide and nucleoside pools.<sup>1–3</sup> There are seven human 5'-nucleotidases with different substrate specificities, cellular localization, and tissue-specific expression patterns:<sup>1,4,5</sup> ecto-5'-nucleotidase (eN), cN-IA (AMP specific), cN-IB (AMP specific), cN-II (IMP and GMP specific), cN-III (CMP and UMP specific), and two 5'(3')-deoxynucleotidases—cytosolic

(cdN) and mitochondrial (mdN). cdN is an ubiquitous enzyme that, in contrast to cN-III and mdN, is not strictly pyrimidine-specific and efficiently dephosphorylates dIMP and dGMP as well as dTMP and dUMP. In addition, cdN exhibits limited activity toward dAMP and no activity toward dCMP.<sup>6</sup> mdN is highly homologous to cdN (sequence homology of 78%) but has a remarkably narrow specificity toward dUMP and dTMP, which are considered to be its physiological substrates.<sup>7</sup> Its high pyrimidine specificity suggests that mdN regulates the level of mitochondrial dTTP and prevents the accumulation of mutagenic dUTP.<sup>6</sup>

In addition to their regulatory role, 5'-nucleotidases can dephosphorylate the 5'-phosphate esters of therapeutically relevant nucleoside analogs, thus negatively affecting their pharmacological efficacy. Both cdN and mdN are capable of efficiently dephosphorylating modified therapeutic nucleoside 5'-phosphates. In particular, cdN efficiently dephosphorylates the 5'-phosphates of zidovudine (AZT) and fludarabine (FdUR), which are used for HIV-1 and cancer (leukemias and solid tumors) treatment, respectively. The rate of cleavage of FdUMP, an active metabolite of fludarabine, is two-fold higher than the dUMP cleavage rate.<sup>6</sup>

Primary and acquired resistance toward nucleoside analogs is a limiting factor in their clinical use, and resistance seems to be linked to high expression and increased activity of cytosolic 5'-nucleotidases.<sup>7–9</sup> In particular, araC-resistant leukemia cell lines with increased cN-II activity are less sensitive to

<sup>a</sup>Institute of Organic Chemistry and Biochemistry, Academy of Sciences of the Czech Republic, v. v. i., Flemingovo 2, 166 10 Prague 6, Czech Republic.

E-mail: rosenberg@uochb.cas.cz, brynda@img.cas.cz

<sup>b</sup>Institute of Molecular Genetics, of Sciences of the Czech Republic, v. v. i., Videněská 1083, 14220 Prague 4, Czech Republic

<sup>c</sup>Department of Chemistry of Natural Compounds, Institute of Chemical Technology, Prague, Technická 5, 166 28 Prague, Czech Republic

† Electronic supplementary information (ESI) available: (1) Calculated geometry and NMR parameters for *C3'-endo* and *C2'-endo* conformations of [6'R] and [6'S]-epimers of compound **9i**. (2) Backbone NMR chemical shift perturbations obtained for cdN complexes (compounds **12d**, **13**, **15**, **31** and **32**). (3) Calculated distances of the metal ion and coordinating atoms in 3 different structures. (4) Selectivity graph of measured compounds. (5) Crystal Data and Diffraction Data Collection and Refinement Statistics. (6) Experimental section. (7) <sup>1</sup>H and <sup>13</sup>C-NMR spectra of final compounds tested for their inhibition activities. See DOI: 10.1039/c4ob01332h

‡ Both authors contributed to this work equally.

fludarabine,<sup>10</sup> and recent results identified a relapse-specific activating mutation in cN-II in childhood acute lymphoblastic leukemia (ALL).<sup>11,12</sup> In parallel, increased activity of cdN and cN-III was found in the cells of patients with acute myeloid leukemia (AML) and ALL, and patients with clinical remission of ALL had even higher cdN activity than at the time of diagnosis.<sup>13</sup>

Long-term treatment with antiviral and anticancer nucleoside drugs is accompanied in almost all cases by serious drug-induced health problems.<sup>14,15</sup> This is a consequence of mitochondrial toxicity induced in certain tissues.<sup>16,17</sup> Nucleoside analogs can serve as substrates for the less-selective mitochondrial DNA polymerase gamma, causing chain termination and mtDNA depletion.<sup>16,17</sup> Avoiding mitochondrial toxicity would require nucleoside analogs (i) whose 5'-triphosphates possess a low affinity toward mitochondrial DNA polymerase and/or (ii) whose 5'-monophosphates are good substrates for mdN.<sup>18</sup> Alternatively, nucleoside analogs that are good substrates for mdN could be combined with a selective cdN inhibitor.

Therefore, human cdN can be considered a promising therapeutic target, as its inhibition may increase the effectiveness of chemotherapy and antiviral treatment. Selective inhibition of mdN should be further investigated for its effects on various tumor cell lines.

Nucleoside phosphonic acids with a non-cleavable P-C linkage have been studied as potential inhibitors of various nucleotidases. The first nucleoside phosphonate inhibitors (**1a** and **1b**), which block the activity of 5'-nucleotidase from *Crotalus adamanteus* venom, were reported in 1973 by Hampton *et al.* (Fig. 1).<sup>19</sup> In 1998, Garvey *et al.*<sup>20</sup> described the ddTMP analog **2** (Fig. 1) as a potent inhibitor of rabbit heart cN-I with an apparent  $K_i$  of 63 nM. Recently, Meurillon *et al.*<sup>21</sup> reported an inhibition study of cN-II with a variety of cytosine and uracil nucleoside phosphonic acids (based on scaffold **3**) with millimolar  $K_i$  values.

Our group has synthesized many structurally diverse adenine, guanine, 2,6-diaminopurine, cytosine, uracil, and thymine nucleoside phosphonic acids.<sup>22–33</sup> Of these compounds, two types of structurally diverse nucleoside phosphonic acids, **4**<sup>34</sup> and **5**<sup>31,32</sup> (Fig. 2), inhibited cdN and mdN.<sup>18,35</sup> Whereas **4** inhibited both enzymes, **5** showed selectivity toward the mitochondrial enzyme.<sup>18</sup>

Detailed analysis of the crystal structures of mdN in complex with inhibitors **4** and **5**<sup>35</sup> showed that **4** binds to the enzyme active site in a manner similar to the natural 5'-nucleotide substrate, while the binding mode of **5** is different. The

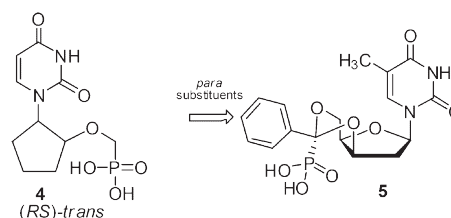


Fig. 2 Two structurally diverse inhibitors of human cdN and mdN.

phosphonate moiety of **5** does not interact with the nucleoside phosphoester binding site but with another site distal from the catalytic residues.<sup>35</sup> A positively charged region formed by Arg163 and Arg177 and partially by Lys165 and Ser131 was identified in the vicinity of the *para* position of the benzylidene ring in the crystal structure of the mdN-**5** complex.<sup>35</sup> With the aim of increasing inhibitor affinity, we designed a series of inhibitors with various substituents introduced at the *para* position of the benzylidene ring of **5**. At the same time, we focused on fine-tuning the inhibitor selectivity toward either cdN or mdN. Although the active sites of the two enzymes are very similar in terms of sequence and overall structure, detailed structural analysis revealed several regions with variable sequences.<sup>36</sup> One variable region lies close to the positively charged region targeted by our proposed inhibitor substitutions. Specifically, this region comprises Ile133, Lys134, and Met135 in mdN (corresponding to cdN residues Leu202, Leu103, and Lys104). Also, Arg177 in mdN corresponds to Lys146 in cdN. This variability provides an opportunity for modification of the basal inhibitor scaffold to achieve specificity for cdN or mdN.

Here, we present novel inhibitors of human mdN and cdN based on (*S*)-1-[2-deoxy-3,5-*O*-(phosphonobenzylidene)- $\beta$ -*D*-threo-pentofuranosyl]thymine derivatives. We synthesized compounds with a series of polar electron-rich substituents (some with a negative charge) in the *para* position of the benzylidene ring and tested these nucleoside benzylidene phosphonates for their inhibitory activity toward both enzymes. Structural characterization of inhibitor complexes with cdN and mdN revealed the existence of two alternative binding modes of the substituted compounds in the active site of both enzymes and emphasized the key role of the *para* substituent of the benzylidene moiety in determining the binding specificity. In addition, our data suggest that each of the isoenzymes requires a specific binding mode for effective inhibition.

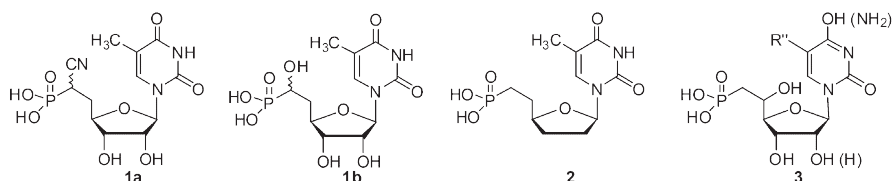


Fig. 1 Chemical structures of nucleotide inhibitors of snake venom (**1a,b**), rabbit heart (**2**), and human cN-II 5'-nucleotidases (**3**).



## Results and discussion

### Chemistry

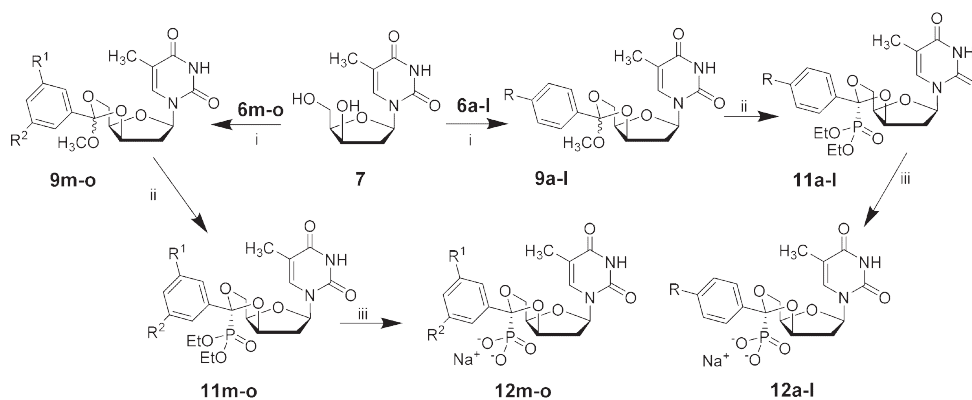
The starting fifteen orthoesters **6a–o** (Table 1) were prepared in three steps from the corresponding *N,N*-methylphenylbenzamides.<sup>37</sup> The acid-catalyzed reaction of orthoesters **6a–o** with *xyl*T 7 in DMF yielded nucleoside orthobenzoates **9a–o** in high yield (Scheme 1). For the preparation of nucleoside orthoesters **9a–h**, we used dry HCl in Et<sub>2</sub>O as a catalyst, whereas for **9i–o**, pyridinium tosylate provided a much cleaner reaction without opening the nucleoside orthoester ring or forming a mixture of 3'- and 5'-*O*-acyl derivatives. In contrast to compounds **9a–h** and **9j**, which were obtained as single *R*-epimers, the compounds **9i** and **9k–o** were epimeric mixtures with the *R*-epimer prevailing (Fig. 3). NMR spectroscopy

revealed that the furanose ring adopts a <sup>3</sup>E (C3'-*endo*) conformation, while the annealed 1,3-dioxane ring is in a chair conformation. Thus, the relatively bulky phenyl substituent is in an equatorial position on the six-membered 1,3-dioxane ring (Fig. 3). The use of a strong acid (HCl in Et<sub>2</sub>O) may lead to a quasi-reversible transesterification reaction: partial re-opening of the formed cyclic orthoester ring and repeated closure provides the thermodynamic products **9a–h**. On the other hand, the use of pyridinium tosylate as a weak acid maintains the intact cyclic orthoester ring affording the kinetic products. The epimeric mixtures of compounds **9i–o** (the obtained ratios from the NMR spectra are given in the Experimental section in ESI†).

The NMR spectra showed that compounds **9a–h** and **9j** were obtained as only a single C6'-epimer, while compounds **9i** and **9k–o** were C6'-epimeric mixtures. The configuration at

Table 1 Prepared orthobenzoates **6a–o**

Compounds <b>6</b>	R	R	Compounds <b>6</b>	R <sup>1</sup> , R <sup>2</sup>
	<b>a</b> <sup>38</sup> <b>b</b> <sup>39</sup> <b>c</b> <sup>39</sup> <b>d</b> <b>e</b> <sup>37</sup> <b>f</b>	F Cl Br I NO <sub>2</sub> COOMe		<b>m</b> <sup>40</sup> <b>n</b> <sup>40</sup> <b>o</b>
		<b>g</b> <b>h</b> <b>i</b> <b>j</b> <sup>37</sup> <b>k</b> <b>l</b> <sup>41</sup>	SMe CN CF <sub>3</sub> OCH <sub>3</sub> vinyl Ph	C <sub>6</sub> H <sub>5</sub> , H I, H I, Br



Scheme 1 Synthesis of substituted phosphonobenzylidene derivatives of 1-[2-deoxy-β-D-threo-pentofuranosyl]thymine. Reagents and conditions: (i) HCl/DMF or TsOH·py/DMF; (ii) (EtO)<sub>2</sub>PCI/CH<sub>3</sub>CN; (iii) TMSBr/2,6-lutidine/CH<sub>3</sub>CN; for R, R<sup>1</sup>, and R<sup>2</sup> see Table 1.

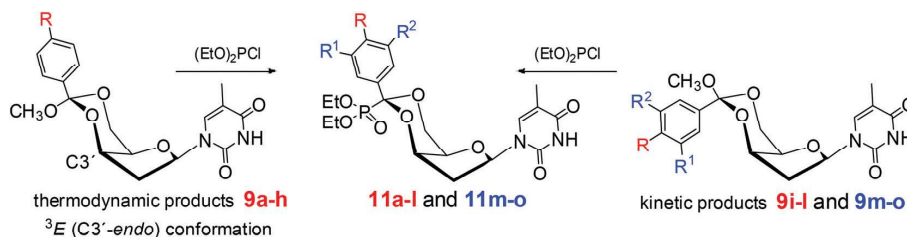


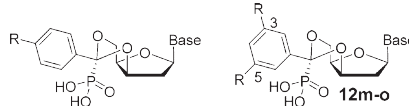
Fig. 3 Configurations of the thermodynamic and kinetic products.

C6' was determined from the observed NOE contacts of the C(6')-OMe group and the <sup>1</sup>H chemical shifts of the C(5)-Me group of thymine and the H-3' of the furanose ring. The NOE contacts between C(6')-OMe and the H-6 of thymine could be observed only in the C6'-epimers with a [6'S] configuration, while for C6'-epimers with a [6'R] configuration, an NOE between C(6')-OMe and H-3' was observed (see ESI Fig. 1S†). In series **9a–o**, both epimers clearly differ in their <sup>1</sup>H chemical shifts of the C(5)-Me group of thymine and the H-3' of the furanose ring. The C6'-epimers with a [6'R] configuration show a significant upfield shift of the signal belonging to the C(5)-Me

group as a result of the shielding effect of the phenyl ring ( $\delta$  1.12–1.20 in [6'R] compared to  $\delta$  1.77–1.80 in the [6'S]-epimers). A reverse shielding effect is observed for H-3' ( $\delta$  4.27–4.35 in [6'S] compared to  $\delta$  4.66–4.71 in [6'R]-epimers).

The conformation of both C6'-epimers was studied by molecular modeling and theoretical calculations of the NMR parameters. Two potential chair conformations of the annealed 1,3-dioxane ring stabilize either the <sup>3</sup>E (C3'-endo) or the <sup>2</sup>E (C2'-endo) conformation of the furanose ring. Because the interproton coupling constants in **9a–o** are not influenced by the substitution of the aromatic ring at C6', we have chosen

**Table 2** Inhibition of mitochondrial and cytosolic nucleotidases by benzylidene ring *para*-substituted derivatives of (S)-1-[2-deoxy-3,5-O-(phosphonobenzylidene)- $\beta$ -D-threo-pentofuranosyl] derivatives of pyrimidine nucleobases



R	Base	Cmpnd	Relative activity $v_i/v_0^a$		$K_i$ ( $\mu\text{M}$ )		$K_i/K_M$		Selectivity index <sup>b</sup>
			mdN	cdN	mdN	cdN	mdN	cdN	
H	T	<b>5</b>	0.61	0.67	11.6 $\pm$ 2.0	610 $\pm$ 125	0.156	0.630	0.25
	U	<b>12r</b>	0.44	0.97	31.1 $\pm$ 3.1	410 $\pm$ 120	0.362	0.424	0.85
	U <sup>5-cl</sup>	<b>24</b>	0.69	0.56	11.8 $\pm$ 0.87	52.2 $\pm$ 4.5	0.137	0.054	2.5
F	T	<b>12a</b>	0.55	1.19	13.0 $\pm$ 1.9	n.d.	0.151	n.d.	n.d.
	Cl	<b>12b</b>	0.63	1.03	30 $\pm$ 15	n.d.	0.349	n.d.	n.d.
Br	T	<b>12c</b>	0.79	0.82	31.8 $\pm$ 9.8	n.d.	0.370	n.d.	n.d.
I	T	<b>12d</b>	0.42	0.82	2.71 $\pm$ 0.42	416 $\pm$ 66	0.032	0.430	0.073
	U	<b>12p</b>	0.72	0.66	19.7 $\pm$ 4.1	115 $\pm$ 11	0.229	0.119	1.9
	T	<b>12q</b>	0.69	0.81	14.2 $\pm$ 2.9	307 $\pm$ 38	0.165	0.317	0.52
	T	<b>11d</b>	0.81	0.77	n.d.	n.d.	n.d.	n.d.	n.d.
IO <sub>2</sub>	T	<b>31</b>	0.44	0.07	5.90 $\pm$ 1.1	6.60 $\pm$ 1.4	0.069	0.0068	10
	U	<b>32</b>	0.73	0.18	43.0 $\pm$ 11	12.1 $\pm$ 1.5	0.500	0.0125	40
NO <sub>2</sub>	T	<b>12e</b>	0.58	0.71	22.1 $\pm$ 3.3	950 $\pm$ 370	0.257	0.981	0.26
	COOH	T	<b>13</b>	0.73	0.44	7.90 $\pm$ 2.2	11.6 $\pm$ 1.7	0.092	0.0120
U	<b>15</b>	0.70	0.22	16.9 $\pm$ 2.1	11.0 $\pm$ 0.86	0.197	0.0114	17	
COOMe	T	<b>12f</b>	0.96	1.01	n.d.	n.d.	n.d.	n.d.	n.d.
CONH <sub>2</sub>	T	<b>14</b>	0.77	0.92	n.d.	n.d.	n.d.	n.d.	n.d.
CHO	T	<b>22</b>	0.80	0.73	n.d.	n.d.	n.d.	n.d.	n.d.
CN	T	<b>12h</b>	0.54	0.77	23.0 $\pm$ 2.6	177 $\pm$ 28	0.267	0.183	1.5
P(O)(OH) <sub>2</sub>	T	<b>28</b>	0.69	0.54	28.0 $\pm$ 2.0	52.7 $\pm$ 4.7	0.326	0.054	6.0
B(OH) <sub>2</sub>	T	<b>30</b>	0.74	0.70	n.d.	n.d.	n.d.	n.d.	n.d.
SCH <sub>3</sub>	T	<b>12g</b>	0.57	0.98	33.3 $\pm$ 4.3	n.d.	0.387	n.d.	n.d.
S(O)CH <sub>3</sub>	T	<b>23</b>	0.81	0.88	n.d.	n.d.	n.d.	n.d.	n.d.
NH <sub>2</sub>	T	<b>16</b>	0.89	0.82	n.d.	n.d.	n.d.	n.d.	n.d.
NHCHO	T	<b>20</b>	0.69	0.72	n.d.	n.d.	n.d.	n.d.	n.d.
NC	T	<b>21</b>	1.12	1.07	n.d.	n.d.	n.d.	n.d.	n.d.
N <sub>3</sub>	T	<b>26</b>	0.79	0.79	n.d.	n.d.	n.d.	n.d.	n.d.
CF <sub>3</sub>	T	<b>12i</b>	1.05	0.94	n.d.	n.d.	n.d.	n.d.	n.d.
OCH <sub>3</sub>	T	<b>12j</b>	1.20	0.80	n.d.	n.d.	n.d.	n.d.	n.d.
Phenyl	T	<b>12l</b>	1.11	0.78	n.d.	n.d.	n.d.	n.d.	n.d.
3-Phenyl	T	<b>12m</b>	0.72	0.82	n.d.	n.d.	n.d.	n.d.	n.d.
3-I	T	<b>12n</b>	0.87	0.64	n.d.	n.d.	n.d.	n.d.	n.d.
3-Br-5-I	T	<b>12o</b>	1.19	0.85	n.d.	n.d.	n.d.	n.d.	n.d.

<sup>a</sup> Values were obtained for a ratio of the substrate (dUMP) to the inhibitor of 10 : 1 at substrate concentrations of 100  $\mu\text{M}$  (mdN) and 1 mM (cdN).

<sup>b</sup> The selectivity index  $[(K_i/K_M)_{\text{mdN}}/(K_i/K_M)_{\text{cdN}}]$  is expressed as a ratio of the  $K_i$  values for the mdN and cdN enzymes normalized to the enzymatic constant  $K_M$  of the individual enzymes [ $(K_M)_{\text{mdN}} = 86 \pm 14 \mu\text{M}$ ,  $(K_M)_{\text{cdN}} = 968 \pm 79 \mu\text{M}$ ]. <sup>c</sup> Mono-ethyl ester of **12d**.



the C6'-epimers of **9i** as representative examples of a detailed conformational analysis of compounds **9a–o**. Geometric optimization was performed for both the C3'-*endo* and C2'-*endo* conformers of each C6'-epimer, and the optimized geometries were then used to calculate the  $^1\text{H}$  and  $^{13}\text{C}$  NMR chemical shifts using the same DFT B3LYP/6-31G\* method with an implicit solvent (PCM model; solvent = DMSO) in both steps. The vicinal couplings  $J(\text{H,H})$  were calculated for the optimized geometries (shown in ESI Fig. 1S†) with the MSpin program of the MESTRELAB package<sup>42</sup> using the Diez-Altona-Donders equation.<sup>43</sup> The comparison of the observed and calculated NMR parameters together with the calculated conformational data ( $P$  and  $\phi_{\text{max}}$  of the furanose ring and the  $\chi$  angle for the nucleoside base orientation) and the relative energies of the C3'-*endo* and C2'-*endo* forms are given in ESI Table 1S.† Mean average error values (MAE) are used to quantify the agreement between the observed and calculated data. As shown in ESI Table 1S,† the relative energies, the comparison of the observed and calculated  $^3J(\text{H,H})$  values and the  $^1\text{H}$  and  $^{13}\text{C}$  chemical shifts clearly indicate that the C3'-*endo* conformation is highly preferred (>99%) for both the [6'*R*]- and [6'*S*]-epimers.

The reaction of *xylo*dU **8** with orthoesters **6d**, **6f**, and **10** in DMF with 10 M HCl as an acid catalyst in Et<sub>2</sub>O yielded products **9p–r** exclusively as the *R*-isomers (Scheme 2).

A similar stereoselective behavior was observed with the 3',5'-*O*-acetal derivatives of *xylo*T.<sup>27</sup> The reaction of nucleoside orthoesters **9a–r** with diethyl chlorophosphite in acetonitrile afforded the fully protected phosphonates **11a–r** as single epimers (**a–o** Scheme 1 and **p–r** Scheme 2). The stereospecificity of this reaction seems to be the result of the stable intermediate Im2 (Scheme 3) with the phenyl substituent in an equatorial position, which most likely subsequently undergoes

an S<sub>N</sub>1 reaction to form diethyl methyl phosphite (Scheme 3). The proposed mechanism is similar to that of the previously reported mechanism for the formation of 2',3'-*O*-phosphonoalkylidene derivatives of ribonucleosides.<sup>32</sup>

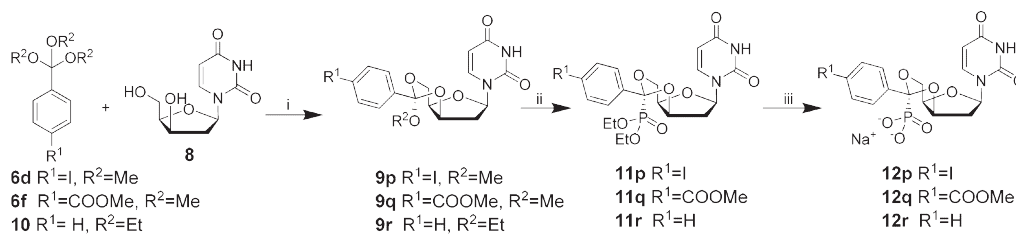
The deprotection of the phosphonate ester groups was carried out with bromotrimethylsilane in acetonitrile in the presence of 2,6-lutidine, providing phosphonic acids **12a–r** in moderate yields.

The carboxy derivative **13** was prepared in nearly quantitative yield by saponification of methyl ester **12f** in 0.5 M NaOH at r.t. The reaction of ester **12f** with 28% aqueous NH<sub>3</sub> at 100 °C for 24 h yielded carboxamide derivative **14** as the major product as well as free acid **13** (Scheme 4).

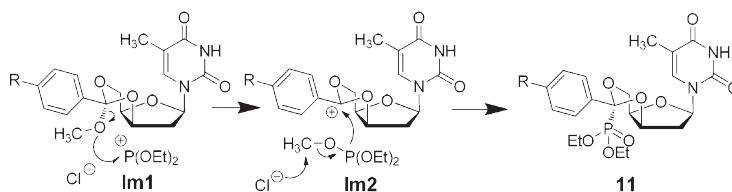
The same reaction conditions were used for the preparation of carboxylate **15** from *para*-methoxycarbonyl derivative **12q** (Scheme 4).

The catalytic hydrogenation of nitro derivatives **11e** and **12e** on Pd/C yielded the corresponding amino derivatives **16** and **17**, respectively. The obtained amino derivative **17** was converted to formamide **18** by reaction with ammonium formate in refluxing acetonitrile, and this compound yielded, in a subsequent reaction with phosphoryl chloride, isocyanide **19**. Amide **18** and isocyanide **19** were converted to free phosphonic acids **20** and **21**, respectively, by treatment with bromotrimethylsilane (Scheme 5).

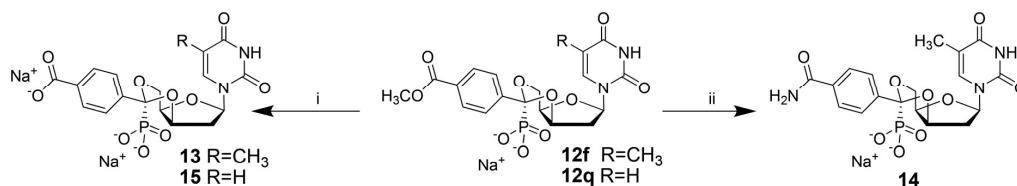
The synthesis of benzaldehyde derivative **22** (Scheme 6) started from styrene compound **12k**, which was oxidized by OsO<sub>4</sub> in the presence of sodium periodate to afford **22** in nearly quantitative yield in one step. Similarly, a high yield of sulfoxide compound **23** was obtained by oxidation of the methylthio derivative **12g** with an aqueous solution of NaIO<sub>4</sub> (Scheme 7).



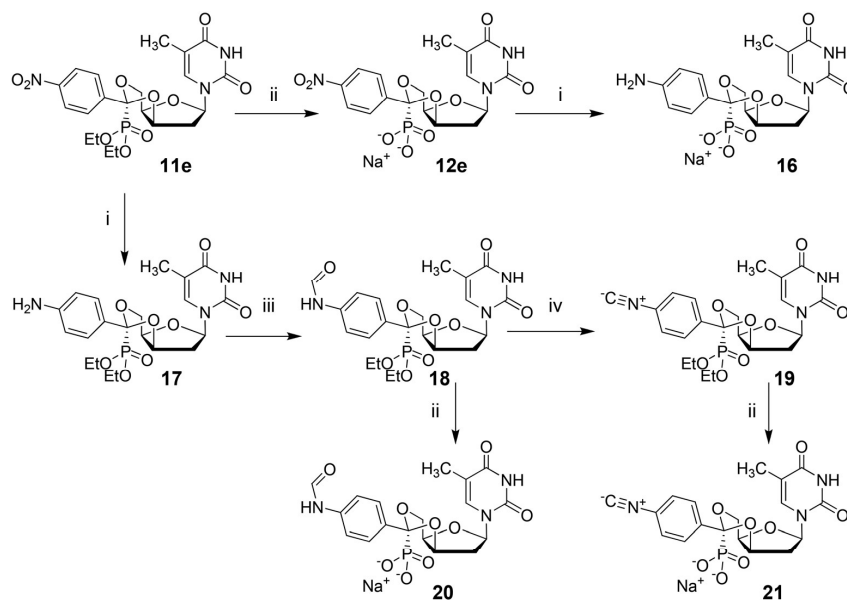
**Scheme 2** Synthesis of substituted phosphonobenzyldene derivatives of 1-[2-deoxy-β-D-threo-pentofuranosyl]uracil. Reagents and conditions: (i) HCl/DMF; (ii) (EtO)<sub>2</sub>PCl/CH<sub>3</sub>CN; (iii) TMSBr/2,6-lutidine/CH<sub>3</sub>CN.



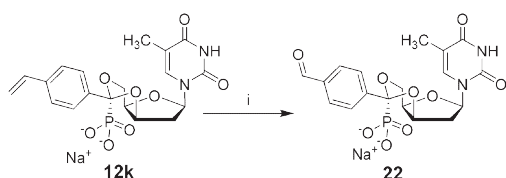
**Scheme 3** Proposed mechanism of the stereospecific phosphorylation.



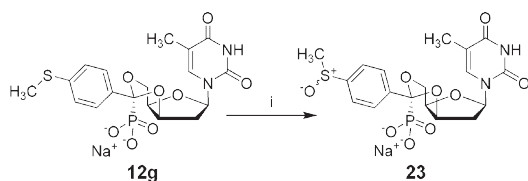
**Scheme 4** Transformation of the *para*-methoxycarbonyl group into carboxylate and carboxamide moieties. Reagents and conditions: (i) 0.05 M NaOH; (ii) 28%  $\text{NH}_4\text{OH}/100\text{ }^\circ\text{C}/24\text{ h}$ .



**Scheme 5** Synthesis of the phosphonobenzylidene derivatives of 1-[2-deoxy- $\beta$ -D-threo-pentofuranosyl]thymine **16**, **20**, and **21**. Reagents and conditions: (i)  $\text{H}_2/\text{Pd-C}$ ; (ii)  $\text{TMSBr}/2,6\text{-lutidine}/\text{CH}_3\text{CN}$ ; (iii)  $\text{HCOONH}_4/\text{CH}_3\text{CN}$ ; (iv)  $\text{POCl}_3/\text{Et}_3\text{N}/\text{CH}_2\text{Cl}_2$ .



**Scheme 6** Synthesis of 4-formylbenzylidene derivative **22**. Reagents and conditions: (i)  $\text{OsO}_4/\text{NaIO}_4/\text{tBuOH}/\text{H}_2\text{O}$ .

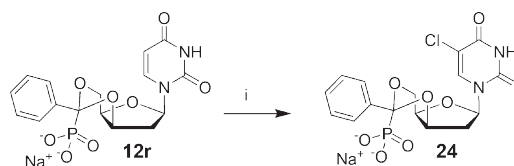


**Scheme 7** Synthesis of sulfoxide derivative **23**. Reagents and conditions: (i)  $\text{NaIO}_4/\text{H}_2\text{O}$ .

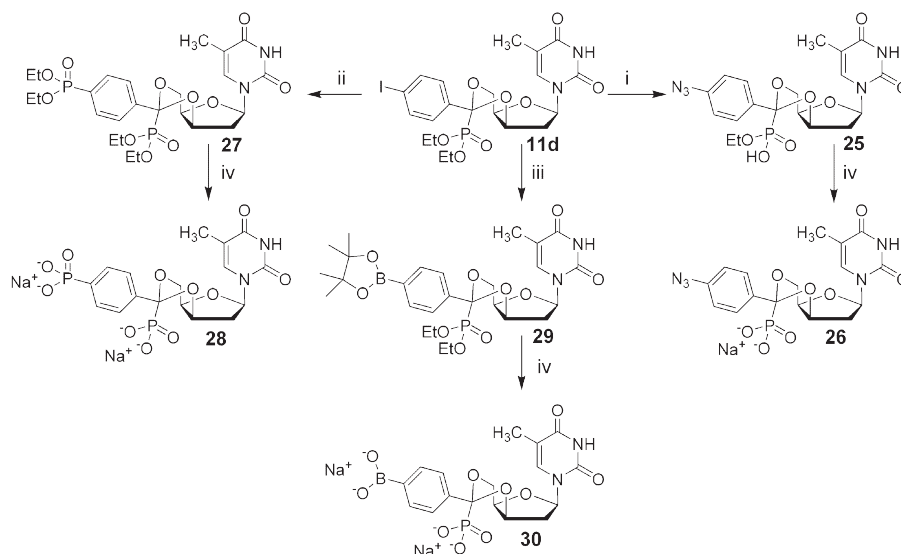
The chlorination of the uracil base<sup>44</sup> of derivative **12r** by *N*-chlorosuccinimide in pyridine at elevated temperature provided 5-chlorouracil derivative **24** (Scheme 8).

Iodophenyl derivative **11d** was a useful starting material for several transformations on the phenyl ring (Scheme 9).

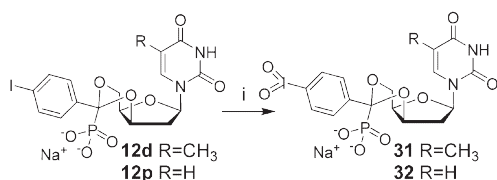
Thus, compound **11d** was treated<sup>45</sup> with  $\text{NaN}_3$ , *L*-ascorbic acid, *L*-proline and  $\text{CuSO}_4$  in aqueous DMSO to yield azido derivative **25** as the mono ethyl phosphonate. This derivative



**Scheme 8** Synthesis of 5-chlorouracil derivative **24**. Reagents and conditions: (i)  $\text{NCS}/\text{py}$ .



**Scheme 9** Synthesis of azido compounds **25** and **26** and phosphoryl **28** and boronate **30** derivatives. Reagents and conditions: (i)  $\text{NaN}_3/\text{CuSO}_4 \cdot 5\text{H}_2\text{O}/\text{Na}_2\text{CO}_3/\text{L-ascorbic acid}/\text{L-proline}/\text{DMSO-H}_2\text{O}$  9 : 1; (ii)  $\text{HOP}(\text{OEt})_2/\text{Pd}(\text{dppf})\text{Cl}_2/\text{KOAc}/\text{Et}_3\text{N}/\text{THF}$ ; (iii)  $\text{bis}(\text{pinacolato})\text{diboron}/\text{Pd}_2(\text{dba})_3/\text{XPhos}/\text{KOAc}/\text{dioxane}/110^\circ\text{C}$ ; (iv)  $\text{TMSBr}/2,6\text{-lutidine}/\text{CH}_3\text{CN}$ .



**Scheme 10** Synthesis of iodoxy compounds **31** and **32**. Reagents and conditions: (i)  $\text{MCPBA}/\text{CH}_3\text{CN}/\text{H}_2\text{O}$ .

was treated with  $\text{TMSBr}$  and 2,6-lutidine to provide phosphonic acid **26**.

The coupling reaction<sup>46</sup> of **11d** with diethyl phosphite, catalyzed by  $\text{Pd}(\text{dppf})\text{Cl}_2$ , yielded tetraethyl diphosphonate **27**, which afforded bisphosphonic acid **28** on treatment with  $\text{TMSBr}$  and 2,6-lutidine.

The coupling reaction<sup>47</sup> of **11d** and bis(pinacolato)diboron, catalyzed by  $\text{Pd}_2(\text{dba})_3$  and  $\text{XPhos}$ , yielded boron derivative **29**. Its treatment with  $\text{TMSBr}$  and 2,6-lutidine afforded boronic acid **30**.

Iodophenyl derivatives **12d** and **12p**, as the free acids, were oxidized by *meta*-chloroperbenzoic acid, providing iodoxy derivatives **31** and **32**, respectively (Scheme 10).

### Biochemistry

**Inhibition studies.** All synthesized phosphonic acids, as well as lead compound **5**, were screened for their inhibitory effect on mdN and cdN activity *in vitro* (Table 2). Activity assay was based on hydrolysis of dUMP in the presence of tested compounds. Substrate concentrations for preliminary tests

were chosen to be similar to  $K_M$  (1 mM for cdN, 100  $\mu\text{M}$  for mdN) and the concentration of tested compounds was 10 times lower than the substrate concentration. Seventeen selected compounds that showed a similar or lower relative enzyme activity  $v_i/v_0$  than lead compound **5** were subjected to a kinetic study to obtain the  $K_i$  values (Table 2). To compare the selectivity of the inhibitors toward mdN and cdN, we introduced a selectivity index (SI), defined as the ratio of  $K_i$  values normalized by the appropriate enzymatic constant  $K_M$ , which was determined experimentally (86  $\pm$  14  $\mu\text{M}$  for mdN and 968  $\pm$  79  $\mu\text{M}$  for cdN). The smaller the SI (<1) is, the higher the selectivity of the inhibitor for mdN is, and the higher the SI (>1) is, the higher the selectivity for cdN is.

The inhibitory effect of compound **5** on mdN had been previously investigated by others, and a  $K_i$  value of 70  $\mu\text{M}$  had been determined using specific assays with labeled dUMP.<sup>18</sup> In our HPLC assay, we followed the quantity of 2'-deoxyuridine released from dUMP by a nucleotidase-catalyzed hydrolysis. This method provided a  $K_i$  value for compound **5** and mdN of 11.6  $\pm$  1.6  $\mu\text{M}$ . A mixed inhibition mode for compound **5** was proposed from the analysis of the linearized Lineweaver–Burk plots. For the analysis of the inhibition mode, we did not use the Lineweaver–Burk plots because of the possible misinterpretation of the linearized data described for tightly binding inhibitors.<sup>48</sup> Instead, we used a non-linear regression fit of the non-transformed data into the Williams–Morrison equation for the respective inhibition modes. The direct comparison of the inhibition data fit into the equations describing competitive, uncompetitive and non-competitive<sup>48</sup> inhibition modes clearly indicated the competitive inhibition of mdN and cdN by compound **5**.

The introduction of iodo, iodoxy and carboxy substituents onto the *para* position of the phenyl ring of lead compound **5** improved the inhibitory effect of the iodo compound **12d**, iodoxy compound **31**, and carboxy compound **13** toward mdN by factors of five, two and 1.7, respectively (Table 2). In contrast to carboxy derivative **13**, aldehyde **22**, which could form a hemiacetal linkage with the hydroxyl of Ser131, showed weak inhibition activity. The inhibitory effect of iodo compound **12d** toward the cdN enzyme was not significantly affected; therefore, its selectivity toward mdN is more than three times higher compared to that of lead compound **5**. On the other hand, the presence of many other substituents improved the inhibition of cdN. Specifically, the compounds bearing iodoxy (**31**, **32**) and carboxy (**13**, **15**) groups showed the highest inhibition of cdN, with  $K_i$  values more than a hundred times lower than that of lead compound **5**. Additionally, the selectivity towards cdN changed dramatically; in the case of iodoxy derivative **32**, the selectivity index reached a value of 40 (Table 2, ESI Fig. 3S†).

The additional preference of mdN to bind the thymine over the uracil inhibitors was identified by comparing the  $K_i$  values of the compounds with the same substituent on the phenyl moiety but a different nucleobase (compounds **5/12r**, **12d/12p**, **13/15**, and **31/32**). However, an analogous preference for cdN was not established due to the lack of structural information.

We also evaluated the inhibition properties of two anionic compounds related to carboxy compound **13**: boronic acid derivative **30** and bisphosphonic acid derivative **28** bearing an additional phosphonic acid group. Compound **30**, which could form a hemiacetal bond with the Ser131 hydroxy group and thus strengthen the binding of **30** to the catalytic site, exhibited only weak inhibition. On the other hand, the phosphonic acid derivative **28** was less than half an order of magnitude weaker than carboxy derivative **13** for the inhibition of both enzymes but showed selectivity for cdN (SI = 6).

**Structural studies.** To determine the binding mode and interactions contributing to the inhibitory properties of this class of compounds, selected compounds were soaked into a crystal of mdN. The crystal structures of the mdN complexes with **12d**, **12e**, and **13** were solved by a difference Fourier technique using the structure of free mdN as a model (PDB code 4L6A<sup>36</sup>). The statistics for the diffraction data and structure refinements are summarized in ESI Table 3S.† In all cases, the asymmetric unit contained one molecule of mdN with one compound bound in the active site. All mdN residues could be traced in a well-defined electron density map.

The structure of the complex with iodo compound **12d**, the most potent inhibitor of mdN from our series, was refined using diffraction data to a resolution of 1.78 Å. The electron density map used to model the inhibitor was of excellent quality (Fig. 4A); the occupancy factor for the inhibitor was reduced to 0.85 to correctly explain the density.

The structure of the mdN complex with **12e** was refined using diffraction data to a resolution of 1.37 Å. The electron density map used for inhibitor placing clearly showed the position of the inhibitor, which was modeled with an occupancy

factor of 0.7 (Fig. 4C). Other non-protein electron densities in the active sites of the structures were modeled as phosphate and magnesium ions (Fig. 4). The phosphate ion originated from the crystallization solution, which contained 20 mM potassium phosphate. Phosphate binding was observed in the other structure of the free enzyme (PDB codes 1MH9<sup>49</sup> and 4L6A<sup>36</sup>) and in the structure of the mdN complex with compound **5** (PDB code 1Q92<sup>35</sup>).

The structure of the mdN complex with carboxy derivative **13** was refined to a resolution of 1.67 Å using diffraction data. The electron density map of the active site of the protein shows two alternative arrangements of ligands in the enzyme active site: carboxy compound **13** with an occupancy factor of 0.6 is overlaid with a phosphate ion with an occupancy factor of 0.4. Interestingly, the magnesium ion in this structure was replaced by a potassium ion (Fig. 4E). The identity of the metal ion was confirmed by the value of the electron density map and also by the coordinating distances (ESI Table 3S†).

The binding modes of iodo compound **12d** and nitro compound **12e** are similar to each other (Fig. 4A and C); the phosphonate group interacts with the areas of the active site distal from the catalytic residues, while the base moiety is deeply buried in the active site. This binding mode is very similar to that of compound **5**, as published by others;<sup>35</sup> the root-mean-square deviations (RMSD) for the superposition of the 28 corresponding atoms of **5** with **12d** and **12e** are 0.407 and 0.614 Å, respectively.

Although similar in structure, carboxy compound **13** binds to the mdN active site differently from **12d** and **12e**, with the phosphonate group coordinating to the catalytic magnesium ion. This binding pose is unique among all published mdN inhibitors<sup>35</sup> and resembles the binding mode of substrates (2'-deoxythymidine, uridine, and 2'-deoxyuridine 5'-monophosphates) in crystal structures of D41N mutant (PDB codes 1Z4L, 1Z4M, and 1Z4I, Fig. 4F).<sup>50</sup>

Iodo compound **12d** and nitro compound **12e** participate in numerous polar interactions with the mdN active site (Fig. 4B and D), and most of them are analogous to the interactions described previously for compound **5**.<sup>35</sup> The thymine base 3-NH group of **12d** or **12e** forms a hydrogen bond with the main chain carbonyl of Phe75. The O2 carbonyl oxygen of the thymine forms a hydrogen bond with the main chain amide of Val77 and a water-mediated hydrogen bond with the Ser78 hydroxyl group. The carbonyl oxygen at C4 of the base forms bonds with two water molecules; one of them is coordinated by a Mg<sup>2+</sup> ion, and the other water forms a hydrogen bond with a carboxyl group of Glu50. The polar interactions of the pentofuranosyl moiety of **12d** or **12e** include one water-mediated hydrogen bond to Ser78 and the interaction of the hydrogen atoms at C1' and C2' with the  $\pi$ -electrons of the Trp96 aromatic side chain. The phosphonate groups of **12d** and **12e** bind to a positively charged pocket and form direct hydrogen bonds with the main chain amide of Lys134 and the side chains N $\eta$ 1 and N $\eta$ 2 of Arg163. Additionally, the phosphonate group forms water-mediated hydrogen bridges with Glu97 and Trp96.



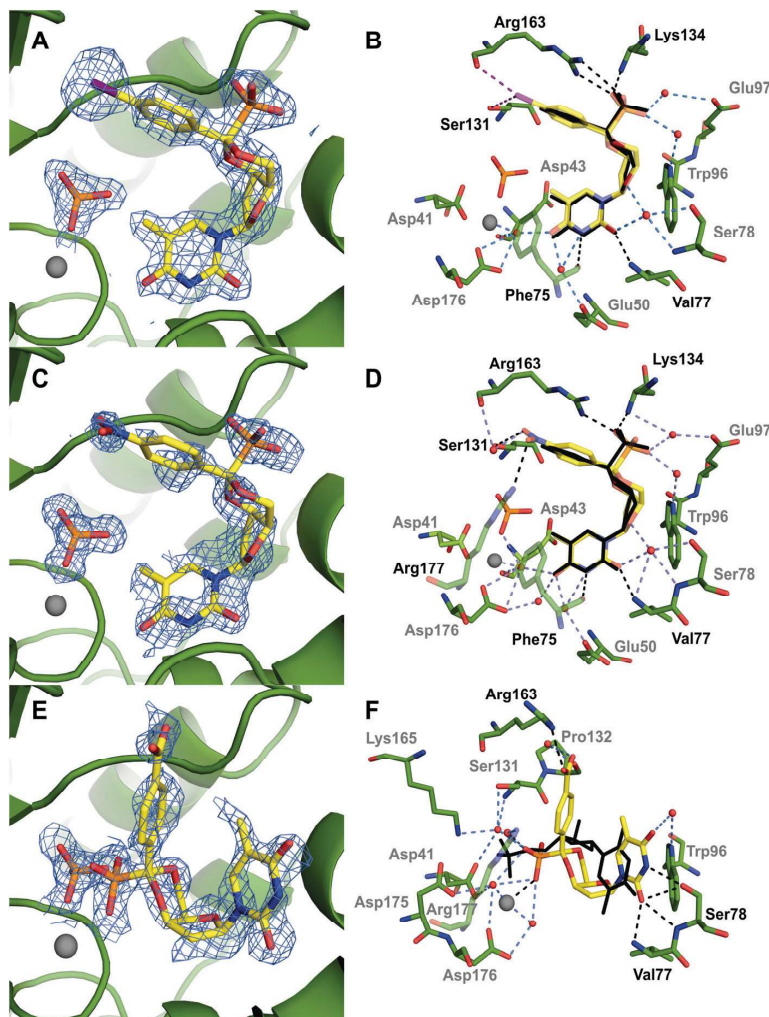


**Fig. 4** Details of the active site of the enzyme in crystal structures of mdN complexes with **12d** (panels A, B), **12e** (C, D), and **13** (E, F). The inhibitors are shown as stick models, and carbon atoms are yellow, oxygen atoms are red, nitrogen atoms are blue, phosphorus atoms are orange and iodine atoms are purple. In the protein, the carbon atoms are colored green. Phosphate and magnesium ions bound to the enzyme are also shown as sticks and balls, respectively. In panels (A, C and E), the  $2F_o - F_c$  electron density map is contoured at  $1.0\sigma$ . In panels (B, D and F), the polar interactions between the inhibitor and mdN are represented by dashed lines. Direct hydrogen bonds and water-mediated hydrogen bonds are colored black and light blue, respectively. Halogen bonds in panel (B) are shown in purple. Residues participating in direct and water-mediated hydrogen bonds are named in black and gray, respectively. In panels (B and D), the structure of lead compound **5** from crystal structure 1Q92<sup>35</sup> is shown in black lines. In panel (F), the structure of the substrate analog from crystal structure 1Z4L<sup>50</sup> is shown in black.

The iodo or nitro substituents at the *para* position of the phenyl ring provide additional interactions not present in complexes with lead compound **5**. The iodo group of **12d** forms two halogen bonds<sup>51,52</sup> (Fig. 4B). The first interaction is with a partially negatively charged carbonyl oxygen of Arg163 at a distance of 3.6 Å with a C–I–O angle of 166°. The second interaction is the hydrogen bond with the hydroxyl group of the Ser131 side chain (distance 4.0 Å, C–I–O angle 106°). The bond distances and angles are in agreement with the values

expected for the interaction of a halogen with a Lewis base (carbonyl oxygen) and a Lewis acid (H-atom of the hydroxyl group).<sup>51–53</sup>

The nitro group of **12e** forms direct hydrogen bonds with the side chains of Ser131 and the Nη1 atom of Arg177. The larger volume of the nitro group compared to the iodine in **12d** results in a slight shift of the nitrophenyl moiety away from Ser131 (0.47 Å) and also a small rotation (~15.4°) of the phosphonate group (Fig. 4D). Because of this small structural

change, the hydrogen bond network of the **12e** phosphonate group differs marginally from those in **12d** and **5**.

In compound **13**, the phosphonate group is buried in the mdN active site and contributes to the coordination of the potassium ion (Fig. 4F). In addition, several water-mediated hydrogen bonds are formed between the phosphonate group and Asp41, Ser131, Lys165, Asp175, Asp176, and Arg177. The base moiety forms direct hydrogen bonds *via* the N3 atom with the Ser78 hydroxyl group and *via* the O2 atom with the main chain amide of Val77. A water-mediated hydrogen bond is also formed between the base carbonyl and Trp96. The carboxyl group at the *para* position of the phenyl ring forms one direct hydrogen bond with the guanidine group of Arg163 and one water-mediated hydrogen bond with the carbonyl of Pro132.

We have characterized the interactions of cdN with selected compounds (**12d**, **13**, **15**, **31** and **32**) using protein-detected NMR spectroscopy, as the extensive soaking trials did not yield crystals of cdN with bound small molecules. cdN provides well-resolved NMR spectra, which allowed for the backbone resonances to be completely assigned.<sup>54</sup> The effects of the added compounds were followed using 2D <sup>15</sup>N/<sup>1</sup>H TROSY spectra of <sup>15</sup>N-labeled cdN. The chemical shift perturbations induced by the selected compounds are summarized as graphs of the minimal shift values (Fig. 2S; ESI†). As expected, the most perturbed residues were localized around the active site of cdN, suggesting that all the tested compounds bind to the same region of the enzyme, possibly with similar conformations. In particular, two regions of cdN, Gly13-Asp16 and Phe44-Arg47, were found to be consistently affected by all inhibitors. However, a detailed analysis revealed certain differences in the distribution of changes in the cdN backbone signal positions upon binding of various compounds. Significant differences were first observed between compounds **12d** and **13**; **12d** affected Arg47, and **13** strongly perturbed the signal from Arg132 and its neighboring residues Thr131, Asp133, Lys134 and Thr135. Considering the relatively small difference between the covalent structures of **12d** and **13**, the distribution of the compound-specific local changes observed in the cdN spectra suggests a different orientation of these compounds in the active site, with the carboxylic group of **13** displacing the side chain of Arg132 in a manner similar to that observed in the X-ray structure of the complex with mdN (Fig. 4F); **12d** adopts the reverse orientation. The presence of two different binding modes for the highly similar compounds **12d** and **13** is further supported by the difference of >2 ppm between the positions of the <sup>31</sup>P signals from the phosphonate groups in the 1D <sup>31</sup>P NMR spectra obtained for both complexes. Compound **15** showed overlapping perturbations with **13** within the region around Arg132, although there were additional changes in other residues, including Val61-Phe71 and Lys104-His106, suggesting that different contacts were established by the uracil base (**15**) compared with the thymine base of **13**. The additional effects of **31** and **32** cannot be unambiguously interpreted.

## Conclusion

We have shown that the introduction of various substituents into the *para* position of the phenyl ring of the mdN-specific inhibitor **5** can lead to an improvement in the inhibitory activity toward mdN and also fine tune the selectivity toward cdN. To our knowledge, compounds **12d** and **31**, with different substituents (iodo and iodoxy), are the most potent and specific inhibitors of mdN and cdN, respectively, reported to date. On the other hand, uracil iodoxy compound **32** exhibited a four times higher selectivity index towards cdN than compound **31**, suggesting the important role of the pyrimidine nucleobase type on the selectivity (compare also **12d** and **12p**).

The crystallographic data provided evidence for the existence of two different binding orientations for compounds **12d** and **13** in the active site of mdN and underlined the crucial role of the substituent on the binding specificity. The NMR data obtained for the analogous cdN complexes confirmed similar binding behavior. Based on the inhibition kinetics and structural data, we propose that inhibitors more specific towards mdN are preferentially binding to the mitochondrial and cytosolic enzyme in the orientation represented by lead compound **5**, while for inhibitors more specific towards cdN, the proteins favor the opposite orientation, similar to that observed for the complex of mdN with compound **13**. This suggests that each of the isoenzymes requires a specific binding mode for effective inhibition.

## Abbreviations

ALL	Acute lymphoblastic leukemia
AML	Acute myeloid leukemia
AZT	Zidovudine
cdN	Cytosolic 5'(3')-deoxynucleotidases
cN-II, cN-IA and cN-III	Cytosolic 5'-nucleotidases
eN	Ecto-5'-nucleotidase
FUDR	Fludarabine
FdU	5-Fluoro-2'-deoxyuridine
FdUMP	5-Fluoro-2'-deoxyuridine 5'-phosphate
$K_i$	Inhibition constant
$K_M$	Michaelis-Menten constant
mdN	Mitochondrial 5'(3')-deoxynucleotidases
RMSD	Root-mean-square deviation
SI	Selectivity index

## Acknowledgements

Financial support by grants 203/09/0820, 13-24880S, and 13-26526S (Czech Science Foundation) and by Research Centers KAN200520801 (Acad. Sci. CR) is gratefully acknowledged. This work was also supported in part by projects RVO 61388963 and 68378050 awarded by the Academy of Sciences of the Czech Republic and by the Ministry of Education of the Czech



Republic – LK11205 (programme “NAVRAT”). The authors are indebted to Eva Zborníková, MSc for LC-MS measurements and the staff of the Mass Spectrometry Department of the Institute of Organic Chemistry and Biochemistry AS CR (Dr Josef Cvačka, Head) and Zdeněk Fiedler for the measurements and interpretations of HR mass spectra and IR spectra.

## References

- S. A. Hunsucker, B. S. Mitchell and J. Sychala, *Pharmacol. Ther.*, 2005, **107**, 1–30.
- V. Bianchi, E. Pontis and P. Reichard, *Proc. Natl. Acad. Sci. U. S. A.*, 1986, **83**, 986–990.
- S. Eriksson, *Curr. Med. Chem.*, 2013, **20**, 4241–4248.
- P. Bianchi, E. Fermo, F. Alfinito, C. Vercellati, M. Baserga, F. Ferraro, I. Guzzo, B. Rotoli and A. Zanella, *Br. J. Haematol.*, 2003, **122**, 847–851.
- K. Wallden, P. Stenmark, T. Nyman, S. Flodin, S. Graslund, P. Loppnau, V. Bianchi and P. Nordlund, *J. Biol. Chem.*, 2007, **282**, 17828–17836.
- V. Bianchi and J. Sychala, *J. Biol. Chem.*, 2003, **278**, 46195–46198.
- S. A. Hunsucker, J. Sychala and B. S. Mitchell, *J. Biol. Chem.*, 2001, **276**, 10498–10504.
- C. M. Galmarini, J. R. Mackey and C. Dumontet, *Leukemia*, 2001, **15**, 875–890.
- D. A. Carson, C. J. Carrera, D. B. Wasson and T. Iizasa, *Biochim. Biophys. Acta*, 1991, **1091**, 22–28.
- S. Yamamoto, T. Yamauchi, Y. Kawai, H. Takemura, S. Kishi, A. Yoshida, Y. Urasaki, H. Iwasaki and T. Ueda, *Int. J. Hematol.*, 2007, **85**, 108–115.
- J. A. Meyer, J. Wang, L. E. Hogan, J. J. Yang, S. Dandekar, J. P. Patel, Z. Tang, P. Zumbo, S. Li, J. Zavadil, R. L. Levine, T. Cardozo, S. P. Hunger, E. A. Raetz, W. E. Evans, D. J. Morrison, C. E. Mason and W. L. Carroll, *Nat. Genet.*, 2013, **45**, 290–294.
- G. Tzoneva, A. Perez-Garcia, Z. Carpenter, H. Khiabani, V. Tosello, M. Allegretta, E. Paietta, J. Racevskis, J. M. Rowe, M. S. Tallman, M. Paganin, G. Basso, J. Hof, R. Kirschner-Schwabe, T. Palomero, R. Rabadan and A. Ferrando, *Nat. Med.*, 2013, **19**, 368–371.
- H. K. Erdemli, B. Adam and N. Bavbek, *Acta Medica (Hradec Kralove)*, 2004, **47**, 129–131.
- G. Moyle, *Clin. Ther.*, 2000, **22**, 911–936; discussion 898.
- W. Lewis and M. C. Dalakas, *Nat. Med.*, 1995, **1**, 417–422.
- W. Lewis, B. J. Day and W. C. Copeland, *Nat. Rev. Drug Discovery*, 2003, **2**, 812–822.
- K. Brinkman, H. J. ter Hofstede, D. M. Burger, J. A. Smeitink and P. P. Koopmans, *AIDS*, 1998, **12**, 1735–1744.
- C. Mazzon, C. Rampazzo, M. C. Scaini, L. Gallinaro, A. Karlsson, C. Meier, J. Balzarini, P. Reichard and V. Bianchi, *Biochem. Pharmacol.*, 2003, **66**, 471–479.
- A. Hampton, F. Perini and P. J. Harper, *Biochemistry*, 1973, **12**, 1730–1736.
- E. P. Garvey, G. T. Lowen and M. R. Almond, *Biochemistry*, 1998, **37**, 9043–9051.
- M. Meurillon, Z. Marton, A. Hospital, L. P. Jordheim, J. Bejaud, C. Lionne, C. Dumontet, C. Perigaud, L. Chaloin and S. Peyrottes, *Eur. J. Med. Chem.*, 2014, **77**, 18–37.
- D. Rejman, A. Rabatinova, A. R. Pombinho, S. Kovackova, R. Pohl, E. Zbornikova, M. Kolar, K. Bogdanova, O. Nyc, H. Sanderova, T. Latal, P. Bartunek and L. Krasny, *J. Med. Chem.*, 2011, **54**, 7884–7898.
- D. Rejman, N. Panova, P. Klener, B. Maswabi, R. Pohl and I. Rosenberg, *J. Med. Chem.*, 2012, **55**, 1612–1621.
- Z. Tocik, I. Dvorakova, R. Liboska, M. Budesinsky, M. Masojdkova and I. Rosenberg, *Tetrahedron*, 2007, **63**, 4516–4534.
- D. Rejman, P. Kocalka, M. Budesinsky, R. Pohl and I. Rosenberg, *Tetrahedron*, 2007, **63**, 1243–1253.
- D. Rejman, P. Kocalka, M. Budesinsky, I. Barvik and I. Rosenberg, *Tetrahedron: Asymmetry*, 2007, **18**, 2165–2174.
- O. Pav, I. Barvik, M. Budesinsky, M. Masojdkova and I. Rosenberg, *Org. Lett.*, 2007, **9**, 5469–5472.
- R. Liboska, M. Masojdkova and I. Rosenberg, *Collect. Czech. Chem. Commun.*, 1996, **61**, 313–332.
- S. Kralikova, M. Budesinsky, I. Tomeckova and I. Rosenberg, *Tetrahedron*, 2006, **62**, 9742–9750.
- A. Kralikova, M. Budesinsky, M. Masojdkova and I. Rosenberg, *Tetrahedron*, 2006, **62**, 4917–4932.
- M. Endova, M. Masojdkova, M. Budesinsky and I. Rosenberg, *Tetrahedron*, 1998, **54**, 11187–11208.
- M. Endova, M. Masojdkova, M. Budesinsky and I. Rosenberg, *Tetrahedron*, 1998, **54**, 11151–11186.
- I. Kosiova, O. Simak, N. Panova, M. Budesinsky, M. Petrova, D. Rejman, R. Liboska, O. Pav and I. Rosenberg, *Eur. J. Med. Chem.*, 2014, **74**, 145–168.
- R. Liboska, M. Masojdkova and I. Rosenberg, *Collect. Czech. Chem. Commun.*, 1996, **61**, 778–790.
- A. Rinaldo-Matthis, C. Rampazzo, J. Balzarini, P. Reichard, V. Bianchi and P. Nordlund, *Mol. Pharmacol.*, 2004, **65**, 860–867.
- P. Pacht, M. Fabry, I. Rosenberg, O. Simak, P. Rezacova and J. Brynda, *Acta Crystallogr., Sect. D: Biol. Crystallogr.*, 2014, **70**, 461–470.
- R. A. McClelland, G. Patel and P. W. K. Lam, *J. Org. Chem.*, 1981, **46**, 1011–1012.
- W. A. Sheppard, *Tetrahedron*, 1971, **27**, 945–951.
- K. H. G. Brinkhaus, E. Steckhan and D. Degner, *Tetrahedron*, 1986, **42**, 553–560.
- R. Breslow and P. S. Pandey, *J. Org. Chem.*, 1980, **45**, 740–741.
- I. Barba, R. Chinchilla and C. Gomez, *Tetrahedron*, 1990, **46**, 7813–7822.
- MSPin software program, version 1.2.1-49*, MestReLab Research S.L., 2008.
- E. Diez, J. Sanfabian, J. Guilleme, C. Altona and L. A. Donders, *Mol. Phys.*, 1989, **68**, 49–63.
- D. Rai, M. Johar, N. C. Srivastav, T. Manning, B. Agrawal, D. Y. Kunimoto and R. Kumar, *J. Med. Chem.*, 2007, **50**, 4766–4774.

- 45 Y. K. Wang, D. X. Wang, C. H. Xu, R. Wang, J. J. Han and S. Y. Feng, *J. Organomet. Chem.*, 2011, **696**, 3000–3005.
- 46 M. Kalek, M. Jezowska and J. Stawinski, *Adv. Synth. Catal.*, 2009, **351**, 3207–3216.
- 47 K. L. Billingsley, T. E. Barder and S. L. Buchwald, *Angew. Chem., Int. Ed.*, 2007, **46**, 5359–5363.
- 48 R. A. Copeland, *Enzymes: a practical introduction to structure, mechanism, and data analysis*, Wiley, New York, 2nd edn, 2000.
- 49 A. Rinaldo-Matthis, C. Rampazzo, P. Reichard, V. Bianchi and P. Nordlund, *Nat. Struct. Biol.*, 2002, **9**, 779–787.
- 50 K. Wallden, B. Ruzzenente, A. Rinaldo-Matthis, V. Bianchi and P. Nordlund, *Structure*, 2005, **13**, 1081–1088.
- 51 M. R. Scholfield, C. M. Zanden, M. Carter and P. S. Ho, *Protein Sci.*, 2013, **22**, 139–152.
- 52 P. Auffinger, F. A. Hays, E. Westhof and P. S. Ho, *Proc. Natl. Acad. Sci. U. S. A.*, 2004, **101**, 16789–16794.
- 53 P. Politzer, P. Lane, M. C. Concha, Y. G. Ma and J. S. Murray, *J. Mol. Model.*, 2007, **13**, 305–311.
- 54 A. Hnizda, R. Sklenickova, P. Pachl, M. Fabry, Z. Tosner, J. Brynda and V. Veverka, *Biomol. NMR Assign.*, 2013, DOI: 10.1007/s12104-013-9531-1.



Cite this: *Med. Chem. Commun.*, 2015, 6, 1635

## Structure-based design of a bisphosphonate 5'(3')-deoxyribonucleotidase inhibitor†

Petr Pachtl,‡<sup>a</sup> Ondřej Šimák,‡<sup>ab</sup> Pavlína Řezáčová,<sup>ac</sup> Milan Fábry,<sup>c</sup> Miloš Buděšínský,<sup>a</sup> Ivan Rosenberg\*<sup>a</sup> and Jiří Brynda\*<sup>ac</sup>

Received 3rd June 2015,  
Accepted 20th July 2015

DOI: 10.1039/c5md00235d

www.rsc.org/medchemcomm

Cellular 5'-nucleotidases regulating nucleotide/nucleoside pools are capable of dephosphorylating phosphomonoesters of important nucleoside analogue drugs, thus decreasing their therapeutic efficacy. Based on previously known inhibitor–enzyme complex structures, we developed a promising inhibitor by mimicking the phosphate ion and achieved 50- and 100-fold increases in the inhibitory potency towards cdN and mdN, respectively. Crystal structures of both complexes showed major differences in the inhibitor binding mode towards both enzymes.

5'-Nucleotidases are ubiquitous enzymes that catalyse the dephosphorylation of nucleoside monophosphates and thus regulate the levels of nucleotides and nucleosides.<sup>1,2</sup> In addition to their regulatory roles, 5'-nucleotidases can also dephosphorylate 5'-phosphate esters of therapeutically relevant nucleoside analogues and thus negatively affect their pharmacological efficacy. To date, seven human 5'-nucleotidases that differ in substrate specificity, cellular location, and tissue-specific expression have been identified and characterized (reviewed in ref. 1).

Two human 5'-nucleotidases, cytosolic 5'(3')-deoxyribonucleotidase (cdN) and mitochondrial 5'(3')-deoxyribonucleotidase (mdN), share 61% sequence identity. As their names indicate, they differ in subcellular localization. The enzymes specifically dephosphorylate dUMP and dTMP as preferred substrates. Overexpression of cdN in cultured human cells leads to an increase in dT, dU, and dC levels without affecting the ribonucleoside pool.<sup>3,4</sup> mdN is involved in regulation of mitochondrial dTMP and dUMP levels and thus, in the latter case, prevents accumulation of mutagenic dUTP.<sup>5</sup>

Both cdN and mdN are capable of efficiently dephosphorylating 5'-phosphates of modified nucleosides used as therapeutic agents. For example, cdN efficiently dephosphorylates 5'-phosphates of zidovudine (AZT), a

compound used for HIV-1 treatment. FdUMP, an active metabolite of floxuridine (FUDR) that is used in cancer

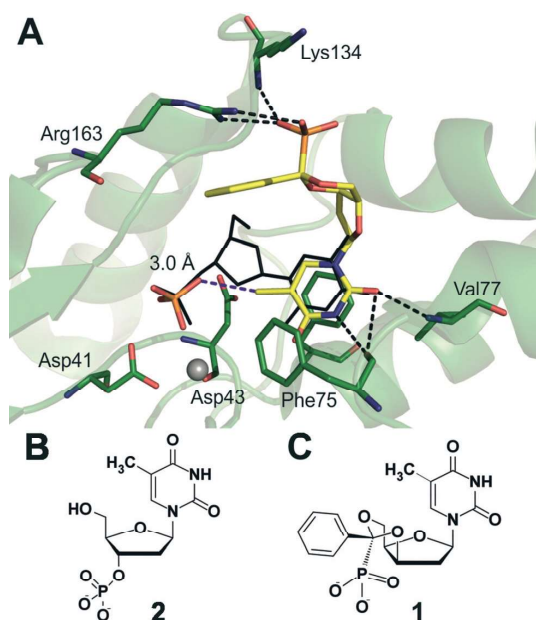


**Fig. 1** Structure of mdN with two compounds. (A) Structure of mdN (green) in complex with **1** (yellow) (PDB code 1Q91). Compound **1** and interacting residues are shown as sticks. Direct hydrogen bonds are shown as dashed black lines. The position of 3'-dTMP (**2**) from its complex with an inactive mdN mutant (PDB code 1Z4L) is indicated by solid black lines. The dashed blue line indicates the distance (3 Å) between the base methyl and the phosphate oxygen. Carbon atoms are coloured green or yellow; oxygen atoms are coloured red, nitrogen blue, and phosphorus orange. (B) Structural formula of 3'-dTMP (**2**). (C) Structural formula of **1**.

<sup>a</sup> Institute of Organic Chemistry and Biochemistry, Academy of Sciences of the Czech Republic, Prague, Czech Republic. E-mail: rosenberg@uochb.cas.cz, brynda@img.cas.cz; Tel: +420 220 183 210, +420 220 183 381

<sup>b</sup> Department of Chemistry of Natural Compounds, University of Chemistry and Technology Prague, Prague, Czech Republic

<sup>c</sup> Institute of Molecular Genetics, Academy of Sciences of the Czech Republic, Prague, Czech Republic

† Electronic supplementary information (ESI) available. See DOI: 10.1039/c5md00235d

‡ These authors contributed equally.

treatment (solid tumours in the colon, kidneys, and stomach), is cleaved by cdN twice as fast as the natural substrate dUMP.<sup>6</sup> Dephosphorylation of nucleotide analogues by human 5'-nucleotidases decreases the concentration of the active drug, which can contribute to the development of drug resistance and thus limit the clinical use of these analogues.<sup>7–9</sup> For example, increased activity of cdN and cN-III (CMP specific cytosolic 5'-nucleotidase III) has been found in the cells of patients with acute myeloid leukaemia (AML) and acute lymphoblastic leukaemia (ALL), and patients with clinical remission of ALL have even higher cdN activity than at the time of diagnosis.<sup>10</sup> Inhibition of cdN may therefore increase the effectiveness of chemotherapy and antiviral treatment. Selective inhibition of mdN should be investigated to determine its potential effects on various tumour cell lines.

Previous studies have identified two inhibitors of cdN and mdN (PMcP-U and DPB-T).<sup>9</sup> Based on the inhibitor DPB-T (compound 1, Fig. 1C), we recently published an SAR study on inhibitor modification at the *para* position of the phenyl ring.<sup>11</sup> This work showed twelve additional inhibitors of both enzymes and three X-ray crystal structures of the mdN-inhibitor complex.

Here, we present a new modification of the inhibitor DPB-T based on previously published structures. By modifying the uracil base, we obtained a highly promising type of inhibitor. We also present the crystal structures of both enzymes in complex with this new inhibitor, showing different binding modes towards cdN and mdN. Inhibitor DPB-T (compound 1), the structure of which is derived from 3'-dTMP (2),<sup>9</sup> inhibits mdN and cdN with  $K_i$  values of  $11.6 \pm 1.6 \mu\text{M}$  and  $610 \pm 130 \mu\text{M}$ , respectively.<sup>11</sup>

The crystal structure of 1 bound to the active site of mdN reveals that its binding mode is different from that of substrate 2 (Fig. 1).<sup>12</sup> The phosphonate group of 1 does not interact with the catalytic site, but rather points towards the opening of the active site, where it forms two hydrogen bonds with the guanidine group of Arg163 and the peptide amide of Lys134.<sup>12</sup> A phosphate ion originating from the crystallization conditions occupies the active site position where substrate 2 phosphate groups bind during catalysis. Phosphate ion binding has also been observed in free and inhibitor-bound mdN structures.<sup>11–15</sup>

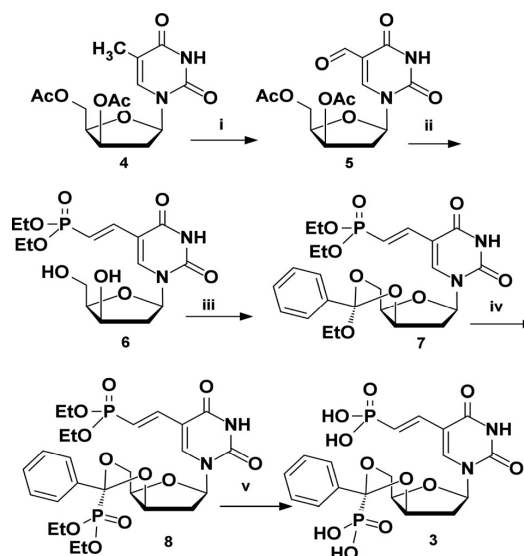
This observation led to the structure-assisted rational design of compounds that combine 1 and the inorganic phosphate into a single molecule. The distance between the methyl carbon at the C5 position of the thymine base in 1 and the oxygen atom of the phosphate is 3.0 Å (Fig. 1). Thus, we attached a phosphonate group to C5 of the thymine base in 1. This phosphonate coupling was synthetically achieved through a double bond linkage and resulted in 3.

The synthesis of inhibitor 3 started from acetylated "xyloT" derivative 4, which was oxidized by a procedure developed by Matsuda *et al.*<sup>16</sup> to 5-formyl-xyloT derivative 5. This aldehyde reacted with tetraethyl methylenediphosphonate by a Horner–Wadsworth–Emmons type reaction to yield the *trans*-vinylphosphonate, and the following deacetylation yielded compound 6. Acid-catalysed transesterification of

triethyl orthobenzoate with 6 yielded orthoester 7 as an *R*-isomer exclusively. The reactions<sup>17</sup> of orthoester 7 with diethyl chlorophosphite depicted in Scheme 1 led to the production of bisphosphonate derivative 8 as a single epimer. The deprotection of the phosphonate ester groups was performed with bromotrimethylsilane in acetonitrile in the presence of 2,6-lutidine, providing desired phosphonic acid 3. Detailed experimental procedures and NMR analytical data of newly prepared compounds are provided in the ESI.†

Crystals of mdN and cdN complexes were prepared by soaking 3 into previously grown crystals. The crystallization was performed in hanging drops at 18 °C. Diffraction data for mdN and cdN in complex with 3 were collected at the BESSY Berlin, Beamline MX14.1 and MX14.2.<sup>18</sup> The structure of mdN in complex with 3 was solved using the difference Fourier method, using an identical protein structure (PDB code 4 L6A<sup>13</sup>) as the initial model. Atomic coordinates and experimental structure factors have been deposited with the PDB under codes 4YIH and 4YIK for complexes of 3 with cdN and mdN, respectively. All figures showing structural representations were prepared with the programme PyMOL.<sup>19</sup> Crystal parameters and data collection statistics are summarized in Table S1.†

Compound 3 was assayed for inhibition of mdN and cdN using dUMP as a substrate (Table 1).<sup>11</sup> The  $K_i$  value for inhibition of mdN was more than 150-fold less than that of 1. We also observed an increase in inhibitory potency towards cdN, but it was not as significant. Thus, 3 displayed high selectivity for mdN over cdN. Compound 3 was successfully crystallized in complex with mdN and cdN. Crystal structures



**Scheme 1** Chemical synthesis of compound 3. Reaction conditions: i:  $\text{Na}_2\text{S}_2\text{O}_8$ ,  $\text{CuSO}_4 \cdot 5\text{H}_2\text{O}$ , 2,6-lutidine,  $\text{CH}_3\text{CN}/\text{H}_2\text{O}$ . ii: 1) Tetraethyl methylene diphosphonate, NaH, THF, 2) 2 M MeONa/MeOH. iii: Triethyl orthobenzoate, dry HCl/Et<sub>2</sub>O, DMF. iv:  $(\text{EtO})_2\text{P}(\text{Cl})$ ,  $\text{CH}_3\text{CN}$ , v: TMSBr, 2,6-lutidine,  $\text{CH}_3\text{CN}$ .

**Table 1** Inhibition of cytosolic and mitochondrial nucleotidases by compounds 1 and 3

Compound	$K_i$ [ $\mu\text{M}$ ]		Selectivity index <sup>a</sup>
	cdN	mdN	
1	$610 \pm 130^b$	$11.6 \pm 1.6^b$	$4.67^b$
3	$21.7 \pm 2.2$	$0.128 \pm 0.018$	19.98

<sup>a</sup> The selectivity index  $[(K_i/K_M)_{\text{mdN}}/(K_i/K_M)_{\text{cdN}}]$  is expressed as a ratio of the  $K_i$  values for the mdN and cdN enzymes normalized to the enzymatic constant  $K_M$  of the individual enzymes  $[(K_M)_{\text{mdN}} = 86 \pm 14$ ,  $(K_M)_{\text{cdN}} = 968 \pm 79 \mu\text{M}]$ . <sup>b</sup> Values from ref. 11.

determined at high resolution provided a structural basis for understanding the selectivity of 3 for mdN.

The crystal structure of mdN in complex with 3 revealed that the inhibitor binds in the position expected from our rational design. The position and interactions of the inhibitor are very similar to those of 1 (Fig. 2A and B). The phosphonate group forms two hydrogen bonds with the two nitrogen atoms of the guanidine group of Arg163 and the peptide amide of Lys134. Two more hydrogen bonds are formed by the base of the inhibitor with the carbonyl group of Phe75 and the amide group of Val77. Additional interactions are formed by the secondary phosphonate group attached to the base of the inhibitor. The inhibitor forms a strong coordinate-covalent interaction with the magnesium ion in the mdN active site. The position of the secondary

phosphonate group does not fully overlay with the position of the phosphate ion that was used as a guide for the design of 3. The distance between phosphorus atoms in the superposed structures is 2.24 Å (Fig. 2B) indicating potential space for optimization of the linker length and torsion restraints.

Surprisingly, the crystal structure of 3 in complex with cdN revealed a different binding mode (Fig. 2). The phosphonate group positions are exchanged in cdN compared with the complex of 3 with mdN. In cdN, the phosphonate group attached to the sugar moiety is coordinated to the active site magnesium ion, while the secondary phosphonate group attached to the base points towards the opening of the active site. Interestingly, although the inhibitor positions in mdN and cdN differ substantially, the interacting residues are preserved. The base moiety of 3 forms a hydrogen bond with the backbone amide of Arg47, which corresponds to Val77 in mdN. In cdN, an alternative hydrogen bond forms between the base moiety of 3 and the amide of Ala46. The base-attached phosphonate group of 3 forms hydrogen bonds with the guanidine group of Arg132 and the amide of Val103, corresponding to mdN residues Arg163 and Lys134, respectively. The phosphonate group attached to the sugar moiety in 3 is coordinated to the active-site magnesium ion, similar to the phosphate group of substrates. The binding mode of 3 in complex with cdN more closely resembles substrate binding than the binding of parental compound 1.

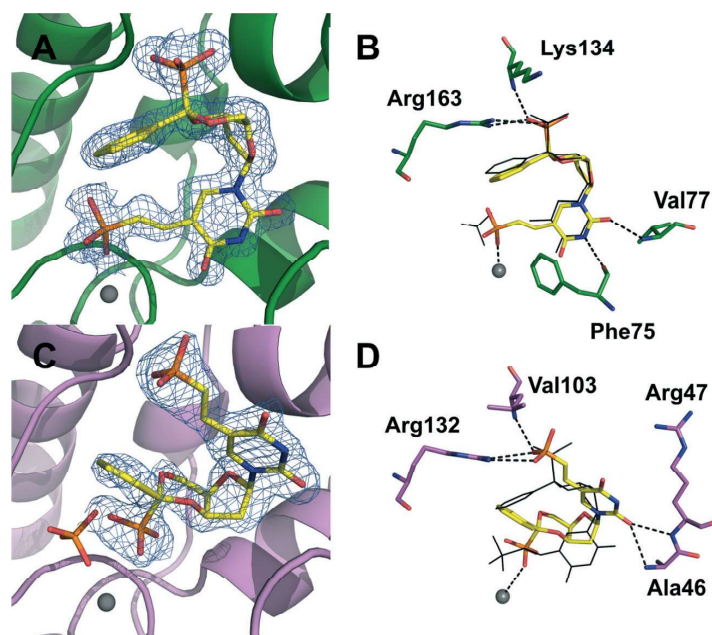


**Fig. 2** Structures of mdN and cdN in complex with 3. (A, B) Structure of mdN (green) in complex with 3 (yellow) (PDB code 4Y1K). On panel (B), the black line indicates the position of 1 in complex with mdN (PDB code 1Q91). (C, D) Structure of cdN (magenta) in complex with 3 (yellow) (PDB code 4Y1H). On panel (D), the black line indicates the position of 3 from its complex with mdN (PDB code 4Y1K). Compound 3 and interacting residues are shown as sticks. Direct hydrogen bonds are shown as black dashed lines. Carbon atoms are coloured yellow, green, or magenta; oxygen atoms are coloured red, nitrogen blue, and phosphorus orange.



We report the successful application of structure-based design of a bisphosphonate inhibitor of cdN and mdN. Attachment of a second phosphonate group, the position of which was inspired by the phosphate ion found in the crystal structures of cdN and mdN, decreased the  $K_i$  values 50- and 100-fold for cdN and mdN, respectively. The inhibitory properties of 3 towards cdN ( $K_i = 21.7 \pm 2.2 \mu\text{M}$ ) are comparable to the best inhibitors for this enzyme described to date.<sup>11</sup> For mdN, 3 has the lowest  $K_i$  value ( $0.128 \pm 0.018 \mu\text{M}$ ) of all reported inhibitors.<sup>11,12</sup> Interestingly, 3 assumes two different binding modes when bound to these two highly homologous enzymes. The structure of 3 in complex with mdN showed that the additional phosphonate group binds in the expected position: deeply buried and coordinating with the active-site magnesium ion. A small difference (approximately 2 Å) between the ideal position of the phosphate ion in the active site and the phosphonate group in 3 provides some space for future compound optimization. The crystal structure of cdN in complex with 3 represents the first structure of this enzyme in complex with an inhibitor. Compound 3 has an unexpected binding mode, with the secondary phosphonate group interacting with the entrance to the active site and the phosphonate group attached to the base coordinating with the active site magnesium ion. Our results suggest that selective inhibition of cdN and mdN could be achieved by designing bisphosphonate compounds with different binding modes for each enzyme.

## Abbreviations

ALL	Acute lymphoblastic leukaemia
AML	Acute myeloid leukaemia
AZT	Zidovudine
cdN	Cytosolic 5'(3')-deoxynucleotidase
FUDR	Fludarabine
FdU	5-Fluoro-2'-deoxyuridine
FdUMP	5-Fluoro-2'-deoxyuridine 5'-phosphate
$K_i$	Inhibition constant
$K_M$	Michaelis-Menten constant
mdN	Mitochondrial 5'(3')-deoxynucleotidase
RMSD	Root-mean-square deviation
SI	Selectivity index

## Acknowledgements

Financial support from grant 203/09/0820, 13-26526S and 13-24880S (Czech Science Foundation) under research projects RVO 61388963 and RVO 68378050 is gratefully acknowledged.

## References

- 1 S. A. Hunsucker, B. S. Mitchell and J. Spychala, *Pharmacol. Ther.*, 2005, **107**, 1–30.
- 2 V. Bianchi, E. Pontis and P. Reichard, *Proc. Natl. Acad. Sci. U. S. A.*, 1986, **83**, 986–990.
- 3 C. Gazzola, M. Moras, P. Ferraro, L. Gallinaro, R. Verin, C. Rampazzo, P. Reichard and V. Bianchi, *Exp. Cell Res.*, 1999, **253**, 474–482.
- 4 C. Rampazzo, P. Ferraro, G. Pontarin, S. Fabris, P. Reichard and V. Bianchi, *J. Biol. Chem.*, 2004, **279**, 17019–17026.
- 5 V. Bianchi and J. Spychala, *J. Biol. Chem.*, 2003, **278**, 46195–46198.
- 6 C. M. Galmarini, J. R. Mackey and C. Dumontet, *Leukemia*, 2001, **15**, 875–890.
- 7 D. A. Carson, C. J. Carrera, D. B. Wasson and T. Iizasa, *Biochim. Biophys. Acta*, 1991, **1091**, 22–28.
- 8 S. A. Hunsucker, J. Spychala and B. S. Mitchell, *J. Biol. Chem.*, 2001, **276**, 10498–10504.
- 9 C. Mazzon, C. Rampazzo, M. C. Scaini, L. Gallinaro, A. Karlsson, C. Meier, J. Balzarini, P. Reichard and V. Bianchi, *Biochem. Pharmacol.*, 2003, **66**, 471–479.
- 10 H. K. Erdemli, B. Adam and N. Bavbek, *Acta Med.*, 2004, **47**, 129–131.
- 11 O. Simak, P. Pachel, M. Fabry, M. Budesinsky, T. Jandusik, A. Hnizda, R. Sklenickova, M. Petrova, V. Veverka, P. Rezacova, J. Brynda and I. Rosenberg, *Org. Biomol. Chem.*, 2014, **12**, 7971–7982.
- 12 A. Rinaldo-Matthis, C. Rampazzo, J. Balzarini, P. Reichard, V. Bianchi and P. Nordlund, *Mol. Pharmacol.*, 2004, **65**, 860–867.
- 13 P. Pachel, M. Fabry, I. Rosenberg, O. Simak, P. Rezacova and J. Brynda, *Acta Crystallogr., Sect. D: Biol. Crystallogr.*, 2014, **70**, 461–470.
- 14 A. Rinaldo-Matthis, C. Rampazzo, P. Reichard, V. Bianchi and P. Nordlund, *Nat. Struct. Biol.*, 2002, **9**, 779–787.
- 15 K. Wallden, A. Rinaldo-Matthis, B. Ruzzenente, C. Rampazzo, V. Bianchi and P. Nordlund, *Biochemistry*, 2007, **46**, 13809–13818.
- 16 A. Ono, T. Okamoto, M. Inada, H. Nara and A. Matsuda, *Chem. Pharm. Bull.*, 1994, **42**, 2231–2237.
- 17 M. Endova, M. Masojdkova, M. Budesinsky and I. Rosenberg, *Tetrahedron*, 1998, **54**, 11151–11186.
- 18 U. Mueller, N. Darowski, M. R. Fuchs, R. Forster, M. Hellmig, K. S. Paithankar, S. Puhlinger, M. Steffien, G. Zocher and M. S. Weiss, *J. Synchrotron Radiat.*, 2012, **19**, 442–449.
- 19 W. L. DeLano, *Abstracts of Papers of the American Chemical Society*, 2009, vol. 238.



## Structure-Assisted Drug Design

## Structure-Based Optimization of Bisphosphonate Nucleoside Inhibitors of Human 5'(3')-deoxyribonucleotidases

Petr Pacht,<sup>[a]</sup> Ondřej Šimák,<sup>[a,c]</sup> Miloš Buděšínský,<sup>[a]</sup> Jiří Brynda,<sup>[a,b]</sup> Ivan Rosenberg,<sup>[a]</sup> and Pavlína Řezáčová<sup>\*,[a,b]</sup>

**Abstract:** Cellular 5'-nucleotidases, enzymes regulating nucleotide/nucleoside pools, are capable of dephosphorylating phosphomonoesters of important nucleoside analogue drugs, thus decreasing their therapeutic efficacy. Human cytosolic (cdN) as well as mitochondrial (mdN) variants of this enzyme represent interesting targets for development of inhibitory compounds. In this work, bisphosphonate nucleoside derivatives were designed by using a structure-based approach. A second phosphonate group was attached onto a base moiety and by optimi-

zation of the linker an increased inhibitor potency towards mdN and cdN was attained. The best compound exhibited inhibition of both enzymes in a nanomolar range, making it the most potent inhibitor of these enzymes prepared to date. In addition, the compounds showed selectivity towards the cdN variant. A series of crystal structures were solved for several inhibitors in the complex with mdN or cdN that provided a structural basis for understanding the inhibition profile of bisphosphonate compounds.

## Introduction

Cellular pools of nucleotides and nucleosides are regulated by 5'-nucleotidases.<sup>[1]</sup> These ubiquitous enzymes catalyze dephosphorylation of nucleotide monophosphates and there were eight 5'-nucleotidases identified and characterized in humans. They differ in substrate specificity, cellular localization, and tissue-specific expression.<sup>[1a,2]</sup> In addition to their physiological activity, 5'-nucleotidases can also dephosphorylate the 5'-phosphate esters of therapeutically relevant nucleoside analogs. This activity negatively affects pharmacological efficacy of nucleoside analogs and limits thus their clinical use.<sup>[3]</sup>

Primary and acquired resistance toward nucleoside analogs is suggested to be linked to the high expression and increased activity of cytosolic 5'-nucleotidases.<sup>[3]</sup> For example, araC-resistant leukemia cell lines with increased activity of cytosolic 5'-nucleotidase II (cN-II) are less sensitive to fludarabine,<sup>[4]</sup> and recent results identified a relapse-specific activating mutation in cN-II in childhood acute lymphoblastic leukemia (ALL).<sup>[5]</sup> Increased activity of cytosolic 5'(3')-deoxynucleotidase (cdN) and cN-III has also been found in the cells of patients with acute myeloid leukemia (AML) and ALL and patients with clinical remission of ALL.<sup>[6]</sup>

There are two 5'(3')-deoxynucleotidases differing in cellular localization and sharing 61 % sequence identity: cytosolic cdN and mitochondrial mdN. cdN efficiently dephosphorylates FdUMP, the 5'-phosphates of floxuridine (FdUR), a compound used in treatment of colon, kidney and stomach solid tumors. Interestingly, FdUMP is cleaved by cdN twice as fast as the natural substrate dUMP. Another medicinal compound cleaved by cdN is 5'-phosphate of zidovudine (AZT), a compound used for HIV-1 treatment.<sup>[8]</sup> The mdN is involved in regulation of mitochondrial dTMP and dUMP levels and thus prevents accumulation of mutagenic dUTP.<sup>[9]</sup> Both 5'(3')-deoxynucleotidases thus represent targets for development of inhibitory compounds. The obvious challenge is to design a specific inhibitor of the two highly similar enzymes.

The first identified inhibitor of cdN (DPB-T, compound **1**, Figure 1A)<sup>[3c]</sup> had the  $K_i$  value in a micromolar range (610  $\mu\text{M}$ )<sup>[10]</sup> and was shown it inhibit mdN with the  $K_i$  value of 11.6  $\mu\text{M}$ .<sup>[9]</sup> The modification of the *para* position of the phenyl ring yielded inhibitors of cdN, and mdN with the  $K_i$  values in the low micromolar range.<sup>[10]</sup>

The modification of the base moiety by the second phosphonate group gave rise to the bisphosphonate compound (compound **2**, Figure 1A) exhibiting a selective inhibition of mdN.<sup>[11]</sup> Crystal structures of mdN and cdN in complex **2** revealed a different binding mode of the compound in the active site cdN compared to mdN explaining the inhibitory properties.

In this work, we present further development of the bisphosphonate compounds driven by the structural data. By modification of the length and structure of the linker connecting the second phosphonate modification to the base moiety, we fine-tuned the inhibitory properties and selectivity towards mdN and cdN enzymes.

[a] Institute of Organic Chemistry and Biochemistry of the CAS Flemingovo nám. 542/2, 16610 Prague 6, Czech Republic  
E-mail: pavlina.rezacova@uochb.cas.cz  
<http://www.uochb.cz/rezacova>

[b] Institute of Molecular Genetics of the ASCR, v.v.i. Videňská 1083, 14220 Prague 4, Czech Republic

[c] Department of Chemistry of Natural Compounds, UCT Prague Technická 5, 16628 Prague, 6 Czech Republic

Supporting information and ORCID(s) from the author(s) for this article are available on the WWW under <https://doi.org/10.1002/ejoc.201800515>.

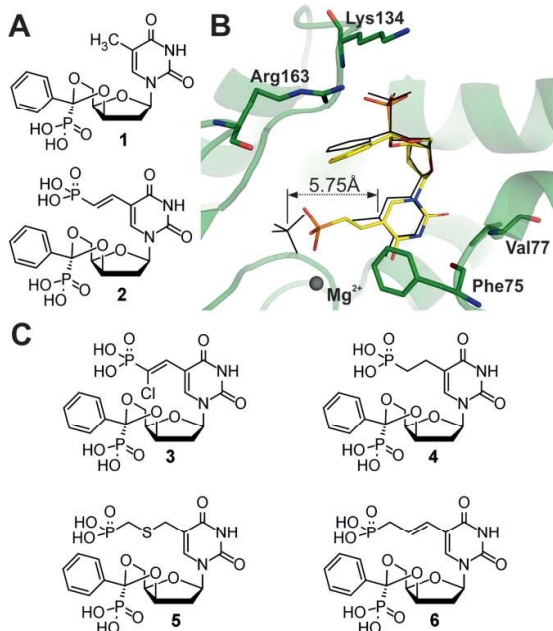


Figure 1. A) Chemical formulas of previously published inhibitors. B) Superposition of crystal structures of mdN in complex with **1** and **2**. Protein is shown in ribbon representation with interacting residues in sticks and magnesium ions as a gray ball. Position of compound **2** (PDB code 4YIH<sup>[11]</sup>) is shown in stick representation with carbon atoms colored yellow, oxygen atoms red, nitrogen blue and phosphorus orange. Position of the phosphate ion (PDB code 1Q91<sup>[3c]</sup>) is shown in black lines. The distance of the phosphorus atom and base atom C5 of compound **1** is shown. C) Chemical formulas of compounds designed in this work.

sulted in compound **2** with significantly better inhibitory properties (Table 1) and the crystal structure provided structural information on compound interaction with the mdN active site (Figure 1B). Superposition of the crystal structure of mdN in complex with **1** and **2** revealed a difference in the position of the phosphonate moiety and phosphate ion whose position was mimicked by the structure-based design. The phosphate ion is more buried in the catalytic site compared to the phosphonate moiety of **2**, the distance between the phosphorus atom positions was 2.24 Å. The aim of this work was to optimize the linker connecting the phosphonate to the base. Taking into account the synthetic feasibility, we designed four compounds differing in length and conformation of the linker (Figure 1C). We used an ethyl moiety to explore the effect of more flexible linker with length similar to that present in **2**. Vinyl linker substituted by halogen atom was chosen to probe effect of electro-negative atom in the linker. Chlorine atom was selected for its size and possibility to form halogen bonds. In addition, two longer linkers with three atoms were designed with allyl and methylthiomethyl group, respectively.

Table 1. Inhibition of cdN and mdN.

Compound	$K_i$ [nM] cdN	$K_i$ [nM] mdN	Selectivity index <sup>[a]</sup>
<b>1</b>	610000 ± 130,000 <sup>[b]</sup>	11600 ± 1600 <sup>[b]</sup>	4.67 <sup>[b]</sup>
<b>2</b>	21700 ± 1,400 <sup>[c]</sup>	128 ± 18 <sup>[c]</sup>	19.98 <sup>[c]</sup>
<b>3</b>	34600 ± 4,300	310 ± 110	9.90
<b>4</b>	2330 ± 270	27.7 ± 2.7	7.46
<b>5</b>	2140 ± 250	68 ± 22	1.86
<b>6</b>	72.0 ± 6.4	15.1 ± 5.6	0.42

[a] The selectivity index  $[(K_i/K_M)_{cdN}/(K_i/K_M)_{mdN}]$  is expressed as a ratio of the  $K_i$  values for the cdN and mdN enzymes normalized to the enzymatic constant  $K_M$  of the individual enzymes [ $(K_M)_{cdN} = 968 \pm 79 \mu\text{M}$ ;  $(K_M)_{mdN} = 86 \pm 14$ ]. [b] Values from<sup>[10]</sup>. [c] Values from<sup>[11]</sup>.

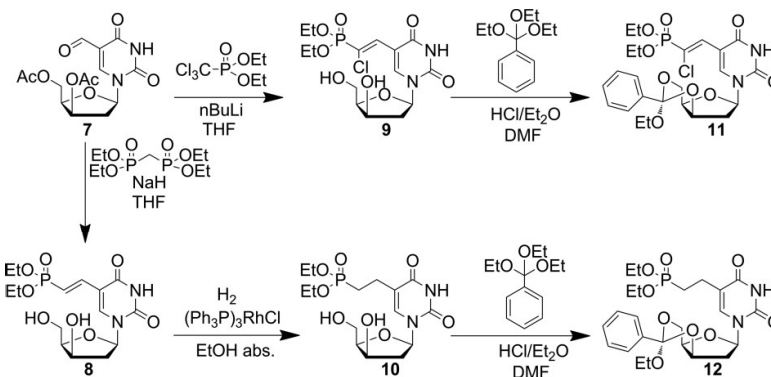
## Results and Discussion

### Design

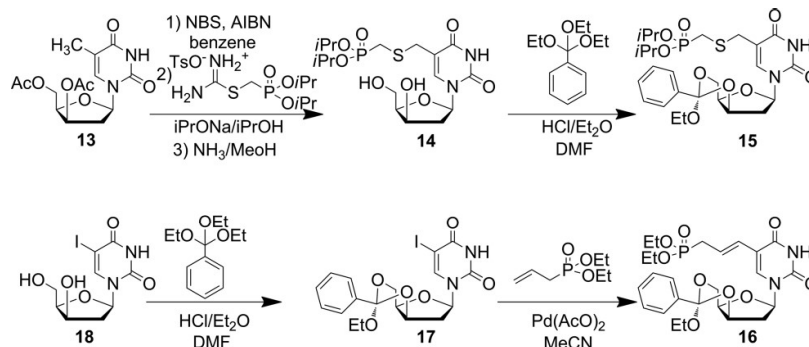
Design of compound **2** was led by the notion that the active site of mdN in complex with **1** has a phosphate ion interacting with catalytic residues and magnesium ion (Figure 1B).<sup>[11]</sup> Attachment of phosphonate group to the base moiety of **1** re-

### Chemistry

The synthesis of the compounds with the two-atom linker started with known aldehyde **7**, which was transformed by the Horner–Wadsworth–Emmons reaction to *E*-vinylphosphonate, and *Z*-vinylchlorodiphosphonate, respectively. The following de-



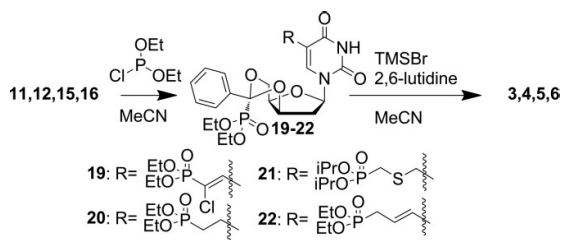
Scheme 1. Synthesis of phosphonates with two-atom linker.



Scheme 2. Synthesis of phosphonates with three-atom linker.

acetylation yielded compounds **8** and **9**. Hydrogenation of **8** by palladium led to the reduction of both double bonds and to the fully saturated derivative. Regioselective catalytic reduction of the vinyl derivative **8** by Wilkinson's catalyst yielded ethyl phosphonate **10**. The acid catalyzed reaction of **9** and **10** with triethyl orthobenzoate yielded orthoesters **11** and **12**, respectively, as an *R* isomer exclusively (Scheme 1).

Preparation of thio derivative **15** started by the radical bromination of xylofuran derivative **13** with NBS. The obtained bromide was rapidly filtered through silica gel and without further purification treated with *S*-(diisopropylphosphonomethyl)isothiouronium tosylate<sup>[12]</sup> to obtain thiophosphonate **14**. Transesterification reaction with triethyl orthobenzoate yielded orthoester **15**, as *R* isomer only (Scheme 2). The allyl phosphonate **16** was prepared by the Heck type reaction of allyl phosphonate and 5-iodo-orthoester **17** obtained from the reaction of 5-iodo-xylofuran<sup>[13]</sup> and triethyl orthobenzoate (Scheme 3).



Scheme 3. Synthesis of deprotected phosphonic acids.

From the reaction of all four orthoesters **11**, **12**, **15**, and **16** with diethyl chlorophosphite four corresponding bisphosphonates **19**, **20**, **21**, and **22** were obtained as single epimers. The deprotection of the phosphonate ester groups was performed with bromotrimethylsilane in acetonitrile in the presence of 2,6-lutidine, providing the desired bisphosphonic acid-containing compounds **3**, **4**, **5**, and **6**.

### Activity Evaluation

Bisphosphonic compounds **3–6** were tested for the *in vitro* inhibitory activity towards recombinant cdN and mdN using a

high-performance liquid chromatography activity assay based on the monitoring of the dUMP substrate depletion (Table 1).<sup>[10]</sup>

Compound **3** with the vinyl linker substituted by chlorine, had  $K_i$  values roughly twofold higher relative to the parent compound **2**. Compound **4**, a reduced form of **2**, showed a significantly higher inhibitory effect towards both enzymes (five times towards mdN, ten times towards cdN). Compound **5** with a linker containing additional sulfur atom exhibited improvement of inhibitory properties towards cdN similar to **4** (about 10-fold decrease in  $K_i$  value), inhibition of mdN improved about two times compared to the parent compound **3**.

Compound **6**, containing a linker extended by one carbon atom exhibited the largest improvement in inhibitory properties, particularly towards cdN.  $K_i$  values for both enzymes fell to a nanomolar range and compound **6** exhibited a higher specificity for cdN.

### Structure Evaluation

To obtain structural information on interaction of the inhibitors, compounds **4–6** were co-crystallized with mdN and co-crystals of cdN with **6** were also obtained. The crystals diffracted to high resolution and crystal structures were refined using data to the resolution of 1.37 to 1.85 Å. The mdN crystals exhibited  $P4_32_1$  symmetry and contained one molecule in the asymmetric unit, whereas the cdN crystal belonged to  $P1$  space group and contained two enzyme molecules in the unit cell. In all crystal structures, the compounds were modelled to a well-defined electron density maps with full occupancy (Figure 2). In the active site of mitochondrial enzyme compounds **4–6** acquired a pose similar to those of **1** and **2** (PDB codes 1Q91 and 4YIK<sup>[3c,11]</sup>). Matching parts of the inhibitors, i.e. phenyl ring, neighboring phosphonate group, and sugar mimicking double ring, did not show any significant differences in their conformation. RMSD for superposition of 19 corresponding atoms of **2** and **4–6**, respectively, did not exceed 0.37 Å. Polar interactions observed between **2** and mdN were also preserved for **4–6**: main-chain of Lys134 and side-chain of Arg163 interacted with the first phosphonate group and main-chain of Phe75 and Val77 interacted with the base moiety (Figure 2). As expected, variation in posi-



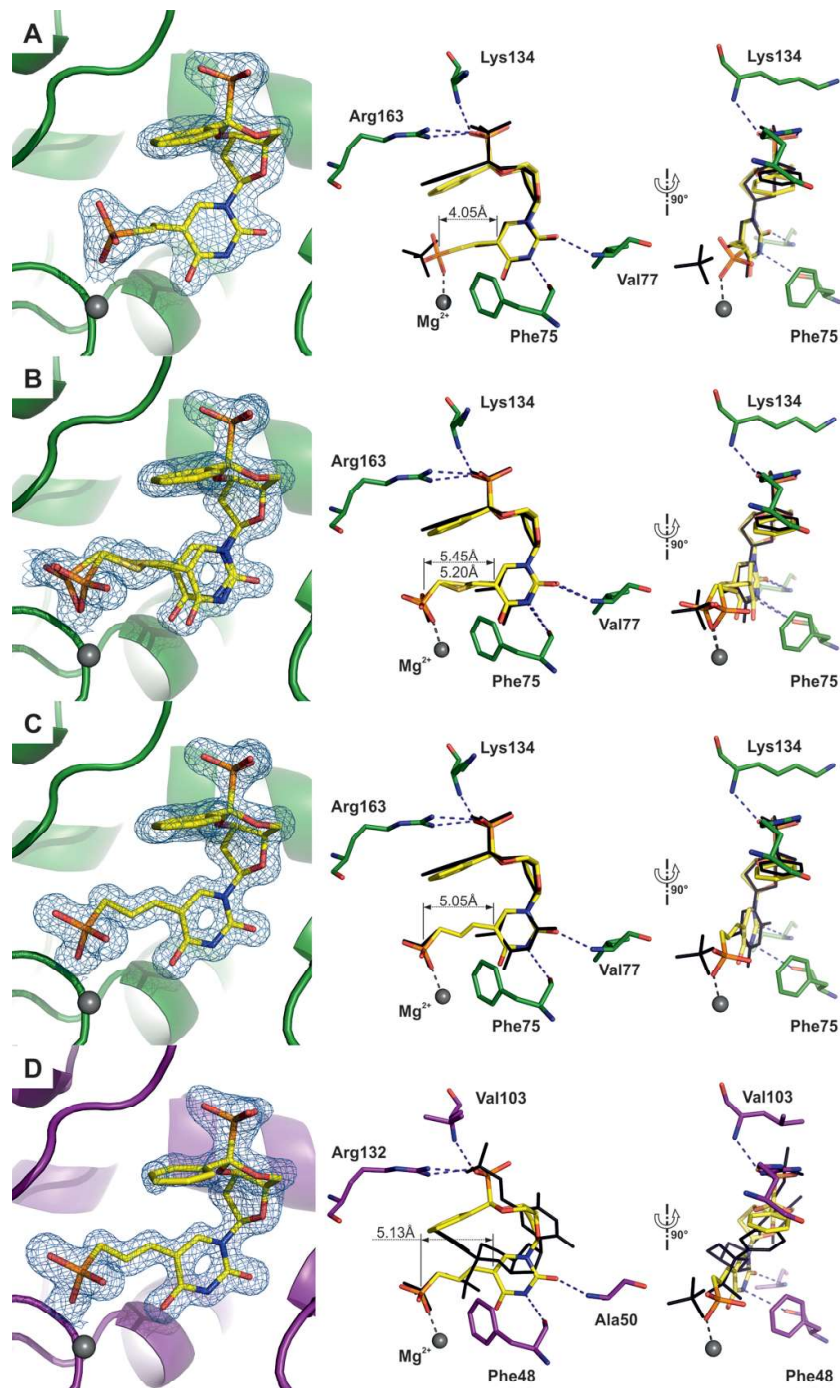


Figure 2. Structures of mdN in complex with compound **4** (A), **5** (B), and **6** (C) and cdN in complex with **6** (D). In panel A–C, binding pose of **1** is indicated as black line (PDB code 1Q91). In panel D, the black line represents the position of **2** in complex with cdN (PDB code 4YIH). Compounds **4**, **5**, **6** and interacting residues are shown as sticks. Potential direct hydrogen bonds are represented as blue dashed lines. Coordinate covalent bonds are shown as grey dashed lines. Carbon atoms are colored yellow, green (mdN) or purple (cdN); oxygen atoms are colored red, nitrogen blue, and phosphorus orange. Magnesium ion is presented as grey ball. All  $2F_o - F_c$  electron density maps are contoured at  $1.5\sigma$ . The distance of the phosphorus atom and base atom C5 is shown for every compound.



tion of the second phosphonate moiety was observed for different compounds depending on the linker properties.

Compound **4** showed the same position of the phosphonate group as compound **2** (RMSD of phosphate atom and corresponding oxygen atoms was 0.36 Å), however, a small difference was observed in the position of the linker and a slight shift of the base of inhibitor, perhaps due to the flexibility of the reduced linker.

Compound **5** with a linker extended by a sulfur atom, showed two alternative conformations of the phosphonate moiety. At one conformation, modelled with occupancy 0.3, the phosphonate group mimicked the position of the phosphate anion in the structure of mdN in complex with **1** (Figure 3A). The distance between the two phosphorus atoms was 0.54 Å. Interestingly, the phosphonate moiety was in the favorable position to make interactions with enzyme residues, which were not observed for compound **2**. In addition to the coordination of magnesium ion, the phosphonate group is available for hydrogen bond interactions with catalytic residue Asp43 and to residues Thr130, Ser131 and Lys165. Additional polar contacts of the phosphonate group with aspartates 175 and 176 were mediated through water molecules (Figure 3A). Second alternative conformation, modelled with occupancy 0.7, positioned the phosphonate group 1.25 Å away from the minor conformation with no change in position of oxygen coordinating magnesium ion (Figure 3B). This change resulted in a movement of the base moiety, with RMSD for 15 atoms with alternative positions was 0.91 Å. In this position, phosphonate was available for polar interactions with Asp41, Ser131 and Lys165. Four additional interactions were maintained via water mediated hydrogen bonds (Figure 3B). No polar interaction of sulfur atom with enzyme active site was observed.

The phosphonate group in compound **6** has a single binding pose in the mdN active site corresponding to the major alternative pose of **5**. The phosphonate group in this position established the same interactions described above for **5** (Figure 3B). Very similar pose and interactions of phosphonate moiety was also found in cdN co-crystal structure: direct hydrogen bonds were formed by carbonyl oxygen of Asp14, hydroxyl from Ser104 and amino group of Lys138 (different numbering in mdN and cdN structures stems from the presence of a 31 amino acid residues long signal peptide in mdN). Overall RMSD for **6** when bound to cdN or mdN was 0.35 Å, reflecting a high similarity in binding pose in both enzyme active sites. In addition, the interactions of **6** with cdN were analogous to those with mdN: the phosphonate moiety formed one hydrogen bond with backbone amide of Val103 and two hydrogen bonds with the guanidine group of Arg134. The inhibitor base interacts with Phe48 carbonyl oxygen and nitrogen from Ala50 (Figure 2D).

The binding of **6** to cdN and mdN though the same binding mode was a surprising observation. The co-crystal structure of cdN with **2** previously showed an alternative binding mode, in which the phosphonate moiety attached to the base pointed away from the catalytic site (Figure 2D). The extended linker between the base and phosphonate in **6** apparently allowed this phosphonate group to reach and form an interaction with

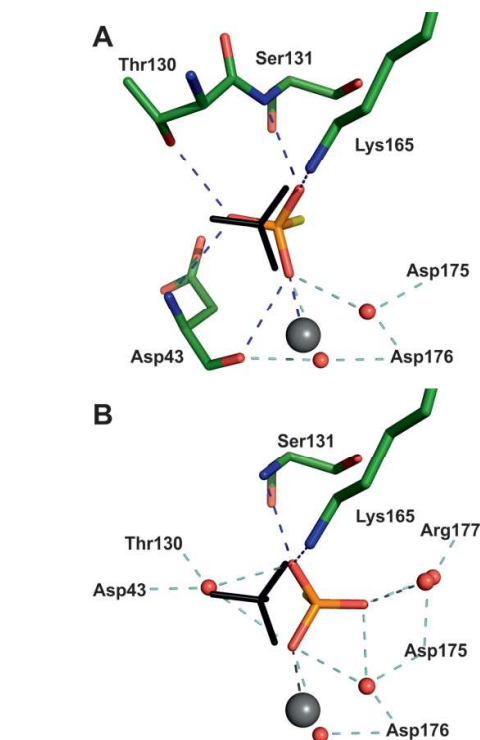


Figure 3. Detail of two phosphonate binding positions (A – less favoured, B – more favoured) of compound **5** in complex with mdN superposed with phosphate anion from structure 1Q91<sup>[34]</sup> (black solid line). Carbon atoms are coloured yellow (inhibitor) and green (mdN); oxygen atoms are coloured red, nitrogen blue, and phosphorus orange. Magnesium ion is presented as a grey ball. Waters involved into water mediated hydrogen contacts are shown as red balls. Stick model shows only residues available for direct hydrogen bonds, potential polar interactions are indicated as dashed lines, direct hydrogen bonds in blue, water mediated hydrogen bonds in cyan and coordinate covalent bonds in grey.

the catalytic site of cdN leading to an alternative inhibitor binding. This altered binding mode explains the significantly better inhibition of cdN by **6** when compared to **2**.

## Conclusions

By using a structure-based approach, we designed nucleoside derivatives targeting active sites of human cdN and mdN. Four novel bisphosphonate nucleoside derivatives targeting the position of the phosphate ion, product bound to the catalytic site, were prepared and their inhibitory properties were evaluated by using an in vitro assay. The length of the linker between the base and secondary phosphonate group proved to be crucial for efficient inhibition of enzyme activity and crystal structures provided a structural basis for understanding the structure activity relationship. Addition of a halogen substituent onto the two-atom linker (compound **3**) did not improve the inhibitory property; the  $K_i$  values were higher than those of the parent compound (Table 1). In compound **4**, we extended the length

and flexibility of the two-atom linker by reduction of a double bond. A phosphonate moiety was able to form a coordinate covalent bond with the magnesium ion in mdN, however the position was different from that of the phosphate ion (Figure 2A). Further extension of the linker containing two carbon atoms and one sulfur atom (compound **5**) allowed the phosphonate moiety to reach the ideal position for magnesium ion coordination, however the linker was too long and this resulted in shift of the inhibitor base moiety (Figure 2B). Compound **6**, with a three-carbon-atom linker, showed inhibition of both enzymes in the nanomolar range, making it the most potent inhibitor of these enzymes reported to date. X-ray analysis revealed that the phosphonate moiety occupied a novel position, which is favorable for coordination of magnesium ions and does not significantly change the position of the inhibitor base (Figure 2C). Unlike the parent compound **2**, the same binding pose was observed for mdN and cdN enzymes for **6** (Figure 2D). This altered binding mode elucidates the significantly better inhibition of cdN by **6**, that resulted in selectivity of this compound to cdN over mdN (Table 1).

Structural information on interactions with mdN and cdN active sites explained the inhibition profile and can be utilized in future inhibitor design efforts.

## Experimental Section

### Chemistry

**General Procedures:** Unless otherwise stated, all used solvents were anhydrous. TLC was performed on TLC plates pre-coated with silica gel (silica gel/TLC-cards, UV 254, Merck) using the following mobile phases: C-1 (chloroform-ethanol 9:1), T-1 (toluene-acetone 1:1), H-3 (ethyl acetate/acetone/ethanol/water 6:1:1:0.5) IPAV (2-propanol-25 % ammonia/water, 7:1:2). Compounds were detected using UV light (254 nm), spraying with a 1 % solution of 4-(4-nitrobenzyl) pyridine in ethanol followed by heating and treating with gaseous ammonia (for the detection of alkylating agents, such as halogen derivatives and phosphonic acid diesters; blue color). The purity of the final compounds was greater than 95 % as determined by LC-MS using a Waters AutoPurification System with 2545 Quaternary Gradient Module and 3100 Single Quadrupole Mass Detector using Luna C18 column (100 × 4.6 mm, 3 μm, Phenomenex) at a flow rate of 1 mL/min. The A, B, and C mobile phases were used representing 50 mM NH<sub>4</sub>HCO<sub>3</sub>, 50 mM NH<sub>4</sub>HCO<sub>3</sub> in aq. 50 % CH<sub>3</sub>CN, and CH<sub>3</sub>CN, respectively (A→B over 10 min, B→C over 10 min, and C for 5 min). Preparative RP HPLC was performed on an LC5000 Liquid Chromatograph (INGOS-PIKRON, CR) using a Luna C18 (2) column (Axia 250 × 21.2 mm, 5 μm, Phenomenex) at a flow rate of 10 mL/min. A gradient elution of methanol in 0.1 M TEAB (pH 7.5) (A, 0.1 M TEAB; B, 0.1 M TEAB in aq. 50 % methanol; C, methanol) was used. All final compounds were lyophilized. The mass spectra were collected on an LTQ Orbitrap XL (Thermo Fisher Scientific) using ESI ionization. The phosphorus content in the compounds was determined using a simultaneous energy-dispersive X-ray fluorescence spectrometer SPECTRO iQ II. NMR spectra were collected in [D<sub>6</sub>]DMSO or D<sub>2</sub>O on a Bruker AVANCE 600 (<sup>1</sup>H at 600.13 MHz, <sup>13</sup>C at 150.9 MHz). Chemical shifts (in ppm, δ scale) were referenced to the residual [D<sub>6</sub>]DMSO signal (δ = 2.5 ppm for <sup>1</sup>H and 39.7 ppm for <sup>13</sup>C) or to the 1,4-dioxane signal (δ = 3.75 ppm for <sup>1</sup>H and 69.3 ppm for <sup>13</sup>C) as an internal standard in D<sub>2</sub>O. Coupling constants (*J*) are given in Hz. The complete assignment of <sup>1</sup>H

and <sup>13</sup>C signals was performed by an analysis of the correlated homonuclear H,H-COSY and heteronuclear H,C-HSQC and H,C-HMBC spectra. The relative configuration of the compounds was checked using 2D-H,H-ROESY experiments. The numbering for signal assignment is shown below. UV/Vis spectra were collected on spectrophotometer CARY 100 Bio UV Spectrophotometer (Varian Inc.), samples were dissolved in 50 % MeOH. The purity of the final compounds was greater than 95 %. The <sup>1</sup>H NMR and <sup>13</sup>C NMR spectroscopic data of all prepared compounds are in Supporting information in Table S1 and Table S2, respectively.

### Method A

**Preparation of Nucleoside Orthoesters:** A solution of chlorovinylphosphonate **9** (dried by co-evaporation with DMF) and triethyl orthobenzoate (2–3 equiv.) in dry DMF (0.1 M solution) was carefully acidified with the 10M HCl in dry Et<sub>2</sub>O (slightly red color on a wet pH paper), and the mixture was stirred under an argon atmosphere at room temp. for 12 h (TLC in H-3). The reaction was quenched by the addition of Et<sub>3</sub>N and then Amberlyst A21 was added, the suspension was filtered and concentrated under reduced pressure. The resulting crude nucleoside orthoester **11** was purified on a silica gel column by elution with a linear gradient of CHCl<sub>3</sub> in toluene (0→100 %) followed by EtOH in CHCl<sub>3</sub> (0→10 %).

### Method B Preparation of nucleoside diethyl phosphonates

Orthoester **11** dried by co-evaporation with acetonitrile was treated with diethyl chlorophosphite (2 equiv.) in dry acetonitrile (0.05 M solution) in argon atmosphere at –40 °C. The heterogeneous mixture was stirred under slowly increased temperature to 0 °C (TLC in T-1). When finished, the reaction mixture was cooled to –40 °C and 1 M TEAB in 50 % EtOH was added and the solution was concentrated in vacuo. The obtained crude phosphonate **19** was purified by silica gel chromatography with a linear gradient of EtOH in CHCl<sub>3</sub> (0→10 %).

### Method C

**Preparation of Nucleoside Bisphosphonic Acids:** Diethyl phosphonate **19** dried by co-evaporation with MeCN was treated under an argon atmosphere with bromotrimethylsilane (15 equiv.) and 2,6-lutidine (6 equiv.) in dry MeCN (0.05 M solution) at room temp. overnight (TLC IPAV). When finished, the reaction was concentrated in vacuo, the residue was treated shortly with 2M TEAB and the obtained solution was evaporated to dryness. The residue was co-evaporated with EtOH and purified by the preparative HPLC on the C18 column using a linear gradient of methanol in 0.1M TEAB buffer. The product was converted into the sodium salt on Dowex 50 in Na<sup>+</sup> form.

**Diethyl Z-2-[1-(2-Deoxy-β-D-threo-pentofuranosyl)uracil-5-yl]-chlorovinylphosphonate (**9**):** Diethyl trichloromethylphosphonate (1.64 mL, 8.82 mmol) was dissolved in dry THF (30 mL) and the solution was cooled under argon atmosphere to –80 °C. Then 1.6M *n*BuLi in hexane (5.6 mL, 9 mmol) was added and the reaction mixture was stirred 1 h. After then the solution of aldehyde **5** (1 g, 2.94 mmol) in dry THF (10 mL) (before reaction was dried by co-evaporation with dry THF) was added. The resulting mixture was slowly warmed to room temp. and then stirred for 24 h. The progress of reaction was monitored by TLC C-1. When finished, the reaction mixture was poured on silica gel column and chromatographed with a linear gradient of EtOH in CHCl<sub>3</sub> (0→10 %) to give a mixture of partially deacetylated products. This mixture was treated with 0.1M MeONa in dry MeOH (20 mL) whilst stirring overnight and then neutralized by the addition of solid DOWEX 50 in H<sup>+</sup> cycle. Filtration and evaporation of the solution provided desired chlorovinylphosphonate **9** (306 mg, 24 % over two steps) and *E*-

isomer (96 mg, 8% over two steps). HRMS [M + H]<sup>+</sup> for C<sub>15</sub>H<sub>23</sub>O<sub>8</sub>N<sub>2</sub>ClP: calcd. *m/z* 425.08751, obs. 425.08758. IR (KBr):  $\tilde{\nu}$  = 3422, 3059, 2986, 1715, 1694, 1612, 1466, 1441, 1404, 1395, 1370, 1284, 1238, 1164, 1101, 1090, 1052, 1022, 987, 815, 794, 779, 760 cm<sup>-1</sup>.

**Diethyl 2-[1-(2-Deoxy-β-D-threo-pentofuranosyl)uracil-5-yl]ethylphosphonate (10):** To the solution of vinylphosphonate **8** (400 mg, 1 mmol) in absolute ethanol (20 mL) was added Wilkinson's catalyst (40 mg, 0.044 mmol). Reaction was stirred under hydrogen atmosphere (0.1 MPa) overnight. The progress of reaction was monitored by LCMS. Reaction mixture was then evaporated and chromatographed through silica gel column with a linear gradient of H-3 in EtOAc to give diethyl phosphonate **10** (356 mg, 89%) as light-yellow oil. HRMS [M + Na]<sup>+</sup> for C<sub>15</sub>H<sub>25</sub>O<sub>8</sub>N<sub>2</sub>Na: calcd. *m/z* 415.12407, obs. 415.12395; IR (KBr):  $\tilde{\nu}$  = 3424, 3062, 2985, 2932, 1705, 1689, 1470, 1443, 1408, 1394, 1370, 1278, 1219, 1165, 1105, 1090, 1054, 1028, 971, 794, 779, 761 cm<sup>-1</sup>.

**Diethyl Z-2-[1-(2-Deoxy-3,5-O-ethoxybenzylidene-β-D-threo-pentofuranosyl)uracil-5-yl]chlorovinylphosphonate (11):** Orthoester **11** was prepared from chlorovinylphosphonate **9** (380 mg, 0.9 mmol) using Method A as colorless oil (394 mg, 79%). HRMS [M + H]<sup>+</sup> for C<sub>24</sub>H<sub>31</sub>O<sub>9</sub>N<sub>2</sub>ClP: calcd. *m/z* 557.14502, obs. 557.14504. IR (CHCl<sub>3</sub>):  $\tilde{\nu}$  = 3389, 3174, 2984, 1710, 1689, 1612, 1494, 1454, 1450, 1434, 1402, 1394, 1369, 1307, 1297, 1280, 1243, 1160, 1129, 1108, 1098, 1084, 1058, 1024, 988, 910, 701, 611 cm<sup>-1</sup>.

**Diethyl 2-[1-(2-Deoxy-3,5-O-ethoxybenzylidene-β-D-threo-pentofuranosyl)uracil-5-yl]ethylphosphonate (12):** Orthoester **12** was prepared from diethyl phosphonate **10** (356 mg, 0.9 mmol) using Method A as colorless oil (388 mg, 82%). HRMS [M + Na]<sup>+</sup> for C<sub>24</sub>H<sub>33</sub>O<sub>9</sub>N<sub>2</sub>NaP: calcd. *m/z* 547.18159, obs. 547.18154. IR (CHCl<sub>3</sub>):  $\tilde{\nu}$  = 3395, 3172, 3093, 3067, 2989, 1703, 1684, 1641, 1603, 1494, 1467, 1452, 1435, 1406, 1393, 1369, 1360, 1306, 1299, 1273, 1241, 1163, 1138, 1098, 1059, 1033, 970, 701, 615 cm<sup>-1</sup>.

**Diisopropyl 2-[1-(2-Deoxy-β-D-threo-pentofuranosyl)uracil-5-yl]methylthiomethylphosphonate (14):** To the refluxing solution of *xyloD* **13** (660 mg, 2 mmol) in benzene (30 mL) was added NBS (430 mg, 2.4 mmol) and simultaneously AIBN (40 mg, 0.24 mmol). Reaction mixture was stirred under reflux for additional 3 h. The progress of reaction was monitored by TLC T-1. When finished, the reaction mixture was rapidly filtered through silica gel column (elution 20% acetone/toluene). After evaporation of solvents crude bromide was used without further purification in next step.

To a dry isopropyl alcohol (45 mL) was added under argon atmosphere NaH (60% suspension in mineral oil) (720 mg, 18 mmol). Dense suspension appeared in the reaction mixture. After 1 h *S*-(diisopropylphosphonomethyl)isothiuronium tosylate (3.838 g, 9 mmol) was added to the reaction mixture. Previously prepared bromide was added after next 30 min. Stirring was continued overnight and the progress of reaction was monitored by TLC T-1. Reaction was neutralized by DOWEX 50 in H<sup>+</sup> cycle, filtered and washed with MeOH. Solvents were evaporated, the residue was dissolved in CHCl<sub>3</sub> and filtered through Celite.

The filtrate was evaporated and was dissolved in MeOH saturated by NH<sub>3</sub> and stirred overnight. Reaction was evaporated and poured on silica gel column and chromatographed with a linear gradient of H-3 in EtOAc (0→80%) to give methylthiomethylphosphonate **14** (389 mg, 42% over three steps) as colorless oil. HRMS [M + H]<sup>+</sup> for C<sub>17</sub>H<sub>30</sub>O<sub>8</sub>N<sub>2</sub>PS: calcd. *m/z* 453.14550, obs. 453.14550. IR (CHCl<sub>3</sub>):  $\tilde{\nu}$  = 3616, 3536, 3505, 3392, 3302, 2984, 2877, 2822, 1706, 1685, 1467, 1436, 1415, 1404, 1388, 1377, 1358, 1275, 1257, 1231, 1180, 1143, 1106, 1065, 1047, 1015, 1000, 890 cm<sup>-1</sup>.

**Diisopropyl 3-[1-(2-Deoxy-3,5-O-ethoxybenzylidene-β-D-threo-pentofuranosyl)uracil-5-yl]methylthiomethylphosphonate (15):** Orthoester **15** was prepared from methylthiomethylphosphonate **14** (380 mg, 0.84 mmol) using Method A as colorless oil (427 mg, 87%). HRMS [M + H]<sup>+</sup> for C<sub>26</sub>H<sub>38</sub>O<sub>9</sub>N<sub>2</sub>PS: calcd. *m/z* 585.20301, obs. 585.20304. IR (CHCl<sub>3</sub>):  $\tilde{\nu}$  = 3394, 3172, 3063, 2983, 2876, 1706, 1686, 1638, 1603, 1493, 1466, 1452, 1435, 1407, 1387, 1376, 1305, 1277, 1255, 1241, 1178, 1143, 1129, 1105, 1082, 1060, 1034, 1009, 995, 914, 889, 702, 615 cm<sup>-1</sup>.

**Diethyl 3-[1-(2-Deoxy-3,5-O-ethoxybenzylidene-β-D-threo-pentofuranosyl)uracil-5-yl]allylphosphonate (16):** To the mixture of orthoester **17** (486 mg, 1 mmol) and diethyl allylphosphonate (1.47 g, 8 mmol) in dry MeCN (10 mL) was added Pd(OAc)<sub>2</sub> (460 mg, 2 mmol) and few drops of dry Et<sub>3</sub>N (green color on wet pH paper). Reaction mixture was heated to 70 °C for 24 h. The progress of reaction was monitored by TLC T-1. When finished, reaction mixture was filtered through Celite and washed by MeCN. The filtrate was evaporated and poured on silica gel column and chromatographed with a linear gradient of EtOH in CHCl<sub>3</sub> (0→10%) to give allylphosphonate **16** (318 mg, 59%) as light-yellow oil. HRMS [M + H]<sup>+</sup> for C<sub>25</sub>H<sub>34</sub>O<sub>9</sub>N<sub>2</sub>P: calcd. *m/z* 537.19964, obs. 537.19967. IR (CHCl<sub>3</sub>):  $\tilde{\nu}$  = 3394, 3175, 3093, 3063, 3026, 1705, 1688, 1619, 1495, 1465, 1452, 1435, 1393, 1368, 1251, 1241, 1162, 1134, 1119, 1100, 1080, 1059, 1031, 982, 970, 701, 615 cm<sup>-1</sup>.

**1-[2-Deoxy-3,5-O-Ethoxybenzylidene-β-D-threo-pentofuranosyl-5-iodo-uracil (17):** Orthoester **17** was prepared from 5-iodoxyloD **18** (450 mg, 1.3 mmol) using Method A as colorless oil (500 mg, 81%). HRMS [M + Na]<sup>+</sup> for C<sub>18</sub>H<sub>19</sub>O<sub>6</sub>N<sub>2</sub>Ia: calcd. *m/z* 509.01800, obs. 509.01824. IR (CHCl<sub>3</sub>):  $\tilde{\nu}$  = 3385, 3175, 3092, 3063, 2981, 2945, 1706, 1604, 1492, 1451, 1432, 1405, 1392, 1367, 1320, 1296, 1272, 1240, 1196, 1140, 1102, 1081, 1032, 914, 701, 609 cm<sup>-1</sup>.

**Diethyl Z-2-[1-(2-Deoxy-3,5-O-diethylphosphonobenzylidene-β-D-threo-pentofuranosyl)uracil-5-yl]chlorovinylphosphonate (19):** Compound **19** was prepared from orthoester **11** (300 mg, 0.54 mmol) using Method B as colorless oil in a yield of 248 mg (71%). HRMS [M + Na]<sup>+</sup> for C<sub>26</sub>H<sub>35</sub>O<sub>11</sub>N<sub>2</sub>ClNaP<sub>2</sub>: calcd. *m/z* 671.12968, obs. 671.12959. IR (CHCl<sub>3</sub>):  $\tilde{\nu}$  = 3390, 3168, 3001, 2985, 1707, 1689, 1612, 1494, 1457, 1453, 1434, 1394, 1369, 1316, 1300, 1280, 1276, 1243, 1162, 1131, 1097, 1075, 1053, 1035, 976, 913, 697, 620, 611 cm<sup>-1</sup>.

**Diethyl 2-[1-(2-Deoxy-3,5-O-diethylphosphonobenzylidene-β-D-threo-pentofuranosyl)uracil-5-yl]ethylphosphonate (20):** Compound **20** was prepared from orthoester **12** (350 mg, 0.67 mmol) using Method B as colorless oil in a yield of 382 mg (93%). HRMS [M + Na]<sup>+</sup> for C<sub>26</sub>H<sub>38</sub>O<sub>11</sub>N<sub>2</sub>NaP<sub>2</sub>: calcd. *m/z* 639.18430, obs. 639.18402. IR (CHCl<sub>3</sub>):  $\tilde{\nu}$  = 3395, 3170, 3094, 3069, 1699, 1628, 1493, 1467, 1451, 1433, 1406, 1392, 1369, 1314, 1300, 1270, 1242, 1193, 1163, 1138, 1097, 1080, 1059, 1035, 974, 913, 697, 616, 553 cm<sup>-1</sup>.

**Diisopropyl 2-[1-(2-Deoxy-3,5-O-diethylphosphonobenzylidene-β-D-threo-pentofuranosyl)uracil-5-yl]methylthiomethylphosphonate (21):** Compound **21** was prepared from orthoester **15** (427 mg, 0.73 mmol) using Method B as colorless oil in a yield of 355 mg (72%). HRMS [M + H]<sup>+</sup> for C<sub>28</sub>H<sub>43</sub>O<sub>11</sub>N<sub>2</sub>P<sub>2</sub>S: calcd. *m/z* 677.20573, obs. 677.20568. IR (CHCl<sub>3</sub>):  $\tilde{\nu}$  = 3394, 3169, 3088, 3062, 2998, 2985, 2876, 1702, 1686, 1639, 1603, 1495, 1466, 1451, 1434, 1404, 1387, 1376, 1350, 1314, 1299, 1273, 1242, 1179, 1163, 1142, 1130, 1103, 1085, 1080, 1060, 1052, 1025, 1013, 993, 914, 889, 697, 616 cm<sup>-1</sup>.

**Diethyl 2-[1-(2-Deoxy-3,5-O-diethylphosphonobenzylidene-β-D-threo-pentofuranosyl)uracil-5-yl]allylphosphonate (22):** Com-



Compound **22** was prepared from orthoester **16** (300 mg, 0.56 mmol) using Method B as colorless oil in a yield of 260 mg (74 %). HRMS  $[M + H]^+$  for  $C_{27}H_{39}O_{11}N_2P_2$ : calcd.  $m/z$  629.20236, obs. 629.20235. IR (CHCl<sub>3</sub>):  $\tilde{\nu}$  = 3394, 3169, 3092, 3062, 2996, 1701, 1688, 1616, 1494, 1466, 1452, 1434, 1405, 1393, 1369, 1315, 1298, 1273, 1242, 1163, 1134, 1097, 1082, 1052, 1035, 971, 914, 698, 617 cm<sup>-1</sup>.

**Z-2-[1-(2-Deoxy-3,5-O-phosphonobenzylidene-β-D-threo-pentofuranosyl)uracil-5-yl]chlorovinylphosphonic Acid (3):** Compound **3** was prepared from diethyl phosphonate **19** (53 mg, 82 μmol) using Method C as colorless oil in a yield of 12 mg (27 %). HRMS  $[M + Na]^+$  for  $C_{18}H_{17}O_{11}N_2ClNaP_2$ : calcd.  $m/z$  556.98993, obs. 556.99005. IR (KBr):  $\tilde{\nu}$  = 3435, 1695, 1639, 1471, 1449, 1409, 1312, 1285, 1134, 1074, 963, 703, 554 cm<sup>-1</sup>.

**2-[1-(2-Deoxy-3,5-O-phosphonobenzylidene-β-D-threo-pentofuranosyl)uracil-5-yl]ethylphosphonic Acid (4):** Compound **4** was prepared from diethyl phosphonate **20** (84 mg, 140 μmol) using Method C as colorless oil in a yield of 20 mg (29 %). HRMS  $(M - H)^-$  for  $C_{18}H_{21}O_{11}N_2P_2$ : calcd.  $m/z$  503.06261, obs. 503.06233. IR (KBr):  $\tilde{\nu}$  = 3434, 3065, 2958, 1690, 1603, 1493, 1477, 1448, 1313, 1280, 1258, 1221, 1138, 1071, 977, 947, 702, 575, 499 cm<sup>-1</sup>.

**2-[1-(2-Deoxy-3,5-O-phosphonobenzylidene-β-D-threo-pentofuranosyl)uracil-5-yl]methylthiomethylphosphonic Acid (5):** Compound **5** was prepared from diisopropyl phosphonate **21** (53 mg, 78 μmol) using Method C as colorless oil in a yield of 28 mg (67 %). HRMS  $[M + Na]^+$  for  $C_{18}H_{20}O_{11}N_2NaP_2S$ : calcd.  $m/z$  557.01662, obs. 557.01554. IR (KBr):  $\tilde{\nu}$  = 3435, 3060, 2812, 1687, 1605, 1478, 1448, 1433, 1413, 1313, 1301, 1282, 1257, 1136, 1066, 1034, 972, 699 cm<sup>-1</sup>.

**2-[1-(2-Deoxy-3,5-O-phosphonobenzylidene-β-D-threo-pentofuranosyl)uracil-5-yl]allylphosphonic Acid (6):** Compound **6** was prepared from diethyl phosphonate **22** (80 mg, 130 μmol) using Method C as colorless oil in a yield of 15 mg (23 %). HRMS  $(M - H)^-$  for  $C_{19}H_{21}O_{11}N_2P_2$ : calcd.  $m/z$  515.06261, obs. 515.06275. IR (KBr):  $\tilde{\nu}$  = 3439, 3062, 2925, 1636, 1603, 1472, 1409, 1313, 1281, 1136, 1074, 974, 700, 690, 553 cm<sup>-1</sup>.

**Protein Preparation:** Both enzymes were prepared using the recombinant expression in *E. coli* and purified as described previously.<sup>[10,14]</sup>

**Activity Assay:** Enzyme activity was determined by high-performance liquid chromatography with spectrophotometric detection of dUMP substrate and dU product at 262 nm. Typically, 2–4 nM enzyme in 20 mM Tris-HCl, 20 mM MgCl<sub>2</sub>, 2 mM EDTA and 2 mM DTT, pH 7.5, was treated with dUMP at a concentration comparable to enzyme  $K_M$  value (1 mM and 100 μM for cdN and mdN, respectively) for 6 min at 37 °C in a final volume of 100 μL. The reaction was stopped by the addition of 3 μL of 30 % (v/v) TCA and 5 μL of a reaction mixture was applied to a Zorbax C18 column (150 mm×3 mm, 2.5 μm particle size, Agilent) mounted to an Agilent 1100 system. The separation was done using isocratic elution in 75 mM KH<sub>2</sub>PO<sub>4</sub> buffer. After each run, the column was washed with 100 % methanol supplemented with 0.05 % (v/v) TFA. None of the reactions reached more than 10 % of the substrate conversion.

**Inhibition Assay:** To determine the  $K_i$  values, a series of activity assays were performed in the presence of compounds **3**, **4**, **5**, and **6**. The concentration of inhibitors in the reaction mixture was adjusted to fit a range of relative enzyme activity between 0.03 and 1. For each compound, the reaction mixtures with 11 different inhibitor concentrations were analyzed in triplicates. To estimate the apparent  $K_i$  value, the initial velocities of the inhibited reactions at varying inhibitor concentrations were fitted using the Williams–

Morrison equation.<sup>[15]</sup> The true  $K_i$  value was then calculated presuming the competitive type of inhibition. To compare the selectivity of the inhibitors toward mdN and cdN, we introduced a selectivity index (SI), defined as the ratio of  $K_i$  values normalized by the appropriate enzymatic constant  $K_M$ , which was determined experimentally (86 ± 14 μM for mdN and 968 ± 79 μM for cdN). The smaller the SI (<1) was, the higher selectivity of the inhibitor for mdN was, and the higher the SI (>1) was, the higher the selectivity for cdN was.

**Crystallization:** The crystals of mdN for soaking were obtained using the hanging drop vapor diffusion technique with a precipitating solution containing 20 mM KH<sub>2</sub>PO<sub>4</sub>, PEG 8000 8 % (w/v), glycerol 10 % (v/v) whereas nuclei from similar drop were transferred using a streak seeding technique with the cat whisker.<sup>[16]</sup> The crystals grew to a final size within three days. The crystals of mdN complexed with compounds **4** and **5** were obtained by soaking for 12 h in 1 μL crystallization drop supplemented with 1 mM compound and 90 mM MgCl<sub>2</sub> solution. Crystals were flash-cooled without additional cryoprotection.

The crystal of mdN complexed with compound **6** were obtained from crystallization screen JCSG+ from Molecular Dimension by mixing 200 nL of crystallization condition A7 with protein solution containing mdN in concentration 20 g L<sup>-1</sup>, 20 mM Tris buffer pH 8.0, 20 mM MgCl<sub>2</sub>, 10 % glycerol (v/v), 3 % (v/v) β-mercaptoethanol, 1 mM EDTA, and compound **6** in 1 mM concentration. Crystal appeared in 6 d and was harvested after 30 d. For cryoprotection, the crystals were soaked for 10 s in a reservoir solution supplemented with 30 % (v/v) glycerol.

The crystal of cdN in complex with compound **6** were obtained using crystallization screen Morpheus (Molecular Dimensions Limited) by mixing 200 nL of crystallization condition H2 with protein solution containing cdN in concentration 20 g L<sup>-1</sup>, 20 mM Tris buffer pH 8.0, 20 mM MgCl<sub>2</sub>, 10 % glycerol (v/v), 3 % (v/v) β-mercaptoethanol, 1 mM EDTA, and compound **6** in 1 mM concentration. Crystal appeared in 20 d and was harvested after 90 d. Crystal was flash-cooled without any additional cryoprotection by plunging into liquid nitrogen.

**Data Collection and Structure Determination:** The diffraction data for crystal of mdN soaked with compound **4** were collected at 100 K at in house rotating anode MicroMax 007 HF, Rigaku with Pilatus 300 K detector at a wavelength of 1.541 Å. The diffraction data to 1.85 Å resolution were integrated and reduced using XDS.<sup>[17]</sup> The diffraction data for crystals of mdN complexed with **5** and **6** and cdN in complex with **6** were collected at 100 K at the MX14.1 beamline at the BESSY II electron storage ring operated by the Helmholtz-Zentrum Berlin, Germany<sup>[18]</sup> at a wavelength of 0.918 Å. The diffraction data to 1.48 Å and 1.38 Å resolution were integrated and reduced using XDS<sup>[17]</sup> and its graphical interface XDSGUI. All mdN crystals exhibited the symmetry of space group  $P4_32_12$  and contained one molecule in the asymmetric unit with a solvent content of about 60 %. Crystal exhibited the symmetry of space group  $P1$  and contained two molecules in the asymmetric unit with a solvent content of 45 %. Crystal parameters and data collection statistics are summarized in Table 2.

The structures of mdN were determined by the difference-Fourier method using coordinates from the isomorphous structure of the identical protein (PDB code 4YIK). The structure of cdN was determined by molecular replacement using program MOLREP<sup>[19]</sup> with coordinates from the structure of the identical protein (PDB code 4L57). Refinement was carried out using the program REFMAC 5.8.<sup>[20]</sup> Program Coot<sup>[21]</sup> was used for model building. The refinement statistics are given in Table 2.

Table 2. Crystal data and diffraction data collection and refinement statistics.<sup>[a]</sup>

	mdN 4	mdN 5	mdN 6	cdN 6
PDB code	6G22	6G2L	6G2M	6G2N
<b>Data collection statistics</b>				
Space group	<i>P</i> <sub>4</sub> <sub>3</sub> <sub>2</sub> <sub>1</sub> <sup>2</sup>	<i>P</i> <sub>4</sub> <sub>3</sub> <sub>2</sub> <sub>1</sub> <sup>2</sup>	<i>P</i> <sub>4</sub> <sub>3</sub> <sub>2</sub> <sub>1</sub> <sup>2</sup>	<i>P</i> <sub>1</sub>
Cell parameters (Å; °)	118.88 137.64 118.81; 90 90 90	73.80 73.80 106.63; 90.0 90.0 90.0	73.86 73.86 106.12; 90.0 90.0 90.0	38.88 47.23 61.79; 67.86 88.69 77.37
Number of molecules in AU	1	1	1	2
Wavelength [Å]	1.54187	0.9184	0.9184	0.9184
Resolution [Å]	43.19–1.85 (1.96–1.85)	46.88–1.48 (1.57–1.48)	46.86–1.37 (1.45–1.37)	42.41–1.40 (1.49–1.40)
Number of unique reflections	47,028 (7,578)	49,376 (7,653)	62,295 (9,903)	68,116 (11,048)
Redundancy	3.35 (1.77)	7.77 (7.89)	10.1 (10.2)	2.22 (2.21)
Completeness (%)	97.9 (97.3)	99.5 (96.8)	99.9 (99.7)	87.8 (87.9)
R <sub>meas</sub> <sup>[b]</sup>	0.058 (0.588)	0.070 (0.802)	0.061 (1.248)	0.026 (0.556)
Average I/σ(I)	15.03 (1.46)	16.04 (2.05)	23.56 (1.93)	18.84 (1.91)
CC <sub>1/2</sub> (%)	99.9 (70.8)	99.9 (79.3)	100.0 (68.3)	100.0 (71.4)
Wilson B (Å <sup>2</sup> )	30.2	26.0	22.8	27.42
<b>Refinement statistics</b>				
Resolution range (Å)	43.19–1.85 (1.897–1.85)	46.87–1.48 (1.52–1.48)	46.86–1.37 (1.41–1.37)	42.87–1.40 (1.44–1.40)
No. of reflections in working set	24,019 (1,743)	48,259 (3,262)	60,197 (4,354)	66,015 (4,886)
No. of reflections in test set	1,264 (91)	1,116 (75)	2,100 (151)	2,100 (155)
R value (%) <sup>[c]</sup>	15.4 (27.1)	12.0 (24.9)	12.3 (25.8)	15.1 (34.6)
R <sub>free</sub> value (%) <sup>[d]</sup>	19.3 (31.8)	15.1 (27.6)	14.9 (31.6)	19.2 (32.2)
RMSD bond length [Å]	0.019	0.018	0.018	0.017
RMSD angle [°]	1.881	1.908	2.181	2.02
Number of atoms in AU	1,898	2,023	2,007	3,508
Number of protein atoms in AU	1,611	1,658	1,656	3,144
Number of water molecules in AU	238	300	291	294
Mean B value protein/waters/compounds [Å <sup>2</sup> ]	26.88/36.16/26.12	22.51/35.80/19.88	19.63/33.56/15.87	27.7/34.2/23.6
Ramachandran plot statistics <sup>[e]</sup>				
Residues in favored regions [%]	98.4	99.0	99.0	98.4
Residues in allowed regions [%]	1.6	1.0	1.0	1.6

[a] The data in parentheses refer to the highest-resolution shell. [b]  $R_{meas} = \sum_{hkl} [n/(n-1)]^{1/2} \sum_i |I_i(hkl) - \langle I(hkl) \rangle| / \sum_{hkl} \sum_i I_i(hkl)$ , where the  $I_i(hkl)$  is an individual intensity of the  $i$ th observation of reflection  $hkl$  and  $\langle I(hkl) \rangle$  is the average intensity of reflection  $hkl$  with summation over all data. [c]  $R$ -value =  $\| |F_o| - |F_c| \| / |F_o|$ , where  $F_o$  and  $F_c$  are the observed and calculated structure factors, respectively. [d]  $R_{free}$  is equivalent to  $R$  value but is calculated for 5% of the reflections chosen at random and omitted from the refinement process.<sup>[12]</sup> [e] As determined by Molprobrity.<sup>[13]</sup>

The quality of the final models was validated with Molprobrity.<sup>[22]</sup> All figures showing structural representations were prepared with the program PyMOL.<sup>[23]</sup> The atomic coordinates and experimental structure factors have been deposited with the Protein Data Bank under the accession codes 6G22, 6G2L, 6G2M, and 6G2N.

## Acknowledgments

This work was supported by the Ministry of Education of the Czech Republic (programme "NPU I") project LO1304. Diffraction data were collected on BL14.1 at the BESSY II electron storage ring operated by the Helmholtz-Zentrum Berlin. The authors wish to thank Vaclav Veverka for critical proofreading of the manuscript.

**Keywords:** Inhibitor design · Crystal structures · Bisphosphonate nucleoside · Enzymes

[1] a) S. A. Hunsucker, B. S. Mitchell, J. Sychala, *Pharmacol. Ther.* **2005**, *107*, 1–30; b) V. Bianchi, E. Pontis, P. Reichard, *Proc. Natl. Acad. Sci. USA* **1986**, *83*, 986–990.

[2] J. Buschmann, B. Moritz, M. Jeske, H. Lilie, A. Schierhorn, E. Wahle, *J. Biol. Chem.* **2013**, *288*, 2441–2451.

[3] a) D. A. Carson, C. J. Carrera, D. B. Wasson, T. Iizasa, *Biochim. Biophys. Acta* **1991**, *1091*, 22–28; b) S. A. Hunsucker, J. Sychala, B. S. Mitchell, *J. Biol. Chem.* **2001**, *276*, 10498–10504; c) C. Mazzon, C. Rampazzo, M. C. Scaini, L. Gallinaro, A. Karlsson, C. Meier, J. Balzarini, P. Reichard, V. Bianchi, *Biochem. Pharmacol.* **2003**, *66*, 471–479.

[4] S. Yamamoto, T. Yamauchi, Y. Kawai, H. Takemura, S. Kishi, A. Yoshida, Y. Urasaki, H. Iwasaki, T. Ueda, *Int. J. Hematol.* **2007**, *85*, 108–115.

[5] a) G. Tzoneva, A. Perez-Garcia, Z. Carpenter, H. Khiabaniyan, V. Tosello, M. Allegretta, E. Paietta, J. Racevskis, J. M. Rowe, M. S. Tallman, M. Paganin, G. Basso, J. Hof, R. Kirschner-Schwabe, T. Palomero, R. Rabadan, A. Ferrando, *Nat. Med.* **2013**, *19*, 368–371; b) J. A. Meyer, J. Wang, L. E. Hogan, J. J. Yang, S. Dandekar, J. P. Patel, Z. Tang, P. Zumbo, S. Li, J. Zavadil, R. L. Levine, T. Cardozo, S. P. Hunger, E. A. Raetz, W. E. Evans, D. J. Morrison, C. E. Mason, W. L. Carroll, *Nat. Genet.* **2013**, *45*, 290–294; c) A. Hnizda, M. Fabry, T. Moriyama, P. Pachl, M. Kugler, V. Brinsa, D. B. Ascher, W. L. Carroll, P. Novak, M. Zaliava, J. Trka, P. Rezacova, J. J. Yang, V. Veverka, *Leukemia* **2018**, *32*, 1393–1403.

[6] H. K. Erdemli, B. Adam, N. Bavbek, *Acta Medica (Hradec Kralove)* **2004**, *47*, 129–131.

[7] P. D. Adams, P. V. Afonine, G. Bunkoczi, V. B. Chen, I. W. Davis, N. Echols, J. J. Headd, L. W. Hung, G. J. Kapral, R. W. Grosse-Kunstleve, A. J. McCoy, N. W. Moriarty, R. Oeffner, R. J. Read, D. C. Richardson, J. S. Richardson, T. C. Terwilliger, P. H. Zwart, *Acta Crystallogr., Sect. D* **2010**, *66*, 213–221.



- [8] C. M. Galmarini, J. R. Mackey, C. Dumontet, *Leukemia* **2001**, *15*, 875–890.
- [9] V. Bianchi, J. Sychala, *J. Biol. Chem.* **2003**, *278*, 46195–46198.
- [10] O. Simak, P. Pachel, M. Fabry, M. Budesinsky, T. Jandusik, A. Hnizda, R. Sklenickova, M. Petrova, V. Veverka, P. Rezacova, J. Brynda, I. Rosenberg, *Org. Biomol. Chem.* **2014**, *12*, 7971–7982.
- [11] P. Pachel, O. Simak, P. Rezacova, M. Fabry, M. Budesinsky, I. Rosenberg, J. Brynda, *MedChemComm* **2015**, *6*, 1635–1638.
- [12] I. Kosiova, M. Budesinsky, N. Panova, I. Rosenberg, *Org. Biomol. Chem.* **2011**, *9*, 2856–2860.
- [13] N. C. Srivastav, N. Shakya, M. Mak, B. Agrawal, D. L. Tyrrell, R. Kumar, *J. Med. Chem.* **2010**, *53*, 7156–7166.
- [14] a) A. Hnizda, R. Sklenickova, P. Pachel, M. Fabry, Z. Tosner, J. Brynda, V. Veverka, *Biomolecular NMR assignments*, **2013**; b) P. Pachel, M. Fabry, I. Rosenberg, O. Simak, P. Rezacova, J. Brynda, *Acta Crystallogr., Sect. D* **2014**, *70*, 461–470.
- [15] a) R. A. Copeland, *Enzymes: a practical introduction to structure, mechanism, and data analysis*, 2nd ed., Wiley, New York, **2000**; b) J. W. M. Williams, *Methods Enzymol.* **1979**, *63*, 437–467.
- [16] E. A. W. Stura, I. A., *Methods* **1990**, *1*, 38–49.
- [17] W. Kabsch, *Acta Crystallogr., Sect. D* **2010**, *66*, 125–132.
- [18] U. Mueller, N. Darowski, M. R. Fuchs, R. Forster, M. Hellmig, K. S. Paitankar, S. Puhlinger, M. Steffien, G. Zocher, M. S. Weiss, *J. Synchrotron Radiat.* **2012**, *19*, 442–449.
- [19] A. Vagin, A. Teplyakov, *Acta Crystallogr., Sect. D* **2010**, *66*, 22–25.
- [20] G. N. Murshudov, P. Skubak, A. A. Lebedev, N. S. Pannu, R. A. Steiner, R. A. Nicholls, M. D. Winn, F. Long, A. A. Vagin, *Acta Crystallogr., Sect. D* **2011**, *67*, 355–367.
- [21] P. Emsley, B. Lohkamp, W. G. Scott, K. Cowtan, *Acta Crystallogr., Sect. D* **2010**, *66*, 486–501.
- [22] S. C. Lovell, I. W. Davis, W. B. Arendall 3rd, P. I. de Bakker, J. M. Word, M. G. Prisant, J. S. Richardson, D. C. Richardson, *Proteins* **2003**, *50*, 437–450.
- [23] W. L. DeLano, *Abstr. Pap. Am. Chem. Soc.* **2009**, 238.

---

Received: March 29, 2018